THE ROLE OF INCLUSIONS IN THE INITIATION AND PROPAGATION OF FATIGUE CRACKS IN LOW ALLOY STEELS

by

P.S.J. Crofton, MSc, DIC

A thesis presented for the degree of
Doctor of Philosophy
of the
University of London

July 1980

Department of Mechanical Engineering
Imperial College of Science & Technology
London SW7 2BX

ABSTRACT

The role of inclusions in the initiation and propagation stages of fatigue crack growth in low alloy steels has been studied. Special attention is given to fatigue caused by repeated internal pressurisation in axisymmetric components.

Large diameter ratio thick cylinders containing double opposed cross-holes have been tested for five low alloy steels. Analysis of the results shows that the fatigue limit under a repeated internal pressure regime is independent of steel composition. The fatigue limit is shown to increase with tensile strength, but to be more dependent on the geometry of the intersection between the main bore and cross-hole.

A technique has been developed to measure crack growth rate in plain cylinders subjected to repeated internal pressure fatigue cycling. Results are given to show that a fracture mechanics formalism gives a sensible representation of crack growth in cylinders.

Fatigue crack initiation and propagation has been investigated in two steels of nominally similar composition but with differing inclusion contents. It is shown that anistropy in mechanical properties is reflected in the fatigue behaviour of these two steels. Fractographic analysis shows that inclusions are a major cause of fatigue crack initiation in both steels. The same fracture mechanism is observed to occur in repeated direct stress fatigue tests in air as occurs when these steels are subjected to repeated pressurisation in the form of thick cylinders. A consistent theory is developed to show that a mode I fatigue crack propagation limit is determining at the fatigue limit of these steels. Differences in fatigue crack propagation rate measured in air are explained in terms of the inclusion population in the respective steels.

The significance of the experimental findings are discussed in the light of a proposed design code for pressure vessels working in the kilobar region.

Finally, recommendations for further work are made to determine the range of materials and situations to which the proposed direct stress fatigue criterion can be applied.

ACKNOWLEDGEMENTS

The author wishes to thank Dr J. Rogan, under whose supervision this work was carried out. His generous provision of financial support throughout the course of this work is greatly appreciated.

Special thanks are also due to the many staff members of this Institution for valuable advice and practical help. In particular, the assistance of Dr D.P. Isherwood, Dr C.L. Tan, Mr P. Grant, Mr G. Eles, Mr G.C. Klintworth and Mrs E.A. Hall is gratefully acknowledged.

Finally, the author is especially grateful to his wife for her patience and forebearance during the course of this work.

CONTENTS

NOMENCLATURE

a, b, c	:	crack length or half length for central cracks
a_o, b_o, c_o	:	semi-axes of ellipsoidal or cylindrical inclusions
C	:	material constant in Paris' law
D	:	diameter ratio of cylinders
K	:	stress intensity factor
K_{Ic}	:	plane strain fracture toughness (opening mode)
K_{max}	:	maximum value of stress intensity
K_{min}	:	minimum value of stress intensity
ΔK	:	range of stress intensity ($K_{max} - K_{min}$)
ΔK_{th}	:	range of stress intensity below which a fatigue crack will not propagate (threshold value)
L	:	longitudinal axis of forging (length)
m, n	:	exponent in Paris' law
N	:	number of load cycles
P	:	internal pressure
Q	:	short transverse axis of forging (thickness)
R	:	stress ratio (K_{max}/K_{min})
T	:	long transverse axis of forging (width)
W	:	wall thickness or specimen net thickness in direction of crack growth
x, y, z	:	coordinates or directions in an orthogonal system

Greek Symbols

ε_θ	:	hoop or tangential strain in a cylindrical component
σ	:	normal stress
σ_θ	:	effective hoop or tangential stress in a cylindrical component

σ_H : hoop or tangential stress in a cylindrical component (Lamé value)

CHAPTER 1

INTRODUCTION

1.1 INTRODUCTION

The increasing world demand for raw materials and energy conservation has recently begun to pose new problems for designers and engineers. Existing design methods are often too phenomenological in approach to justify further reductions in "safety factors" to satisfy the demand for increased efficiency in engineering situations. Therefore, it is apparent that an ever increasing understanding of the way in which materials respond to applied forces must be gained to satisfy the demand for progress.

In the field of high pressure engineering, this concept is particularly true since accepted working pressures have risen dramatically in the past decade. Tubular polyethylene reactors designed in the 1960's were typically limited to working pressures of 275 MPa. The current generation of reactors operate at internal pressures of 375 MPa. At the same time, reactor bore size has increased from 25 mm to 50 mm and greater.

Similarly, deep sea submersibles, armaments, pumps, water jet cutting equipment and, to a lesser extent, nuclear reactor pressure vessels, are all operating at pressures considered unrealistic until recently. Perhaps the most surprising feature of this design advance is that it has been achieved to a large extent without recourse to any new fundamental technique in pressure containment or exclusion.

The homogeneity and quality of the materials used have improved and fracture mechanics analysis has been extensively developed, but in several important respects the analysis of pressurised systems has not

kept pace with requirements. In any comprehensive design procedure, the possibility and likely consequences of failure of the system are of paramount importance. Linear elasticity and plasticity theorems are well established and can be invoked to describe and predict failure through monotonic overload. The failure situation which is not so well understood is that of crack propagation resulting from fatigue loading or environmental effects.

The fatigue phenomenon has been recognised and researched for well over 100 years. It is a measure of the complexity of the basic fatigue process that, in spite of intensive research efforts, the majority of engineering failures are still attributable to fatigue. Whether a complete understanding of the mechanisms of fatigue failure will reduce the proportion of failures in this category is a subjective point. It is sufficient to say that, at present, no analytical models exist which can generally predict stress levels at which fatigue failure will occur. Therefore, the only recourse a designer has is to the phenomenological approach which has characterised the systematic investigation of the fatigue process to date.

The work undertaken and reported here is an attempt to quantify, through the use of linear elastic fracture mechanics and various material parameters, the response of a typical ferrous pressure vessel material to repeated pressure-induced fatigue crack growth.

In high pressure containment systems, the most commonly encountered geometry is that of the thick-walled cylinder. This geometry is treated in detail in a general fashion such that the results of the investigation can be applied to other materials and geometries through the use of the relevant parameters. The results of the investigation can be shown to apply to any pressurised system where crack growth is augmented by the

pressurising medium, and should therefore be of use to designers and engineers alike.

In the following sections, the nature of fatigue failure and fatigue mechanisms is discussed and a critical review of the relevant literature is presented. Since this work can be broadly divided into two approaches, a continuum approach and a metallurgical approach, the literature is reviewed in two parts. It will be shown later that both approaches are a necessary means of modelling the behaviour of a material subjected to repeated pressure-induced crack growth, whereas either approach used alone is insufficient.

1.2 OBJECTIVES OF PRESENT WORK

The design of pressure vessels to contain static internal pressure is generally thought to be fairly straightforward. Elastic stress analysis of axisymmetric components is sufficiently generalised that the yield pressure of a cylindrical element can be predicted to within a few per cent. Indeed, the inaccuracy present in the prediction is more likely to arise from the choice of yield criterion than in the calculation of stress.

When the design methods for pressure vessels subjected to fatigue loading are reviewed, the lack of complete understanding of the basic mechanisms is obvious. Fatigue design for pressurised components subjected to greater than 100,000 stress reversals is still largely empirical. The vast majority of published data on long life fatigue of pressure systems was carried out in the late 1950's and throughout the 1960's.

Since this time, fracture mechanics has developed to the stage where the metallurgical parameters governing the fracture behaviour of steels and aluminium alloys can be explained. It is therefore pertinent to ask whether a fracture mechanics formalism can be applied to the fatigue process at the microstructural level. Similarly, as with all empirical data, it is relevant to review the established values occasionally. Advances in steel producing techniques in the last 20 years has led the manufacturers to claim increased homogeneity and fatigue properties for almost all classes of steels. If this is indeed the case, then the typical values of fatigue strength for pressurised components as found in the 1960's may now be overly conservative.

The major objective of this work is therefore to test the assumption that "modern steels" produced using vacuum techniques are more isotropic and fatigue resistant than their predecessors. In particular, the effects

of material anisotropy are investigated with respect to their influence on fatigue and fracture properties. This work should be of great use to designers and engineers who, at present, are forced to specify minimum fracture and tensile properties in a transverse direction without any real feel for their significance.

During the course of this work, it became apparent that the results enable a more fundamental criterion for fatigue of thick-walled cylinders to be suggested. Although this had not originally been intended as an objective, the simplification afforded by this failure criterion (if accepted) should prove of great use to all users and manufacturers of high pressure equipment.

1.3 OUTLINE OF PRESENT WORK

The work presented here can be divided into three distinct parts. In the first part of the experimental programme, the notched fatigue strength of five forgings of varying composition and origin are compared. Thick cylinders containing double opposed cross-holes were tested under various pressure regimes to try to demonstrate that steel composition influences fatigue performance.

Secondly, a series of thick cylinders was tested under repeated internal pressure conditions in order to develop a technique for measuring crack growth rate in a thick cylinder.

Finally, the bulk of the experimental work was undertaken in a comparison of fatigue anisotropy in plain cylinders of two steels of nominally identical chemical composition but containing widely varying inclusion populations. Measurements of fatigue crack growth rate in air were taken for these two steels and compared with the behaviour of cylinders in the mortal region as a function of orientation.

It was the original intention of this work to study the fatigue behaviour of thick cylinders with and without stress raisers at the fatigue limit and during the propagation stage. This proved overly ambitious and was abandoned.

The presentation of this work follows the sequence given above, except where a common procedure was applied to all the steels is used. Therefore, the mechanical properties and preliminary metallurgical investigations are reported for all the steels, irrespective of their later usage.

Chapter 2 gives a review of the literature relating to fatigue mechanisms. This review is divided into sections covering fatigue from a micro-structural aspect as well as from the continuum mechanics viewpoint.

In the following chapter, the experimental procedures used in this investigation are detailed. The construction of electronic apparatus is described, as are the reasons for selection or certain experimental techniques. Finally, the machines used to provide the fatigue loading are described and the methods used to test specimens are given.

The results of the experimental programme and preliminary metallurgical investigations are given in Chapter 4, together with the techniques used for data reduction.

In Chapter 5, the results obtained are discussed in the light of other published research in this field. Some further results are presented and compared with existing data to provide a coherent theory for the prediction of a fatigue limit in thick cylinders. This hypothesis is tested against the existing fatigue limit criteria for pressurised systems. A comparison of fatigue crack growth behaviour in air and in thick cylinders is made on the basis of metallurgical observations and the

differences explained. The errors introduced by the assumptions made and methods adopted are estimated and discussed.

Suggestions are given in Chapter 6 as to the applicability of existing fatigue and fracture criteria in a proposed design code for monoblock pressure vessels.

Finally, the conclusions reached as a result of this investigation, and the recommendations arising from it are summarised in Chapter 7.

CHAPTER 2

REVIEW OF THE LITERATURE

2.1 EARLY HISTORY OF FATIGUE

The recognition of fatigue as a failure mode occurred at a late stage in the development of engineering on the large scale in this country. Rankine (1843) noted that railway axles had a tendency to fail after several years' use and attributed the behaviour to a time-dependent deterioration of the metal. The use of iron as a structural material, especially in the form of girders, led to the realisation that failure could occur under repeated loading at loads less than the singly applied failure load. This situation, when appreciated, gave impetus to experimental work to quantify the strength of metals under repeated load.

Probably the first systematic investigation of the fatigue phenomenon was undertaken by Wohler (1871) between 1858 and 1870. His design of a fatigue testing machine and format for the presentation of results are still in use today (a tribute indeed).

Early in this century, corrosion enhanced fatigue became recognised as a problem and this started the serious investigation of fatigue mechanisms which is still continuing.

2.2 THE MECHANISMS OF FATIGUE

Early investigations into the mechanisms by which fatigue failure occurs contributed little as the structure of metals was not appreciated. A generally accepted explanation for fatigue was that a metal changed from a fibrous to a crystalline structure as a result of fluctuating stresses. This impression arose because of the faceted nature of most fatigue failures in poor quality cast iron, the common engineering

material of the day. Even in the early part of this century, therefore, the avoidance of low energy modes of failure was appreciated.

With the observation by Ewing & Humfrey (1903) that fatigue was associated with detectable deformation on the surface of a metal, the importance of slip in metal crystals was apparent.

Two competing theories of the time both explained fatigue as occurring by slip bands broadening to form cracks. Ewing & Humfrey (1903) proposed that the constant motion of slip band surfaces led to a 'fretting' type situation where metal was worn away by solid friction until a crack was formed. Beilby's (1921) 'amorphous' theory argued that, because of the repeated stressing, metal in the slip band surfaces underwent an amorphous change to a less ductile but stronger material, this process then repeating itself until a crack had formed.

In 1923, Gough & Hanson proposed a theory of fatigue based on the ability of a material to work or strain harden and thereby decrease the plastic deformation occurring.

If the range of applied stress was below the fatigue limit, then plastic deformation slowly declined to zero and therefore no failure would occur, whereas if the range of applied stress was above the fatigue limit, saturation work hardening occurred and failure inevitably resulted.

To prove this theory, Gough (1933) undertook a series of experiments with single crystals of pure, ductile metals. From his tests, it was apparent that fatigue cracks originated from regions of intense slip. With a few tests on polycrystalline aluminium, the same characteristics were also evident, although it was noted that grain boundaries inhibited crack growth.

More recent work by many authors (Wood (1956), Cottrell & Hull (1957), Forsyth (1957), Cina (1960)) has confirmed the basis of Gough's

observations and enabled a distinction to be made between static and fatigue deformation. Slip bands that appear as a result of static deformation are fairly evenly distributed over all the surface grains of a polycrystalline aggregate of a ductile metal. When a polycrystalline aggregate of a ductile metal is subjected to fatigue loading, however, slip bands are first generated in crystals which are favourably oriented with respect to the applied stress. Further stress cycling leads to broadening of these initial slip bands and only limited occurrence of more slip bands close to those already in existence.

With the advent of electron microscopy and dislocation models, it has been possible to show that in pure ductile metals fatigue crack initiation is preceded by the formation of 'extrusions' and 'intrusions' on the metal surface. Because of the reversal of stress in a fatigue situation, slip bands broaden to form a series of grooves and ridges, or extrusions and intrusions.

It is now generally accepted that intrusions generated at a surface in ductile metals by reversed slip are the site from which microcracks grow, and various dislocation and geometric mechanisms are invoked to explain their formation (Backofen (1959), Grosskrentz (1963), Mott (1958), Wood (1959), May (1960)).

Once a microcrack has formed, it can be treated on two levels:

1. Continuum mechanics can be invoked to describe the propagation and behaviour of the fatigue crack under the influence of external loading.

or 2. A microstructural (sub-continuum) approach can be adopted to explain the growth of a fatigue crack.

The reconciliation of these methods should bring about a full understanding of the fatigue process.

Both models can be used with varying degrees of success to describe the response of a fatigue crack to loading intensity, environment and time. The former method currently offers greater accuracy in the prediction of fatigue lives and is therefore of more immediate use, although the latter approach should serve to give a fundamental understanding of the processes involved. In either case, the observed behaviour of all fatigue cracks which has to be explained can be divided into three distinct stages.

1. Stage I growth: Once a microcrack has formed from an intrusion or surface 'defect' under the action of repeated stress, it continues to propagate along slip bands aligned parallel to planes of maximum shear stress.
2. Stage II growth: When the crack length becomes significant with respect to the body in which it is set, the crack tip stress field becomes dominant and the propagating plane deviates to a plane normal to the maximum principal stress. A characteristic of this stage II type crack propagation is the occurrence in some materials of striation or ripple markings corresponding to discrete crack advancement with cyclic loading*.

   Stage II crack growth occupies the greatest proportion of fatigue crack length but is usually a very minor proportion

---

* The striations commonly observed on metallic engineering components which have failed in service, and which are readily visible to the naked eye, are *not* striations produced by crack front advance with each load cycle. This change in surface topology or coloration occurs as a result of changes in loading intensity or due to environmental conditions during periods of no external fluctuating load.

(≈ 10%) in terms of cyclic life. Whether or not a fatigue crack can adopt its final mode is a function of the crack tip stress field.

3. Stage III crack growth is characterised by reversion of the crack to a plane of maximum shear stress in ductile materials when final failure occurs by a tensile instability mode, the remaining section of material being unable to support the applied loads.

   With less ductile materials, stage III crack propagation is often absent as a fast fracture intervenes, leading to failure in the same plane as for stage II but within one cycle of applied load.

The mechanism for fatigue crack formation from persistent slip bands is not generally true for materials in all conditions. Ransom & Mehl (1952) have shown quite conclusively that in wrought, high strength materials, fatigue cracks can initiate from hard particles in the matrix. Therefore, inclusions in the form of oxides, silicates, aluminates, etc., can initiate crack growth without evidence of persistent slip bands forming in surface grains remote from the flaw. Similarly, in brittle materials, defects in the form of second phase particles, scratches or other geometrical discontinuities initiate fatigue cracks without localised slip band formation.

It has been shown by Frith (1956) that steels with tensile strengths of 900 MN/m^2 or greater will tend to nucleate fatigue cracks at inclusions when tested in the form of smooth specimens. Since, in general, a steel will have a preferred orientation related to the working direction, the effect of inclusion orientation can be critical in determining the mode

of crack initiation. Inclusions of an elongated nature when stressed normal to their long axis have a more damaging effect than when lying parallel to the stress axis. It has been suggested that this fact alone can account for the observed anisotropy of fatigue properties in heavily worked steels.

2.2.1 Effect of Stress Conditions

2.2.1.1 Mean stress

The majority of fatigue data on both ferrous and non-ferrous materials has been accumulated for the case of zero mean stress. This has occurred because the earliest accurate fatigue testing procedures utilised rotating bending machines which inherently cycle between equal values of tensile and compressive stress. In reality, engineering components are rarely, if ever, subjected to such anti-symmetric loading.

With the development of direct stress machines, it became possible to investigate the effect of a mean stress superimposed on an alternating stress. Since the loading system of most interest to engineers is one of a mean tensile stress, together with an alternating tensile stress, this has received most attention.

Various empirical laws have been introduced to predict the fatigue limit under mean stress conditions. Of these, the most generally accepted are due to Soderburg (1890), Goodman (1899) and Gerber (1874). These can be expressed mathematically as follows:

Soderburg's Law: $$\pm \sigma_L = \pm \sigma_o \left(1 - \frac{\sigma_m}{\sigma_y}\right)$$

Goodman's Law: $$\pm \sigma_L = \pm \sigma_o \left(1 - \frac{\sigma_m}{\sigma_t}\right)$$

$$\text{Gerber's Law:} \qquad \pm \sigma_L = \pm \sigma_o \left(1 - \left[\frac{\sigma_m}{\sigma_t}\right]^2\right)$$

where $\pm\sigma_L$ is the fatigue limit or strength at a given endurance

$\pm\sigma_o$ is the fatigue limit or strength under zero mean stress conditions

σ_y is the yield strength of the material

σ_t is the ultimate tensile strength of the material

and σ_m is the mean tensile stress in the fatigue cycle

When plotted on the basis of range of stress at the fatigue limit versus mean tensile stress, these three relationships appear as below.

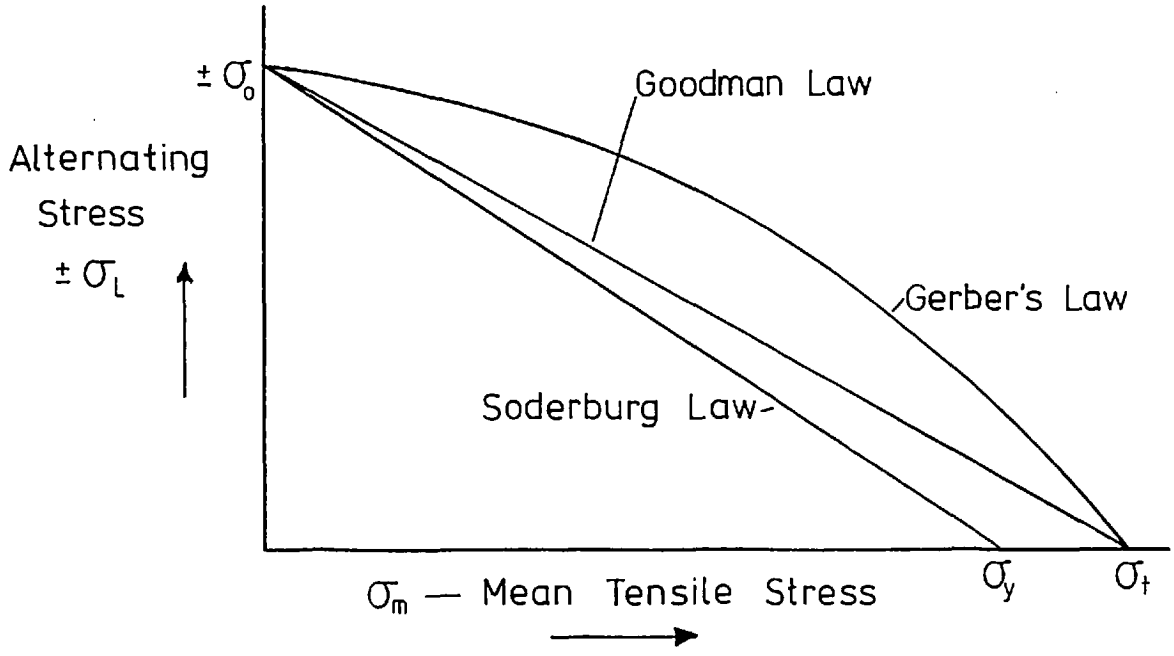

Most experimental data for wrought steels fall between the Goodman (sometimes referred to as the Modified Goodman) Law and Gerber's Law. Hence, the general use of the Goodman or Soderburg Law is acceptable since they provide a conservative estimate of the effect of mean tensile stress.

2.3 CONTINUUM MECHANICS APPROACH TO FRACTURE

2.3.1 Linear Elastic Fracture Mechanics (LEFM)

The original work in this field was undertaken in an attempt to explain quantitatively the difference between the theoretical strengths of crystalline solids and glasses and their observed strengths.

Griffith postulated that all solids contain defects of finite size (which could not be easily removed) and that these defects led to a gross reduction in fracture strength.

In a classic paper (1920), he recognised that these defects could be regarded as incipient cracks and that the driving force for crack extension was the difference between the energy released from crack extension (i.e. the strain energy in the surrounding elastic material) and the energy needed to create two new surfaces.

Using glass rods as his experimental material, as they approximate a Hookean material, he found that, as can be done using the expressions due to Inglis (1913) for the stress and strain distribution at the top of an elliptical crack in an infinite plate, the decrease in strain energy in the material surrounding his defect could be calculated:

$$\text{strain energy} = \frac{\pi c^2 \sigma^2}{2E}$$

where $2c$ = crack length

σ = stress perpendicular to major axis of elliptical crack

The surface energy needed to create these surfaces is given by:

$$\text{Surface energy} = 4c\,S$$

where S = surface energy/unit area. For the crack to spread, the differential of these two terms is required:

$$\frac{\pi\ 2c\ \sigma_b^{\,2}}{E}\ \delta c \;=\; 4S\ \delta c$$

and hence the Griffith fracture stress:

$$\sigma_b \;=\; \left(\frac{2\ E\ S}{\pi\ c}\right)^{\frac{1}{2}} \tag{2.1}$$

The simplicity of this thermodynamic approach is evident as it ignores the details of the fracture process occurring at the crack tip and implies a $(1/c)^{\frac{1}{2}}$ dependency of fracture stress with crack length.

The significance of this work was not fully recognised until after the Second World War when the problem of brittle fracture of mild steel structures became pressing. Much attention was devoted to the impact resistance of steels and criteria were developed for the avoidance of brittle fracture largely based on conventional Charpy V notch tests.

Although Griffith originally developed his fracture theory for very brittle materials, it had been realised independently by both Irwin (1957) and Orowan (1945) that this type of approach could be used to characterise failure in more general engineering materials. Experimentation using cracked sheets of aluminium had shown that the constant, $2S$, in Griffith's original expression was too low to account for the observed results. This led Orowan to rewrite Griffith's original expression to include a term expressing the energy absorbed in the production of a plastic zone at the crack tip:

$$\sigma_b \;=\; \left[\frac{E\ (2S + S_p)}{\pi\ c}\right]^{\frac{1}{2}} \tag{2.2}$$

where S_p is a measure of the energy absorbed in producing a plastic zone at the crack tip, providing the plastic zone is small in relation to the overall geometry. Then, since it was found that $S_p >> 2S$, equation (2.2) can be expressed as:

$$\sigma_b = \left[\frac{E\ S_p}{\pi\ c}\right]^{\frac{1}{2}} \tag{2.3}$$

and values of S_p deduced from tests on cracked specimens of varying crack length, $2c$.

Westergaard (1939), by consideration of the stress field condition at the tip of a crack in biaxial tension and with the use of complex functions, derived an expression to describe the stress normal to the crack tip in the form of a series:

$$\sigma_{11} = \sigma \sqrt{(c/2r)} \cos\frac{\theta}{2}\left(1 + \sin\frac{\theta}{2}\sin\frac{3\theta}{2}\right) + \ldots$$

where θ is the angle with respect to the crack plane of an element at a distance r from the crack tip. Now, when $r << c$, the expression can be reduced to:

$$\sigma_{11} = \sigma \left(\frac{c}{2r}\right)^{\frac{1}{2}} \tag{2.4}$$

which can then be rewritten as:

$$\sigma_{11} = \frac{K'}{\sqrt{2r}} \tag{2.5}$$

(where $K' = \sigma \sqrt{c}$), which, when K' is more usually defined as:

$$K = \sigma \sqrt{\pi\ a} \tag{2.6}$$

gives us a single parameter with which to describe the stress close to a crack tip.

Irwin (1957), by a rigorous analysis of the relationship between fracture stress and crack length, was able to derive a parameter which quantifies the potential energy release rate just preceding unstable crack propagation. This parameter, G_{crit}, became known as the fracture toughness. With the recognition that the strain energy release rate, G, could be related to the stress intensity factor, K, by a simple relationship:

$$G = \frac{K^2}{E}(1-\nu^2) \qquad \text{(plane strain)} \qquad (2.7)$$

$$G = \frac{K^2}{E} \qquad \text{(plane stress)} \qquad (2.8)$$

the foundation of linear elastic fracture mechanics was laid. By the use of a single parameter to describe the state of stress at a crack tip, the fracture stress of a quasi-brittle material may be calculated, irrespective of component geometry. Fracture is shown to occur when K reaches a critical valued denoted as K_{Ic} for a crack loaded in direct tension (mode I). This critical stress intensity can be shown to be a material property within the limits of temperature, loading rate, material condition and environment.

2.4 THE APPLICATION OF LEFM TO FATIGUE CRACK PROPAGATION

2.4.1 Crack Growth Rate Models

The use of a stress intensity approach to fatigue crack propagation was first proposed by Paris & Erdogan (1963), who noted that most fatigue crack propagation data could be well approximated by an expression of the form:

$$\frac{da}{dN} = C\,\Delta K^m \tag{2.9}$$

where a = crack length

N = number of cycles

C = material constant (intercept)

ΔK = range of stress intensity = $K_{max} - K_{min}$

and m = stress dependence (exponent)

Whilst a material may not be truly quasi-brittle or even approaching a condition where an LEFM approach would be valid in terms of fracture, the gross stresses obtained in a high cycle low plastic strain amplitude test ensure that the fracture process should be dependent only on the size of the reversible plastic zone at the crack tip.

From the standard expression first derived by Irwin to account for crack tip plasticity, r_y, the radius of the plastic zone is given by:

$$r_y = \frac{\Delta K^2}{6\pi\,(2\sigma_y)^2} \qquad \text{(plane strain)} \tag{2.10}$$

This implies that from fundamental considerations the exponent m should take a value of two or very close to it. However, with high strength materials, exponents of the order of ten have been observed, values of m greater than two being common.

Paris and his co-workers found that, in general, most materials exhibited a dependence on the range of stress intensity factor raised to the fourth power. It is now generally accepted, however, that for ferrous materials a plot of *log da/dN* versus *log* ΔK yields a sigmoidal relationship of the form shown in Figure 2.1. Only the central region

B-C can be adequately represented by equation (2.9). The so-called general exponent of four encompasses all three regions AB, BC and CD of the crack growth rate behaviour.

Several more generalised crack growth rate laws have been evolved to explain the occurrence of three regions of crack growth behaviour and to incorporate the physical singularities of zero growth and fast fracture (Barsom (1974), Klesnil & Lukas (1972), Duggan (1977), McEvily & Groeger (1977)). The simplest of these involve the introduction of additional terms to account for the experimentally found crack growth threshold, the influence of mean stress and the singularity which is implied when K_{max} equals K_{Ic}. That due to Forman (1966) is of interest since it includes all the above mentioned.

Forman postulated that crack growth dependence would be best modelled by an expression of the type:

$$\frac{da}{dN} = \frac{C\ (\Delta K - K_{th})^m}{(1-R)\ K_c - \Delta K} \qquad (2.11)$$

The existence of a stress intensity value below which a crack will not propagate has been found by many workers and is generally termed K_{th}.

By inspection, it is obvious that in equation (2.11):

$$\frac{da}{dN} \rightarrow 0 \qquad \text{as} \qquad \Delta K - K_{th} \rightarrow 0$$

Similarly, fast fracture or unstable crack propagation is deemed to occur when K_{max} attains a critical value denoted by K_c. Therefore, since it is evident that:

$$\frac{\Delta K}{(1-R)} = K_{max}$$

(where R is the stress intensity ratio = K_{min}/K_{max} in a cyclic loading cycle), the expression reduces to:

$$\frac{da}{dN} = \frac{C\ (\Delta K - K_{th})^m}{\Delta K\ ((K_c/K_{max}) - 1)} \qquad (2.11a)$$

Hence, $da/dN \to \infty$ as $K_{max} \to K_c$. This type of equation satisfies the physical realities of zero growth at low stress intensities and unstable crack propagation at a critical value of stress intensity, but it also implies an effect of mean stress in increasing crack propagation rates.

Some authors (Ritchie & Knott (1973)) show convincing experimental evidence for an effect of mean stress, whilst others working with similar materials (Richards & Lindley (1972)) find no effect.

From theoretical considerations, mean stress should have no effect since the size of reversed plastic zone embedded at the crack tip is merely a function of the range of stress intensity and not its absolute value (provided $K_{max} < K_c$). Fractographic examination of cracked specimens has shown conclusively that mean stress effects are always associated with limited scale monotonic failure modes occurring simultaneously with subcritical crack propagation by a ductile striation mechanism. Hence, it would appear that microstructure can play a determining rôle in the crack propagation rate behaviour of a body.

A further concept in the continuum mechanics modelling of fatigue crack growth has recently been introduced by Elber (1970). By considering a fatigue crack growing under zero to tension loading, it was shown that the crack may be partially or completely closed at zero load. The explanation for this behaviour is given in terms of the compressive residual stresses left in the wake of an advancing fatigue crack leading to premature closure. The theoretical calculation of the stress level at

which crack tip closure occurs is currently not possible and most workers resort to experimental determination of the stress intensity at which closure occurs, K_{cl}. In the literature to date, many values of K_{cl} have been reported for differing loading histories and specimen configurations, but, in general, K_{cl} is of the same order as K_{th} for a given material. This fact poses the question as to the existence of a K_{th} since it is tempting to ascribe a zero crack growth situation to the condition:

$$K_{cl} = K_{th} \tag{2.12}$$

for a given material and loading situation. It is, however, now generally accepted that K_{cl} is larger than K_{th} (Schmidt & Paris (1973), Kikuwa, Jono & Tanaka (1976)). The significance of the crack closure concept is realised in the region AB (Figure 2.1) and the transition from this region to the stress intensity dependent crack growth regime, BC. In attempting to derive a generally applicable crack growth law by a continuum mechanics approach, many workers (McEvily & Groeger (1977), Ritchie (1977)) have investigated the threshold propagation region. It is in this region that the bulk of the cyclic life of a component is spent if a crack is propagating under constant range of applied load.

The conclusions that have been reached can be summarised as follows:

(a) K_{th} exhibits a dependence on stress ratio, crack closure stress and environment.

(b) Crack growth in this regime is not necessarily continuous.

(c) Microstructure can be determining, both as regards K_{th} values and initial rate of crack propagation.

From a design point of view, the use of a linear elastic fracture mechanics formalism for the calculation of residual life of cracked components has been shown to be an adequate approach. This is to be expected since most cracks, when detected, are of sufficient size to ensure that the maximum normal stress (region BC, Figure 2.1) is controlling. Crack growth in this regime is accepted as being continuum controlled and therefore adequate knowledge of the material parameters yields good correlations.

Several workers (Forman (1968), Jack & Price (1970), Schlitz (1979)) have used the LEFM approach in predicting total life and fatigue limit of initially uncracked components. The results of these predictions are more variable. To predict the total cyclic life of an initially unflawed component, several assumptions must be made. The most basic is the size of the initial defect or microflaw from which a fatigue crack can grow. In high strength steels, inclusions have been shown (Zacky, Gerberich & Parker (1968), Frith (1955), Buch & Chodorowski (1964), Ranson (1954), Lankford (1977)) to be the initiation sites from which fatigue cracks propagate. Careful estimation of inclusion size and orientation should therefore give a good estimate of initial 'crack' size since, at a free surface, an inclusion can debond from the matrix after very few cycles of applied stress and therefore be regarded as a crack. Hence, by integrating expressions of the type given by Paris or Forman, the total life of the component can be deduced. Indeed, this is the approach that has been used generally. To estimate the fatigue limit of a component, the K_{th} value for that material is substituted into the stress intensity factor expression:

$$K = K_{th} = \sigma f(\frac{a}{w}) w^{\frac{1}{2}}$$

Knowing the value of K_{th} and the size of initial flaw or defect, and hence $f(a/w)$, a stress can be calculated which should correspond to the minimum stress needed to propagate a crack and therefore the fatigue limit.

The limitation of this approach is twofold. Firstly, it is implicitly assumed that crack propagation occurring at all values of stress intensity range is continuum controlled which has been shown not to be the case. Secondly, the choice of a suitable stress intensity factor is critical. Inclusions in high strength steels are generally either ellipsoidal or approximately spherical in shape and thus present special geometries where they intersect free surfaces for which no accurate general form stress intensity factors exist.

This area is currently the subject of much research interest from a microstructural point of view, but it is doubtful if an adequate continuum mechanics model will be forthcoming to predict fatigue limits without consideration of sub-continuum factors.

2.5 FLUCTUATING PRESSURE FATIGUE

2.5.1 Fatigue of Thick-Walled Cylinders Subjected to Repeated Internal Pressure

The state of stress in a thick-walled cylinder was first analysed by Lamé (1833). He demonstrated the dependence of the stress system on the diameter ratio (hereafter referred to as D) and not on the absolute size of the cylinder. The uneconomical nature of stress distribution in a thick-walled cylinder is immediately obvious in that material nearest the inner diameter takes a greater proportion of the load than the less highly strained outer diameter.

The importance of fatigue failure in thick-walled cylinders

was evident in 1861, when Rodman reported on a series of experiments undertaken to evaluate materials for cannon manufacture. Indeed, all the early impetus towards understanding the nature of fatigue failure in cylindrical vessels was aimed at producing better cannons (Longridge (1860), Jacob (1920)).

The first systematic investigation of fatigue in cylinders subjected to repeated internal pressure was reported by Morrison, Crossland & Parry in 1956. There followed a series of papers (Morrison, Crossland & Parry (1959,1960), Parry (1956,1965)) by the same authors giving fatigue results for a large range of materials and configurations. The main points to arise from their work were as follows:

i) At the fatigue limit, the range of shear stress gives the best failure criterion.

ii) There is no simple correlation between the uniaxial fatigue strength of a material and its fatigue strength under the multi-axial stress conditions of the thick cylinder. Rather, there appeared to be an unexpected relationship between the range of reversed shear stress required to cause failure in a torsional fatigue test and the range of shear stress required to cause failure in the same material in the form of a thick cylinder:

$$\Delta\tau_t = 2\Delta\tau_c \qquad (2.13)$$

No explanation was offered for this anomaly other than the suggestion that the pressurising oil in the crack had an unexpectedly large effect.

iii) Mean shear stress appeared to have a significant effect on the

range of shear stress at the fatigue limit for the range of materials and sizes tested.

iv) Tests on materials which would commonly be regarded as ductile always led to the same type of failure: a fatigue crack initiating at the inner diameter and growing in a longitudinal radial plane normal to the maximum principal stress, final failure occurring in a "leak before burst" mode. Repeated internal pressure fatigue tests on plain cylinders of a low modulus material, beryllium copper, gave similar early growth patterns, but failure occurred by fast fracture of the specimen from end to end before the fatigue crack had penetrated the full wall thickness. The same response was observed in a notably brittle material, tungsten carbide; but here, the depths of the fatigue cracks before fast fracture were very small.

Crossland (1976), in a recent review of the fatigue and fracture of thick-walled pressure vessels, proposes two possible explanations for the apparent difference in fatigue strength of materials when tested in repeated torsion and in the form of thick cylinders. He argues that in a low D ratio vessel, the state of stress is equivalent to a fairly high volumetric tension plus a superimposed shear stress, whereas in a high D ratio the converse is true. The volumetric tension is low compared to that in a thin-walled vessel. Therefore, if repeated volumetric tensile stress is weakening and the effect of pressure acting on the bore material is weakening, the two effects may be self-cancelling.

The more fundamental explanation proposed is that fluid enters the crack or flaw, exerting pressure on the flanks of the cylinder. This effectively increases the range of stress intensity such that, if the

material has a threshold range of stress intensity factor, then this is determining at the fatigue limit.

The application of fracture mechanics criteria has been attempted by Shannon (1970), who showed that for long straight-fronted cracks, typical of fatigue cracks in rifled gun barrels, fracture mechanics parameters gave good agreement with experimental results in predicting residual strength. The use of yielding fracture mechanics is shown to involve enormous computational difficulties, but LEFM can be invoked if limited crack tip plasticity is occurring.

Fatigue life predictions have been attempted by Haslam (1969, 1972) and Haslam & Marsh (1969) in a series of three similar papers intended to be of use to designers. Using material constants C and m derived from the work of Frost, Pook & Denton (1971), he combines a modified stress intensity factor with Paris' equation to derive a fatigue life expression. This relationship is dependent only on range of pressure, diameter ratio, material crack growth rate constants and a knowledge of initial defect size. In comparison with the experimental data of Morrison, Crossland & Parry (1960), the expression produces conservative results according to the author.

The reason for this most probably lies in the choice of stress intensity factor and initial defect size.

When the work at Bristol University (Morrison, Crossland & Parry (1956,1959,1960)) is considered as a whole, the need for a simple endurance criterion of use to a designer is obvious. The extreme difficulty of carrying out high pressure fatigue tests ensures that a simple criterion, based for example on uniaxial fatigue properties, would be adopted.

Tomkins (1973) has proposed such a criterion based on

considering the fatigue limit of a thick cylinder from a plasticity onset point of view. He shows that for a typical pressure vessel steel, the results of push/pull, reversed torsion and thick cylinder fatigue tests are identical when plotted on a Von Mises equivalent stress basis.

From Von Mises criterion yielding occurs when:

$$\bar{\sigma} = \text{constant}$$

where $\bar{\sigma}$, the equivalent stress, is given by:

$$\bar{\sigma} = \frac{1}{\sqrt{2}} [(\sigma_1 - \sigma_2)^2 + (\sigma_2 - \sigma_3)^2 + (\sigma_3 - \sigma_1)^2]^{\frac{1}{2}}$$

where σ_1, σ_2 and σ_3 are the principal stresses. Therefore, the fatigue limit of a thick-walled cylinder can be predicted from uniaxial fatigue data provided that the basis of equivalent stress is used to relate the differing stress systems. As justification for this approach, the author cites evidence that in all fatigue tests micro regions of plastic behaviour occur. Hence, the fatigue limit of a material is a threshold stress range level, below which micro yielding does not occur.

From continuum mechanics, Tomkins further derived a crack growth law for the thick cylinder configuration.

For a crack growing in a stage I regime, i.e. propagating on a plane of maximum shear stress, as does occur in the initial stages of crack growth in ductile materials:

$$\frac{da}{dN} = C_1 \gamma^+ (\tau^+)^2 a \qquad (2.14)$$

where γ^+ = shear strain prevailing

τ^+ = shear stress prevailing

a = crack length

and C_1 = material constant

Crack growth in this regime is therefore nominally unaffected by pressure acting in the crack.

Fluid pressure can enter the crack when:

$$\tau > 0$$

but its only effect is to increase the normal stress acting across the plane of maximum shear stress from σ_n to a value of $(\sigma_n + p)$.

Using a similar argument to that employed to derive equation (2.14), Tomkins considers the propagation of a stage II crack. In this instance, the propagation is normal stress dependent and hence hoop stress controlled. Therefore:

$$\frac{da}{dN} = C_2 \gamma^+ (\sigma^+)^2 a \qquad (2.15)$$

where σ^+ = normal stress prevailing

γ^+ = shear strain prevailing

a = crack length

and C_2 = material constant $\neq C_1$

Then, since pressure can enter the crack and exert pressure on its flanks when $\sigma_\theta > -p$, the driving stress for crack growth becomes $(\sigma_\theta^+ + p)$. Now, it is obvious that from Lamé equations:

$$\sigma_\theta + p = \frac{2p\,K^2}{K^2 - 1} \quad , \qquad \text{where } K = \text{diameter ratio}$$

$$= 2\tau_r$$

hence:
$$\frac{da}{dN} = C_2\,\gamma^+\,(2\tau^+)^2$$

This model for crack propagation in thick cylinders has attractions in that it separates the initial stage of crack propagation which is nominally shear stress range controlled from the normal stress range controlled propagation. It is, however, at variance with more conventional crack growth laws in that the influence of the second stress is included in both parts of the model. Secondly, although the effect of pressure acting in the crack is included, the effect of the stress/strain gradient in the cylinder wall is ignored. This may not be significant in that the influence of bore stresses dominates behaviour for the greater proportion of the total endurance.

More recently, Frost & Sharples (1978) have provided a simple fracture mechanics analysis to explain the shear stress range fatigue failure criterion in thick cylinders.

If cracks are assumed to be a consequence of initial defects in a material, as seems to be the case for wrought materials, then the fatigue strength of a thick-walled cylinder should be a function of the transverse fatigue properties of that material. Using this premise, the authors relate the mode I K_{th} for a material to its plain specimen transverse fatigue limit through:

$$\Delta K_{th} = \lambda\,\sigma_t\,(\pi\,a_o)^{\frac{1}{2}} \qquad (2.16)$$

where σ_t is the repeated tension fatigue limit, and a_o is some characteristic length term related to initial defect size. The term λ is included to account for defect shape characterisation. Then, if internal pressure can be assumed to act in the crack, the effective driving force for crack extension is given by:

$$\sigma = p + \frac{p\,(K^2+1)}{K^2-1} = \frac{2\,p\,K^2}{K^2-1} \qquad (2.17)$$

therefore: $\sigma = 2\tau$

hence: $$\Delta K_{th} = \frac{2\,\lambda\,p\,K^2}{K^2-1}\,(\pi\,a_o)^{\frac{1}{2}} \qquad (2.18)$$

If, as seems reasonable, the shape of a defect in a transverse fatigue specimen is comparable with that in a thick-walled cylinder, equation (2.17) may be substituted in equation (2.18), giving:

$$\sigma_t = \frac{2\,p\,K^2}{K^2-1}$$

Now, $(p\,K^2/K^2-1)$ is the bore shear stress in a thick-walled cylinder at the fatigue limit, denoted σ_{bs}, whence:

$$\sigma_t = 2\sigma_{bs}$$

Therefore, for a given material, the bore shear stress criterion for cylinders of differing diameter ratio would appear to be a natural consequence of a fracture mechanics analysis.

Various data in the literature attributable to Morrison, Crossland & Parry and Haslam are reanalysed according to this criterion and the fit is shown to be excellent.

2.5.1 (a) Fatigue of Thick Cylinders Subjected to Repeated Internal Pressure About a Mean Pressure

The influence of mean pressure has received little attention experimentally in spite of its importance in practical engineering situations. Almost certainly, the explanation for this lies in the extreme difficulty and cost in carrying out systematic internal pressure fatigue tests to long lives with varying mean pressures.

Burns & Parry (1967) have published the most comprehensive paper on this aspect of thick-walled cylinder fatigue behaviour. The effect of mean shear stress was investigated experimentally by constructing a number of compound cylinders with a known degree of interference and hence radial pre-stress of the inner component. These cylinders were designed to give a mean shear stress at the bore of either +60 MPa or zero at design pressure. Tested under repeated internal pressure (i.e. $P_{min} = 0$), the results of this series of tests using both EN25 and 0.15% C steel inner components showed the benefits of decreased mean stress.

A further series of tests was carried out by the same authors on monoblock cylinders of EN25 steel. By varying the minimum pressure in the cycle, cylinders of diameter ratio 1.4 and 2.0 were tested with an associated mean shear stress of 230, 280, 305 MPa and 230 MPa, respectively.

For a given endurance (10^6 to 10^7 cycles), it was concluded that the fatigue strength of thick-walled cylinders is primarily dependent on the maximum range of shear stress, together with the associated mean stress. The safe range of shear stress was found to decrease with increasing mean stress, as illustrated in Figure 5.2. The severity of the decrease in allowable shear stress range with increasing mean stress is most noticeable when compared with mean stress tests on the same steel carried out in direct stress or torsion. A further interesting feature

is the apparent minimum in allowable range of shear stress at high mean shear stress. The possible reason for the occurrence of this apparent minimum is given by Burns & Parry as the onset of cyclic strain softening or yielding.

In a thesis concerning fatigue of thick cylinders subjected to internal and external pressure, Kendall (1972) re-analysed much existing fatigue data for EN25 steel at endurances of between 10^5 and 10^6 cycles. This author attempted to show the effect of various stress parameters on the allowable range of shear stress for a given endurance. In particular, the variation of shear stress range with the following:

i) Maximum hoop stress
ii) Maximum normal stress on the plane of maximum range of shear stress
iii) Mean shear stress on the plane of maximum range of shear stress

Kendall found little correlation between the results of thick cylinder tests and direct stress or torsional fatigue tests on more conventional specimens using the above stress parameters. However, specimens of EN25 steel were tested as open-ended cylinders with fluctuating internal pressure and static external pressure in an attempt to further elucidate which were the most important stress conditions in determining fatigue endurance. Most of these tests were carried out with an approximately constant value of maximum direct stress. The conclusions reached by this author are that there is a non-linear relationship between direct stress and fatigue strength. Fatigue strength increasing as direct stress decreases. Further, Kendall finds that the influence of

mean shear stress on the plane of maximum range of shear stress is much less important in its effect that direct stress.

A further reference to the effect of mean stress is found in the work of Rogan (1975), who tested thick cylinders of 0.13% C 13.0% Cr stainless steel. By varying the minimum pressure in a repeated pressure test, this material was tested at various mean shear stress levels in cylinders of diameter ratios varying from 1.8 to 2.6. The effect of mean shear stress was investigated for cylinders in the "as-received", pressure tested (single application of pressure just sufficient to cause bore yielding) and autofrettaged.

At an endurance limit of 10^6 cycles, the effect of mean shear stress was least noticeable for the "as-received" material and increasingly more noticeable for pressure tested and autofrettaged cylinders. In all three cases, the effect of increasing mean shear stress was to decrease the safe or allowable shear stress range at the bore of the cylinder. The reason cited for the weak effect of mean shear stress on "as-received" cylinders was the low ratio of yield to ultimate tensile strength of this particular material condition. Rogan assumes that cyclic strain hardening occurs sufficient to offset the weakening effect of high mean stress.

This same reason is given by Burns & Parry (1967) to explain the apparent minima in their high mean stress tests.

Haslam (1972) has published some details of tests carried out on cylinders of mild steel at high mean pressure. Using cylinders of diameter ratio 1.025, he finds that the effect of tensile mean stress as expressed by the Gerber parabolic law models the behaviour of cylinders subjected to a mean stress, providing the local effective hoop stress is given by the empirical expression:

$$\sigma_\theta = P\left(\frac{D^2+1}{D^2-1} + \frac{5}{D+1}\right)$$

where σ_θ = local effective hoop stress at the bore of the cylinder

D = diameter ratio

The results of the tests undertaken by Haslam do not, however, seem very consistent when viewed in the light of more conventional fatigue tests at mean stress. For high mean fluctuating pressure tests, it is found that the results lie outside the Gerber parabola constructed from repeated axial fatigue and burst test results. More conventional mean stress tests from uniaxial fatigue tend to lie on or slightly under the Gerber parabola. Further, the choice of mild steel as an experimental material is perhaps unfortunate, especially as it does not approach the normal low alloy steel behaviour.

2.5.2 Fatigue Strength of Other Thick-Walled Configurations

Most of the available literature on the fatigue strength of thick-walled cylinders has concentrated on the plain cylinder configuration. However, there is another situation of real practical importance - that of the side hole or cross-bored cylinder. This is not readily amenable to a fracture mechanics analysis because of the lack of suitable stress intensity factor calibrations. Several workers have considered this problem from the elastic stress concentration point of view.

Fessler & Lewin (1956) measured the stress state at the intersection of two thick cylinders by a photoelastic technique. The theory developed gave good agreement with experimental results, except at the peak values. The theoretical elastic stress concentration factor, defined as peak stress/Lamé hoop stress in the bore of the main cylinder, gave a value of 3.7 which was 32% greater than the measured value of 2.8.

Little (1965) has offered a listing of the theoretically derived stress concentration factors for thick cylinders with various geometries of intersection. The values he gives agree well with the maximum tensile hoop stress and maximum shear stress elastic stress concentration factors derived from other simple analyses (Morrison, Crossland & Parry (1959)).

Morrison, Crossland & Parry (1959) have reported results on a series of fatigue tests on cylinders with cross-holes. From these, the strength reduction factor at the fatigue limit was found to be 2.1, whereas a theoretical shear stress concentration factor of 2.5 was found.

Two papers by Gerdeen (1972) and Gerdeen & Smith (1972) show that the geometry of the intersection of a cross-hole with a cylinder is critical in determining the elastic stress concentration factor. He shows that the effect of the shear stress, σ_{rr}, acting on the intersection

is to reduce the stress concentration factor. Previous workers have neglected shear stress effects. By a superimposition technique, Gerdeen predicts that the minimum stress concentration will be offered by an intersection of equal diameter cylinders with an intersection radius of between 0.3 and 0.4 of the main diameter. In the second paper, an experimental investigation using model cylinders of resin was used to check the predictions of the former theoretical paper. By varying the ratio of main bore to side bore diameters and the radius of intersection, Gerdeen found his theoretical predictions to be accurate.

In a paper by Körner (1974), a summary of the existing work on cross-hole cylinders is given and an attempt is made to predict the fatigue strength of a cross-hole cylinder from a knowledge of the elastic stress concentration and uniaxial fatigue properties of the material. The lack of agreement he finds leads him to conclude that there is no substitute for full size or model tests.

2.5.3 Stress Intensity Factors for Thick-Walled Cylinders

The rigorous derivation of stress intensity factors has one limitation in that the state of stress at a crack tip is regarded as being determined solely by the applied stress normal to the plane of the crack (see Figure 2.2). This denies the effect of any stress parallel to the plane of the crack in being determined in a fracture process. For brittle or quasi-brittle materials, this assumption is justified by experiment if monotonic fracture is considered. However, when subcritical crack growth mechanisms are operative, as in the fatigue process, this assumption may not be justified.

In considering the thick-walled cylinder geometry, it is thought that under fatigue conditions cracks nucleate at the bore of the

material under the action of repeated shear stress and grow in a longitudinal radial plane. Therefore, crack growth is occurring on a plane normal to the direction of maximum principal stress. Hence, any stress intensity factor solution for a thick-walled cylinder must be of the form:

$$K_1 = f(\sigma_\theta)\, g(c)$$

Because of the curvature and doubly connected nature of a thick-walled cylinder, the exact solution of stress intensity factors for part-through cracks is not possible. No suitable stress functions can be derived which satisfy all the boundary conditions implicit in the geometry.

The simplest procedure appears to be to search the literature for a solution to a geometry which most closely resembles that of a thick-walled cylinder and to modify that solution. This is the technique that has been used by most of the workers to date.

Tiffany & Masters (1965) and Tiffany, Lorenz & Hall (1966) have assumed that Irwin's solution for a plate containing a crack and subjected to a gross stress, σ, could be used to describe a part-through crack in a thick-walled cylinder.

Irwin's (1962) original expression is given by:

$$K_1 = \frac{1.095\, \sigma \sqrt{\pi\, c}}{\left\{\Phi^2 - 0.212\, (\sigma^2/\sigma_{ys}{}^2)\right\}^{\frac{1}{2}}}$$

but this is more generally written so that:

$$Q = \Phi^2 - 0.212\, \frac{\sigma^2}{\sigma_{ys}{}^2}$$

where Q is termed the shape factor and is a correction for crack shape

which can be evaluated from tables. Therefore:

$$K_1 = \frac{1.095\ \sigma\ \sqrt{\pi\ c}}{Q^{\frac{1}{2}}} \tag{2.19}$$

Substituting σ_θ for σ in equation (2.19) gives:

$$K_1 = \frac{1.1\ \sigma_\theta\ \sqrt{\pi\ c}}{Q^{\frac{1}{2}}} \tag{2.20}$$

Further solutions for a part-through thickness crack in a plate subjected to a gross stress σ are due to Paris (1965), Kobayashi (1965) and Anderson (1970), and reviewed by Orange (1975). These solutions are modifications of Irwin's original expression to account for the effect of plastic zone size in determining crack depth, and including front and back face correction factors. In general, they do not vary by more than 15% and will not be treated in detail for the reason given below.

Although the approach of these authors appears valid, no account is taken of the effect of pressure acting in the crack and thereby augmenting σ_θ.

Bowie (1956) derived a solution for the stress intensity factor at the tip of an infinite notch emanating from a pressurised hole in an infinite plate. Using boundary collocation techniques, he was able to produce a graph of K_1/K_o versus crack depth for values of k ratio up to 2.5 (Figure 2.3).

One interesting point with this analysis is that, as $a \to 0$:

$$K_1 \to 1.1\ \sigma\ \sqrt{\pi\ c} \tag{2.21}$$

i.e. the solution for a crack in a semi-infinite plate.

A solution arrived at independently by Shannon (1970) and Underwood, Laselle, Scanlon & Hussain (1970) consists of taking the semi-infinite plate solution and superimposing the solution for a pressurised notch in a half-space due to Bueckner (1960), thus:

$$K_1 = 1.12\ \sigma_\theta \sqrt{\pi c} + 1.13\ p \sqrt{\pi c} \qquad (2.22)$$

Underwood (1972) found that this gave good agreement with an experimentally determined compliance K calibration at crack depths of up to 0.6 (c/W).

Converting σ_θ from the semi-infinite plate part of equation (2.22) into terms of pressure gives:

$$\sigma_\theta = p \left[\frac{(r_2/r)^2 + 1}{D^2 - 1} \right] \qquad (2.23)$$

where $r = r_i + c$, and hence equation (2.22) can be rewritten as:

$$K = 3.06\ p \sqrt{\pi c} \qquad (2.24)$$

This expression simulates both tangential stress due to pressure and the direct effect of pressure acting in the crack or notch. Whilst it was originally developed for long straight fronted cracks, insertion of a shape factor yields an expression which the author deems applicable to the furthest front of a semi-elliptical crack set in the wall of a thick-walled cylinder.

Goldthorpe (1973) has derived a stress intensity calibration for a long straight fronted crack by assuming that as the crack depth approaches zero, the stress intensity factor tends to that for an infinite plate. Hence:

$$K_I = 1.12\ \sigma\ \sqrt{\pi\ c} \tag{2.25}$$

Then, from the fracture mechanics point of view, the effect of pressure, p, acting in the cylinder can be represented by a cylinder subjected to an external tension of $-p$. Thus, since:

$$\sigma_{id} = \frac{2k^2}{k^2 - 1}\ p \tag{2.26}$$

where σ is the stress at the inside diameter of a cylinder subjected to an external pressure of $-p$.

We have from equations (2.25) and (2.26):

$$K_I = 2.24\ p\ \left(\frac{k^2}{k^2 - 1}\right)\ \sqrt{\pi\ c} \tag{2.27}$$

which can be rewritten as:

$$K_I = 1.12\ (\sigma_\theta + p)\ \sqrt{\pi\ c}$$

where σ_θ is the hoop tension at the inside diameter of a cylinder subjected to an internal pressure, p.

The author then uses this expression to extend the expressions derived by the authors previously cited to small crack depths.

When this approach is adopted and compared graphically, it can be seen that there is little discrepancy between the expressions of Underwood, Shannon and Bowie for values of c/W in the range:

$$0.1 < c/W < 0.75$$

It would seem reasonable therefore that the stress intensity factor for long straight fronted cracks should converge to a discrete value at small crack depths. Indeed, this value is implicit in Bowie's analysis and has previously been mentioned.

A further point of interest arises from Goldthorpe's work and has also been considered by Crymble, Goldthorpe & Austin (1975). In a thick cylinder subjected to fatigue loading, it is generally assumed that only one crack can propagate to a signficant size. Whilst this is generally true, a situation can arise, especially in a high strain, low cyclic life component, where multiple cracks are initiated. The presence of a multiplicity of cracks will obviously disturb the stress field in the component. Comparison with other multiple crack configurations (Bowie (1956), Kutter (1970)) suggests that the stress intensity factor will decrease and this was found to be the case for a pressurised thick-walled cylinder. However, it was shown by Kutter (1970) that two equal depth diametrically opposed cracks cause a substantial increase in stress intensity relative to that for the single crack case.

Therefore, when considering the likely behaviour of a thick-walled cylinder subjected to internal pressure, it is necessary to know with some certainty the number of cracks in the cylinder if a fracture mechanics approach is to be adopted.

All of the expressions considered have been derived for long straight fronted cracks typical of those emanating from rifling in mortar barrels. In this situation, the geometry of the components is such that the point of highest stress intensity is also the point of deepest crack penetration.

In plain cylinders, fatigue cracks are generally semi-elliptic in shape since they are nucleated and grow from what is essentially a

point source. Recent work by Tan (1978), using three-dimensional finite element codes and the boundary integral equation (BIE) method, indicate that the point of highest stress intensity is not at the point of deepest penetration but at a point on the crack periphery at some small angle to the free surface (Figure 2.5). For the case of a semi-elliptic crack set in the wall of a thick cylinder, the implication is that if fast fracture is a possibility, it may equally well occur in a longitudinal direction rather than in the assumed radial direction. Rogan (1975) has noted this type of behaviour in thick cylinders of cold reduced, hot reduced and cold drawn materials after full penetration of the wall thickness by a semi-elliptic crack.

Therefore, the modification of existing stress intensity factor expressions for thick-walled cylinders with long straight fronted cracks by the use of existing shape factors to define the semi-elliptic crack problem is suspect.

2.5.4 Stress Intensity Factors for Semi-Elliptic Cracks in Thick-Walled Cylinders

Only one analytical stress intensity factor expression was found in the literature, due to Throop (1970). This author considers the stress intensity factor for a semi-elliptic crack in a thick-walled cylinder to be the sum of two calibration functions, such that:

$$K = (Y_p + Y_a)\, S\, b^{\frac{1}{2}}$$

where b = crack depth

S = maximum tangential stress at the bore of the cylinder

and where Y_p is a calibration function due to the effect of pressure acting in the crack given by:

$$Y_p = 0.625 \frac{R_i (w-1)}{(b/2a)^{\frac{1}{2}}} \left(\frac{w^2-1}{w^2+1}\right) \left(\frac{b}{B}\right)^3 m$$

and Y_a is a calibration function to take account of the tangential stress gradient in the wall thickness:

$$Y_a = \left(\frac{3.77}{\Phi^2}\right)^{\frac{1}{2}} \left(\frac{1}{w^2+1}\right) \left(1 + \frac{w^2}{[1+(b/B)(w-1)]^2}\right)$$

In these expressions, R_i is the inside radius of the cylinder, w is the ratio of internal to external diameter, b is the crack depth at the point of deepest penetration of the wall thickness, B. The factor m is a measure of the efficiency with which the pressurising medium penetrates and exerts forces within the crack. Φ is the elliptic integral function of the crack depth, b, and the half crack length, a, given by:

$$\Phi = \int_0^{\pi/2} \left[1 - \frac{a^2-b^2}{a^2} \sin^2 \phi\right]^{\frac{1}{2}} d\phi$$

On detailed examination of the derivation of this expression, two facts become obvious. The factor m in the expression for Y_p is taken as 0.5 to satisfy experimental results rather than physical reality. This term had been introduced to characterise the efficiency with which fluid pressure enters the crack and exerts additional forces. It is difficult to see why in the monotonic loading situation, the effect of pressure acting in the crack should not be wholly additive to the remotely applied forces.

Secondly, the expression for Y_p is linearly dependent on R_i

the inside radius of the cylinder. This implies a size effect, albeit quite small, which has not been found to be the case for either monotonic or fatigue loading of thick-walled cylinders. Therefore, although this formulation gives realistic numerical values of stress intensity factor for semi-elliptic cracks, it should be treated conservatively until further analytical corroboration is available.

Two further stress intensity factor calibrations for semi-elliptic cracks in pressurised cylinders exist in the literature, but both have been derived empirically for cylinders of finite dimensions or range of dimensions. The extension of these expressions to cylinders of differing diameter ratios outside the ranges covered should be treated cautiously.

By means of a semi-empirical approach, Haslam (1969) has derived a stress intensity factor for a thick-walled cylinder containing a semi-elliptic defect. He considers that the stress intensity factor can be adequately represented by:

$$K_1 = \sigma \sqrt{\pi c}$$

where σ is equated to a modified hoop stress, σ_{eff}, to take account of pressure acting in the crack such that:

$$\sigma_{eff} = P \left(\frac{D^2 + 1}{k^2 - 1} + \frac{5}{k + 1}\right)$$

whence:

$$K = \sigma_{eff} \sqrt{\pi c}$$

No justification is given for the additional factor $5/k+1$ other than the fact that it approximates the behaviour of cylinders of diameter ratios up

to 3. Haslam further shows that his expression agrees almost exactly with that of Underwood (1972) for diameter ratios from 1.2 to 4. The agreement is difficult to understand since Underwood's expression is for a straight fronted crack, whereas that of Haslam's is intended for semi-elliptic crack profiles. It can be seen quite readily that the stress intensity factor at the point of deepest penetration of a semi-elliptic crack will be less than that for a straight fronted crack because of the constraint from surrounding material in the former.

Mishioka & Hirawaka (1975) have experimentally determined a stress intensity factor calibration for a particular geometry and wall diameter ratio. Their experimental technique involved measuring crack growth rates through the wall of a thick-walled cylinder and determining the 'equivalent K' from tests carried out on a more tractable geometry. Their results agree closely with the shape factor modified expression due to Underwood (1972) (Figure 2.6). However, the use of such a technique does assume that pressure acts fully on the flanks of the crack and that this effect is independent of wall diameter ratio.

Since all stress intensity factors for thick-walled cylinders should include the effect of pressure acting in the crack as well as the stress gradient acting through the wall of finite dimensions, the separation of these effects should prove a useful means of analysing the applicability of the existing solutions.

2.6 THE INFLUENCE OF MICROSTRUCTURE ON FRACTURE AND FATIGUE

2.6.1 Fatigue

Most early researchers (Thompson & Wadsworth (1958), Gough (1933), Forsyth (1957)), from whose observations the theory of fatigue failure has been developed, used specimens of pure face or body centred

cubic metals. When testing specimens of pure iron, copper or aluminium, it was observed that the fatigue crack appeared to initiate at the free surface from persistent slip bands in suitably oriented grains. The appearance of narrow, persistent slip bands on the surface of a metal subjected to a repeated stress was correctly distributed to reversed slip occurring in the metal grains. Fatigue cracks were observed to grow from such slip bands and in cases to propagate completely through the specimen.

Whilst this behaviour is essentially the basis for fatigue crack formation in pure metals, the extension of this idea of initiation phenomenon to realistic engineering alloys is not simple. In components of high strength steel or aluminium, fatigue failure can invariably be shown to have originated at a geometric discontinuity. This is not unreasonable since any geometric discontinuity in a structure offers a source of stress concentration. Therefore, when the cause of failure in machine parts of complex geometry is investigated, sudden section changes (Dorey & Smedley (1956), Gregor (1960)), air holes or other similar macro discontinuities are found to be the preferred site for fatigue crack initiation.

If, however, fatigue tests are carried out on plain, well polished components of high strength materials, a different preferred initiation site is frequently encountered. Fatigue crack initiation sites can then usually be traced to inclusions or internal defects which intersect or lie slightly below the surface of the component. The importance of inclusions and other micro discontinuities in promoting fatigue crack initiation has been realised for some 25 years, but quantitative work on the subject is scarce.

With the realisation that inclusions, in particular, can act as stress concentrators to a sufficient degree to decrease fatigue life

and endurance limit, the reason for gross anisotropy in fatigue properties became clearer. Ransom (1954) undertook a series of experiments to compare the fatigue strength of commercially available SAE 4340 steels (0.4% C, 1.8% Ni, 0.85% Cr, low alloy steel) with those of an essentially inclusion-free steel of the same composition. By carrying out bending and torsional fatigue tests on specimens cur from different axes of steel billets, he was able to show that for commercial steels:

(a) Fatigue cracks initiated at elongated inclusions when the direction of forging was normal to the direction of stressing.
(b) The large variation in fatigue endurance limits for specimens stressed normal and parallel to the direction of forging was due to the presence of elongated inclusions.

The comparison of the results obtained using specimens of commercially available steels with those from specimens of the vacuum melted 'inclusion-free' steel showed the advantages of low inclusion content steels. For the vacuum melted steel at essentially the same tensile strength level, the fatigue endurance limit was raised and the variation with direction of stressing was largely removed. The fact that the variation in endurance limits between longitudinal and transverse stresses specimens was not completely removed is interesting in that it indicates that inclusions are not the sole cause of fatigue anisotropy. With this 'inclusion-free' steel, it was also observed that fatigue cracks seldom initiated at the few existent inclusions.

A further significant work on the relationship between inc inclusions and fatigue strength of steels was reported by Cummings, Stulen & Schulte (1958). These authors were able to show qualitatively

that the size and distribution of inclusions played a determining rôle in both fatigue crack initiation and propagation. Using 'aircraft quality' SAE 4340 (1.8% Ni, 0.85% Cr, 0.4% C, low alloy steel), heat treated to a tensile strength of 965 MN/m^2, rotating bending fatigue tests were carried out at a constant nominal stress. Over 100 specimens were tested at a single stress level and it was found that in every case failure had initiated from inclusions at or near the free surface. Since the inclusions in this steel were approximately spheroidal, the geometric mean diameter of the exposed cross-section of the inclusions was chosen as their size parameter. By plotting this size parameter versus the life of the individual specimens, it was shown that for single nucleus fatigue fractures, the size of the initiating inclusion was inversely proportional to fatigue life. Further tests were performed on large numbers of specimens at constant stress above and below this initial level. It was observed that for stresses close to the nominal yield stress of the material, cracks were initiated at inclusions of all sizes and linked together often by a shear mechanism to form the final fracture plane. Also, it was noted that the first visible crack was initiated from the largest inclusion. Using an intermediate stress level, cracks were again observed to initiate first at the largest inclusion but often final failure occurred from the linkage of two smaller cracks initiated from inclusions of an average size. At very low stress levels close to the fatigue limit of the material, a single large inclusion predominated and final failure invariably occurred after propagation from a crack initiated at such an inclusion.

The inclusions in this particular electric arc melted steel are given as being of the complex manganese alumino silicate type, which are fairly typical of modern low alloy steels but the existence of other

types, not recognised by the authors, is quite likely. If this was the case, then further information on the relative severity of inclusion type for a given size would have been most useful. However, the importance of this work cannot be under-estimated since it shows qualitatively that the fatigue life and strength of high strength steels depends largely on inclusion size and distribution.

Working in the UK, Frith (1954) has shown that the conclusions of the authors cited previously are essentially correct in that inclusions can provide the initiation site for fatigue cracking. This author has demonstrated that there is little difference between the fatigue properties of steels made by electric arc or normal open hearth melting practices. Using rotating bending specimens, Frith was able to show that, in general, the longitudinal fatigue ratio (i.e. fatigue endurance limit/ultimate tensile strength) decreased with increasing tensile strength level for both types of melting. The work of this author is of particular interest in that he tries to correlate the fatigue properties of his test steels with an assessment of the inclusion numbers through the 'Fox' count. The lack of correlation leads him to assume that a better parameter is needed to describe the severity of inclusions according to their chemical composition as well as size and occurrence. It was noted in this work that inclusions which did not deform on hot working and those non-deformable types surrounded by a manganese sulphide envelope produced cavities in the metal which appeared to be of greatest severity from a stress concentration point of view.

In response to the need for a better means of quantifying inclusion size, shape and spatial distributions, Atkinson (1960) investigated the fatigue properties of very high tensile strength ($\simeq$ 1930 MN/m^2) steels. By assuming that an inclusion can effectively be

regarded as a cavity equivalent to the volume of the inclusion, Atkinson uses the theoretical stress concentration factor associated with such a defect to give a parameter capable of describing the size and shape of inclusions. Examination of metallographic sections parallel to the direction of applied stress shows a number of inclusions to which a value can be ascribed. These values are then assumed to be additive and a total 'count number' is derived for a specified field size. This means of characterising inclusion distributions was termed a Fairey count. Comparison of the 'Fairey' counting technique with the 'Fox' count for the steels investigated by Atkinson showed there to be a better correlation between fatigue properties and the former means of inclusion assessment, although the evidence is by no means definitive.

During the 1960's, very little useful data was published on the quantitative or qualitative relationships between fatigue strength and inclusion content of steels. However, the increasingly widespread availability of scanning electron microscopes and imaging systems in the early 1970's led to a renewed interest in attempting to quantify these relationships.

Thornton (1971) has published a review paper on the influence of non-metallic inclusions on mechanical properties of steels containing a section devoted entirely to fatigue properties. It is apparent from his discussion of the literature up to 1970 that the original manual methods of inclusion population estimation were being superseded by automatic counting methods. The use of the Quantimet (Quantitative Television Microscopy) instrument has enabled hitherto untried correlation parameters to be tested quickly and cheaply. It is perhaps unfortunate that the early promise of this instrument has not been fulfilled. Comparison of inclusion counts made manually with those from the Quantimet

have shown the automatic system to be suspect (Hauser & Wells (1970)). Instead of reducing the operator error found in the manual counting techniques, the Quantimet has been shown to be more susceptible to human error in programming the machine.

Conversely, the scanning and conventional transmission electron microscopes have enabled considerable advances to be made. Most attention has been focused on the effect of inclusions on fatigue crack propagation.

Hauser & Wells (1970) compared the mechanical properties of SAE4340 steels melted by different methods. Their material in the form of 0.067 inch thick sheet was processed from melts produced by:

(a) Electric arc, air atmosphere
(b) A degassed heat
(c) Two vacuum arc remelted heats
(d) A vacuum induction melt
(e) A vacuum induction remelted heat

The effect of these differing melting processes was to provide steels with varying inclusion contents as measured by their respective percentage volume fractions. Although no quantitative evaluation of the influence of inclusions on fatigue properties was offered by these authors, their observations on the relative severity of inclusions in initiating fatigue cracks are important. It was found that alumina/aluminate stringers and globular calcium aluminates were principally responsible for fatigue crack initiation. The steels produced by methods (a) and (b) were found to contain large sulphide particles, but these were never proved to be responsible for crack initiation.

The effect of inclusion content on fatigue crack propagation

rate has been studied by Shih & Araki (1973). Using plain carbon steels in unidirectional bending, these authors showed that the fatigue crack propagation rate was dependent on steel inclusion content, although not to any great degree. The vacuum degassed steel used in their programme which gave the lowest micrographic areal percentage fraction of inclusions appeared to give the same Paris exponent (1963) as air melted and conventionally poured steels, but a different material constant, C_o. Inclusions of the non-deformable type, such as alumina and silicates, were found at the fatigue crack initiation site. It was further observed that these inclusions were generally spherical, and an inclusion at least 20 μm in diameter was necessary to initiate a crack. Whether any significance can be attached to this limiting size of inclusion is debatable, but it is interesting to note that other authors (Stulen, Cummings & Schulte (1956), Cummings, Stulen & Schulte (1958)) quote limiting sizes (Hauser & Wells (1970)).

Thornton (1972) published a thesis specifically on the topic of the influence of inclusions on stage II fatigue crack propagation in a low alloy steel. Using specially prepared charge, eleven tapered plates of nominal AISI 4330 composition were cast. Deoxidation practice was varied for each casting to provide differing inclusion contents. Essentially, three types of inclusion system were generated, although not all were necessarily present in a given cast. Quantitative assessment of the volume fraction of inclusions present was achieved by lineal analysis under a conventional light microscope. Inclusions were identified by both conventional metallographic techniques as well as by electron beam microprobe analysis and energy dispersive X-ray analysis of the fracture surface.

Fatigue crack propagation rates were measured for each cast

using single edge notch plate specimens and analyses of results according to the conventional Paris (1963) law formalism.

From the comparison of different casts, Thornton was able to show that the slowest crack growth rates were associated with the highest volume fraction of inclusions. However, these particular casts were also the ones which, in general, contained spherical well-dispersed inclusions. The casts of steel with irregularly shaped interdendritic inclusions, such as Type II sulphides, showed the highest growth rate but the lower volume fraction of inclusions.

This apparent anomaly can be readily explained by recourse to the work of Baker & Charles (1972), who have shown that Type II sulphides can readily form interdendritic films of lath-like inclusions lying in the prior austenite grain boundaries and providing a low energy fracture path through the matrix.

In his conclusion, Thornton observes that fatigue crack propagation rates are more sensitive to morphology, composition and distribution variations than to total volume fraction of inclusions. He does not mention the fact that his specimens were cut from castings and therefore cannot be considered representative of more normal forged or hot worked engineering components.

Heiser & Hertzberg (1972) have considered the anisotropy of fatigue crack propagation in a hot rolled steel plate. Using the common American notation, as depicted below, the authors measured the fatigue crack propagation rates in a Mn-C steel heat treated to provide four differing microstructures: (i) Pearlite-ferrite (bonded); (ii) Pearlite-ferrite (homogenised); (iii) Martensite-ferrite (bonded); (iv) Martensite-ferrite (homogenised).

The effect of specimen orientation and microstructure on

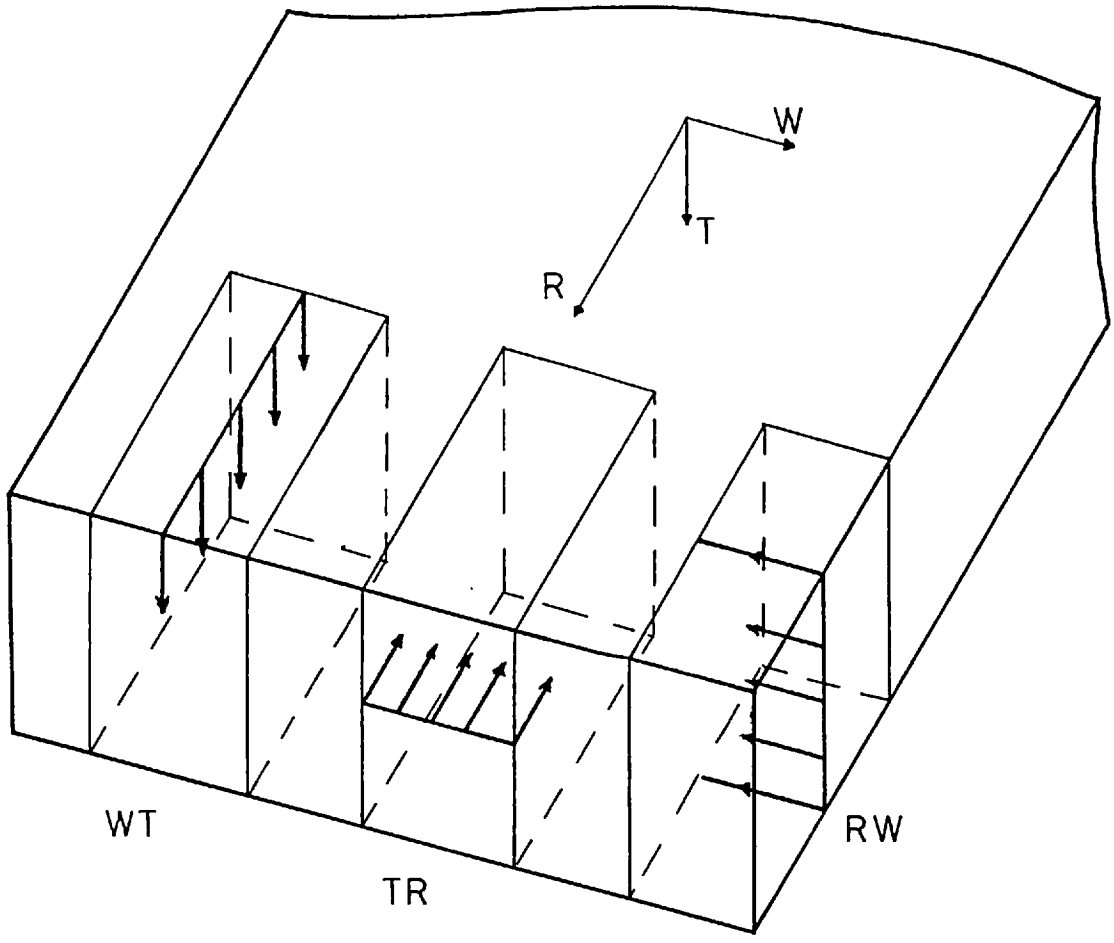

fatigue crack propagation was measured by correlation with the simple Paris (1963) law. It was found that the dependence of crack growth rate on stress intensity range was a function of microstructure and orientation of microstructural constituents relative to the fracture plane. All the martensite microstructures showed a similar ranking in that fatigue crack propagation rate was greatest in the TR orientation, least in the WT, and intermediate in the RW orientation. With the pearlite microstructures, crack growth rate was greatest in the RW orientation, and least in the WT orientation. A further important conclusion was drawn from the work by these authors, namely, that the relative differences in fatigue crack propagation rate increased for higher stress intensities. Attempts to correlate the striation spacing obtained fractographically with the measured crack growth rates showed that the fatigue cracking process is a summation of different mechanisms. The striation spacings measured were shown to be independent of orientation and therefore local fracture at

inclusion/matrix interfaces was considered to be responsible for the measured anisotropic crack growth behaviour. The ease with which such localised fracture processes occur will obviously be a function of the orientation of inclusions or brittle micro-constituents, according to the authors.

No quantitative evaluation of inclusion size, shape or spacing was offered by these authors, so further correlations based on their data are impossible, but their work is of importance in showing qualitatively for the first time that the effect of anisotropy of fatigue crack growth rate increases with increasing stress intensity range.

The reasons for this type of behaviour will be discussed in detail in the discussion of this work.

From the literature reviewed here and in many other publications not cited, it is apparent that inclusions can initiate and contribute to the propagation of fatigue cracks. It is also evident from experimental observation that not all inclusions are injurious in the initiation of fatigue cracks.

The work of Brooksbank & Andrews (1970) is deserving of attention in this respect. These authors postulate that microstresses can develop around inclusions during cooling from the molten state. The intensity of these microstresses varies according to inclusion type (in the compositional sense) and therefore the potency of certain inclusion types in initiating fatigue cracks can be explained.

Using the idea first propounded by Laszlo (1943), these authors show that textural or "tesselated" stresses can arise as a result of differences in thermal contraction between the inclusions and the steel matrix. These microstresses, which are generally referred to as textural or tesselated stresses, are of the general form:

$$\pm \phi \{[\alpha_2 - \alpha_1] T\}$$

where ϕ is a function of the elastic moduli of the matrix and inclusion, and of inclusion size, shape and distribution, α_2 and α_1 are the coefficients of thermal expansion of the matrix and inclusion, respectively, and T is the negative temperature difference. The expression $[\alpha_2 - \alpha_1] T$ is often termed the "strain potential" of an inclusion since it is to some extent a measure of the severity of textural stress that can be generated around an inclusion.

For the types of inclusions where $\alpha_2 < \alpha_1$, tensile stresses will be generated around inclusions and these can, in general, be considered to be deleterious to fatigue properties. Inclusions for which $\alpha_2 > \alpha_1$ will be associated with voids when cooled from the liquid state and are not considered to be as harmful as the former. Indeed, there is some evidence (Hewitt & Murray (1968)) that the voids associated with such inclusions can act as sinks for hydrogen gas evolved during welding processes and are thus positively beneficial.

From this hypothesis, Brooksbank & Andrews have developed generalised equations to predict the stresses associated with various sizes, shapes and varying composition of inclusion. The compilation of these data is very interesting in that the types of inclusions, notably aluminates and aluminas, that are shown to have the greatest strain potential are those most often found at the initiation sites of fatigue cracks. Conversely, the sulphides show least strain potential and are seldom, if ever, implicated in fatigue crack initiation. A situation which frequently arises in low alloy steels is that of duplex inclusions. Typically, oxide inclusions which may be spherical or fragmentary are

found surrounded by envelopes of manganese or calcium sulphide. Analysis of this situation from a textural stress aspect shows that the sulphide envelope considerably reduces the strain potential and hence deleterious effect of this type of oxide inclusion. From fatigue tests on ball bearing steels and other high carbon, rolling element, steels, it has been frequently shown that the fatigue limit increases with sulphur content (Lyne & Kasak (1963), Coole (1970)). This apparently anomalous behaviour can be explained in terms of the Brooksbank model for duplex inclusions. Increase of sulphur content in these steels leads to the damaging oxide type inclusions being enveloped in sulphide which reduces their ability to initiate fatigue cracks.

From the foregoing review of the literature, several well-established facts emerge:

(1) Inclusions can initiate fatigue cracks.

This tendency increases with tensile strength of the material, increased fatigue loading, reduced ductility or material cleanliness.

(2) The composition of an inclusion responsible for fatigue crack initiation is more important than its absolute size or shape.

(3) Improvements in material fracture toughness do not necessarily increase fatigue endurance.

In the majority of cases, only one inclusion is responsible for fatigue crack initiation and therefore a steel containing very few large

well-dispersed inclusions may show good fracture toughness but poor fatigue crack initiation resistance.

(4) The reduction of total volume fraction of inclusions will increase fatigue crack propagation resistance only when the size of particles is reduced simulataneously with increased inter-particle spacing.

CHAPTER 3

EXPERIMENTAL PROCEDURES

3.1 AIMS OF PROJECT

The aims of this work have been previously outlined in Chapter 1. In the following sections, these aims are restated in greater detail. The materials used are briefly described as are the experimental methods adopted.

The major aim of this work was to test the hypothesis that the current generation of steels used in pressure vessel fabrication are more isotropic and hence have a greater fatigue resistance than steels produced previously. In particular, the fatigue limit in thick cylinders as a function of composition and orientation is studied. Crack propagation rates in air are measured and related to the shape of fatigue cracks generated in the thick cylinder geometry. As a result of the investigation undertaken, a more realistic fatigue failure criterion is suggested. This criterion is based on the influence of micro-structural discontinuities inherent in all engineering materials.

3.2 EXPERIMENTAL PROGRAMME

3.2.1 Notched Fatigue Strength of Thick Cylinders

Since it may be postulated that material cleanliness or, more correctly, homogeneity will have a discernible influence on the fatigue endurance and fatigue limit of a steel subjected to a repeated internal fluid pressure, the first part of this work involved testing this hypothesis.

Several forgings of high strength, low alloy steel were obtained at approximately equal tensile strength levels. The forgings

were then machined to provide small test cylinders of known orientation relative to the major axes of the original forging. Cross-holes were drilled through the wall of each cylinder so as to intersect the main bore normally and the intersection was carefully and reproduceably radiused using a specially developed tool.

These specimens were then tested under various stress regimes in the autofrettaged and non-autofrettaged condition using fluctuating internal pressure generated by reciprocating a ram in an enclosed volume of hydraulic oil.

The comparison of these results enabled the influence of material inhomogeneity on notched fatigue strength to be established. No attempt was made to monitor the crack growth rate in this configuration of specimen.

3.2.2 Plain Cylinder Fatigue Strength

A batch of 40 specimens was produced from a single bar of 3¼ Ni,Cr case hardening steel (formerly EN36B BS970) in the form of plain cylinders. These specimens were tested to failure using repeated internal oil pressure and techniques were developed for initiating cracks from predetermined point defects and measuring the crack growth rate.

Two further block forgings were then obtained of similar composition and mechanical strength, but having widely differing inclusion contents. These blocks were cut and machined to provide thick-walled cylinder specimens of known orientations. The plain cylinder fatigue strength was ascertained for both blocks and measurements of fatigue crack growth rate made for various specimen orientations.

A comparison of the fatigue crack growth rates for the various orientations within and between each block forging indicates the influence

of inclusion type, size and spatial distribution.

The estimation of the plain cylinder fatigue limit for each orientation further enables an alternative fatigue failure criterion for internally pressurised thick-walled cylinders to be suggested.

3.2.3 Fatigue Tests in Air

To evaluate the difference in crack propagation occurring in an air environment compared to that under a pressurised oil environment, conventional circular cross-section fatigue specimens were prepared. Approximately twenty specimens were prepared from each of the three axes of the two forgings showing the large inclusion content disparity. These specimens were tested in repeated tension and examined fractographically to determine the mode of failure, initiation site and preferred crack path.

A minimum of two specimens from each direction in both forgings were also tested to determine the fatigue crack growth rate of the material for a given plane of crack propagation.

3.2.4 Plane Strain Fracture Toughness Tests

Conventional fracture toughness specimens were also prepared from the forging with highest volume fraction of inclusions in an attempt to predict the mode of failure of thick cylinders of this material containing cracks.

Analysis of these results, assuming linear elastic fracture mechanics to be applicable, showed that the mode of failure of such cylinders should be stable irrespective of the direction of crack propagation.

However, it has been noted by the author and two independent

workers in this field that thick cylinders of nominally "fail-safe" material and dimension have failed in an unstable manner when subjected to repeated internal pressure fatigue loading. Therefore, a further series of fatigue tests was performed utilising thick cylinders of the steel forging of lowest fracture toughness to try to reproduce and explain this phenomenon.

3.2.5 Further Internal Pressure Fatigue Tests

The phenomenon of unstable fracture of thick-walled cylinders subjected to internal pressurisation by hydraulic fluid has not been widely publicised, but one feature is common to all reports. Namely, that fracture may have occurred in an unstable manner when fluid pressure is absent from the flanks of the crack. In an attempt to simulate these conditions, liners of a low modulus material were inserted loosely into thick cylinders of the steel forging and subjected to a repeated internal pressure until failure of the steel cylinder occurred. The mode of failure of these cylinders was then investigated fractographically and using more usual metallographic sectioning techniques.

3.3 MATERIALS

3.3.1 Steels

The steels used in this programme of work were all chosen as being typical of low alloy steels from which forged high pressure components are fabricated.

Forged components are invariably specified for high pressure containment applications, since the stress system encountered is always biaxial and often triaxial. Therefore, designers always attempt to specify materials with high transverse strength and ductility. Forging

is generally considered to be the best method of obtaining these characteristics.

3.3.2 Nomenclature for Steels Tested

Throughout the experimental work, the various materials under test were assigned identification letters based on the origin of the material or some physical property. This system will be adhered to in the reporting of this work.

i) Cross-bored cylinders from various forgings:

M : Mitsubishi

J : Japan

Y : Y block

BO : Böhler

OES : Outer end sleeve

ii) Plain cylinders (D = 2) for crack growth rate technique and evaluation:

CH : Case hardening

iii) Plain cylinders (D = 3) from forgings of differing inclusion contents:

B : Bad

G : Good

Various suffixes can be added to these designations to indicate a particular condition for testing. The most common is:

A : Autofrettaged

Others are defined as they occur in the text.

3.3.3 Orientation

The convention used to describe the orientation of a particular crack plane and direction of crack growth is a modification of that laid out in ASTM E-399. The system followed is that of a two-letter description referring to the three orthogonal axes of the original forging. In the American system, L, S and T are the normal letters appended to directions, whereas in Europe the letters L, Q and T seem to be commonplace, where:

L = length, longitudinal, rolling direction, extrusion direction, axis of forging

Q ≡ S = thickness, short transverse direction

T = width, long transverse direction

Thus, the first letter of any two-letter designation refers to a plane normal to that direction and the second letter indicates the direction of crack propagation in that plane.

At first sight, this system may appear cumbersome for axisymmetric components, such as thick cylinders, and a system based on the more realistic polar axis would seem more applicable. However, given that the materials tested in this work were in the majority taken from forged blocks, the quantitative description of inclusion size, shape and spacing necessitates an orthogonal system.

3.4 SPECIMEN PREPARATION

(a) Cross-Drilled Cylinders: All the specimens tested in this section were machined from the original forgings to the dimensions shown in Drawing 3.1. The outside diameter and bore of the specimen were fine turned and the ends threaded before cross-drilling. Double opposed cross-holes were jig drilled in each specimen and the cross-holes reamed. Finally, a special tool was placed in the main bore and the driving rod inserted through the cross-hole. The intersection of the cross-hole and main bore was then radiused to the dimensions shown in Drawing 3.1, detail (a).

Specimens from the J, Y, BO, M, OES series were all tested in the "as-received" condition at tensile strength levels indicated in Table 4.3.

(b) Plain Cylinders - Technique Development: These specimens were produced primarily as convenient test cylinders on which the techniques for crack propagation rate measurement could be developed. All the cylinders were machined from bar stock to the dimensions given in Drawing 3.3. No attempt was made to produce a very fine internal surface finish nor to relieve internal stresses set up through the machining process.

(c) Plain Cylinders: Only two forgings were used to carry out this part of the experimental programme. As stated previously, these forgings were of similar composition and tensile strength level but contained radically different inclusion populations. The forging with the larger volume fraction of inclusions was referred to as 'B' and that with the smaller volume fraction as 'G'.

Specimens were prepared by sawing up the original block forgings into square section blanks, great care being taken to ensure that the original

position and orientation of the blank was retained. Cutting plans for fogings B and G are given in Figures 3.1 and 3.2, respectively. The sawn blanks were then rounded and the main bore drilled and finally honed to size. Typical specimen dimensions are given in Drawing 3.4. It had been intended to test these specimens in the "as-received" condition without any further heat treatment, but a stress relieving heat treatment of half an hour at 590°C in a neutral atmosphere was carried out on all specimens to overcome residual stress effects set up by machining or honing. The surface finish obtained is typical of that which can be achieved in practice without vast expense and is estimated as being of the order of 0.3 μm CLA in the longitudinal or axial direction of the cylinders.

(d) Fracture Toughness Specimens: Plane strain fracture toughness tests were only carried out for forging B for the reasons given later. The specimen configuration chosen was that of the compact tension specimen (CTS). Two specimens were machined from each of the principal directions in the forging to the dimensions given in Drawing 3.5 and to the tolerances laid out in ASTM E-399.

(e) Fatigue Crack Growth Specimens: Due to the limited amounts of materials available from the B and G forgings, three different specimen configurations were utilised.

For forging B, both compact tension and "constant K" double cantilever beam specimens machined to the dimensions shown in Table 3.1 were used. With the G forging material, only double cantilever beam type specimens were tested, although the dimensions were varied to utilise the available material most effectively (Table 3.1).

(f) Repeated Tension Specimens: Approximately twenty blanks were cut, having their longitudinal axis aligned with each of the original orthogonal axes of both the G and B forgings. These were then rounded to the dimensions shown in Drawing 3.8. After turning, these specimens were polished longitudinally in a proprietary polishing machine with successively finer grades of emery paper. The final paper used was grade 000. The specimens were then stress-relieved in vacuo for one hour at 590°C, care being taken not to scratch or indent the surface.

Subsequent testing proved a need to test specimens of the same parallel gauge length dimensions in repeated torsion. Specimens were produced by machining the bottom head of untested tension specimens to provide a suitable flat for location (Drawing 3.8). It was not considered necessary to re-stress relieve these specimens since no machining was undertaken on the parallel gauge length.

The surface finish obtained for both the tension and torsion specimens is estimated as being 0.1 μm CLA in the longitudinal direction and 0.4 μm CLA in the circumferential direction over the gauge length.

3.5 EXPERIMENTAL TECHNIQUES

3.5.1 Mechanical Properties of Materials

(a) Tensile tests: Conventional mechanical properties were measured for each of the steels used in this investigation from 6.5 mm diameter Houndsfield specimens. An Instron Universal Testing machine TTDM of 10,000 lbf capacity was used. Crosshead speed was standardised at 0.1 cm/min.

Charpy V-notch impact tests were carried out for each of the six possible specimen orientations in both the B and G forgings. No attempt was made to precrack these specimens to further enhance the severity of the notch as full size fracture toughness tests were envisaged.

(b) Fracture toughness tests: Plane strain fracture toughness tests were carried out according to the procedures laid out in ASTM E-399 for three crack plane orientations in the B forging. Unfortunately, even in the TQ orientation, which showed the lowest value of fracture toughness, testing at 20°C did not produce a result which would meet the criterion for validity associated with this code. The results are, therefore, presented as being indicative of the plane strain fracture toughness for the TQ and QT orientations. Similarly, the LT orientation test was conducted as a J-integral test and the results presented assuming the equivalence of J and the critical strain energy release rate. Fracture toughness was not measured for the G forging since the necessity for such data is dubious and the quantity of material necessary too great.

(c) Hardness measurements: The macro-hardness value for each steel was measured on small coupons approximately $3 \times 3 \times 1$ cm in size. A standard Vickers hardness testing machine was utilised with an indenting load of either 30 kgf or 50 kgf.

(d) Chemical analysis: Several of the steels tested in this work were supplied with the original mill analysis. These were repeated and all the remaining steels chemically analysed using the spark spectrographic method.

Additional analysis for the total oxygen content of steels B and G was carried out by Henry Wiggins Limited of Hereford.

X-ray fluorescence was used to indicate the presence or absence of rare earth elements, such as Ce, Cs, La and Ca, used in the deoxidation of the original melts of steels B and G. Inclusions found in these two steels were further analysed by microprobe analysis and X-ray dispersive analysis (XRDA) in the JEOL 35 scanning electron microscope.

3.5.2 Quantitative Metallography

(a) Specimen preparation: Samples from each of the forgings used in the investigation were prepared by hack-sawing from the bulk and machining to approximately 25 mm cubes, care being taken to ensure that the original orientation was not lost. These specimens were then ground and polished on rotary machines in the following sequence:

(1) Rough grind 180 C silicon carbide paper water lubricant.
(2) Fine grind 600 grade silicon carbide paper water lubricant.
(3) Coarse polish 6 μm diamond paste synthetic lubricant, 'Padamet' disc.
(4) Fine polish 1 μm diamond paste synthetic lubricant, 'Metron' disc.
(5) Final polish ¼ μm diamond paste synthetic lubricant, 'Metron' disc.

Between stages of polishing, each specimen was ultrasonically cleaned in absolute alcohol and dried in a warm air blast.

Synthetic oil-based lubricants are preferred for the final polishing stages since some inclusions are water soluble and hence may be lost.

(b) Estimation of volume fraction of inclusions: In general, all methods of inclusion density measurement may be classified as either manual or automatic.

Manual methods are preferred but are extremely tedious and prone to operator bias. Conversely, automatic or semi-automatic methods relying on image analysis are very quick and simple to perform but are subject to large errors arising from machine sensitivity calibration and specimen preparation. To minimise the errors associated with either method, both manual and automatic measurements were carried out.

(c) Manual technique: All manual or, more correctly, visual techniques for estimation of such quantities as volume fraction of inclusions rely on making measurements in two dimensions which are then transformed to give a parameter valid for three dimensions. In any multi-phase system, it may be shown that certain stereological relationships exist which allow information derived from a plane to be extended to the volume of the material. Therefore, by estimating the areal fraction of inclusions on a random plane of polish, the volume fraction of inclusions may be deduced. Similarly, stereological relationships exist which allow inter-inclusion spacing to be predicted from a knowledge of volume fraction and size distribution of inclusions.

Specimens approximately 5 cm^2 in area were cut from each of

the steels used in the investigation and prepared by grinding and polishing using the techniques previously outlined. For the steels B and G, planes of polish were prepared such that all the possible combinations of orthogonal axes were included, i.e. LT, LQ and QT planes.

(d) Volume fraction measurements: The areal fraction of inclusions was determined using a point counting technique. The image obtained from the unetched plane of polish using reflected light was brought into focus on the projection screen of the microscope (Vickers M41 Photoplan) at a magnification of ×570. A 6 cm × 6 cm scribed grid was then superimposed on the image. Any point which lies over an inclusion is counted as one 'hit' and points lying on the matrix inclusion interface are counted as one half. By careful selection of the magnification used and interviewing sufficient fields, it can be shown that the areal fraction is given by:

$$A_L = \frac{H}{N_f \times P}$$

where A_L = areal fraction

H = number of 'hits'

N_f = number of fields viewed

P = total number of test points

Then, since: $A_L = V_v$

where V_v is the volume fraction, irrespective of the size distribution of inclusions, the volume fraction may be calculated. The accuracy of such a technique is strongly dependent on the number of fields examined. According to Dehoff (1968), the accuracy of the result may be estimated

from the expression:

$$P_T = \left[\frac{200\ \sigma(P_p)}{(\%\ acc)\ P_p}\right]^2$$

where P_T = total number of points required to achieve the desired accuracy

P_p = point fraction, i.e. number of points per test point

σ = standard deviation

(e) Automatic image analysis for volume fraction of inclusions: A Quantimet 720 image analysing microscope was used to perform a check on the results obtained manually. The principles of operation of such instruments have been amply described elsewhere, hence it is deemed sufficient to describe only the basic mode of operation.

The polished specimen is examined in the reflected light mode under a conventional metallurgical microscope having the usual range of objectives. Contrast between the polished matrix and the inclusions present occurts as a result of their relative reflectivities. Beam splitters are provided in the body of the microscope such that the image can be passed to a video camera and simultaneously displayed on a monitor screen. The displayed image is then interrogated by a line scan on the monitor screen. When a line length of differing reflectivity is traversed, an electrical signal is generated whose amplitude is proportional to the difference in reflectivity. Simultaneously, a separate signal is generated as a square wave of length of which is proportional to the distance traversed across this region. By processing this information electrically, the total lengths and intensities of contrast regions can be summed both for the individual regions of each field and for successive fields.

The data thus generated is processed through a micro-computer such that any parameter for which exact or approximate stereological relationships exist can be deduced via the appropriate software.

In principle, this type of instrument would appear to have great potential but, in practice, it has severe limitations. These limitations are discussed in Chapter 5.

(f) Size and length distribution of inclusions: All comparisons of size and length distributions of inclusions were carried out visually under the Photoplan microscope. Steels M, J, Y, BO and OES were not examined quantitatively for inclusion size and shape. The major effort in this respect was confined to steels B and G since the orientation of the inclusion population could be more easily related to the starting volume with these steels.

A 1 cm graticule subdivided into one hundred units was inserted into the IOX eyepiece of the binocular viewing head. This was calibrated against a stage graticule of 1 mm subdivided into one hundred units for each of the available objectives. The resolution in measuring features on a polished plane with this system is considered to be of the order of 0.5 μm (×40 objective).

For the steels B and G, a minimum of 100 fields were examined on each of the three orthogonal planes. Every inclusion that could be resolved in the particular field was sized for length and diameter. Simultaneously, the inclusion was classified according to composition judged from morphology and colour. The significance of this classification is discussed later.

3.6 REPEATED INTERNAL PRESSURE FATIGUE TESTS

3.6.1 Description of Bristol Machine

The basic fatigue machine described here was originally developed in the Engineering Department of Bristol University by Professors Morrison and Crossland in conjunction with Dr J. Parry. Whilst the principle of operation and construction details of this machine have been amply detailed by the originators (Morrison, Crossland & Parry (1956)), several modifications have been incorporated in this version of the machine.

Following development during the last ten years, the Bristol fatigue machine used for this research work is currently capable of sustained operation with repeated pressure ranges of 0 to 450 MPa at frequencies from 4 to 8 Hz.

A ram is reciprocated through a gland by a double crank arrangement and generates fluid pressure by displacement of a fixed volume of oil. Figure 3.9 shows the double crank arrangement and crosshead to which the guiding plunger is attached. The ram is fixed to this plunger with a collar nut which allows transverse flexibility to ensure good alignment in the gland.

The range of pressure generated above the gland assembly is obviously a function of the displaced volume of oil and its compressibility characteristics. Since the latter cannot be caried, the pressure range is regulated by increasing or decreasing the stroke of the ram. This is effected by varying the phase relationship of the two crankshafts controlling the motion of the crosshead. Input power for the machine is derived from a DC electric motor and V belt drive to one end of the layshaft which is set transversely across the crankcase. At the inboard end of the layshaft, a long pinion gear engages both crankshaft gears.

The stroke of the ram may be altered in discrete intervals by disengaging this gear from one crankshaft gear and rotating this crankshaft with the second at rest.

In operation, this system of pressure generation provides a virtually sinusoidal pressure (time wave form) with the minimum of trouble. Obviously, leakage does occur past the gland seal (Drawing 3.9), but this can be compensated for by a "make up" oil system. Photograph 3.4 shows a typical arrangement of flanges and cone ring joints by which a specimen is mounted above the gland housing. The non-return valve mounted at the top of the stack is provided with approximately 5 bars oil pressure such that if, at bottom dead centre or thereabouts, the pressure in the system falls below this value, the valve opens and admits oil to make up for any leakage.

(a) Machine control system: Speed control and starting of the machine is achieved by having a Variac feeding the DC rectifier bridge which supplies the electric motor. Voltage to the Variac is taken from one line of three phase supply via a contactor with an electrically energised "hold-in" coil. All emergency and normal interlock functions are triggered through relays which are connected serially with this "hold-in" coil. Theoretically, this system provides speed control in the range from 0 to 500 rpm. In practice, the machine must be running at a minimum of 300 rpm to fully utilise the inertia of the flywheel system.

A further drive is taken from one crankshaft end via a chain and sprocket to an auxiliary layshaft which drives the oil pump for the machine and cycle counter.

Failure of a fatigue specimen is detected automatically through the "make up" oil system previously referred to. On starting a test, the

machine speed is gradually increased to the value desired. The ½ hp gear pump supplying the "make up" oil is then started and a valve above the check valve opened to admit oil to the enclosed volume. After the oil has warmed up and dissolved the entrapped air, the stroke is adjusted to the range of pressure required. At this juncture, a needle valve in the line between the gear pump and check valve is gradually closed until the flow is seen to be throttling. This is indicated by a pressure drop in the contact manometer upstream of the needle valve. The valve is then opened slightly to restore the original pressure reading and the set point in the contact manometer brought up to within 5% of the value indicated. Since the leakage rate of the seal remains essentially constant and the frequency of cycling is high, the pressure in the make up oil line appears constant. When specimen failure occurs, however, the check valve opens to admit more oil over a greater proportion of the cycle. The throttled pressure line cannot meet the demand so that the pressure in the line drops sharply. This causes the contact manometer to complete an electrical circuit which reverses the polarity of a relay. Continuity is broken to the "hold in" coil of the main contactor and therefore both the DC drive motor and AC pump motor stop. Power to all control systems cannot be re-established without switching out this interlock manually.

Further interlocks are provided to stop the machine in the event of electrical overload through overspeed or increased seal friction. Of these, the most efficient is the semi-conductor fuse, rated at 15 A, which protects the rectifier bridge and electric motor from overheating.

(b) Pressure range measurements: Beneath the non-return valve and in series with the specimen is a cylinder which acts as a pressure gauge. Normally constructed from an EN25 type steel, this cylinder is internally

nitrided and then strain gauged externally with a half bridge arrangement of two active tangential 120 ohm gauges. Before commencing to test fatigue specimens and intermittently during testing, the output from this half bridge is calibrated statically against a secondary pressure standard using the same instrumentation. The pressure gauge is energised with a high frequency carrier wave from a Peekel (Model 540 DNH) amplifier. The signal is demodulated and fed to the Y plates of a Telequipment (S61 Model) oscilloscope. An in-phase constant level signal is also extracted from the amplifier and connected to the X plates of the oscilloscope to produce a "Lissajous type" figure. By means of external capacitative and resistive balance, this figure can be artificially nulled against the horizontal graticule of the oscilloscope screen. This provides a means of measuring the signal intensity both statically during calibration and dynamically during operation. Attributed to Roberts (1952), this means of measuring fatigue load is estimated to be accurate to within ±1%.

3.6.2 Double Cross Bore Specimens

All the specimens tested under the repeated internal pressure regime were connected to the Bristol machine as shown in Photograph 3.4 through a system of flanges and cone ring joints.

In the case of cross-bored specimens, provision had also to be made to seal the cross bores without introducing undue extraneous forces. This was achieved by having a mild steel ring of slightly larger internal diameter than the specimen with two radial threaded holes diametrically opposed. The intersections of the cross bores with the outside surface were chamfered at 60^{o} and hardened ball bearings placed over these bores. The mild steel ring was then brought into position and the ball bearings seated firmly by back-up Allen screws. A moderate torque ($\simeq$ 7 Nm) was

more than sufficient to provide a perfect seal with the minimum of force due to the small contact land between ball and specimen.

At the outset of every test, a note of specimen number, time, machine speed and all other relevant parameters was taken. Due to the energy absorbed in compressing and decompressing the pressurising medium, in this case a medium viscosity hydraulic oil, the temperature of the oil and specimen rises. This leads to an increase in the effective compressibility of the oil and hence a decrease in the range of pressure generated. Therefore, it was essential during the first 2-3 hours of any test to constantly monitor the range of pressure and increase it when necessary. Specimen failure, as previously described, automatically causes the machine to stop such that the number of cycles endured can be calculated from the cycle counter.

The range of pressure selected for the first test of any particular material was deliberately kept high to ensure failure. From the result of this first test, further pressure ranges were selected to ensure maximum economy in the use of specimens in arriving at the fatigue limit pressure range. In the testing of all the repeated internal pressure specimens, both plain and cross-bored, the range of pressure endured without failure for greater than 2×10^6 cycles is arbitrarily defined as the fatigue limit. The justification for and errors introduced by this assumption are discussed in Section 5.7.1.

3.6.3 Plain Cylinder Tests (Diameter Ratio = 2)

The purpose of testing these cylinders under repeated internal pressure was to develop techniques for initiating and monitoring crack growth.

For reasons to be discussed later, it was decided to attempt

to initiate cracks from a "point" source of the smallest possible size at the inner surface of the cylinder. Since these cylinders are relatively compact (Drawing 3.3), introducing a reproducible defect mechanically appeared impossible. The solution of this problem was therefore attempted using a modified spark erosion technique, albeit of a primitive nature.

(a) Introduction of point defects in cylinders: A Unitek (Model 1039B) power supply was obtained. This unit had originally been intended for use in spot welding by the capacitance discharge resistance heating method. Energy output from a bank of capacitors is variable from zero to 15 watt seconds in two discrete ranges.

The power supply is connected as in Photograph 3.1 to a specially fabricated specimen holder. An adjustable height arm containing a replaceable tungsten electrode is inserted in the bore of the cylinder until the electrode is approximately half way along the cylinder length. The arm is then lowered until the electrode rests lightly on the inner diameter of the cylinder. Single phase 220 V AC suitably rectified is used to charge the capacitor bank in the power supply. An external switch is then closed which causes a solenoid operated relay to discharge the capacitor bank to ground via the specimen.

Due to the profile of the electrode and the high resistance path between it and the specimen surface, a very high current flows, locally melting the steel surface under the electrode. A crater-like defect is produced approximately 1 mm in diameter.

From preliminary trials with longitudinally sectioned specimens, it was observed that the maximum available energy produced the most consistent defects. Further, it was noted that the most reliable indication of a successful discharge was a loud crack. Therefore, all

defects introduced were produced using the maximum available energy and repeating the discharge until the loud crack was heard.

The specimen holder has a further function to perform in that for the purposes of crack growth rate monitoring, it is necessary to know the location of the induced defect with respect to the outside surface. A scribe point was therefore inset in a bushing in the base of the specimen holder. This pointer can be raised vertically to meet the tungsten electrode in a vertical plane. After a defect has been produced and with the specimen still in position, the pointer is raised to produce a mark on the outside surface of the cylinder, giving the radial direction from the defect to the outside surface.

(b) Crack growth monitoring technique: By virtue of the small size of cylinders chosen for this and the larger diameter ratio tests, the wall thickness available for crack growth is small. The technique adopted for crack depth sensing must therefore show good resolution. To this end, and for reasons discussed at a later stage, it was decided that a strain sensing device might give the best results.

A simple two-dimensional finite element study of an internally pressurised circular ring containing a radial crack was carried out. Obviously, the crack modelled in this study can only be straight fronted, but the results obtained should be indicative of the behaviour of the response of the body with a semi-elliptic crack. From the study, it was apparent that the range of strain at a point on the external diameter of the ring in the plane of the crack would vary sensibly with crack depth. It was also evident that the strain at points removed only a few degrees circumferentially was substantially different for the same internal loading. The system adopted must therefore approach as closely as

possible to the concept of measuring or sensing strain at a point.

Various mechanical strain indicating, and clip-on type, devices were considered but rejected because of either poor reduction, susceptibility to external vibration or thermal effects. The ideal system should be capable of resolving small changes in strain range, be impervious to mechanical shock, vibration, and temperature change. It must also be easily interfaced to recording equipment in what is arguably a noisy environment, electrically and mechanically. Further, the method used should be cheap and give readily reproducible results.

The method adopted was to use a single electrical resistance strain gauge per specimen. This method of dynamic strain range measurements fulfils most of the requirements cited with the exception of thermal drift. However, it was considered that this problem was not too great.

(c) Choice of strain gauge and bonding agent: From a review of manufacturers' catalogues and price lists, it was apparent that a suitable gauge could be obtained at reasonable cost. Various problems were forseen which dictated the type of gauge used. Primarily, the strain gauge selected must be of the smallest possible gauge length to avoid fatigue failure in the high strain gradients expected tangential to the crack plane. Conversely, the gauge must have a large resistance to enable large excitation voltages to be used. Finally, it would be preferable if the gauge grid were encapsulated to avoid damage during specimen mounting.

The major compromise necessary revolves around the gauge length and resistance. Eventually, a TML FLA-X-350-11 strain gauge of 350 ohms nominal resistance was chosen. This strain gauge is obtainable in both 3 mm and 6 mm gauge length versions and is of Cu/Ni foil encapsulated in a

transparent epoxide backing with integral leads. At the dynamic strain range expected for the greater part of each gauges life, the fatigue life quoted is in excess of 10^7 cycles. Further, this gauge was obtainable with self-compensating temperature characteristics compatible with low alloy steel, albeit not over an extensive temperature range.

Having selected this strain gauge, it was decided by reason of experience to use a cyanoacrylate type adhesive. This type of adhesive has many advantages in that it is cheap, requires no special curing procedures and is easy to use. The commonly quoted disadvantage of poor long-term performance is a function of relative humidity. In this particular application, testing was expected to be of limited duration (1 to 3 days) and the choice of cyanoacrylate is felt to be perfectly justifiable.

(d) Strain gauge instrumentation: The choice of suitable instrumentation for strain gauge energisation and signal processing is dictated by the speed of fatigue loading capability of the Bristol machine. This machine is only capable of imposing loading frequencies of between 4 and 8 Hz without considerable modification. Therefore, the output from the strain gauge bonded to the test cylinder will be of this frequency. It is necessary to process this very low frequency AC signal to provide a measure of the strain range being experienced by the strain gauge.

Manufacturers of commercial strain gauge equipment were approached with the problem but no suitable equipment was available. Carrier wave systems are unsuitable because of the low frequency of the signal. Similarly, DC amplifier systems are not suitable because the signal frequency is too high. Therefore, it was decided to build a system capable of providing a DC signal proportional to the dynamic strain range.

The bridge configuration adopted was a half bridge comprising the active gauge and a fixed resistor as a ballast. A high precision wire wound "Rhopoint" resistor with a very low thermal resistance coefficient was used in this position. Setting this resistance at 350 ohms makes the overall circuit resistance 700 ohms, enabling 10 V DC to be used as energisation. The active strain gauge therefore draws ≈ 15 mA at 5 V which is not excessive, 25 mA being considered the maximum allowable. Signal output from the strain gauge under fatigue loading consists of a constant 5 V with a superimposed ±5 millivolts at 5 Hz. This signal is processed through the circuitry shown schematically in Figure 3.3. The first stage is the removal of the DC voltage component through a filter designed to pass only frequencies of greater than 0.5 Hz. The remaining AC voltage component then goes through two stages of amplification before rectification by a diode bridge network. At this stage, the signal produced reverts to being a DC voltage proportional to the dynamic strain range. The signal is then further amplified before being passed to the recording and visual display equipment.

The complete circuitry, including the simple constant voltage bridge energiser, are shown in Figures 3.4 and 3.5. Two complete amplifier systems were built since two fatigue machines were available for testing cylinders.

(e) Display and data recording: From the outset, it was intended to measure crack growth rates in thick cylinders over the entire range which can occur in high cycle fatigue. A preliminary calculation based on Paris' law with assumed material constants and stress intensity factor calibration indicated that tests could last up to 16 hours. Automatic data recording equipment was therefore considered necessary.

Multi-channel scanning data acquisition systems are readily available and compatible with low voltage DC signals but were well beyond the budget of this work.

As two fatigue machines were available, it was necessary to design a system capable of giving a hard copy and visual display from two separate inputs. Previously, the author had carried out a study of fatigue crack initiation in thick cylinders as part of an attempted validation of Miner's law using the strain gauge technique referred to above. In this instance, the dynamic strain range was recorded continuously by means of an Ultraviolet Light Oscillograph recorder. Whilst this system is nominally attractive, the necessary ultraviolet light-sensitive paper is very expensive for long term testing. Further, no means was ever successfully developed to drive or pull the light-sensitive paper at more economical rates. This system was therefore ruled out for this application. The use of a conventional pen recorder with a motorised roll chart was precluded for similar reasons.

The system adopted comprised a digital voltmeter (DVM) with a $3\frac{1}{2}$ digit display for each amplifier channel coupled to a single 12 digit printer. It was known from the finite element study and practical tests that the range of strain at a point on the free surface of a cylinder being internally fatigue loaded at first declines and then increases with increasing crack depth. (This behaviour is only observed when strain measurements are taken at a point on the free surface lying in the extended crack plane.)

In order to accurately measure and record this behaviour, it was intended that the signal to the DVM be amplified to ≈ 100 millivolts at the outset. The DVM selected has a 199,9 millivolt range so that the signal can drop to zero or increase to a maximum of 199,9 millivolts with

a theoretical resolution of 1 part in 1999. This type of DVM (Weston Model 1230-274910) has the further advantage of having a parallel binary coded digital (BCD) output socket. The printer selected (Electron Systems Limited ES6) was directly compatible with this BCD signal. An interface comprising an EL7410 and SN7404N was constructed enabling the output from each DVM to be sampled and passed to the printer in a four digit format. The printer was further modified to accept an external BCD level signal as a print command. A 230 V, 50 Hz driven timer mechanism was provided with mechanical latches to make and break a pair of contacts once every five minutes. Using the spare BCD level voltage capacity from one DVM, these contacts were energised so that on opening and closing the printer was activated. Since the print command signal is received on opening and closing of contacts, this period was adjusted to exactly 20 seconds. In effect, therefore, the current signal level at the DVM is sampled every five minutes and again some 20 seconds later.

After much aggravation with the amplifier system stability, both channels were built into a cabinet to provide electrical screening necessary in the noisy electrical environment. The final display and recording system appears as in Photograph 3.2. The third DVM apparent was interfaced to the printer as a reserve but was never seriously utilised.

3.6.4 Specimen Testing Programme (Diameter Ratio = 2) CH Steel

This series of tests was started by the testing of plain cylinders under repeated internal pressure without any induced defects. To ensure that failure occurred in the parallel gauge length (Drawing 3.3) of the specimens, the bore at either end was heavily polished for some 25 mm. Connection of the specimen to the fatigue testing machine and the

procedures for testing were the same as for the double-cross specimens. The fatigue limit was again arbitrarily defined as the pressure range endured to 2×10^6 cycles of repeated internal pressure.

Once this limit had been established, a series of tests was carried out with cylinders having induced defects. Using the technique previously outlined, cylinders were prepared with spark discharge defects. Strain gauges were applied over the supposed defect and connected to the system described.

From the outset, it was found that a successful defect initiated crack was a matter of chance with these cylinders since the bore finish was not sufficiently good. However, as sufficient specimens were available and the success rate was greater than 50%, no corrective action was taken.

It was desired to establish a calibration curve of crack depth versus strain gauge output since the two-dimensional finite element model was known to be inaccurate. Therefore, approximately ten cylinders were subjected to repeated internal pressure fatigue loading and the test stopped after a certain amount of crack growth. The specimens were removed from the machine and cut open to reveal the fatigue crack. In all cases, the depth and aspect ratio of the fatigue crack was measuring using a ×30 binocular head mounted on a slideway (Prior Limited). From these readings, a graph of crack depth in the radial direction versus normalised tangential hoop strain change was constructed.

The production of this calibration curve enabled several tests to be carried out in which a crack was initiated from a defect and allowed to propagate through the complete wall thickness. Analysis of the strain range recorded as a function of time enabled a crack growth rate versus range of stress intensity graph to be plotted. These graphs, plotted

according to the well-known Paris (1963) law formalism, proved to give sensible results in terms of the exponent and material constant. Although no direct comparison with these values as obtained in more conventional tests was possible, the reproducibility was good. Therefore, no further development of the technique was undertaken and the next stage of specimen testing was commenced.

3.6.5 Specimen Testing Programme (Diameter Ratio = 3) B and G Steels

Cylindrical specimens from both forgings were tested according to the same procedures and are therefore treated as one.

All specimens were tested in the same manner as the cross-drilled and CH specimens, i.e. under a repeated pressure regime. The first series of tests was undertaken to establish the repeated pressure fatigue limit for the various orientations of specimen axis. Initially, one specimen was tested at a high range of pressure (≈ 330 MPa) to ensure fatigue failure. Dependent on the endurance at this range of pressure, the following test was carried out with a proportionately reduced range of pressure. This procedure was intended to enable the fatigue limit to be found with the fewest specimens used in the mortal region. Whilst being relatively successful for steel G, the fatigue anisotropy inherent in steel B was so marked that no benefit was incurred by the adoption of this procedure.

It will be readily appreciated that there are six primary crack plane orientations based on the three orthogonal axes, namely, LT, TL, QT, TQ, LQ and QL. For each fatigue failure, the crack plane was noted and classified either as a primary plane, intermediate, e.g. LT/TL, or as being close to a primary plane, e.g. cl. LT.

In all the orientations of fatigue crack encountered, the

aspect ratio and/or profile was accurately determined using the binocular measuring head and slideway described.

3.7 FATIGUE TESTS IN AIR

(a) Fatigue Crack Growth Rate - Steels B and G: The fatigue crack growth rate in laboratory air for steel B was measured in three of the six possible configurations of crack plane and growth direction. Initially, testing was started using a "constant K" (Drawing 3.7) type double cantilever specimen configuration. A Dowty Rotol Limited servo-hydraulic machine (Type 300-328009) of 12,000 lbf dynamic capacity was used to provide the fatigue loading. A binocular head with cross-wires inset in one eyepiece (×30 magnification) mounted on a slideway, actuated by a lead screw, was used to monitor crack length.

From the outset of the test, the compliance of the specimen was measured by manually increasing the load applied to the specimen in increments up to approximately 70% of the dynamic load and noting the deflection of the actuator indicated by a linear displacement transducer. This servo-hydraulic machine has been modified in that the original thermionic value servo amplifiers have been replaced by modern semi-conductor devices from RDP Howden Limited. Three $4\frac{1}{2}$ digit DVM's are provided to give the maximum, minimum and mean load or displacement. Therefore, the measurement of changing specimen compliance is relatively easy so long as care is taken not to increase the dynamic plastic zone size at the crack tip during the quasi-static measurement.

Despite the 50% side grooving provided in this particular configuration of specimen, it was soon found that the growing fatigue crack would not stay in plane for all specimens other than the QL and TL. This meant that the crack was moving into thicker section material,

completely invalidating the test. To overcome this problem, the specimen was merely reversed by cutting off the reduced section and providing two new loading pin holes at the opposite end of the specimen (Drawing 3.7). Whilst not particularly aesthetic, this configuration of specimen proved to have a good range of stress intensity variation with crack length. No further trouble with cracks running out-of-plane was experienced.

After precracking of the specimen at a relatively high mean load, the loading range was reduced such that the range of stress intensity varied from approximately zero to 20 $MN/m^{3/2}$ (i.e. R = 0.05). The test proper was then started, crack length was measured at ≈ 1 mm intervals and the compliance of the specimen tested. With increasing crack length, the range of stress intensity increased sufficiently not to necessitate further increases in loading range. A frequency of loading of 20 Hz was used to precrack and start the crack growth rate test. As the specimen compliance increases, the deflection at the loading shackles increases, and it was found necessary to reduce the loading frequency to reduce the loading frequency to ensure constant load range.

To check the validity of the results obtained using this "reversed constant K" specimen configuration, the test series was repeated using compact tension specimens (CTS), 1.75 inches thick, originally intended for K_{Ic} determination. The testing procedure was exactly as outlined above, except that a larger load cell had to be utilised in the servo-hydraulic machine since the section of these specimens necessitates much higher load ranges.

Fatigue crack growth rates in air for steel G were measured in the same fashion, excepting that a micro-processor controlled hydraulic machine was used for some tests. A Mayes 250,000 Newton capacity servo-hydraulic machine was used for all the tests on steel G (Model No.

ESH 250B, Serial No. 367-D-77). This machine is identical in mode of operation to the Dowty previously referred to, but is more flexible and is thought to provide more reproducible results. The applied force is measured through a strain gauged load cell of Class 1A accuracy. Displacement of the loading train is measured from actuator movement by a built-in LVDT.

All crack growth rate specimens of steel G were of the double cantilever beam (DCB) type, but of varying absolute size (see Table 3.1 and Drawing 3.6). Whilst this use of non-standard size specimens is obviously open to criticism since it introduces greater errors, the adoption of differing dimensions was necessary to fully utilise the available material.

The crack growth rate specimens were all pre-cracked at high mean load and then tested at low stress ratio, with the minimum load in the fatigue cycle being approximately zero, giving $R \simeq 0.05$. Crack length was always monitored visually with the equipment previously described, although in some later tests an AC potential drop system due to Klintworth (1977) was used.

For all crack growth rate tests on both steels, conventional pin and shackle arrangements were used in conjunction with a single universal joint in the loading train. The use of only one universal joint in the loading train is not thought to have any negative influence on the accuracy of loading or axiality of the load since no asymmetric crack growth was observed.

(b) Repeated Tension Tests - Steels B and G: Specimens prepared from each axis of both forgings (B and G) were tested in repeated tension fatigue in the Mayes servo-hydraulic machine. The fatigue specimens

(Drawing 3.8) were connected into the loading train by the use of a split collet system at either end (Photograph 3.3). This system was used in preference to threaded end specimens since it reduced the amount of machining necessary and was amenable to copy turning for specimen production. The split collets were produced from a good quality low alloy steel which was hardened and tempered to approximately 260 Hv. Although great care was taken to ensure that the seat radius of the collets was square to the reacting face, it was thought desirable to use a low yield strength such that localised deformation could occur. Therefore, before fatigue testing of these specimens was started, the collet grip arrangement was utilised to tensile test one specimen from each axis of both forgings. No measurable deformation was observed, but it is thought that this procedure enhances the likelihood of true axiality of fatigue loading.

All the specimens tested were subjected to a nominally zero to maximum sinusoidal load cycle. It was found that the minimum load in the cycle had to be kept slightly tensile since the machine operates in a closed loop load control system. Unlike the crack growth rate tests where a true zero load could be obtained if desired, the collet arrangement provides no resistance to compressive load and catastrophic failure will and did occur when a zero load condition was reached.

The only special precaution found necessary during testing was to ensure that the load range did not shift about the mean load. Since the purpose of these tests was to establish a fatigue limit in repeated tension, specimens were set up and then left to fatigue under automatic servo loop load control. The machine is equipped with load trips which could be set in conjunction with the specimen stiffness control to stop the machine without the two ends of specimens coming into contact after

failure. This is essential since it was desired to investigate the fracture surfaces to establish the origin of failure.

As a result of the relatively small gauge length and high stiffness of the specimens, it was found that a cycling rate of 20 Hertz could be achieved even when crack propagating was occurring. Only in the last few crack propagation cycles did the compliance of the cracked specimen influence the applied load range.

A few specimens were also tested in repeated tension fatigue in an attempt to measure the fatigue crack growth rate at a very early stage in the crack development process. The technique used is basically that developed by Lankford (1977).

After final polishing of the selected specimen, the gauge length is further electro-polished and then examined microscopically to establish the likely site of crack initiation - usually at the longest inclusion lying normal to the specimen axis. This inclusion and the surrounding area are then replicated with cellulose acetate tape and a positive metal replica made for scanning electron microscope examination. The specimen is then inserted in the testing machine and subjected to repeated fatigue loading for a given number of cycles and then the replication process repeated. Under the scanning electron microscope, the amount of crack growth may be measured and recorded. The process is then further repeated until the incipient crack becomes of "engineering size" and can be monitored visually in the testing machine.

Whilst giving valuable information as to the behaviour of cracks at very short crack lengths, the process was found to be extremely tedious and not suited to this particular specimen configuration. The reasons for this are discussed further in a later chapter.

(c) Repeated Torsion Tests - Steels B and G: Specimens of both Steels B and G to the dimensions shown in Drawing 3.9 were tested under torsional fatigue conditions. Two Schenck (Type 3/MP) constant displacement machines of nominally 60 Nm capacity were used. These machines are of the variable eccentric crank type, the applied load being measured through a torque bar. The operation and procedures for using this machine have been previously described by the author (Crofton (1972)). In essence, a constant angular displacement is provided at one end of the specimen, which is connected in series with a torque bar. By measuring the twist induced at the specimen/torque bar grip, the applied moment can be calculated. The torque bar is also equipped with an arrangement which permits the application of a static moment independent on the dynamic displacement.

Tests were carried out in both repeated torsion and fully reversed torsion. From previous fatigue tests on specimens of similar dimensions, it is known that the loading cycle is essentially sinusoidal and that no problems of hysterical heating occur with the maximum testing frequency available, namely, 50 Hertz. Therefore, this cyclic frequency was used for all tests.

This series of tests was performed to establish the fatigue limit in shear of both steels in order to compare this value with the limiting bore shear stress range obtained from the thick cylinders tested. Therefore, because of limited time and specimens, no attempt was made to obtain data in the mortal region of the fatigue curve. A preliminary estimate of the expected fatigue limit in reversed torsion was made and specimens tested at slightly above this level of stressing. Where failure occurred, the range of shear stress was reduced for the next specimen and, conversely, increased if failure did not occur.

It may well be argued that a constant deflection machine of this type can significantly affect the results obtained in the mortal region of a fatigue strength versus number of cycles to failure plot. Once a crack has initiated, the compliance of a specimen of the dimensions used in this work alters considerably. It was noted frequently that the machine would cut out automatically if the trip system was set too close, but this invariably indicated eventual failure. In some instances, this was many hundreds of thousands of cycles later. However, since the mortal region is not used in the correlations developed, this effect can be safely ignored.

CHAPTER 4

RESULTS OF EXPERIMENTAL PROGRAMME

4.1 MATERIALS - CHEMICAL ANALYSIS

All the steels used in the course of this work were analysed for conventional element content by spark spectrography. Steels B and G were further investigated for rare earth element content and oxygen in order to try to establish the de-oxidation practice used in their production. The results of these analyses, relative errors in analysis and source of the analysis are shown in Tables 4.1 and 4.2.

4.2 MECHANICAL AND PHYSICAL PROPERTIES

Tensile test data for all of the steels used in this investigation were derived from 6.3 mm diameter Hounsfield specimens. These results, together with hardness values, are shown in Table 4.3. Fracture toughness values and Charpy impact values from room temperature tests are given in Table 4.4.

4.3 QUANTITATIVE METALLOGRAPHY

All of the steels used, except CH, were subjected to conventional microscopic examination in order to determine volume fraction of inclusions. Several of these steels were also subjected to automatic inclusion content assessment techniques to derive the same parameter. These results are shown in the form of histograms of relative frequency of occurrence versus feature size. In the case of the Quantimet inclusion content assessment, all inclusions are counted irrespective of their nature. The size distribution of inclusions generated by the automatic counting and scanning assessment is given in the form of equivalent circle

diameters, i.e. irrespective of the actual shape of an inclusion intersected on the plane of polish, the surface area is assessed numerically and converted to the appropriate circle diameter.

In the visual technique, all inclusions were assessed optically and the results are given in the form of histograms of relative frequency of occurrence versus equivalent circle diameter. These results are given for the steels assessed automatically in Figures 4.1 to 4.7 and visually in Figure 4.8. Other parameters amenable to automatic assessment, such as volume fraction, mean inclusion spacing, mean inclusion diameter and number of inclusions per square millimetre, are given for the steels investigated in Table 4.5. Also shown in this table are the comparable quantities as assessed visually under the conventional light microscope.

As a result of analysis of these results, and in order to qualify the effect of inclusions in the fatigue process, further parameters were measured visually. These results are presented in the discussion.

4.4 QUALITATIVE METALLOGRAPHY

In addition to deriving quantitative information about the inclusion populations in each of the steels used in this investigation, it is also desirable to know the composition of these inclusions.

For the steels J, Y, M, BO, OES and CH, the chemical composition of the inclusion population was estimated by visual assessment. The shape, size and colour of an inclusion under a conventional light microscope enables a reasonably accurate deduction to be made about its chemical composition. Etching techniques are available to differentiate between the less common inclusion types but these were not utilised.

Initially, the total inclusion population was considered and all the major inclusion types noted for each steel. These results are given in

Table 4.6. The inclusions were then classified as being "hard" or "soft", and the relative proportion of each classification based on area was estimated. Table 4.7 shows the results of this classification for all the steels mentioned, except CH, B and G. The significance and basis for this classification is discussed in the following chapter.

(Probably one of the most difficult tasks in qualitative metallography is to select a typical field of a polished steel surface since it is invariably a blank field if it is truly typical. The temptation to present something of interest makes the production of a typical micrograph highly subjective. Bearing this apologia in mind, the micrographs included here give a useful comparison between steels B and G.)

Sections taken from each of the forgings were polished, as previously outlined. Photomicrographs 4.6 and 4.7 are typical unetched fields of steels B and G, respectively, taken at the same magnification. Prior austenite grain size was determined for both steels by deep etching with saturated aqueous solution of picric acid plus a wetting agent. Both steels were found to have an ASTM grain size number of 8, irrespective of orientation. Etched sections (Nital) are shown in Photomicrographs 4.8 (B) and 4.9 (G). Steel B is a tempered martensite containing a lot of inclusions by current standards. Types I and III manganese sulphides were identified, together with some evidence of type II networks in isolated regions. The sulphide stringers were heavily elongated (Photomicrograph 4.10) in the longitudinal direction. From visual observation on a plane of polish containing the L direction of the forging, manganese sulphides of 100 μm length were not uncommon. Normal to the L direction, 10 μm diameter sulphides were observed, but are probably type III. A second, darker grey inclusion of similar morphology to the manganese sulphide was often noted accompanying the primary sulphide.

This is thought to be calcium sulphide or a solid solution complex sulphide. The manganese sulphide was invariably enveloped to some extent by the darker constituent (Photomicrograph 4.11). A third, almost black inclusion type was found, but this invariably occurred in stringers with other complex inclusions (Photomicrograph 4.12). Typical complex inclusions were identified as belonging to the silicate, calcium aluminate and spinel families (probably galaxite). These stringers varied in size from the relatively short and thin (18 μm × 5 μm) to quite sizeable (450 μm × 35 μm), invariably being orientated in the working direction.

Electron probe microanalysis of steel B positively confirmed the presence of complex calcium aluminates with silicates, silica, alumina and mixed manganese sulphide, calcium aluminate inclusions.

In comparison, steel G showed very few inclusions and those found are much smaller. Two types of inclusion were identified. The larger is a two or three phase inclusion, generally consisting of two concentric rings of varying grey colour. The lighter grey (MnS) tends to surround the darker constituent, again tentatively identified as calcium sulphide (Photomicrograph 4.13). Often a third, lighter phase was present at the core of these spherical inclusions (Photomicrograph 4.14). Typical sizes ranged from 5 μm to 15 μm. The second type identified was more irregular in shape but smaller and is thought to be silica. Electron probe analysis confirmed the composition of this second type as being silica. Similarly, the larger spheres were found to have aluminium cores surrounded by manganese, calcium and sulphur. This would seem to verify that this inclusion is either pure alumina surrounded by concentric rings of calcium and manganese sulphides or that a calcium aluminate phase is also present.

4.5 REPEATED INTERNAL PRESSURE FATIGUE TESTS: DOUBLE CROSS-BORE SPECIMENS (D = 3)

The results of repeated internal fatigue tests for double cross-bore specimens of steels J, Y, M, BO and OES are shown in Figure 4.9. The number of specimens tested and the inherent scatter in results means that the curves drawn can only be regarded as tentative at the fatigue limit.

Similar tests at high mean pressure for the same range of steels are shown in Figure 4.10. In this instance, the paucity of results at or near the fatigue limit does not allow differentiation between the various steels. Therefore, with the exception of steel J, a scatter band is drawn to cover all the results obtained at high mean pressure.

After fatigue testing, a representative sample from each steel was cut open to reveal the fracture surface. Typical fracture surfaces for each of the steels tested are shown in Photographs 4.1 to 4.5. No difference in crack profile was noted for tests performed under repeated pressure or high mean pressure fatigue regimes.

Small sections cut from the fracture surface so as to include the cross-bore/main bore intersections were mounted for scanning electron microscope investigation. Although the initiation site could be located fairly easily under the SEM, no consistent evidence was obtained to incriminate second phase particles in the initiation process.

4.6 REPEATED INTERNAL PRESSURE FATIGUE TESTS: PLAIN CYLINDERS (D = 2); STEEL CH

The specimens tested under repeated internal pressure in this section of the research programme were intended largely for technique development. However, sufficient specimens were tested without spark induced point defects to allow a fatigue curve to be constructed (Figure 4.11). The

curve drawn represents a 50% probability of survival at a given pressure range and endurance. Also shown in this figure are the results from specimens of this steel with cracks initiated from spark induced defects.

Approximately twenty-five specimens were also tested with spark induced defects to provide the initiation site and a single tangential strain gauge normal to the expected crack plane at the outside diameter. The object of these tests was to construct a calibration curve of crack depth versus hoop strain range. To this end, the strain range of the specimens was monitored continuously. When a crack had reached the required depth according to the strain gauge output, the test was stopped. The specimen was then cut open to reveal the crack. Crack depth in a radial direction was measured accurately under a travelling microscope. Further measurements of crack shape were also taken to establish the consistency of crack profile as a function of depth.

Although many specimens were treated in this manner, the calibration curve produced contains the results of only thirteen specimens where the crack was symmetrical with respect to the strain gauge placement in both tangential and longitudinal directions. Figure 4.12 gives the calibration curve produced where the strain range as measured normalised by the original strain range is shown as a function of crack depth normalised by wall thickness. Also shown in this figure is the variation of hoop strain range as calculated (Tan (1979)) by boundary integral equation (BIE) methods.

Analysis of the shape of cracks from the smallest obtained to full wall thickness penetration showed them to be perfect semi-ellipses at all stages of crack growth. A plot of normalised crack growth in the radial and axial directions is given in Figure 4.13. This result is of great significance since it allows a much simpler analysis of crack growth rate

to be used than would be the case for constantly changing crack shapes.

4.6.1 Analysis of Crack Growth in Plain Cylinders ($D = 2$); Steel CH

To obtain a sensible relation between crack growth rate and stress intensity factor range, it is necessary to accurately deduce crack depth as a function of applied load cycles. If these data can be produced continuously and require little smoothing, then central point numerical difference techniques can be adopted to derive the crack growth rate differential, db/dN. It is obvious from the description of the techniques used to monitor crack growth (Section 3.6.3(b)-(e)) that strain range versus time was recorded at discrete intervals. Therefore, using the calibration curve (Figure 4.12), a discontinuous plot of crack depth, b, versus number of cycles, N, was produced for each specimen. Because of this equipment limitation, the analysis of crack growth rate was extremely tedious. Numerical difference techniques could not be used and all data had to be plotted by hand and differentiated graphically. Figures 4.14 and 4.15 show typical b versus N curves derived using the calibration curve referred to. It was found by experience that reciprocation of the slope of normals to the curve drawn provided the most reliable method of determining crack growth rate. Although this method of data reduction may be criticised for its subjectiveness, the repeatibility from specimen to specimen was adjudged to be sufficient for further use of the technique.

Initially, it had been intended to use a finite element stress intensity calibration for a straight-fronted crack for the correlation since no function existed for semi-elliptic cracks. During the latter course of this work, a stress intensity calibration due to Tan (1979) was published and all the results shown here are derived using this function. The values of stress intensity as a function of normalised crack depth

computed using the BIE method assumed a semi-minor to semi-major axis ratio of 0.8. Further, the values given by Tan assume full penetration of the pressurising medium into the crack with consequent additional crack face forces.

Figure 4.16 shows a plot of crack growth rate versus stress intensity factor range for the two specimens of Figures 4.14 and 4.15. Both these specimens were subjected to spark defect initiation and cycled under repeated internal pressure until failure occurred.

4.7 REPEATED INTERNAL PRESSURE FATIGUE TESTS: PLAIN CYLINDERS (D = 3); STEELS B AND G

Plain specimens were tested in repeated pressure orientated such that the longitudinal axis of the cylinder was one of the three primary directions of the original block forgings. Both steels B and G were tested in this fashion and fatigue curves drawn to represent 50% probability of survival. Since the primary objective of this phase of the experimental programme was to establish the fatigue limit as a function of orientation, more specimens were dedicated to this region than was strictly necessary.

The results obtained for steel B are shown in Figure 4.17, whilst those for steel G are given in Figure 4.18. A comparison of the repeated pressure fatigue curves generated is given in Figure 4.19.

All specimens which failed were sawn open to reveal the crack profile and the semi-axis ratio measured. Average values of the semi-minor to major axis ratio are plotted in polar fashion in Figures 4.20 to 4.22 and 4.23 as a function of forging orientation for steels B and G, respectively. The same results are given numerically in Table 4.8.

Preferred planes of crack initiation and growth were observed for

cylinders of steel B. No preferred plane of crack initiation was observed for steel G for any specimen orientation, although an insufficient number of specimens were tested for any subtle tendencies to become obvious.

4.8 FATIGUE TESTS IN AIR

4.8.1 Results of Crack Growth Rate Tests in Air for Steels B and G

An attempt was made at the outset of this series of tests to use curve fitting techniques to speed the processing of data. Despite the use of very high order Chebyshev polynomial expressions to fit compliance versus crack length data pairs, the derivatives were found to be highly erratic. Therefore, this technique was abandoned and the derivatives of compliance with crack length and crack length with cycles were determined graphically as for the thick cylinder tests.

Results of crack growth rate versus stress intensity range for various orientations of steel B are given in Figures 4.24 to 4.27. Also shown in Figures 4.25 and 4.27 are the results from periods of crack growth at high mean stress (R = 0.50) for two different crack plane orientations.

Fatigue crack growth rate tests in air were carried out and results (Figures 4.28 to 4.32) processed in identical fashion for steel G with two minor exceptions. In Figure 4.30, the exponents and intercepts cited are given as a range of values for reasons which will be discussed later. Secondly, Figures 4.31 and 4.32 show the results of crack growth rate tests using a micro-processor controlled servo-hydraulic machine to carry out the tests and process the data.

For tests with both steels B and G, the applicability of the data presented is tabulated in Table 4.9.

4.8.2 Repeated Tension Fatigue Tests in Air for Steels B and G

The results of repeated tension fatigue tests are presented in the form of 50% probability of failure curves for steels B and G in Figures 4.33 and 4.34, respectively. Specimen orientation is identified by reference to the longitudinal axis of the specimen.

A comparison of the fatigue curves of steels B and G is given in Figure 4.35 as a function of specimen orientation. All failed specimens from both steels were examined under the scanning electron microscope to determine the initiation point. These results are given in the discussion chapter of this work.

4.8.3 Torsion Fatigue Tests in Air for Steels B and G

Both fully reversed and repeated torsion fatigue tests were carried out for steels B and G. Owing to the limited number of specimens available, the results presented are somewhat speculative. All the specimens tested in torsional fatigue had their longitudinal axis aligned in the L direction of the original forging. Figures 4.36 and 4.37 show estimated fatigue curves for steels B and G in reversed and repeated torsion fatigue, respectively.

CHAPTER 5

DISCUSSION OF RESULTS AND FURTHER RESULTS

5.1 INTRODUCTION

In practical engineering terms, a good intuitive feel for the minimum acceptable properties of a material is second only to correct stress analysis. It is not uncommon for components to be heavily over-specified as the easy alternative to searching for values or conducting tests. Where values are available in the literature, they are all too often not correctly specified. This discussion of results is therefore written in a fashion which, it is hoped, will add to the existing body of knowledge and contribute to a more fundamental understanding of design for high pressure containment.

The discussion is divided arbitrarily into various sections. In the first, the results of repeated internal pressure fatigue on cross-bored cylinders of typical low alloy steels are discussed in the light of material properties.

The second section (5.3) discusses the techniques of crack growth measurement in cylinders of diameter ratio 2. Results obtained using the procedures detailed are shown to be explicable using an LEFM approach.

Fatigue test results from thick cylinders of steels B and G are discussed in the third section (5.4). A more rational repeated pressure fatigue failure criterion is developed and compared with existing theories. The implications of this hypothesis are discussed in a further section (5.5).

Finally, a section (5.6) is devoted to the significance of the results of crack growth rate tests on steels B and G carried out in air.

5.2 CROSS-BORED CYLINDERS

Together with the plain cylinder, the cross-bored cylinder is one of the most widely used high pressure configurations. It is also one of the most troublesome to design for fatigue resistance.

When the available literature is reviewed critically, the scarcity of reliable data for "modern" steels in the form of cross-bored cylinders is obvious. It is further apparent from the work of Crossland & Skelton (1967) that fatigue endurance is a function of the tensile strength of the steel used.

The introduction of new steel-making techniques in the last decade, which the steel manufacturers claim leads to more homogeneous steel, raises the question as to whether steel-making practice has a marked influence on fatigue endurance. If, as seems likely, this is the case, then it is of obvious interest to designers to know whether a more economic use of material can be justified. It is also of particular interest to see if this presumed advantage accrues to both plain and notched components, such as cross-bored cylinders.

From a more basic standpoint, it is essential to our knowledge of the response of materials that the metallurgical factors controlling fatigue strength be further understood.

To this end, a series of tests was undertaken to evaluate the notched fatigue strength of five industrially procurred low alloy steels. It might be argued, and with some justification, that control of source materials is a *sine qua non* of scientific investigation. Whilst model materials such as Armco iron are readily available, it must be said that these materials can never provide the designer with the hard data needed for industrial design. For this reason alone, it was decided to use low alloy steels typical of current large scale industrial practice.

The following parameters have been investigated to establish which, or what, combination has the most marked influence on notched fatigue strength:

i) Material cleanliness: variously expressed as volume fraction of inclusions, inclusion size, total number of inclusions, inclusion spacing and inclusion type.

ii) Material strength, notably yield and ultimate tensile strength.

iii) Material ductility, expressed as percentage reduction of area and as uniaxial elongation.

5.2.1 Materials

The origin of the steel forgings used has been briefly described in Sections 3.3.2 and 3.4.1. It should be noted that the five steels originate from Japanese, American (North) and European steel-makers so that they may be said to be representative of world steel-making practices.

The thermal history and forging practice are known for only two of the five steels, but it is known that all were originally forgings of approximately the same initial size. Therefore, the influence of variability due to mass effects in heat treatment should not be significant.

Steels J, Y, BO and OES are all typical high pressure component steels reminiscent of EN25 (BS970:1955) in having carbon contents in the range 0.23 to 0.39 wt% with additions of nickel and chromium for hardenability. Conversely, steel M is rather special in that it is a weldable forging steel. This is achieved by having a low carbon content (0.12 wt%) with a higher nickel content (4.9 wt%) than is normal for forged components. The impurity levels (phosphorous and sulphur) are all in the 0.01 wt% region, with the exception of steel OES which shows a highish residual sulphur content of 0.022 wt%. All the steels, with the exception of steel OES which is of unknown melting practice, were produced

by the electro-slag remelt (ESR), vacuum arc remelt (VAR) or vacuum degassing (VAG) processes.

From Table 4.3, it can readily be seen that the yield and ultimate tensile strengths of the steels used vary by 35% and 23%, respectively. Ductility as measured by percentage reduction of area varies by some 40%. This spread in physical properties, whilst undesirable when metallurgical parameters are considered as independent variables is not considered to be too large to make comparisons invalid.

5.2.2 Choice of Specimen Configuration and Pressure Cycle

The configuration of specimen adopted for these tests was a compromise between wishing to retain a geometry similar to that of other authors (Crossland & Skelton (1967), Morrison, Crossland & Parry (1959), Parry (1965)) and making use of simple design improvements. The design of specimen used (see Drawing 3.1) incorporates a cross-bore through both walls of the cylinder set on a diameter. This is similar to that of previous workers cited above. The major difference was that the intersection of the cross-bores with the main bore was carefully and reproduceably radiused. As justification for this, it need only be stated that contrary to some opinion this operation is not impossibly difficult and cannot detract from the fatigue endurance of the cylinder.

The cross-bored cylinders were tested under repeated pressure and high mean pressure. These two pressure regimes are typical of those seen by the vast majority of fluctuating, internal pressure, components and should therefore provide a good basis for comparison of materials.

5.2.3 Comparison of Results

From Figure 4.9, it is readily apparent that too few tests

have been carried out at or near the fatigue limit, for definitive conclusions to be obvious. Bearing this in mind, it is still possible to make some useful comparisons.

The fatigue limits in repeated pressure as drawn cover a range of only 14% which is a small deviation in comparison with the range of yield stress (42%) or tensile strength (26%) of these steels. In the mortal region, steel J has a considerably greater endurance at a given pressure range than any of the other steels. Similarly, this steel has the highest fatigue limit (here, arbitrarily defined as 2×10^6 cycles without failure). Three steels, M, BO and OES, all show approximately the same fatigue limit, whereas steel Y is estimated to have a differentiably lower fatigue limit.

The same tendencies are also present when these steels are tested at high mean pressure (Figure 4.10). Steel J again shows greater endurance at a given pressure range than the other steels, as well as a higher fatigue limit. In this instance, no attempt was made to discriminate the fatigue limits of steels M, Y, BO and OES since they all fall within a reasonable scatter band as indicated.

When compared with other reported work on non-autofrettaged cross-bored thick cylinders, these results become more interesting. Morrison, Crossland & Parry (1959) have published the results of a series of tests on cross-bored cylinders produced from hot rolled bars of EN25. This steel was hardened and tempered to a tensile strength of 865 MPa with a yield stress of approximately 725 MPa. In respect of strength properties, therefore, it most closely resembles steel OES in terms of tensile strength and falls in between steels OES and BO in terms of yield strength. Tested under repeated internal pressure, this steel gave a clear fatigue limit (10^7 cycles) when the range of bore shear stress was

136 MPa. In comparison, the steels tested in this work gave fatigue limits between 220 MPa and 253 MPa bore shear stress range.

It must not be forgotten that the specimens tested in the course of this investigation were radiused, whereas those of Morrison et al were not blended or radiused in any way. The magnitude of the increase in allowable bore shear stress range is, however, remarkable if solely due to the effect of radiusing the intersection of the cross-bore and main bore.

Crossland & Skelton (1967) have published a paper giving details of results of repeated internal pressure tests on cross-bored cylinders of EN25 at varying hardness levels. Again, the specimens were double bored on a diameter with no attempt being made to blend the intersection. Although the intention of the authors was to investigate the fatigue properties as a function of tensile strength in the mortal region, sufficient results were presented to enable the fatigue limits to be deduced. Cylinders were tested at three tensile strength levels, namely, 973 MPa, 1313 MPa and 1700 MPa, giving bore shear stress ranges of 170 MPa, 193 MPa and 226 MPa, respectively, at the fatigue limit. Therefore, a tensile strength level directly comparable with those measured for four of the five steels used in this investigation produced a fatigue limit some 40% lower.

This effect can be more easily seen when presented graphically, as in Figure 5.1. In this figure, bore shear stress range normalised by ultimate tensile stress is plotted against cycles to failure for various cross-bored and plain cylinders of ferritic steels. If the results of Crossland & Skelton were to be added, they would narrowly span those attributed to Parry & Shannon (1977).

Whether such a spectacular increase in fatigue strength is solely due to the effects of radiusing the cross-bore is not entirely

clear. No tests were carried out on plain cylinders of the steels used, so no comparison can be made in terms of the strength reduction or nominal stress concentration factors. It is, however, known from much unpublished and restricted data that the allowable bore shear stress range normalised by tensile strength for modern steels lies above that shown by Parry & Shannon (1977).

As indirect evidence of this trend towards increasing fatigue strength, for whatever reason, a comparison is made in Figure 5.2 of the effect of mean shear stress for plain and cross-bored cylinders of various steels. To the author's knowledge, the solid line depicting the effect of mean shear stress for monoblock and compounded cylinders of EN25 is the only published data on a typical pressure vessel steel. Correct as it undoubtedly is, the effect of mean shear stress on the allowable range of shear stress at the fatigue limit for hot rolled EN25 is shown to be very strong. Some results due to Rogan (1975) on a 13% Cr martensitic stainless steel are also shown, as are the results from the present investigation on cross-bored cylinders.

Two facts are immediately obvious. For AISI410, the effect of mean shear stress on allowable range of bore shear stress at the fatigue limit is not nearly so marked. Secondly, at high mean shear stress, the cross-bored cylinders show an equal and, in one instance, markedly superior (steel J) fatigue strength when compared with monoblock plain cylinders of EN25. In passing, it is also worth noting that the effect of mean stress for cross-bored cylinders is quite small. Since no results for cross-bored cylinders subjected to high cycle internal fluctuating pressure at high mean pressure can be found in the open literature, it is difficult to make comparisons. The response of cross-bored cylinders to high mean stress appears to be similar to that found by

Rogan (1975) for the 13% Cr steel plain cylinders. Since, for most ductile ferritic steels tested uniaxially, the notched fatigue strength does not decrease as rapidly for notched specimens as for plain specimens (Grover, Hyler & Jackson (1959)), this behaviour could be expected. Conversely, it could justifiably be suggested that the response of cross-bored cylinders to high mean stress is the same as that for plain cylinders of EN25 in that at the superior mean stress for cross-bored cylinders, a degree of self-autofrettage has been introduced. The resolution of this uncertainty would require further tests at intermediate mean stress levels with cross-bored cylinders. Unfortunately, no further specimens were available to carry out such tests.

A series of tests was carried out at high mean pressure for steels Y and M in an autofrettaged condition to see whether the inferiority of steel Y persisted after autofrettage. The fatigue curves from this series of tests is shown in Figure 5.3.

Autofrettage was carried out in the closed ended condition and to the same pressure for both steels. The pressure used was 860 MPa. For the yield strengths of steels Y and M, this would correspond to theoretical autofrettage depths of 38% and 30%, respectively.

From Figure 5.3, it can be seen that the difference in fatigue limit estimated for the non-autofrettaged repeated pressure condition persists at high mean pressure. If the upper and lower bounds of the scatter band drawn to represent the fatigue limit under high mean pressure for the non-autofrettaged condition (Figure 4.10) are taken as the actual fatigue limits for steels M and Y, respectively, the effect of autofrettage can be appreciated. The allowable stress range for steel Y increases by 70% and for steel M by 70%. This increase in allowable stress range is almost identical with that found by Morrison et al (1959).

5.2.4 Comparison of Steels

From the outset, it had been decided to investigate the steels used in this part of the experimental programme from a metallurgical standpoint. It has been postulated and indirect evidence presented in the foregoing section that the fatigue strength of cross-bored cylinders (albeit with a radiused intersection) is a function of the metallurgy of the steel. Therefore, it was something of a disappointment and surprise to find such a small variation (14%) in the repeated pressure fatigue limit of five steels with such widely varying physical and chemical parameters.

Various correlations of a simple nature were tried and these are shown graphically in Figure 5.4(a)-(f). In all the attempted correlations, the estimated nominal range of bore shear stress at the fatigue limit in repeated pressure is shown plotted against the parameter in question for each of the five steels tested. The first three correlations are based on physical properties that can be determined directly from a simple tension test. The latter correlations are functions of steel composition and are by no means easy to obtain.

The first and most obvious correlation is that of tensile strength of the steel, since this has previously been shown to be important (Crossland & Skelton (1967)). From Figure 5.4(a), it can be seen that, with the exception of steel Y, there does appear to be a non-linear, but definite relationship between fatigue limit and tensile strength level for cross-bored cylinders. That such a relationship should exist is not surprising, given that this effect has been observed for plain components and is well documented. It is not always observed for notched or flawed components and indeed the effect can be reversed, depending on the severity of the stress concentration and absolute strength level.

This dependence of fatigue strength on tensile strength is not reflected when yield stress is considered. In Figure 5.4(b), the fatigue limit of cross-bored cylinders is shown as a function of yield ratio, here defined as the yield strength of the steel in question divided by its ultimate tensile strength. The yield ratio as such has no fundamental significance in the response of a material to external or internal loads and is generally misused in industry as a measure of inherent ductility. Whilst its indiscriminate use as a qualitative measure of ductility is not to be criticised too severely, this approach does have limitations.

Probably the main use of the quantity defined as yield ratio lies in its ability to indicate whether a material will strain harden or strain soften under fatigue loading. Cyclic strain hardening occurs for most ferritic steels with a yield ratio of less than 0.7 when subjected to dynamic loading. Conversely, strain softening is found to occur for steels with yield ratios of greater than 0.8 when subjected to cyclic loading (Smith, R.W., et al (1963)).

The stress concentrating effect of the cross-bore in a cylinder subjected to repeated internal pressure is such that strain hardening or softening of the material in the vicinity of the intersection might be expected. If this were the case, then it might be further expected that the number of cycles and nominal stress level necessary to initiate a crack would be a function of the degree of strain hardening or softening. From Figure 5.4(b), it is evident that in this instance the theory is not substantiated. Four of the five steels would be expected to strain soften and the fifth, steel OES, would neither harden nor soften. It is interesting to note that the steels showing the highest yield ratio, 0.91 to 0.92, also show the greatest difference in fatigue strength. Again,

with the exception of steel Y, the general tendency is for fatigue strength to increase with yield ratio but this is inseparable from the tensile strength effect of Figure 5.4(a).

A further correlation with a mechanical property of the steels is shown in Figure 5.4(c). Here, the abscissa represents the percentage reduction of area measured from a tensile test in the longitudinal direction. This quantity is often regarded as a measure of ductility of the steel and is included here to indicate how misleading it can be for a thick cylinder geometry. The steel with the lowest percentage reduction of area having the highest fatigue strength. Obviously, from the stress system generated in a cross-bored cylinder, the tangential or hoop stress is most likely to be controlling if shear stress is not the controlling criterion. Therefore, the percentage reduction in area from a tensile test in a transverse direction is the proper parameter to consider. Unfortunately, when these steels were acquired by the author, they had been sawn in such a fashion that a systematic tensile testing programme with specimens from other than the longitudinal direction was not possible.

In an attempt to reclaim this situation, metallurgical parameters were measured to try to obtain some idea of the degree of inhomogeneity of the steels used.

From the work of many authors (Frith (1954), Cummings (1958), Thornton (1972), Heiser & Hertzberg (1972), etc.), it is known that inclusions can influence both the initiation and propagation phases of fatigue crack growth. In terms of the fatigue limit of a cross-bored cylinder subjected to repeated internal pressure, the initiation phase will be the dominant factor in determining the absolute stress level at which failures can occur.

For the case of static loading, i.e. a singly applied load as

in a fracture toughness test, there is evidence that the total volume fraction of inclusions determines to some extent the critical mode 1 stress intensity (Feige & Murphy (1967)). Conversely, Thornton (1972) has found that this is not the case for fatigue loading.

The results of the volume fracture of inclusions analysis are shown in Figure 5.4(a) plotted as a function of the fatigue limit found for each of the five steels tested. No trend of any description is apparent, substantiating the premise that the total volume fraction of inclusions does not have any influence on high cycle notched fatigue crack initiation. A reason for this lack of correlation is not hard to find in that the volume fraction of inclusions is an all encompassing quantity which does not discriminate between size, shape or nature of the inclusions present in a steel.

The effect of inclusion size can be coarsely judged from the mean inclusion diameter of the steel in question (see Table 4.5). This quantity is shown plotted against the bore shear stress fatigue limits of each of the five steels in Figure 5.4(e). Again, no trend is obvious. If, as seems likely for plain components, the size of an inclusion initiating a fatigue crack is controlling at the fatigue limit, then the tensile strength of the material must also be included. When the results of Figure 5.4(e) are replotted as tensile strength divided by mean inclusion diameter, no better result is found.

A further parameter was assessed by plotting the mean inclusion spacing versus the experimentally determined fatigue limits for each of the steels. The mean inclusion spacing can be thought of as a non-linear function of the likelihood of encountering an inclusion at the free surface in the highly stresses cross-bore region. Therefore, the trend, if any, should be towards increasing fatigue limit with increasing

inter-inclusion spacing. This behaviour is observed in Figure 5.4(f), perhaps fortuitously, for steels J, M and OES. The two rogue steels are BO and Y.

From the foregoing, it is tempting to say that the lack of correlation of fatigue strength with metallurgical parameters is so marked that their influence on notched repeated pressure fatigue strength is non-existent. Also, the experimental observation that inclusions were not found at the initiation sites of the fatigue cracks tends to confirm this opinion. Thus, an alternative explanation has to be sought to explain the inherent difference in fatigue strength between steels. That this difference occurs solely as a function of tensile strength is altogether too facile when it is generally accepted that fatigue failure is plasticity controlled (Feltner & Morrow (1961)). When the criterion for fatigue failure is the onset of true plastic straining, then the yield stress rather than the tensile stress would be expected to give better correlation. It cannot be denied that yield stress and/or tensile strength influence fatigue endurance but there must be secondary factors which are not obvious.

The major limitation of the metallurgical factors considered here is their lack of discrimination. Volume fraction of inclusions is a parameter which can be highly misleading. Mean inclusion diameter is also a dubious term, since it is the average diameter of all inclusions irrespective of their severity as stress raisers. Similarly, the mean inter-inclusion distance does not differentiate between large and small, soft or hard inclusions. The equivalent circle diameter size distributions of inclusions (Figures 4.1 to 4.5) for the steels tested does not give any additional information, even when superimposed as in Figure 4.6. From visual determinations of the relative proportions of

"hard" and "soft" inclusions in these steels (see Table 4.7), it might be inferred that steel J would perform better than the others. This does not, however, go any way towards explaining the differences, slight though they are, for the remaining steels.

One final fact worthy of attention is that both steels OES and Y had seen service in massive form as high pressure components. The actual stress levels are not known with any certainty, but it is known that steel Y had been operated at ≈ 280°C for some seven years (60,000 hours).

There is experimental and practical evidence that steels of the 3½ NCMV type can suffer temper embrittlement after prolonged exposure at temperatures of ≈ 290°C (Walker et al (1977)). It is therefore suggested that this may have occurred for steel Y which has a composition not too dissimilar to that of 3½ NCMV. The degree to which a reduction in the fracture toughness and impact resistance of a steel affects the fatigue strength of that steel is open to speculation but could easily explain the differences noted in this work.

In concluding this section of the discussion of results, the important points which have emerged from this investigation can be summarised as follows:

(1) The fatigue strength of radiused cross-bored cylinders of forged steels is considerably in excess of that which would be expected from other literature values.

(2) The effect of mean pressure on the fatigue strength of cross-bored cylinders is less than that found for plain cylinders of comparable steels produced from hot rolled bar.

(3) The differences in fatigue limit for cross-bored cylinders

of different steels tested under repeated pressure persists after autofrettage.

(4) Autofrettage of radiused cross-bored cylinders increases the allowable stress range at the fatigue limit by some 70%.

(5) No factor other than tensile strength could be shown to have any influence on the fatigue limit of the five steels tested in the form of cross-bored cylinders.

(6) No metallurgical evidence was found at the initiation sites of fatigue cracks in cross-bored cylinders which would implicate inclusions or second phase particles in the initiation process.

(7) The fatigue strength of cross-bored cylinders appears to be a function of geometry and perhaps material.

On a purely speculative note, the steels used in this investigation are estimated to have plane strain fracture toughness values in any orientation in excess of 120 MPa.$m^{\frac{1}{2}}$ with the possible exception of steel Y. To give the designer some idea of the possible size limitations in cross-bored cylinders of these steels, Figure 5.5 was constructed. In this figure, a double cross-bored cylinder of diameter ratio 2 is assumed to contain symmetric, opposed semi-circular cracks to a depth in the radial direction given by a/W. The ordinate gives the internal pressure at which fast fracture in the radial direction could be expected to occur for a range of wall thicknesses. It will be appreciated that for the wall thickness of 10 mm, the pressure necessary to cause fast fracture is at about the yield pressure of the diameter ratio 2 cylinder for all crack depths with steels over 1000 MPa yield strength. Therefore, this situation is unlikely to arise in practice.

With increasing wall thickness, however, the critical pressure falls to below typical design working pressures for diameter ratio 2 vessels. Fast fracture from a cross-hole crack is therefore a real possibility, especially with the larger wall thickness, where fracture toughness values of 120 MPa.$m^{\frac{1}{2}}$ might not be achieved. On a more optimistic note, the larger wall thicknesses are not so "pressure sensitive" as the smaller and therefore give more inherent safety. Also, the chance of discovering a growing fatigue crack in a cross-bored vessel is better for the larger wall thickness by virtue of absolute size for a given crack depth to wall thickness ratio.

This figure was produced with a stress intensity factor calibration due to Tan & Fenner (1979) calculated numerically by the BIE method. Although no other stress intensity factors exist for comparison purposes, it is felt by the authors that this solution is likely to be correct to within a few percent from their experience with this calculation method.

5.3 PLAIN CYLINDERS (D = 2)

5.3.1 Crack Growth Tests

As outlined in Sections 3.2.2 and 3.6.3, a series of tests was performed to demonstrate and refine a technique for monitoring crack growth in thick cylinders subjected to fluctuating internal pressure.

The steel used for this test programme was selected more for its availability than for technical reasons. However, from Table 4.1 it can be seen that this steel is of similar composition to the low alloy steels tested as cross-bored cylinders. Designated a case hardening steel, which can also be core refined by heat treatment, the nickel content is higher than conventional low alloy pressure vessel steels. It is

directly comparable in terms of the mechanical properties obtainable with all the steels used in this work.

From general experience and the reported literature from Bristol, Belfast and Imperial College, it is known that a fatigue crack produced by fluctuating internal pressure is semi-elliptic in shape at breakthrough. This implies that initiation occurs at a point in the material. Fatigue cracks originating from line defects at the bore of the material lead to multiple initiation and long straight-fronted cracks or totally asymmetric cracks. This situation is frequently encountered in large guns or howitzers, where the effect of the rifling is akin to that of a line defect.

The purpose of this work was to quantify the crack initiation and propagation process for the more usual situation of semi-elliptic cracks. Since, in contrast to most other fatigue situations, a large surface area of the specimen is highly stressed and largely inaccessible, the initiation site cannot be predicted with any certainty. Therefore, it was essential from the outset to either know the position of the initiation site or to induce the initiation. The latter course of action was chosen.

The size of specimen adopted for this and later sections of this investigation dictated to some extent the technique used to measure crack growth. Ultrasonic crack growth measurement is frequently recommended for its resolution and ease of application. In the case of a thick-walled cylinder of small overall dimensions, ultrasonics cannot be employed because of the surface curvature. The method adopted was that due to Shannon (1973), who has demonstrated that measurement of the changing strain pattern in a cracked body can be related to crack depth. Shannon was able to measure crack depth for long straight-fronted cracks

set in thick-walled cylinders. He further showed that the change in range of strain with crack depth could be predicted with reasonable accuracy by analytical or finite element techniques. Whilst the strain pattern change accompanying a semi-elliptic crack will not be identical to that of a long straight-fronted crack, the method appeared promising, especially for thick-walled cylinders of only some 25 mm outside diameter.

A large mistake was made at this juncture. The intention was to relate the crack growth rate data produced through a fracture mechanics formalism, the Paris law. In this manner, it was hoped to make the results of general use to designers, if only in providing hard evidence of crack growth rates in pressurised thick cylinders. This implies a knowledge of a stress intensity factor for a semi-elliptic crack in a thick-walled cylinder. At the time, only expressions due to Underwood (1972) and Throop (1970) were available, both of which were heavily qualified by the authors in their range of applicability and accuracy. The present author had naïvely assumed that these expressions could be improved upon by making use of a three-dimensional finite element code due to Pereira (1977). This unbridled optimism was shattered on calculating the computing costs involved in producing a stress intensity factor correlation for various crack depths in a thick-walled cylinder of fixed diameter ratio and crack aspect ratio.

Fortunately, the numerical analysis section of the Mechanical Engineering Department were persuaded that this was a problem of great importance. A new numerical analysis technique of great potential and efficiency was applied to the problem and results were promised within two years. To some extent, the investigation undertaken here went into abeyance for a similar period. However, a calculated risk was taken and the experimental programme of crack growth measurement in thick cylinders

was carried out before the means were available to analyse the results.

5.3.2 Considerations in Analysis of Results

The method of initiating cracks from a point defect and measuring the changing strain pattern have been adequately described in Sections 3.6.3 and 3.6.4.

In order to produce the calibration curve of strain range change with crack depth (see Figure 4.12), specimens were fatigued to theoretically predetermined crack depths. Analysis of the aspect ratio of these cracks yielded a valuable piece of information. All the cracks generated irrespective of crack depth were perfect semi-ellipses of semi-minor to major axis ratio (b/a) of 0.8. Photographs 5.1(a)-(g) show a selection of the specimens used to draw Figure 4.13 and to produce the calibration curve (Figure 4.12).

To check that the spark induced initiation did not have a determining effect on the crack shape, further specimens were cracked to various depths, having been allowed to initiate freely. A single strain gauge in the tangential direction at the outside diameter was significantly sensitive to detect a crack growing in a plane circumferentially or axially remote from the gauge. These cracks were found to have exactly the same semi-axis ratio of 0.8, irrespective of crack depth.

The significance of the finding that crack shape remains constant on the macro-scale lies in the fact that the stress intensity factor analysis does not need to be modified continuously to take account of changing crack shape.

This behaviour of consistent semi-axes ratio of cracks could be expected from the following simple analysis.

Consider an elliptical crack set in an infinite medium

perpendicular to a stress applied remote from the plane of the crack. The most extreme differences in crack growth will occur in the direction of the semi-axes, a and b. Using the empirically derived Paris law:

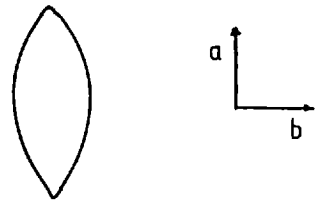

$$\frac{\Delta l}{\Delta N} = C_o \, \Delta K^n \tag{5.1}$$

it can be shown that when n and C_o are identical for the directions a and b:

$$\frac{\Delta b}{\Delta a} = \left(\frac{\Delta K_b}{\Delta K_a}\right)^n = \left(\frac{a}{b}\right)^{n/2} \tag{5.2}$$

a stable crack form will be reached when:

$$\frac{(\Delta b + b)}{(\Delta a + a)} = \frac{b}{a} \tag{5.3}$$

i.e.

$$\frac{\Delta b}{\Delta a} = \frac{b}{a} \tag{5.4}$$

From equation (5.4), it will be seen that a circle will be the final crack shape.

Similarly, if we assume that crack growth in the a direction can be represented by:

$$\frac{\Delta a}{\Delta N} = C_a \, (\Delta K)^n \tag{5.5}$$

and in the b direction by:

$$\frac{\Delta b}{\Delta N} = C_b \, (\Delta K)^m \tag{5.6}$$

then:

$$\frac{\Delta b}{\Delta a} = \frac{C_b \, (\Delta K)^{m_b}}{C_a \, (\Delta K)^{n_a}} = \frac{C_b \, (a)^{n/2}}{C_a \, (b)^{n-m/2}} \tag{5.7}$$

and a stable crack will be formed when:

$$\frac{(b + \Delta b)}{(a + \Delta a)} = \frac{b}{a} \tag{5.8}$$

which, on combining equations (5.7) and (5.8):

$$\frac{C_b \, a^{n/2}}{C_a \, b^{n-m/2}} = \frac{b}{a} \tag{5.9}$$

Therefore, an ellipse of semi-axis ratio b/a will be formed. Evaluation of the intercepts and exponents in the Paris law for the two semi-axis directions will define the ellipse.

If a crack intersecting a free surface in a finite body is now considered, the same reasoning may be applied with the addition of terms to account for the edge effect and finite width of the body. Since the free surface correction term is almost always greater than the net section effect, this leads to the prediction that for isotropic crack growth resistance, an ellipse ($b/a \rightarrow 1$) with major axis at the free surface will always be formed. For anisotropic crack growth resistance, ellipses of more variable semi-axis ratio will be formed with major axis being at the free surface or normal to it, dependent on the absolute values of C_a, C_b, n and m.

The calibration curve, Figure 4.12, enables a crack depth

versus cycles curve to be constructed. Two typical a versus N curves are shown for cyclic internal pressures of 245 MPa and 214 MPa in Figures 4.14 and 4.15, respectively. When the stress intensity factor calibration (Tan (1979)) became available, two further results were checked. The first was the variation in tangential strain at a point lying in the plane of the growing crack (i.e. the calibration curve). From experience, it had been noted that cracks propagating on a plane removed from that expected produced a very different record of strain range with crack depth.

In the BIE equation method used to deduce the stress intensity factor, only surface points used to be discretised. This leads to a considerable reduction in core storage and manipulation time during numerical processing with the digital computer. (Indeed, it is estimated that for problems in elastic fracture mechanics, the BIE method is a factor of 10 more efficient that a three-dimensional finite element solution.) Therefore, it is a simple matter when calculating the displacements of the cracked body necessary to infer the stress intensity, to also arrange for these displacements to be printed. From the computational results for a diameter ratio 2 cylinder with a crack semi-axis ratio of 0.8, the strain at a point on the surface of the cylinder above the crack was plotted as in Figure 4.12. The degree of agreement is encouraging. The differences apparent can be explained qualitatively, if not quantitatively.

The computational model assumes that the fluid pressure acts fully over the crack surface, thereby augmenting the stresses set up in the wall thickness by the internal pressure in the main bore. This effect may not be fully realised in practice when a cyclic frequency of between 5 and 7 Hertz is being used. Oil viscosity, temperature and crack depth may influence the effectiveness of oil pressurising the crack. Secondly,

and this is considered to be the more likely explanation, the computational results are for strain at a point. The strain gauge used in practice has a discrete gauge length. When the computational results of hoop strain at the outside circumference are plotted with respect to crack orientation, it is evident that high strain gradients exist above the crack plane (Figure 5.16). Therefore, the strain gauge to some extent averages the large strain gradients found above a growing crack, producing the differences noted in Figure 4.12.

The second point which was checked by reference to the stress intensity factor calibration of Tan (1979) was the validity of the decision not to use the Underwood or Throop stress intensity calibrations. From Figure 2.4, it can seen that, assuming the accuracy of the results of Tan, the differences in stress intensity at a given crack depth are large. The results from Throop are most consistent but under-estimate the stress intensity by 45% and 65% for cylinders of diameter ratio 2 and 3, respectively, at crack depths of half the wall thickness. The decision to wait for a more fundamentally founded stress intensity factor calibration is therefore considered to have been justified.

5.3.3 Comparison of Results

The results of repeated internal pressure fatigue tests with plain cylinders of steel CH are shown in Figure 4.11. Little need be said about these results, except to comment that the fatigue limit found corresponds to a range of bore shear stress of 387 MPa. Normalised by ultimate tensile strength of the material, this gives a value of 0.44 which is in excess of that expected from Figure 5.1. It will, however, be remembered that these specimens were not stress-relieved after machining. This fact may account for the very good repeated pressure

fatigue strength.

Also shown in Figure 4.11 are the nominal endurances and pressure ranges of cylinders with spark defect induced initiation. It is not possible to say with certainty what influence the defect induced initiation has on total endurance, except by a back calculation from the measured crack growth rate. Since this would not serve any purpose, it has not been attempted. Qualitatively, however, it can be seen from the scatter of results that the defects induced vary in severity. Endurances vary by up to a factor of 3 for approximately equal pressure ranges. This effect is assumed to be confined to the very early stages of crack growth from the defect and does not carry over into the macroscopic crack growth phase.

Using the stress intensity factor calibration previously referenced and the a versus N curves, it was possible to derive the macroscopic crack growth rate as a function of the reigning stress intensity (Figure 4.16). It will be appreciated that this correlation is describing crack growth in a radial direction and so corresponds to the point of deepest crack penetration. It does not necessarily follow as is stated by some authors (Parry & Shannon (1977)) that this point is also the point of highest stress intensity. Reference to Figure 2.5 shows that the stress intensity factor is highest in the material nearest the bore of the cylinder. When the effects of plane stress at the surface are taken into account, the highest value of stress intensity probably occurs at some point around the crack periphery at a small angle from the free surface.

In Figure 4.16, the results of measurements taken from two specimens fatigued at different pressure ranges are shown. The experimental points plotted are gratifyingly consistent in view of the

indirect methods used to measure crack growth rate. Further specimens were tested and analysed, but the results all fall within a few per cent of those shown and are therefore not shown for the sake of clarity.

Assuming the applicability of the empirical Paris law (1963), the results have been further analysed to conform with the relation:

$$\frac{da}{dN} = C \Delta K^n \qquad (5.10)$$

The values of intercept and exponent for this relationship using the experimental data are also given in Figure 4.16. Since no previously reported work can be found in the literature for either this steel tested in air or for that matter for any alloy steel tested in the form of thick cylinders, comparisons are not possible. If crack growth under a repeated internal pressure regime is the same as that in air, then the results presented here might be compared with more conventional crack growth rate tests.

As some indication of the correctness of these results, or lack of it, a comparison of crack growth rates for a selection of alloy steels at a range of stress intensity (R = 0.05 to 0.1) of 20 MPa.m$^{\frac{1}{2}}$ indicates crack growth rates of about 1×10^{-8} m/cycle. The results presented here agree very well with this average figure and the exponents and intercepts are typical.

5.3.4 Fractographic Investigation of Steel CH Fatigue Cracks

A short fractographic and metallographic investigation of

steel CH was undertaken in the same vein as for the cross-bored cylinders. In this instance, however, no statistical analysis of inclusion population was undertaken.

From metallographic polished sections, the steel was observed to contain a normal amount of elongated type I and globular type III sulphides. As this steel had been supplied as rolled bar, the type I sulphide stringers were heavily elongated in the axial direction. A fair proportion of stringers were also observed clustered in the working direction but not deformed transversely. Optical differentiation of the exact chemical composition of these stringers was not attempted but they are thought to be aluminates, probably calcium containing, and silicates. The structure was that of a tempered martensite with no evidence of any abnormality such as micro-segregation.

Three fracture surfaces were cut from the walls of specimens which had failed after being allowed to fatigue without artificially induced initiation. These specimens were cleaned in alcohol in an ultrasonic cleaner, dried with acetone and then mounted on stubs for subsequent scanning electron microscope (SEM) investigation. No carbon shadowing or sputtering was undertaken to improve the image. Using 25 kV at approximately 10 degrees tilt, it was possible to trace back from the river markings on the fracture surface to the initiation site at the bore of the cylinder. In two of the three specimens, evidence of inclusions lying at or very near to the initiation site was found. Photomicrographs 5.1h and 5.1i show the sites associated with inclusions. By making use of the X-ray dispersive analyser attached to the JEOL35 SEM, it was possible to identify aluminium and silicon as being one constituent of the inclusions in Photomicrographs 5.1h and 5.1i, respectively, Due to the fact that the XRDA will not detect the lighter elements, it is not possible

to positively identify these inclusions. It is possible to say that the aluminium containing inclusion was probably alumina since the other elements commonly occurring with aluminium were not found. Similarly, the silicon containing inclusions were probably silica.

No opinion can be offered at this stage as to the significance of this finding since the number of sample fracture surfaces investigated is too small.

5.4 FATIGUE TESTS ON STEELS B AND G

5.4.1 Introduction

The bulk of the experimental programme was carried out with steels B and G. These steels (hopefully) represent the two extremes in modern steel-making. Therefore, the results obtained and the conclusions drawn should serve as useful upper and lower limits for a designer of pressure vessels or any component subjected to fatigue loading produced from this type of steel.

5.4.2 Steels B and G: Background Information

Steel B was originally purchased by an industrial high pressure plant in the form of block forgings of the dimensions shown in Figure 3.1. The material specification called for AISI4340 composition. (This analysis is almost directly comparable with that of EN24 (BS970:1955), now called 817M40 (BS970:Pt2:1970).) Although meeting the chemical analysis specification according to a notary public witnessed certificate, this steel could not attain the necessary Charpy impact values in the transverse direction. The blocks were therefore re-heat treated to their present tensile strength level and again failed to meet the required minimum variation in impact values.

The steel designated as G was therefore procurred as a replacement for steel B. Again, the material specified was AISI4340 and block forgings to the dimensions in Figure 3.2 was procurred.

5.4.3 Comparison of Steels B and G

From a chemistry point of view, these steels are very similar in the major alloying additions, but differ significantly in two important respects. For steel B, the manufacturer's analysis (see Table 4.1) claims a sulphur content of 0.015 wt%, the maximum allowable for electric arc melt quality AISI4340. Independent analysis shows this to be a considerable under-estimation of the actual sulphur content. Whether this was a genuine error or not is a subjective point, but a correct analysis would have saved the cost of the attempted re-heat treatment. Secondly, it is apparent from the independent analysis that the residual aluminium content of steel B is much lower than that of steel G. Whilst by no means conclusive, this could imply deoxidation of the original melt other than by addition of aluminium.

When the mechanical properties of these two steels are compared, the differences become stark. Although steel B is at a slightly higher tensile strength level, it exhibits variations in ductility properties out of all proportion to this slightly higher strength level. The percentage variations in reduction of area and elongation are 67% and 45%, respectively, for steel B, but only 15% and 14%, respectively, for steel G. (Percentage variation is defined as the maximum value of a property minus the minimum value divided by the maximum value times 100. It is a useful measure of anisotropy in a steel when applied to the ductility properties, although it says nothing about the absolute level of that property.)

It is interesting to note that in the longitudinal direction,

both steels show very similar values of reduction of area and elongation, the differences only becoming apparent when the transverse directions are considered. Therefore, it is no surprise to find that this behaviour is reflected in the Charpy impact values (Table 4.4). For steel B, all impact fracture planes containing the L direction show very low values, typically 33 Joules at room temperature. Conversely, steel G shows excellent Charpy impact values at both room temperature and -20°C. Fracture toughness tests were carried out for steel B in the three orthogonal directions. The results obtained are shown in Table 4.4. In the longitudinal direction, a J integral test was adopted since it was realised that a valid plane strain fracture toughness utilising LEFM methods would not be applicable. Although only one specimen was tested for each of the three axes (see Photographs 5.2 to 5.4), the results are sensible, except that it might have been expected that the TQ result would be superior to that of the QT. However, the directional axes were assigned to both block forgings only on the basis of as-received dimensions which may not reflect true forging practice.

Both block forgings were subjected to hardness traverses and macro-etching at selected areas on two orthogonal planes. No significant variation in hardness was found for either forging. Steel B responded positively to sulphur printing with variations which were not consistent with any geometrical feature of the block. No evidence of sulphur or impurity segregation at any position was found in steel G.

5.4.4 Comparison of Thick Cylinder Fatigue Results (D = 3): Steels B and G

The first series of repeated internal pressure fatigue tests was carried out to quantify the effects of material anisotropy. Therefore,

no artificial defects were introduced to cause initiation from a preferred point. It will be recalled that all these cylinder specimens were stress relieved after final machining to relieve induced machining stresses. With this particular design of specimen (Drawing 3.4), the flange did not provide the expected degree of reinforcement and failures tended to initiate and propagate at the specimen ends. To overcome this problem, the first 30 mm from each end of the specimen was heavily polished before testing. Great care was taken to ensure that this polishing did not affect the central region.

The results of repeated pressure fatigue tests for cylinders of steel B machined from different axes of the block forging are shown in Figure 4.17. Whilst the effects of anisotropy are well recognised in the fatigue situation, these results are, to the author's knowledge, the first to actually demonstrate this reduction in fatigue strength as a result of fluctuating pressure fatigue.

It was not possible to differentiate between the fatigue limits for cylinders having their longitudinal axis in the Q or T directions. The results for cylinders with these orientations are therefore shown as one curve. The effect of making the longitudinal axis of the cylinder in a direction other than from the longitudinal direction in the forging is to increase the range of pressure at the fatigue limit by 21%. There would also appear to be an increase in the endurance for a given pressure range in the mortal region of some 20%.

The identical testing sequence was also carried out for steel G. The results are shown in Figure 4.18. Again, it was not considered realistic to draw two fatigue limits for specimens from the Q and T directions. Cylinders with their longitudinal axis from either of the transverse directions give repeated pressure fatigue limits 10% greater

than for cylinders lying in the longitudinal direction. Not enough results are available for the mortal region but endurances for all orientations appear equal within the limits of wide scatter of results.

The results from both series of tests can be compared from Figure 4.19. It is evident that steel G is superior, irrespective of orientation of test specimen. When compared on the basis of the same orientations, steel G exhibits fatigue limits 25% and 13% higher than steel B for orientations L and Q/T, respectively. A further result of interest is that the scatter is most marked for orientations Q and T for both steels. For the L axial direction cylinders of both steels, the reproduceability is good.

After failure, all cylinders were sawn open to reveal the fatigue crack profile. Since the directions other than the axial were kept for all cylinders, it was possible to note the origins of the fatigue failures. Table 5.1 summarises these observations. It will be appreciated that the numbers of specimens tested do not allow rigorous analysis. However, taken at face value, steel B would seem to have preferred planes of crack initiation and propagation. Conversely, no trends are evident in the limited number of tests to failure for steel G.

Each cylinder, after being sawn longitudinally normally to the crack plane, was examined by eye to see if other fatigue cracks were present. Of approximately 40 specimens tested, only four were found to contain more than one crack. Of these four cracks, only one had propagated to more than 20% of the wall thickness.

A selection of crack surfaces are shown in Photographs 5.5 to 5.19, covering the complete range of crack planes possible for both steels. Not all of these cracks were allowed to initiate freely, but as for steel CH in the preceding section no differences were apparent for

full wall thickness cracks.

In attempting to explain the differences in fatigue limit, both between the various orientations and the two steels, it was considered necessary to examine the fatigue fractures in detail.

5.4.5 Fatigue Crack Shapes in Thick Cylinders of Steels B and G

The shapes of the fatigue cracks observed were found to be near perfect semi-ellipses. Therefore, these cracks can be characterised in terms of their semi-minor to major axis ratio, b/a. Figures 4.20 to 4.22 show the variation in crack shape as a function of plane of crack growth for steel B. All the results for steel G are shown in Figure 4.23 and the results for both steels are summarised in Table 4.8.

The greatest variation in crack shape occurs for cylinders of steel B. Cylinders with their longitudinal axis in the forging L direction exhibited significantly lower b/a ratios than cylinders cut from either of the remaining axes. This would imply that there is a distinct variation in crack growth resistance in this steel as a function of orientation.

Conversely, steel G showed remarkably consistent crack shapes only slightly under semi-circular, being more extended in the cylinder axial direction. If no variation in crack growth resistance occurs with material, then a perfect semi-circular crack would be expected as described in Section 5.3.2.

5.4.6 Fractographic Investigation of Fatigue Cracks in Cylinders

Sections containing the geometric origin of the fatigue cracks were cut from a large selection of cylinders of both steels which had failed after being allowed to initiate freely. These slices were removed

from the opened specimens as soon as possible after failure on the fatigue machines and kept in a dessicator.

Examination under an optical stereo microscope gave no indication of the cause of fatigue crack initiation but did serve to pin-point the area of interest more closely. Therefore, all the sections were mounted for SEM observation.

Using a JEOL35 scanning electron microscope in the secondary electron mode, specimens from cylinders of steel B were observed. Due largely to inexperience, the author, although perfectly able to find the initiation site of the fatigue cracks, persistently observed that the specimens were "dirty". Large fluorescing masses were observed in the vicinity of and removed from the area of interest. Since this behaviour is similar to that observed when atmospheric dust collects on the specimen surface, the specimens were repeatedly cleaned ultrasonically in alcohol.

Although the intention of the fractographic work was to try to identify inclusions at the initiation site, it was not until a piece of "dust" was analysed *in situ* that inclusions were found.

Photomicrographs 5.20 to 5.26 show the initiation sites at the bore of thick cylinders for various orientations of steel B. In particular, the photomicrographs of specimens TL-15 and QT/TQ-10 show very clearly that inclusions can initiate fatigue cracks in thick walled cylinders subjected to repeated internal pressure.

Of some 20 specimens of steel studied under the scanning electron microscope, the majority were found to have ruptured inclusions at the origin of the fatigue crack. Whilst this may seem strange, given that only one crack surface was investigated for each steel, it would appear that both crack surfaces can show evidence of inclusions. On rupture, some of the inclusion remains attached to each fracture surface.

A similar result was found for steel G. However, here the inclusions were not easy to find and only some 30% of the fractures investigated were proven to have originated from inclusions. Photomicrograph 5.27 shows a typical initiation site where no inclusion was evident.

In situ analysis with the XRDA attachment to the microscope gave the following results:

Steel B: All inclusions contained calcium and aluminium. Approximately one half showed silicon, manganese and sulphur to be additionally present. A few also contained measurable titanium.

Steel G: Analysis showed more than one type of inclusion to be present. All but one of the inclusions incriminated contained manganese and sulphur with one or more of calcium, silicon, aluminium or titanium. The exceptional inclusion contained only aluminium and magnesium.

At this juncture, the previously adhered to format of presentation is departed from to try to make clearer the way in which the conclusions reached in the following sub-sections are arrived at.

5.4.7 Repeated Tension Fatigue Tests

The results of these tests are summarised in Table 5.2 and Figure 4.35, as well as presented individually in Figures 4.33 and 4.34.

Considering first steel B, the results provide no surprises on

qualitative grounds. Specimens taken from the longitudinal direction in the forging showing a fatigue limit some 37% above the transverse directions. Scatter of results is most marked in this direction.

For the transverse axis specimens, there appears to be a slight difference in fatigue limit. Specimens from the Q direction are marginally superior in fatigue strength at the fatigue limit.

The results from steel G show similar but not so marked tendencies. L axis specimens are only 6% superior at the fatigue limit. This fatigue limit for the L axis specimens is a remarkable 96% of the static yield stress.

When compared as in Figure 4.35, it is apparent that steel G is virtually isotropic, whereas steel B represents a fairly severe case of anisotropy. Ranson & Mehl (1952) tested specimens cut from forgings of AISI4340 and determined the fatigue limits in both the transverse and longitudinal directions. These authors found the ratio of transverse to longitudinal fatigue limits to lie between 0.7 and 0.8. Other authors (Evans et al (1956), Frost (1956), Frith (1956)), however, have found this ratio to be larger. Therefore, it is considered that steel B represents an extreme case with a transverse to longitudinal fatigue ratio of 0.72.

It is of interest to note that, unlike the thick cylinder case, the repeated tension results for steel B in the longitudinal direction overlap those of steel G in the transverse directions.

5.4.8 Repeated and Reversed Torsion Tests

Insufficient specimens were available to determine the fatigue limit in repeated torsion for either of the two steels. From the few results shown in Figure 4.37, together with the estimated fatigue curves, it is evident that the shear yield stress for these steels has been exceeded.

This was to be expected for a repeated torsion test, especially with a solid specimen. Since the redistribution of stress cannot be easily evaluated, and due to the few results obtained, this series of tests is excluded from further consideration.

The results of the reversed torsion fatigue tests are more in accord with those found from the direct stress tests. Steel G exhibits a superior fatigue limit which is quite well defined by three specimens which did not fail at endurances of up to 2×10^7 cycles. Unfortunately, not enough specimens were available to adequately define the fatigue limit for steel B. It is, however, evident from the three results available that the reversed shear stress fatigue limit for steel B is some 8% to 10% inferior to steel G.

Morrison, Crossland & Parry (1956) were the first authors to describe fatigue tests under a repeated internal pressure regime and to suggest a failure criterion. Their criterion is based on the experimentally observed fact that for ferritic steels, the range of bore shear stress in a repeated pressure fatigue test is approximately equal to the semi-range of shear stress in a reversed torsion test.

From the results summarised in Table 5.2, this criterion is seen to be applicable for steel B (albeit generously as the reversed torsion fatigue limit is not well defined). For steel G, where both fatigue limits have been determined to better accuracy, the agreement using a shear stress criterion is not good. The reversed torsion fatigue limit under-estimates the repeated pressure allowable shear stress range by 11%.

Since it is proposed to devote a section of the discussion to this topic, no more will be said at present.

5.4.9 Fractography on Repeated Tension and Reversed Torsion Specimens

Under a conventional stereo light microscope, it was evident that fatigue cracks had originated from inclusions for all orientations of steel B tested in repeated tension.

With specimens cut from the T and Q axes, initiation invariably occurred at the same point relative to the axes. An inclusion whose longitudinal axis intersects the surface at some small angle was seen at the origin of all fatigue cracks. These angles were measured and found to lie between 5° and 35°. Inclusion lengths of up to

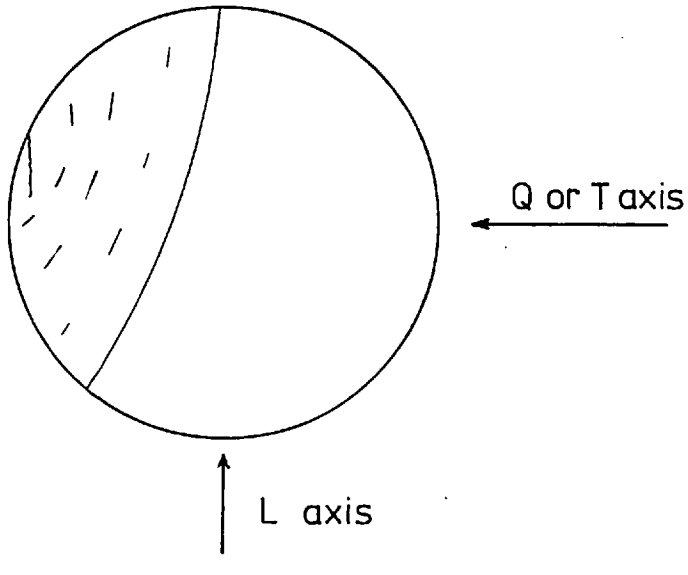

0.3 mm were measured, typical diameters being of the order of 35 μm. It could be seen that only a certain portion of these thread-like inclusions was involved in the initiation. For the T and Q directions, it appears that fatigue crack initiation occurs sub-surface as well as at the surface

of the specimen.

Specimens cut from the L direction were found to have fatigued from inclusions but without any preferred point of initiation, i.e. random with respect to the transverse directions.

Steel G repeated tension specimens were examined under the stereo light microscope, but no useful information was gained as the magnification available is too low and the depth of focus too small. Fatigue cracks were observed to initiate randomly with respect to the transverse axes of the specimen, irrespective of specimen axis.

With the vastly enhanced depth of focus available from the SEM, the origin and modes of fatigue crack initiation became clearer. Photomicrographs 5.28 to 5.34 show typical fatigue crack origins in steel B for each of the three specimen axes. Every crack can be traced to an inclusion at the point of initiation. *In situ* analysis revealed the same element present as for the thick cylinders of the equivalent material. To provide a permanent record of this fact, Photomicrographs 5.35 and 5.36 were taken. In Photomicrograph 5.35, the initiation point of a fatigue crack is shown at 240 times magnification. The following photomicrograph shows the same area being scanned for calcium using the selective analysis facility of the XRDA attachment. A further Photomicrograph 5.37 shows that notall cracks were initiated from inclusions. The origin of this crack can only be ascribed to the surface blemish or scratch not readily apparent on the photomicrograph.

Similar results were obtained for steel G and are shown in Photomicrographs 5.38 to 5.41. It was observed that the point of initiation and inclusions present at this point were easier to find than in the thick cylinder specimens. In general, the inclusions initiating fatigue cracks in steel G were smaller and more symmetric than in steel B

with more tendency for the whole inclusion to be involved in the initiation. Again, analysis showed that the range of inclusions found in repeated tension specimens and in thick cylinder specimens was identical.

The fracture surfaces of the reversed torsion specimens that failed were also investigated fractographically. These proved to be highly distorted, presumably due to mechanical attrition during crack growth. One initiation site was identified positively for steel B and is shown in Photomicrograph 5.42. The inclusion line lying sub-surface was analysed and contained manganese, calcium and aluminium with titanium, although this was not strongly present. No opinion is offered as to the influence of this inclusion line on the initiation of the fatigue crack in the axial shear plane of the specimen. A further photomicrograph is presented for the sake of its inherent interest (Photomicrograph 5.43). This shows the core region of a failed reversed torsion specimen and demonstrates quite nicely circular fatigue striations leading to final ductile failure. That fatigue crack growth striations are so consistent and easily visible at low magnification is merely a function of the very high stress intensity range over this area.

5.4.10 Qualitative Correlation of Results

It has been demonstrated by many workers (Ransom (1954), Cumming et al (1958), Frith (1954), Atkinson (1960), Hauser & Wells (1970)) that inclusions can initiate fatigue cracks in high strength steels. Further, the majority of the authors cited have noted that it is the composition of an inclusion which determines its ability to initiate a fatigue crack. Hard, non-deformable inclusions (at steel hot working temperatures), being far more likely to initiate fatigue cracks than inclusions which are deformed at steel working temperatures. The

explanation for this experimental observation is found in the works of Kiessling (1966,1968,1969,1972) and Brooksbank & Andrews (1968,1969,1972). The former author has postulated the existence of a critical size of inclusion capable of affecting the properties of a steel. Dependent on the property in question, this critical size is shown to be a function of the composition of the inclusion and its physical properties relative to those of the matrix steel. Kiessling bases his theory on conventional LEFM analysis since he observes that matrix cracks are invariably associated with certain types of inclusions.

Brooksbank & Andrews have vastly enhanced the applicability of these theories by calculating numerically the magnitude of textural or tesselated stresses which occur around inclusions. These stresses are shown to occur as a result of the different thermal expansion coefficients, Poisson's ratio and moduli of the inclusion and matrix. Using the mathematical model derived, these authors produced a chart of the stress-raising potential and its converse, void forming potential for a wide range of inclusions in a 1% carbon, chrome bearing steel. This chart is reproduced in Table 5.3.

From this chart, it is evident that calcium aluminates, calcium aluminium silicates, alumino silicates spinels and alumina are all potent stress-raisers. Conversely, manganese sulphide and calcium sulphide are thought to be innocuous or possibly even beneficial.

The results presented here agree excellently in qualitative fashion with the model of Brooksbank & Andrews. Calcium aluminates, spinels, complex alumino silicates and alumina have all been shown to have initiated fatigue cracks in plain specimens as well as in thick cylinders. In comparison with most other investigations reporting similar tendencies, the specimens used here were not finished to a rolling element standard nor

used at high tensile strength level. This point is significant in that it implies that inclusion initiated fatigue occurs at material strength levels and degrees of finish well below those previously found.

Therefore, on the basis of experimental observations, it is evident that the initiation and growth of a micro-crack from an inclusion may be controlling the fatigue process. Consequently, it is suggested that the fatigue limit of steels B and G is controlled by a crack propagation limit. That is, there exists a critical size inclusion from which micro-cracks will not propagate.

In attempting to explain the differences in fatigue limits observed between the two forgings and between different axes in these forgings, the applicability of this hypothesis is assumed. That matrix cracks are pre-existent in the steel surrounding hard, undeformable inclusions is not a prerequisite. Lankford (1977) has shown that for AISI4340 fatigued under a repeated direct stress regime, non-metallic inclusions like calcium aluminates debond and fracture after only one cycle of applied load. This author also found for this steel at $\simeq$ 1000 MPa tensile strength that, after debonding in the first fatigue cycle, slip bands containing micro-cracks could be detected at either side of the inclusion. Further fatigue cycling caused these micro-cracks to propagate towards the inclusion and ultimately away from it until becoming a normal stage II crack. This type of debonding behaviour has been predicted analytically for second phase particles by Jagannadham (1977) based on the differing shear stress moduli of matrix and inclusion. The tendency to inclusion debonding was shown to increase with shear modulus and size of the inclusion.

From the foregoing, it is evident that any parameter which does not discriminate between individual inclusion types cannot be invoked

to explain the differences in fatigue limits between steels B and G. Therefore, although the measured volume fraction of inclusions happens to be lower for the steel with the higher fatigue limit, this may only be fortuitous. The volume fraction of inclusions says nothing about the size or spatial distribution of inclusion types. It has been demonstrated by various workers (Baker et al (1976), Hauser & Wells (1970)) that fracture toughness decreases with increasing volume fraction of inclusions. Baker & Charles show that in systems where micro-void coalescence controls the fracture mechanism, the nature of the inclusion is not particularly significant. This implies that all inclusions are only weakly bonded to the matrix, a fact borne out by tensile testing to low strains and direct visual observation. However, the fracture process of micro-void coalescence involves the simultaneous nucleation and linking of voids in the matrix. The volume of material involved in the fracture process is therefore large. Parameters such as projected length of inclusions or volume fraction, which are 'average' values representative of the volume, would, therefore, be expected to give a measure of agreement. With fatigue crack initiation, the problems are distinctly different and more complex.

As demonstrated by Cummings et al (1958), at stress levels near the fatigue limit, one inclusion initiates the fatigue crack. A small volume of material is involved. Since the inclusion concerned is invariably the most severe stress-raiser for whatever reason, any parameter which measures 'average' properties cannot adequately describe this inclusion. Hence, the problem resolves itself into trying to describe an extreme case. Properties derived from measurements in the bulk of the material will never adequately characterise the extreme case unless the sampling involves the total volume of material.

Using the idea propounded by Kiessling (1966) that a critical size of inclusion exists, this must somehow be related to the fatigue limit of the steel as measured.

Consider first the inclusion populations of both steels. Steel B contains many elongated sulphides which are found not to be involved in the fatigue initiation process. This steel also contains stringers of duplex inclusions which are rotated into the working direction and fragmented by the forging. These inclusions are found to be the source of fatigue cracks.

Figure 5.6(a) shows a schematic representation of these stringer inclusions relative to the forging axes. The stringer inclusions can be crudely represented as ellipsoidal or "cigar shaped". The semi-axes are given by a_o, b_o and c_o, where b_o is equal to c_o to a first approximation.

Similarly, Figure 5.6(b) shows a schematic representation of the complex inclusions found in steel G. Here, however, only the spherical sulphide enveloped inclusions are shown as the smaller silica or silicates are too irregular in shape to be easily represented.

Confining attention initially to the plain specimens of steel B tested under repeated direct stress. It was found experimentally that specimens with their major axis in either the Q or T directions initiated cracks from segments of inclusions lying in the L direction. Therefore, the controlling or characteristic dimension is the $2b_o$ or $2c_o$ of Figure 5.6(a). Measurement of this dimension from fracture surfaces gave values of the order of 35 μm. Since there is a value of stress intensity range below which a crack will cease to propagate in a steel matrix, it should be possible to relate this 'stress intensity threshold', K_{th}, to the fatigue limit of the particular steel. Given that the inclusion

initiating the fatigue crack is very small in relation to the volume of material surrounding it, a stress intensity factor expression for a central crack in an infinite plate can be used, i.e.

$$K_I = 1.12\ \sigma\ \sqrt{\pi\ a} \tag{5.11}$$

where K_I = stress intensity (opening mode)

σ = applied stress

a = crack half length

For a fatigue loading situation where the applied stress varies from 0 to σ, equation (5.11) can be rewritten as:

$$\Delta K_I = 1.12\ \Delta\sigma\ \sqrt{\pi\ a} \tag{5.12}$$

where ΔK_I = range of stress intensity

$\Delta\sigma$ = range of applied stress

Then, if the fatigue limit is controlled by the existence of a non-propagating crack:

$$\Delta K_I = \Delta K_{th} = 1.12\ \sigma_{FL}\ \sqrt{\pi\ a}$$

where ΔK_{th} = range of stress intensity below which crack growth is infinitesimally small, i.e. << 1 lattice spacing/cycle

σ_{FL} = fatigue limited in repeated direct stress

The crack half length, a, is taken as half the typical inclusion width

plus 1 μm to account for the slip band crack occurring after the first applied load cycle. Hence, the predicted ΔK_{th} is of the order of 4.5 MPa.$m^{\frac{1}{2}}$. If a correction is added to the effective crack half length to account for the plastic zone at the embryo crack tip of:

$$r_p = \frac{1}{8\pi} \left(\frac{\Delta K}{\sigma_{0.2}}\right)^2 \tag{5.13}$$

where r_p = plastic zone size in direction of crack growth, assuming plane stress conditions

ΔK = range of stress intensity

$\sigma_{0.2}$ = 0.2% offset yield strength of material

the threshold stress intensity range is only marginally increased to 4.7 MPa.$m^{\frac{1}{2}}$.

This value is of the correct order for threshold stress intensity ranges for AISI4340 steels according to the works of Pook (1972) and Lankford (1977), who quote figures between 4 and 6 MPa.$m^{\frac{1}{2}}$.

Similarly, the calcium aluminate inclusions in steel G were found to range in size from 5 μm to 15 μm. It is likely that the largest inclusions will be responsible for fatigue crack initiation. Therefore, applying the same reasoning as given above yields a ΔK_{th} of 4.5 MPa.$m^{\frac{1}{2}}$.

This treatment is best justified by recourse to the defect shape at the free surface. For the case of the stringers oriented normal to the stress axis as in steel B, the intersection of inclusion and free surface appears as sketched below. The stress axis is normal to the inclusion length (which is normal to the plane of sketch).

Similarly, the roughly spherical inclusions of steel G intersect the free surface with approximately the same geometry. (The

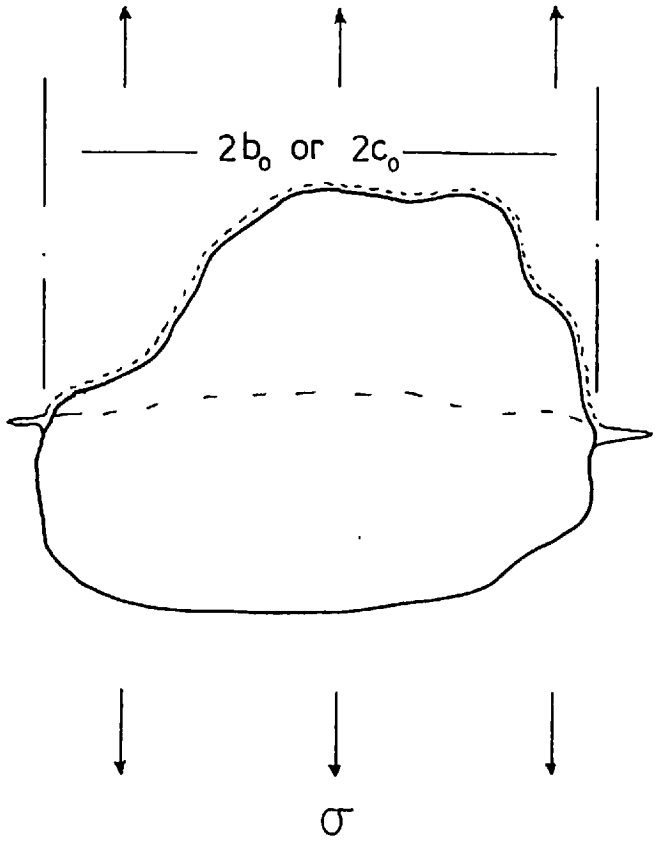

series of tests referred to in Section 3.7(b) were an attempt to measure the length of micro-crack at inclusion equators and hence characterise the early growth behaviour. It was found that the number of possible initiation sites was so large in steel B that the correct site was never chosen for replication. Conversely, in steel G, the number of possible sites was small and all appeared geometrically similar, making correct selection virtually impossible. The attempt was abandoned for this reason and because the collet specimen arrangement was awkward to use without damaging the specimen surface.)

The differences in fatigue limit inferred to exist in the transverse directions of steels B and G subjected to repeated tension may arise for one of two reasons. Either the semi-axes of the sectioned inclusions are not equal as assumed (i.e. $2b_o \neq 2c_o$), or the matrix has an inherently greater intrinsic crack growth resistance in one of the transverse directions. Within the limits of experimental measurements

made in this work, no significant difference in axis ratio could be found for hard inclusions in the transverse directions of steel B. The spherical inclusions of steel G were also measured carefully and no ovality found. Therefore, it must be concluded that if the difference in transverse fatigue limits is tangible, matrix crack growth resistance must be the controlling parameter.

It has also been shown that sub-surface fatigue crack nucleation occurred for the repeated tension specimens. Examination of a stress intensity factor expression for an embedded elliptic crack (Brown & Srawley (1972)) shows that the stress intensity is greatest at the minor axis of the ellipse. Although the inclusion has a finite dimension in the direction of applied stress, it is considered as an ellipse of low b/a ratio. It is expected that crack growth would initiate from the point on the periphery of the ellipse with the highest stress intensity. A simple fracture mechanics analysis would indicate fatigue initiation from the minor axis of the ellipse normal to the applied stress and this is observed in practice (see Photomicrographs 5.37 to 5.44).

Although this treatment produces good correlation for the transverse directions in the steels B and G, a difficulty is encountered for the longitudinal directions in these steels. The choice of a stress intensity factor is difficult. The inclusion stringers, although fragmented in the stress axis, are not such obvious crack initiators. Omission of the 1 μm term from the stress intensity expression used previously does not give a value of range of stress intensity consistent with other threshold values. Also, the omission of this term effectively negates a fracture mechanics analysis since a sharp crack no longer exists.

Inclusions are shown to initiate fatigue cracks in this orientation (Photomicrographs 5.39 and 5.40) but not with the same

consistency as for the transverse directions. Mechanical surface defects, scratches, nicks, etc., were also found to be the initiation sites of fatigue cracks, especially in steel G. Given that for steels B and G in the longitudinal direction the fatigue limits are 0.82 and 0.96 of the static offset yield stress, respectively (in repeated tension), the mechanism for fatigue failure may vary. For specimens with large hard inclusions, a crack propagation limit may be controlling, whereas for others matrix initiated crack propagation from undefined stress concentrators may be the controlling mechanism.

This analysis, although largely qualitative, does explain the observed variations in repeated direct stress fatigue for the two steels tested. The applicability of this analysis can best be judged by recourse to the reported literature. Haddad et al (1979) have shown that for very short crack lengths, the threshold stress intensity approaches the fatigue limit of a material. In order to satisfy their experimental results, these authors postulate that:

$$\Delta K_{th} = \Delta\sigma_{FL} \sqrt{\pi\ (L + L_o)} \qquad (5.14)$$

where ΔK_{th} = minimum stress intensity range which gives rise to crack growth

$\Delta\sigma_{FL}$ = stress range at fatigue limit

L = crack length

L_o = an empirical constant

Other authors (Frost (1974)) have also noted that for mechanically introduced short cracks, the ΔK_{th} appears to vary with crack length. The introduction of the empirical term, L_o, satisfies the physically reasonable

criterion that ΔK_{th} is a material constant independent of crack length. It is thought by Haddad et al (1979) that the empirical constant is a measure of the flow resistance of surface grains due to lack of constraint. However, it can equally well be argued that it is a measure of the plastic zone ahead of the crack. The similarity between the expression given above and that used here to correlate cracks propagating from inclusions are obvious. In this work, a border crack of 1 μm was assumed to be present, but this will probably vary as a function of inclusion size and shape. Large inclusions giving deeper border cracks and vice versa.

Sufficient experimental evidence has been presented to justify the hypothesis that a mode I propagation limit controls the fatigue limit of the steels tested in this work. It is, however, evident that an attempt must be made to define the limits of applicability of this hypothesis.

Of the many factors that have been shown to affect the fatigue limit, residual stress and surface finish are the most relevant for low alloy steels. In attempting to relate the ΔK_{th} value from tests using fracture mechanics type specimens with the fatigue limit in plain polished specimens, these factors must be considered. The ΔK_{th} value derived from a crack propagation test where the stress intensity is incrementally lowered until no crack growth is observed is not dependent on surface finish but may be a function of residual stress. Conversely, the fatigue limit in plain polished specimens can easily be determined by both variables.

In this work, the fatigue limit of plain polished specimens has been found to be controlled by crack propagation from inclusions. All the specimens had been stress relieved in vacuo at 590°C for 1 hour. This heat treatment effectively removes residual stress induced by

polishing or carried over from the steel in its massive form. The effect of surface finish is more difficult to judge but it is the opinion of the author that this is strongly related to tensile strength level. At tensile strength levels of less than 1000 MPa for low alloy steels, it is felt that fine turned surface finishes or better, i.e. $\leq$ 0.75 μm CLA, do not affect the fatigue limit.

Therefore, it is justifiable to expect that that an inclusion controlled fatigue limit mechanism should exist for the majority of well finished plain engineering components.

5.4.11 Quantitative Correlation of Results

It has been shown in the previous sections of the discussion that the fatigue limit of plain specimens is controlled by a mode I crack propagation limit. Identical shape and composition inclusions are found at the initiation sites of fatigue cracks in both plain specimens and thick cylinders. Therefore, it would seem likely that a similar fatigue criterion applies to thick cylinders subjected to a repeated stress regime. This idea has also been proposed by Frost & Sharples (1978) and indirectly by the original workers in this field (Morrison, Crossland & Parry (1956)). In this work, the physical evidence is presented to justify the assumptions made by Frost & Sharples in their treatment. Further, it will be shown that this idea is not confined to inclusion initiated fatigue cracks but can be applied quite generally to defects of any shape, irrespective of material anisotropy.

The fatigue limit in plain specimens of steels B and G is controlled by defects lying normal to the principal stress axis. For thick cylinders of these steels, the maximum principal stress is the hoop stress at the bore of the cylinder. Therefore, the fatigue limit in

repeated pressure is related to the fatigue limit of plain specimens orientated in the tangential direction to the cylinder bore.

For a plain cylinder, we can write that at the fatigue limit:

$$\Delta K_{th} = Y_c \, \sigma_\theta \sqrt{\pi \, b_c} \tag{5.15}$$

where ΔK_{th} = range of stress intensity below which a crack will not propagate

σ_θ = tangential stress range at bore at fatigue limit

b_c = defect characteristic length or depth

Y_c = shape factor describing the defect geometry in thick cylinders

In the case of the plain cylinder, σ_θ must be taken as the nominal hoop stress plus the pressure acting in the defect. Consider a section through a cylinder containing a line defect orientated parallel to the cylinder axis. The defect (exaggerated for clarity) is subjected to a hoop stress, σ_H, dependent only on cylinder dimensions and pressure plus a stress equal to the internal pressure. From the principle of linear superposition, these stresses are additive. Hence:

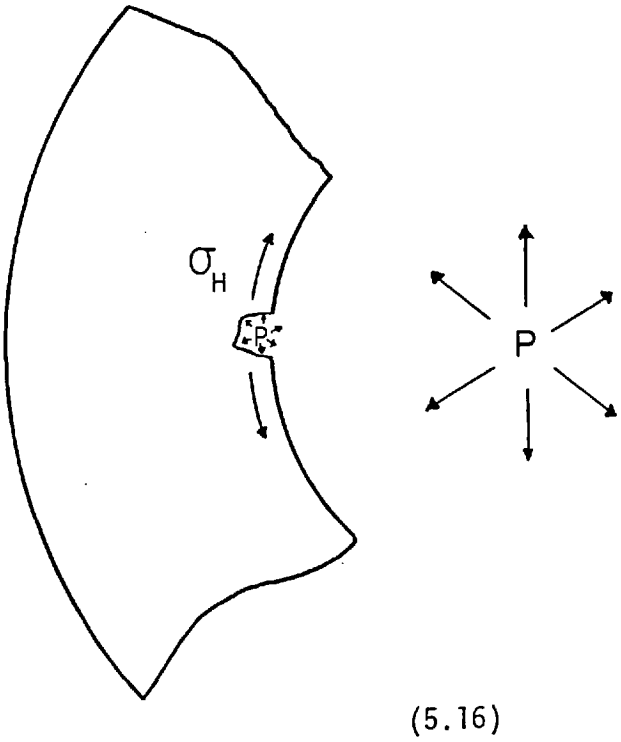

$$\sigma_\theta = \sigma_H + P \tag{5.16}$$

where σ_H = Lamé hoop stress at the bore given by $\sigma_H = P\,(D^2+1/D^2-1)$. For the repeated tension plain fatigue specimen, we can write that at the fatigue limit:

$$\Delta K_{th} = Y_p\,\sigma_p\,\sqrt{\pi\,b_p} \tag{5.17}$$

where ΔK_{th} = range of stress intensity below which a crack will not propagate

σ_p = repeated tension plain fatigue limit

b_p = defect characteristic length or depth

Y_p = shape factor describing the defect geometry in a plain specimen

Now, since the shape of defects or inclusions in thick cylinders is the same as that in plain specimens:

$$Y_c = Y_p \tag{5.18}$$

and:

$$b_c = b_p \tag{5.19}$$

Therefore, as the same material in the same orientation relative to the defect characteristic dimension is being considered, equations (5.15) and (5.17) may be combined to give:

$$\sigma_\theta = \sigma_p \tag{5.20}$$

In essence, equation (5.20) implies that the fatigue limited in repeated tension plain specimens is identical to that of the thick cylinders subjected to repeated internal pressure, providing the effective tangential

stress range is considered for the thick cylinder geometry.

To test the applicability of this relationship, the results of the repeated pressure and repeated tension fatigue tests for steels B and G were used to construct Figure 5.7. The measured range of pressure at the fatigue limit is shown plotted against the expected pressure range predicted using equation (5.20) (assuming that the lower transverse fatigue limit in repeated tension controls the behaviour of cylinders with axis in L direction). The agreement is excellent with the exception of cylinders of steel B cut such that their longitudinal axis is in the Q or T direction of the forging. This discrepancy is not altogether surprising in that fatigue crack initiation is controlled by defects stressed parallel to their major dimension. A great deal of scatter in the results was observed (see Figure 4.33) and the fatigue limit as drawn is probably optimistic. If this fatigue limit in repeated tension were reduced by 8%, the predicted and measured fatigue limits in repeated pressure would coincide exactly. This fact not withstanding, the measure of agreement is very good considering the extreme variations in other mechanical properties of the two steels.

(a) Comparison with previous results

It is fortunate that most previous authors in this field have also attempted to quantify the degree of fatigue anisotropy in their experimental materials. On the debit side, nearly all these reported investigations have been carried out using reversed bending fatigue with zero mean stress to investigate the effect of material anisotropy. From the foregoing, it is clear that a repeated stress regime is the dominating factor in determining the fatigue limit in thick cylinders subjected to repeated internal pressure. Therefore, in comparing the results of

previous thick cylinder tests, transverse repeated direct stress fatigue limits have to be obtained from transverse reversed direct stress data. A dilemma exists in deciding which mean stress criterion to use. Therefore, Figure 5.8 has been constructed using both the Goodman and Gerber criteria to illustrate the variation.

The published results from most previous thick cylinder repeated pressure fatigue tests are shown in Figure 5.8. These results cover a wide range of cylinder diameter ratios, materials and tensile strengths. In this figure, the experimentally determined fatigue limits are plotted against the predicted fatigue limits according to equation (5.20). The fatigue limits are given in terms of the effective direct stress range at the bore, $\Delta\sigma_H + \Delta P$. From equation (5.16), it is evident that the effective direct stress range is twice the Lamé bore shear stress range, since:

$$\Delta\sigma_H + \Delta P = \frac{2\Delta P\, D^2}{D^2 - 1} = 2\Delta\tau \qquad (5.21)$$

In Figure 5.8, the open points refer to transverse repeated direct stress fatigue limits derived using the Gerber criterion, whilst the solid points refer to values derived using the Goodman criterion. The majority of previous results fall on or under the predicted line when the Goodman criterion is used. Hence, it is inherently safe to use this criterion in conjunction with the theory proposed, since the predicted results never exceed the experimentally determined fatigue limits.

It is of interest to note that the best agreement occurs for the ferrous alloys typical of pressure vessel steels, such as AISI4340, EN25 and EN26. Since for uniaxial fatigue tests on most ductile materials the effect of mean stress is usually found to be intermediate between the Goodman and Gerber criteria, this agreement would be expected. What is

perhaps surprising is that metals such as aluminium and titanium which do not show distinct fatigue limits also correlate well on this basis.

In Table 5.4, the predicted fatigue limits derived using the Goodman criterion are tabulated, together with the experimentally determined fatigue limits for thick cylinders of various materials. The differences between the predicted and experimental fatigue limits are given for the effective hoop stress and the more conventional shear stress criteria. With the exception of the austenitic stainless steel tested by Morrison et al (1960), agreement is good for the effective hoop stress criterion. It is evident that the shear stress criterion also gives good correlation with the exception of the EN31 steel.

On the basis of this comparison between the criteria, there is little to say which is the more useful. However, when some of the more anomalous results of fluctuating internal pressure fatigue tests are considered, the superiority of the effective hoop stress criterion can be seen.

(b) Further comparisons

Parry (1956) has given the results of four tests carried out on thick cylinders (D = 1.4) of EN25T with the bore protected by a coating of rubber solution. Tested under repeated internal pressure, these cylinders exhibited very high endurances at large pressure ranges. No explanation based either on the shear stress criterion or any other grounds was given to explain this anomaly.

On the basis of the direct stress controlled fatigue failure criterion, these results are predicted.

The effect of coating the bore with rubber solution is to stop fluid pressure entering a defect or an inclusion. Therefore, the fatigue

limit of such protected cylinders will occur when the range of bore hoop tension is the same numerically as the transverse direct stress fatigue limit of the material. Using the values given by Parry (1956) for this material, the fatigue limit would be predicted to occur at a range of nominal bore shear stress of 382 MPa. Not enough results are presented to define the fatigue limit accurately, but the cylinder which endured 1.2 million cycles before failure must be close to the fatigue limit. This cylinder was cycled at a bore shear stress range of 386 MPa, slightly in excess of the predicted fatigue limit.

Similarly, Haslam (1969a,1969b,1971) has tested cylinders of EN26 with protected bores. He found that this material had a repeated tension fatigue limit of 575 MPa. This would imply a predicted bore shear stress at the fatigue limit of 339 MPa. Experimentally, the fatigue limit was found to occur at a nominal bore shear stress range of 0 to 335 MPa.

The applicability of a direct stress controlled fatigue criterion is not limited to simple monoblock cylinders. Burns & Parry (1967) have published results of repeated internal pressure fatigue tests using compounded cylinders. These authors found that compound cylinders designed to give a bore mean shear stress of between -15 and +46 MPa at full internal pressure had a fatigue endurance of 2×10^7 cycles at a maximum bore shear stress of 402 MPa. Since the material in contact with the fluid is cycling through approximately equal ranges of compression and tension (i.e. mean stress $\simeq$ 0), the fatigue limit should be related to the reversed transverse direct stress fatigue limit. This is found to be the case, the fatigue limit in reversed bending being $\pm$ 402 MPa.

From the foregoing, it is clear that the fatigue limit of cylinders of all dimensions can be predicted from a knowledge of the

transverse direct stress fatigue properties. The criterion developed here on the basis of simple stress analysis and experimental findings is more physically realistic than a shear stress criterion, although the two give identical results in certain situations. As a conclusion to this section of the discussion of results, it is informative to compare the various fatigue failure criteria for internally pressurised cylinders.

5.4.12 Comparison of Fatigue Failure Criteria for Internally Pressurised Cylinders

The critical range of shear stress criterion for fatigue failure in thick cylinders arose naturally from the good correlation found for cylinders of differing diameter ratio. It was assumed by the early workers in this field that fatigue failure is a consequence of plasticity occurring in a material. It is well known that the yielding of ductile metals is controlled by shear stress. The onset of plasticity due to repeated load application should therefore also be shear stress controlled. Further, it was shown that the state of stress at the bore of a thick-walled cylinder could be resolved into a shear stress plus a superimposed triaxial tension. By analogy with other stress systems where the hydrostatic stress component can be shown to have no effect on the yield point, the effect of triaxial tension was initially assumed to be unimportant. However, from practical tests, it was found that the allowable range of bore shear stress was approximately half the range of shear stress from a reversed torsion test. This anomaly was never satisfactorily explained, especially as the magnitude of associated triaxial tension appeared to have no effect on the fatigue limit of thick cylinders.

If a shear stress criterion is controlling in the fatigue

process, then fatigue cracks would be expected to initiate on planes of maximum shear stress. In the thick cylinder, these planes are parallel to the bore and inclined at 45° to tangents drawn to the bore. It is often stated that this is indeed the plane on which fatigue cracks initiate in thick cylinders because of the existence of large shear lips. However, when the initiation site is examined on the micro-scale, it is found that the initiation plane is invariably that containing the radial and axial directions. Remote from the initiation site, shear lips can be formed during fatigue crack propagation because of the free surface effect.

The limitations of a critical range of shear stress criterion have been exposed in the previous section. It is, however, worth stating that the most obvious limitation has never been given serious attention. From the work of Chodorowski (1956), it was evident that material anisotropy had little effect in a reversed torsion fatigue test. This implied that cylinders cut from differing axes relative to the working direction of an ingot should show similar fatigue limits. It is strange that this point was never pursued by the workers at Bristol University or at other institutions. From the results presented in this work, for steel B, the fatigue strength of a thick cylinder is seen to be strongly dependent on material anisotropy. An earlier investigation of this anomaly would have led to a better understanding of the mechanism of fatigue failure in internally pressurised cylinders.

Haslam (1969) has proposed a fatigue failure criterion similar to that developed here from the ideas of Frost & Sharples (1978). Using the idea of an effective hoop stress, Haslam analysed the results of Morrison et al (1956,1960) and others to derive an empirical expression for this stress:

$$\sigma_e = P \left(\frac{D^2 + 1}{D^2 - 1} + \frac{5}{D^2 + 1}\right)$$

where σ_e = effective hoop stress

P = internal pressure

D = diameter ratio

This expression is supposed to simulate the effect of the pressurising medium entering defects or embryonic cracks. On close examination, it can be seen that the so-called "oil effect" is diameter ratio dependent. At low diameter ratios, the effect of pressurising fluid is over-estimated by up to ≈ 23% and for high diameter ratio cylinders, the effect is under-estimated by up to 15%. However, in the range of diameter ratios from 3 to 5, this expression produces good correlation when used in conjunction with the transverse repeated direct stress fatigue strength of a material.

5.5 IMPLICATIONS OF A DIRECT STRESS CONTROLLED FATIGUE CRITERION

If it is accepted that the fatigue behaviour of low alloy steels is controlled by a mode I crack propagation limit, the design of pressurised components can be optimised.

Where high cycle fatigue strength is the governing design criterion, various methods are available to improve fatigue strength. Compound construction, autofrettage, and surface treatments, such as nitriding, have all been used successfully. There are, however, applications where expense or sheer physical size prevent the implementation of these techniques in otherwise plain cylindrical vessels.

Knowing that fatigue failure is controlled by the ingress of fluid into defects, augmenting the stresses developed normally, a simple method of improving fatigue strength is obvious. If the fluid pressure can be excluded from the bore surface, the fatigue strength of a plain cylinder can be improved by a factor:

$$\frac{\sigma_H}{\sigma_H + P} = \frac{2D^2}{D^2 + 1}$$

For low diameter ratios of, for example, 2, this represents an increase in allowable pressure range in repeated pressure of some 60%. As $D \to \infty$, the theoretical allowable pressure range is doubled in comparison with cylinders whose bore is in contact with the pressurising medium. Conversely, the diameter ratio to withstand a given pressure range indefinitely can be reduced substantially. This can often mean the difference between an expensive multi-layer construction and a simpler monoblock construction. For large vessels, section size becomes the limiting factor as the minimum properties required can only be attained with expensive higher alloy content steels. Therefore, any technique which offers the possibility of reducing wall thickness is welcomed by vessel manufacturers.

In the same manner as coating the bore of a cylinder with rubber solution removes the pressurising medium from contact with the bore layers, it is possible to insert thin metallic liners. Ideally, fatigue failure in the liner should also be avoided and this is best accomplished by using a liner of a low modulus material such as beryllium copper, aluminium or titanium alloy. The liner takes only the radial load component and is effectively strain cycling. Correct choice of material and strength level should enable the liner to work indefinitely. It is, however, fairly easy in large vessels to arrange a helical groove at the bore of the monoblock such that if the liner does fail, the contained medium escapes in a controlled fashion, indicating the failure.

Attempts to demonstrate this method of achieving increased fatigue strength experimentally met with a notable lack of success, largely for technical reasons. The first approach consisted in taking a thick

cylinder of diameter ratio 2.55 and attempting to apply a rubber coating to the bore. The rubber solutions currently available do not appear to be remotely similar to those used by Morrison et al (1960). All attempts to spread, dip, smear or paint the solution were unsuccessful. Complete surface coverage was never achieved without air bubbles or holidays appearing. Since the opinion was that the solution was too viscous, heat, solvents and vigorous stirring were also tried to no avail. It is suspected that the previous authors were in possession of a neoprene solution which is now non-obtainable due to the introduction of synthetic alternatives.

The second method tried was to insert thin wall copper tube into a specimen to form a close fitting liner. It was realised from the outset that the copper tube would probably be strain cycled beyond its elastic limit. This fear was realised as fatigue failures were recorded at the same pressure range and endurances as for unprotected cylinders. Annealing the cold drawn copper tube brought some improvement. One specimen was successfully cycled for 0.75×10^6 cycles at a high range of pressure before failure occurred. Photograph 5.44 shows the fatigue crack surface of this specimen. The sequence of events leading up to the fast fracture of the tube can only be surmised. It is suspected that the copper tube failed at an early stage in the test. Fatigue failure of the monoblock occurred according to the "normal" criterion and a crack was initiated. This crack then propagated until the liner shifted, effectively excluding oil from the crack. Further propagation of the fatigue crack occurred until a critical size was reached when fast fracture intervened.

Previous experience with this cold reduced high pressure tubing had never indicated that an unstable crack mode could occur. All fatigue

failures for unprotected cylinders had been by a "leak before burst" mode. The only explanation that can be given is as follows. When the pressurising medium is absent from the crack face, the stress intensity at the crack tip periphery is reduced. Consequently, the plastic zone size associated with the crack tip is reduced. If the plane strain fracture toughness of the material is such that the cylinder wall thickness is approximately the critical crack depth, fast fracture does not occur normally because of interference between the plastic zone and the outer free surface. With a reduced plastic zone size, conditions at the crack periphery, especially in the longitudinal direction, approach more nearly a plane strain condition and fast fracture occurs.

This point was not pursued because of the technical problems and expense in both time and money needed to fully elucidate the problem.

5.6 FATIGUE CRACK GROWTH IN STEELS B AND G

5.6.1 Introduction

Although it has not been previously stated, a secondary objective of this work is to compare fatigue crack growth in air with that found in the internally pressurised thick cylinder geometry.

There is every reason to hope that fatigue crack growth data derived in air might be used to predict the fatigue life of internally pressurised cylinders. Such a simplification would considerably ease the life of a designer and remove some of the restrictions imposed by conservative design codes. However, there is very little positive evidence to justify this assumption.

Haslam (1971,1972) has presented methods based on a LEFM approach which nominally show very good correlation with actual endurances recorded for repeated internal pressure fatigue tests. On detailed

examination, the method used is more than a little suspect, depending entirely on correct choice of material constant, C_o, and exponent, n, in the Paris law. Further, Haslam's analysis assumes that these material constants are independent of orientation, yield strength and material cleanliness (Shih & Araki (1973), Evans et al (1971), Heiser & Hertzberg (1971), Hauser & Wells (1970), Thornton (1972), Priddle (1977)). Similarly, in applying a stress intensity approach to fatigue crack growth, Haslam is effectively denying the influence of the stress biaxiality in the cylinder geometry. Recent work suggests that stress biaxiality does influence fatigue crack growth rates (Hopper & Miller (1977), Pook & Holmes (1975)).

In view of the considerable uncertainty associated with this problem, it is apparent that some useful information might be gained by comparison of crack growth in air with that in a pressurised environment.

5.6.2 Crack Growth in Air: Steel B

The crack growth rates measured in air for steel B are plotted in Figure 5.19. These results are also summarised in Table 5.5, together with the range of applicability of the data generated.

From Figure 5.19, it is evident that a size effect exists for steel B. Crack growth rates measured in 45 mm thick compact tension geometry specimens with LQ orientation being approximately twice those measured in a heavily side-grooved double cantilever bend specimen (crack width = 8.8 mm). This type of behaviour is consistent with the enhanced conditions of plane strain in the thicker specimen but does throw doubt on the general applicability of side-grooved specimens proposed by Green & Knott (1975).

The stress intensity range dependence for crack growth in the LQ orientation varies between 2.5 and 3.0 dependent on thickness. These values are lower than those measured in the transverse directions, which

are typically of the order of 4. It is, however, surprising to see that at low values of stress intensity range, the crack growth rate is considerably lower in the transverse orientations.

A mechanism to explain this anomaly is found in the work of Evans et al (1971). These workers found that for EN24 (directly comparable in composition to AISI4340), the effect of large impurity content was to reduce crack growth resistance in air. It is possible that the effect is confined to the LQ or LT orientations, thereby enabling crack growth to occur at much lower ranges of stress intensity than for the other orientations. That this effect might be confined to the LQ or LT directions is not wholly unrealistic in that, as will be shown later, the lower exponent for this orientation is a function of inclusion orientation. Evans et al (1971) ascribed this enhanced crack growth rate in air to moisture induced changes in crack propagation mode. High purity EN24 was not found to exhibit the same phenomenon.

5.6.3 Crack Growth in Air: Steel G

The results of all crack growth tests in air for steel G are shown in Figure 5.10. Two points are worthy of attention. Firstly, it is again found that the QT orientation exhibits higher crack growth rates than the TQ orientation but with approximately the same stress intensity range dependence. This behaviour was also found for steel B (see Figure 5.19). Secondly, cracks growing in the L direction, i.e. QL or TL orientations, exhibit higher stress intensity range dependence. The effect of enhanced purity therefore appears not to influence the stress intensity range dependence for crack growth in the working direction.

With the exception of the two L direction orientations, the crack growth rate dependence is consistent, although absolute crack growth rates vary as noted above. A further anomaly not apparent in Figure 5.10 can be seen by reference to Figure 4.30.

This fatigue crack growth test in air for an LQ orientation in steel G is shown with a range of stress dependence and correlation coefficients. The actual test was carried out over a period of 3 days. Since crack growth measurements were being made optically, the test was stopped at night. Close inspection of the crack growth rate versus stress intensity range graph shows the experimental points conform to three distinct curves. Starting at low ΔK, there is a region of high stress intensity range dependence followed by a period of lower dependence. This pattern repeats itself three times. Subsequent re-evaluation of the crack growth data proved that the periods of high followed by low stress dependence conform exactly to the start and finish of testing each day.

It is known with certainty that the specimen was not left under a static load overnight. The enhanced fatigue crack growth rate on restarting can, however, be easily explained by the occurrence of environmental effects at the highly energetic crack tip. What is inexplicable is that the subsequent crack growth resumes at the lower stress dependence (n = 2.5) but at higher absolute crack growth rate. In effect, it would appear that stopping and restarting the crack growth test changes the intercept significantly. Therefore, the crack growth exponent is quoted for the two extremes. During steady uninterrupted crack growth, the stress dependence is 2.5. With interrupted crack growth, the overall stress dependence rises to 4.0. The latter value is taken for the purposes of comparison with other orientations, since it leads to a conservative result. This behaviour was only noted for LQ orientation of the specimen in steel G, although this does not discount its existence for other orientations.

5.6.4 Comparison of Crack Growth Rates in Air for Steels B and G

If the results for all orientations of crack growth in air for

steels B and G are compared, they appear as in Figure 5.11. Both steels exhibit approximately equal stress dependence but steel B gives measured crack growth rates a factor of 2 greater than steel G, over most of the applicable stress intensity range. At high stress intensities (> 50 MPa.$m^{\frac{1}{2}}$), the measured crack growth rates appear to converge, but whether this trend would be maintained to even higher ΔK is a subjective point.

The experimental observation that steel B gives the higher absolute crack growth rates is reflected in a comparison between the effect of mean stress between steels B and G.

Figures 4.27 and 4.28 show experimentally measured crack growth rates at a stress ratio of 0.5 in air for steels B and G, respectively (QT orientation). For steel B in this orientation, the effect of mean stress is to dramatically increase the absolute crack growth rate as well as the stress dependence. The addition of a mean stress for steel G is to modestly increase the absolute crack growth rate without altering the stress dependence appreciably.

Thus, steel B is shown to have the inherently greater crack growth rate at a given range of stress intensity, the difference becoming greater with increasing stress ratio. These differences can be successfully explained by recourse to the relative volume fraction and shape of the inclusion populations in the two steels.

It is a well documented phenomenon that the purity of low alloy steels of this type controls the fracture process (Evans et al (1971), Cox & Low (1973), Hahn & Rosenfield (1973), Priest (1971)). Fatigue crack propagation is found to be similarly influenced (Thornton (1972), Evans et al (1971), Ritchie & Knott (1973)). In the case of fatigue crack propagation in air, it has been suggested that crack growth rate is controlled by the formation of ductile striations (Knott (1973)). It can

therefore be shown quite simply that for fatigue crack growth under plane strain conditions, the crack growth rate should be proportional to the stress intensity range raised to the power 2. Experimentally determined crack growth rates invariably show stress dependence of a higher order. The disparity is explained by the occurrence of other fatigue crack fracture micro-mechanisms simultaneously with ductile striation formation. Inclusions or second phase particles which are not strongly bonded to the matrix act as easy crack propagation paths. Therefore, the number and orientation of inclusions traversed by a growing fatigue crack influences the overall crack growth rate.

Heiser & Hertzberg (1971) have shown for a variety of micro-structures that the macroscopic crack growth rate varies with specimen orientation. For a rolled plate of C-Mn steel, they found that crack growth was greatest in the QL orientation, intermediate in the LT orientation and least in the TQ orientation. The differences in crack growth rate becoming more marked with increasing range of stress intensity.

Steel B has the larger and more highly orientated inclusion population and would therefore be expected to show higher crack growth rates than steel G. This is found to be the case but, in contrast to Heiser & Hertzberg's results, there is also a distinct difference in crack growth rates at low ranges of stress intensity. This is thought to be a function of the environmentally influenced crack propagation micro-mechanisms found for steels like EN24 by Priddle (1977) and Ritchie (1973).

It should be pointed out that fatigue crack propagation is probably influenced by all inclusions irrespective of nature. It is, however, probable that a highly orientated inclusion population of, for example, MnS, as found in steel B, has more influence than total volume fraction of inclusions (Thornton (1972)).

Whilst the influence of inclusions in enhancing fatigue crack

propagation cannot be questioned, it does not provide a complete description.

Steel G has an inclusion population which is virtually isotropic, but this steel still displays reproducible differences in crack propagation rate as a function of orientation. It is probable that the matrix crack growth resistance is nominally lowest for growth in the L direction (see Figure 5.10). Since most impurity elements, such as P, As, Sb and Sn, tend to concentrate at the prior austenite grain boundaries, it can be argued that there may be an extended plane of weakness in this direction. If this were the case, then evidence of cracking at prior austenite grain boundaries should be found on the fracture surface.

In order to check this theory and to substantiate the role of inclusions in the fatigue crack propagation process, Ni plated sections of fracture surfaces were examined optically. Fracture surfaces from fatigue crack growth tests in air and in the form of thick cylinders were examined to see if any difference in fracture mode could be found.

5.6.5 Fractography of Fatigue Crack Growth in Steels B and G

Linear analysis of fracture surface sections in the radial direction, from cylinders of steel B, showed that 2.2% of the fracture length was associated with MnS inclusions in the L direction (Photomicrograph 5.45). Radial sections of a TQ fracture surface had 1.2% of the fracture length covered by MnS inclusions (Photomicrograph 5.46).

Fracture planes with an LT orientation were observed to have no inclusions visible at the fracture surface section. However, for this orientation and intermediate orientations, such as LQ/QL, there is considerable evidence of crack blunting. Photomicrograph 5.47 shows the cusp-like fracture surface always found for crack growth normal to the L

direction. These cusps are thought to be generated by the following mechanism. The crack face advances towards an elongated inclusion lying normal to the crack plane. Due to the state of triaxial tension ahead of the crack tip, the inclusion ruptures and debonds. Void growth occurs spherically around the inclusion line. The intervening material between crack tip and inclusion fails by tensile instability after more necking down to leave a blunted crack. Further crack tip growth can then occur only when a sharp crack is re-established at the opposite side of this blunt notch.

A similar mechanism is observed to occur for crack planes slightly removed from normal to the L direction. A portion of the crack tip intersects an inclusion line lying at an angle to the normal. Delamination occurs and this portion of the crack follows the inclusion line direction to its end. The crack tip is then blunted since no more easy fracture path exists. The surrounding crack front has remained in a plane normal to the maximum direct stress and is being held back by this portion of crack front lying out of plane. The blunted segment of crack front must therefore shear back into the major plane before crack growth can continue. This behaviour is observed for the intermediate orientations and leads to a characteristic sawtooth crack plane section (Photomicrograph 5.48).

The major influence on crack growth propagation mechanisms in steel B was found to be the highly directional type I MnS inclusions. Although other inclusions were found on fatigue fracture surfaces, the elongated sulphides are shown to occur ten times more frequently than on a purely random fracture surface line. It must therefore be concluded that this species controls the crack growth dependent on crack orientation. Similar findings for fatigue cracks grown in air were obtained for steel B.

The difference between crack growth in air and that obtained in thick cylinders is not obvious but some fractographic evidence does exist.

Photomicrograph 5.49(a-f) shows a series of photographs taken of a TL orientation fatigue crack in a thick cylinder. Crack growth is from bottom to top. The family of MnS inclusions which run through the complete series are exactly in the radial L direction. To either side of the inclusion line, there are fatigue striations visible at intervals. In general, these striations are all angled towards the inclusion line. Whilst only circumstantial, this would indicate that the crack front leads along the inclusion line. For a similar orientation of specimen fatigued in air, this behaviour could not be found at any position. It is proposed that on a very local scale, a pressurised crack can advance more quickly along an inclusion line of the type shown. Whether this behaviour repeated over the entire crack front noticeably affects the overall crack growth rate will be a function of the amount of inclusion orientation in the radial direction.

Although the same procedures were adopted to investigate fatigue crack fracture sections from steel G as a function of orientation, no distinction could be made. Inclusions were not found in any orientation of fracture plane section. Sections cut from fatigue cracks generated in air and in cylinders were identical with no variation in profile as a function of orientation.

5.6.6 Prediction of Fatigue Endurance in Thick Cylinders

In attempting to predict the fatigue endurance of a component, the most commonly adopted approach is to integrate crack growth rate data between limits of crack length. Where experimental data exist for the crack growth rate of a particular steel orientation, they are invariably given in the form of a Paris law correlation. Macroscopic crack growth rate is plotted against the range of stress intensity at the fatigue crack. In this way, it is hoped that crack growth rate data derived in one specimen geometry can be related to a crack growing in a differing geometry. This approach is valid for cracked bodies where a crack is growing under the influence of a moderate range of stress intensity. Experimental data can be used within its range of applicability to predict the time or number of cycles of applied load for the crack to grow some finite length.

When a total fatigue endurance is required, the applicability of experimental data is dubious. A fatigue crack initiating from some internal flaw or defect in a component spends the greater proportion of the total cyclic life growing at a very low range of stress intensity. As the crack grows, the stress intensity range increases but the crack growth rate increases exponentially. With low alloy steels, the Paris law formalism is only strictly valid over a range of stress intensity (see Figure 2.1) which begins well above the material ΔK_{th}. Consequently, a large part of the total endurance is spent propagating a crack in a region where experimental values are either lacking or of low accuracy.

Therefore, the integration of the crack growth rate data obtained in air for steels B and G would not be expected to give an accurate prediction of endurance in the mortal region for thick cylinders of these steels.

As noted in the previous sections, steel B in the form of thick cylinders exhibited preferred planes of crack initiation. For cylinders with their longitudinal axis taken from the L direction in the forging, fatigue failure was most frequently observed for the QT orientation. Therefore, crack growth rate data for this orientation in air was integrated between the limits of crack growth to provide the total endurance, assuming the applicability of the Paris law formalism over the entire range of stress intensity encountered. Initial crack length was taken as 17.5×10^{-6} metres since this represents the average radial depth of a bisected stringer inclusion in this orientation. Similarly, final crack length was taken as 12.5×10^{-3} metres since this is the total wall thickness available for crack growth in the cylinders of diameter ratio 3.

The results obtained are shown in Figure 5.12, together with the experimental values. Also shown is the predicted fatigue limit based on the mode I propagation limit for this orientation of cylinder.

In the mortal region, the predicted and experimental endurances are apparently in good agreement. This degree of correlation is considered to be purely fortuitous, given the likely accuracy and range of applicability of the experimental crack growth rate data developed in air. Unfortunately, no experimental values were obtained in air for crack growth in the TL or QL orientations. Therefore, the accuracy of extrapolated endurances in the remaining cylinder orientations cannot be checked.

For steel G cylinders with their longitudinal axis in the L direction of the original forging, no preferred initiation plane was observed. Therefore, crack growth can occur in the QT plane, TQ plane or any plane between these. The predicted values of fatigue endurance are therefore shown for both orientations (Figure 5.13). In this instance,

the experimental values of endurance fall between those predicted from the data derived in air.

Taken at face value, the predicted results for the orientations given correlate impressively. However, the stress intensity factor expression for an edge crack, $K_I = 1.1\ \sigma\ \sqrt{\pi\ b}$, was used to derive the endurances shown. The effective hoop stress, $\sigma_H + P$, was used to describe the stress acting across the crack plane. It is difficult to see how this stress intensity factor expression can accurately simulate the biaxial crack growth occurring in the thick cylinder geometry, albeit in the radial direction.

When the more realistic three-dimensional stress intensity expression (Tan (1979)) is used, the predicted endurances are increased by an order of magnitude. Therefore, it is thought that the agreement found using the edge crack stress intensity expression is coincidental. That Haslam (1972) also finds good agreement for fatigue life predictions using arbitrary material constants and stress dependence in the Paris law integration is also indicative of the compliant nature of the edge crack stress intensity factor expression. This can be most easily appreciated when it is realised that doubling the initial flaw size effectively halves the predicted endurance for a material with a stress dependence of 4.

It is therefore concluded that no accurate method of fatigue life prediction exists for a crack growing in a pressurised thick cylinder unless experimental data are found for crack growth at near threshold values. Even if this data were to be found from tests carried out in air, it is doubtful whether these results could be reliably extended to crack growth in cylinders of the same material. The environmental effects found for low alloy steels (Priddle (1977), Evans et al (1971)) tested at near threshold stress intensity range in air may or may not occur in a

pressurised cylinder. If the medium being contained contains moisture, then environmental effects might be expected to be dependent on material purity. Since only a small change in effective crack length at low ranges of stress intensity exerts a powerful influence on total life, the accuracy of any prediction of total life is limited.

5.7 ESTIMATION OF ERRORS

The experimental results reported in this work contain measurements of many different quantities, each with an associated error or degree of uncertainty. However, the major quantitative correlations developed are based on the definition of fatigue limits in plain specimens and thick cylinders and on the size of inclusions or defects initiating the fatigue crack. The estimation of errors associated with these quantities should, therefore, be a measure of the overall error.

5.7.1 Accuracy of Fatigue Limits

For tests under repeated pressure, the fatigue limit for thick cylinders has been arbitrarily defined as the pressure range at an endurance of 2×10^6 cycles. Inspection of all the repeated pressure fatigue test results presented here and those previously published by other workers in the field show that the knee in the fatigue curve occurs at or below 1×10^6 cycles of repeated pressure for steels. The selection of an endurance limit at 2×10^6 cycles is therefore not unreasonable where sufficient test results are available to properly define this limit. For several of the test series carried out, this has not been the case.

In general, therefore, the accuracy of pressure or load measurement does not influence the overall error which is subjective in magnitude, but estimated to be of the order of $\pm$ 3%.

5.7.2 Accuracy in Inclusion Sizing

In an attempt to reduce systematic and human errors involved with inclusion sizing, the inclusion populations of steels B and G were assessed by both visual and automatic techniques. A comparison of Figures 4.7 and 4.8 illustrates the magnitude of the problem in assessing inclusion size.

Automatic inclusion size assessment is dependent entirely on the selection of an appropriate sizing system. Equivalent circle diameters is a reasonable system for a population such as that in steel G but unsatisfactory for steel B. The automatic assessment of steel G shows a probable bimodal distribution of size group occurrence not reflected in the visual assessment. It is thought that for steel G, the Quantimet assessment represents a fairly accurate picture of the size distribution of the inclusions present. However, for steel B, equivalent circle diameter is not a useful sizing system for visual or automatic assessment.

Given that the nature of an inclusion is of overriding importance from a fatigue initiation aspect, the use of automatic assessment techniques will be limited until simultaneous classification can be included in the scanning process.

The values of inclusion size distribution have therefore not been used in any quantitative way in this work because of the inaccuracy involved and the incorrect choice of sizing system adopted.

Instead, visually measured largest inclusion (stringer type) size has been used to derive the transverse threshold range of stress intensity for the steels B and G. The error in assessment of these inclusions is a function of two independent variables. The first is a subjective human error introduced by limited sampling. In general, a

larger inclusion can always be found, but with exponentially decreasing frequency. Secondly, there is an error associated with the measurement of inclusions in the plane of polish.

Of these two error terms, the former is most likely to be controlling. Unfortunately, it is apparent that this error is associated with an extreme value in a distribution function. Whilst statistical models exist for extreme values, they are complex and require the initial distribution function to be accurately defined. Since this data is not available, the error in inclusion sizing must be assumed to be large and biased.

The critical inclusion size controlling the fatigue limit for steels B and G is therefore arbitrarily taken as being subject to an error of +25% and -0%. This degree of error changes the threshold stress intensity by the square root, i.e. a probable under-estimation of the value by some 12%.

5.7.3 Accuracy in Crack Growth Rate Measurement

Errors in the measurement of crack growth rate data as presented here can arise from three sources: errors in fatigue load measurement; errors in crack length measurement; errors in specimen stress intensity factor derivation. The first is insignificant in that fatigue load in air can be measured to better than ± 0.5% of applied load range. Optical crack length measurement is far more subjective and estimated to be no better than ± 1 mm for any given crack length. This error propagates into the stress intensity range derived value as an error of ± 10% at low ΔK_I, but decreasing with increasing ΔK_I. The effect of this degree of error in absolute crack growth rate is theoretically less significant since crack growth rate is a differential term and the error

is likely to be systematic. The magnitude of the error associated with deriving the stress intensity from compliance measurements is not independent of the crack length error. However, the existence or otherwise of gross errors can be found by reference to the empirical formulae of Mostovoy (1967) and Srawley & Gross (1967).

Figure 5.14 shows the variation of stress intensity with crack length for a DCB specimen as predicted by these empirical formulae. The open circles are the derived compliance results from a test in air with a DCB specimen of steel G. The agreement is quite good, indicating that the stress intensity range as derived is probably no more than a few per cent in error. The significant error is, therefore, assumed to be that incurred in crack length measurement and is estimated to lead to a tolerance on stress intensity range of $\pm 7\frac{1}{2}\%$.

Applying similar reasoning to the crack growth rate data derived in cylinders of steel CH is more subjective, but here the data are assumed to be within $\pm$ 15% in terms of stress intensity range. However, the accuracy of the BIE stress intensity factor is not known with certainty but is thought to be such that error in crack depth is the more significant variable.

CHAPTER 6

PRESSURE VESSEL DESIGN

6.1 POSSIBLE APPLICATION OF RESULTS

From the work undertaken here with the two steel block forgings, it is possible to make suggestions as to the relative importance of some mechanical properties in pressure vessel design.

Recently, several authors, notably Ford et al (1978) and the late Witkin et al (1977), have made proposals for the design of monoblock vessels. It is not an unrelated fact that codifying or standards authorities in both Europe and the USA have recently shown interest in the regulation of the high pressure industry in these countries.

The drafting of a design code for pressure vessels working in the 1 to 5 kbar range is admittedly overdue. However, in both Europe and the USA, serious divergence of opinion exists as to the correct procedures for high pressure design and maintenance and impartial opinion is lacking. This function can be admirably fulfilled by the academic engineer when the proposals made are such that over-cautious design is avoided. Similarly, minimum requirements must be specified so as to ensure that no fundamentally unsafe designs can ever be produced.

The proposals of Ford et al (1978) are taken as the basis for comparison since they represent a logical approach to the problem.

6.2 DESIGN FOR STATIC PRESSURE CONTAINMENT

In designing for static pressure containment where fatigue failure is not a problem, the avoidance of yield at operating temperature is regarded as the design basis. The procedures are well established for this elastic analysis and the only possible variable is the magnitude of safety factor to be used. Ford et al suggest that the yield pressure at

full operating temperature should be greater than or equal to 1.25 times the design pressure.

This proposal cannot be faulted provided that it is qualified with a rider that it applies to the main body of the pressure vessel. There often exists a specialised fitting on a pressure vessel where the use of a lower safety factor can be justified. As an example, there is an increasing demand for high pressure (up to 4 kbar) reaction vessels to investigate hydrogenation reactions of interest to the energy industry. These pressure vessels are invariably equipped with stirrer drive assemblies. In the kilobar pressure regime, stuffing box gland seals are notoriously unreliable above 200 rpm and the only viable alternative is a magnetic coupling. These couplings are effectively part of the pressure containing assembly. The tube separating the inner and outer magnet assemblies is therefore a pressure vessel in its own right.

A non-magnetic material must be used for this component and it is desirable for technical reasons to restrict the volume of material used. Hence, it is accepted practice to design this component with a safety factor on yield of only 1.1. An additional margin of safety is inherent in the design through the use of an austenitic stainless steel which exhibits immense ductility after yield. The fact remains, however, that the nominal safety factor is lower than that of the pressure vessel generally. Whilst this procedure is already allowable in some countries, it is to be hoped that any new design codes in the UK will make allowance for this type of situation.

Similarly, in specifying pressure test levels and minimum ultimate pressure requirements, regard should be given to the material stress strain characteristics rather than to set ratios.

Although the possibility of fatigue failure has been excluded by

assumption for this type of pressure vessel, there are other more insidious mechanisms by which sub-critical crack growth can occur. Of these, the most commonly found is stress corrosion cracking. Whilst it is theoretically possible to establish the K_{ISCC} (minimum mode I stress intensity for occurrence of stress corrosion cracking) for a particular material/environment combination, there are many pitfalls for the unwary. Testing must be carried out at the temperature and pressure of operation. The test environment must model exactly the phases found in operation and any changes in their relative proportions. When the costs of such a test procedure are weighed against the usefulness of the data obtained, this type of testing is invariably non-cost effective.

A simpler solution is to design the pressure vessel such that if stress corrosion cracking were to occur, through poor choice of material, the mode of failure would be acceptable. The problem resolves itself into predicting the depth of crack which a particular configuration of vessel can contain without fast fracture being possible. To this end, the fracture toughness of the material is of paramount importance as pointed out by Ford et al. The majority of pressure vessels being axisymmetric, it is usually relevant to confine attention to fracture toughness in the transverse direction since this is a minimum for hollow forged or bar stock pressure vessels.

In making recommendations as to the minimum transverse properties of a constructional steel, it is more relevant to consider the effect of section size than absolute value of fracture toughness.

Consider the case of a cross-bored pressure vessel containing stress corrosion cracks emanating from the intersection. For a fixed diameter ratio vessel constructed from a material with a transverse fracture toughness of 120 $MPa.m^{\frac{1}{2}}$, as shown in Figure 5.5, the internal pressure

sufficient to cause fast fracture is seen to vary strongly as a function of wall thickness. This effect can also be seen for semi-elliptic cracks growing in the longitudinal radial plane from the bore of a pressure vessel.

Figure 6.1 shows the ratio of allowable internal pressure to fracture toughness of a steel versus critical crack depth for various thicknesses of wall section of a diameter ratio 2 vessel. The same parameters are plotted in Figure 6.2 for a diameter ratio 3 vessel. These predictions are for a semi-elliptic crack (b/a = 0.8) where fast fracture is assumed to occur from the point of deepest radial crack penetration (BIE prediction by Tan (1979)).

Given that for a steel of 1000 MPa offset yield strength, reasonable design pressures would be ≃ 350 MPa and ≃ 410 MPa for vessels of D = 2 and D = 3, respectively, it should be possible to specify a minimum fracture toughness. Inspection of Figures 6.1 and 6.2 shows, however, that it is theoretically impossible to construct a large diameter ratio pressure vessel which will fail in a "safe" mode with wall thicknesses much over 50 mm. This may be deduced from the fact that conventionally processed martensitic steels, such as $3\frac{1}{2}$ NCMV or 300 M, do not develop plane strain fracture toughness values much in excess of 180 MPa.$m^{\frac{1}{2}}$ at room temperature (1000 MPa yield strength). Indeed, it is very doubtful if a steel manufacturer would even guarantee attaining this value in thick sections (i.e. over 100 mm).

Intuitively, it is natural to say that the assumptions made or the stress intensity factor used are in error. Accumulated operating experience indicates that vessels of thick sections fail in a safe mode, whereas this analysis would predict the converse.

If the assumptions used in this analysis are reviewed in turn, there

is little comfort.

A crack lying in the radial plane parallel to the longitudinal axis is assumed to be approximated by a semi-ellipse of semi-axis ratio 0.8. Modifying the assumption such that the crack is a perfect semi-circle, i.e. $b/a = 1$, reduces the stress intensity at the point of deepest radial penetration by some 10% at best (see Figure 5.10). A more conservative assumption would be to increase the ellipticity, thereby increasing the stress intensity at the crack tip.

The model used to derive the stress intensity factor assumes that the pressurising medium exerts the equivalent pressure on the crack faces at all positions. For the case of static loading, especially with low viscosity media such as super-critical gases, this is a reasonable assumption.

The BIE method of calculating crack face displacements and subsequently strain energy release rates to derive the stress intensity factor is well tried and gives very good accuracy for problems with known solutions.

Similarly, the use of a critical crack depth to wall thickness ratio of 0.8, in calculating the ratio K_{Ic}/P, effectively ensures that no free surface effects are included.

It is the opinion of the author that the stress analysis of pressurised cracks is in error of omission. The pressure acting in an assumed crack is invariably resolved into a component acting normal to the crack plane. The presumed error lies in ignoring the radial force of fluid pressure at the crack tip.

Consider a section through the wall of a thick cylinder containing a radial crack. The remaining ligament is subjected to a force, P, in the x direction. This force is reacted in the material itself in order to

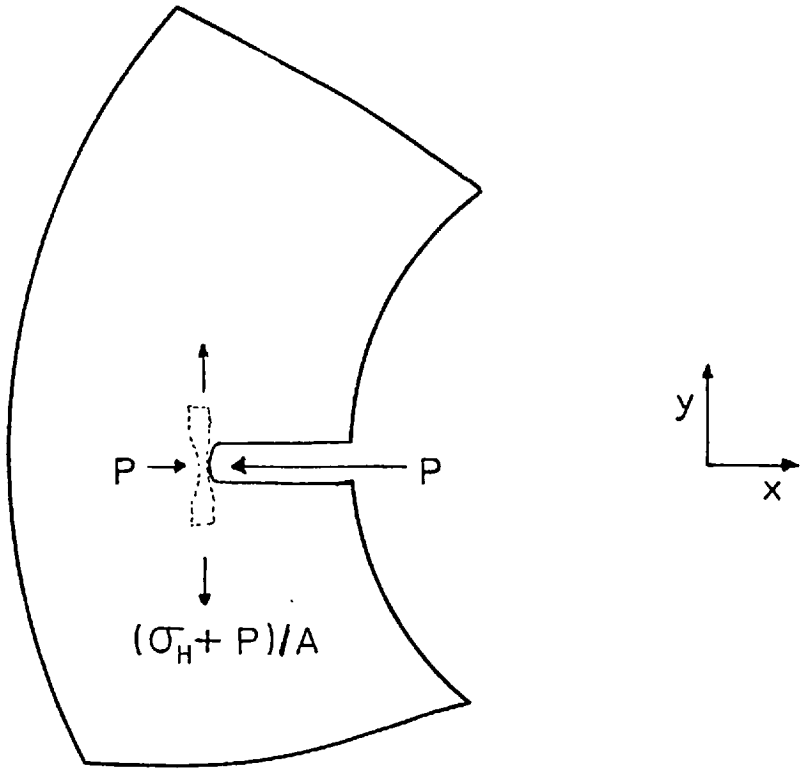

preserve radial equilibrium. This reacting force must be of equal intensity but acting in the opposite direction along the x axis. Taken to the limit, an extremely small element of material at the crack tip (represented by the tensile ligament in the sketch) can be thought of as being subjected to a hydrostatic stress. Conventionally, the stress, $\sigma_H + P$, acting on the unit area of the ligament is assumed to control the fracture process by determining the level of stress intensity. The addition of a hydrostatic pressure component is known to substantially increase strain to fracture in fracture toughness tests (Auger & Francois (1974), Pugh (1977)).

From the above argument, a crack in a material subjected to a substantial internal fluid pressure might therefore be expected to exhibit a higher critical crack opening displacement at the onset of crack propagation than would be predicted from a conventional test at ambient pressure. Alternatively, the plane strain fracture toughness of the material used to calculate a critical crack depth should be found other than at ambient pressure.

Whilst this idea is not contradicted by direct experimental evidence,

there is no easy means of verifying it within the scope of this work. It does, however, provide a reasonable physical interpretation of the observation that, excluding pressure from a sharp crack in a thick cylinder, can lead to unexpected low energy mode failure. That the effect of hydrostatic pressure in extending ductility is universal to all materials is not proven. Some materials show no increase in strain to failure under extreme hydrostatic pressures. Materials which fail under monotonic loading by the initiation and subsequent coalescence of micro-voids such as aluminium alloys and low alloy steels are, however, found to exhibit considerable increases in ductility under moderate (3 kbar) pressures. Presumably, the hydrostatic pressure component effectively increases the critical strain needed to initiate void growth.

Until the existence of a radial pressure effect can be proven, the designer must make conservative assumptions. The correlations provided in Figures 6.1 and 6.2 are a reasonable design basis and can be extended to other diameter ratios by use of the square root size factor. The absolute size of the vessel will determine whether or not a fail safe design can be constructed for a given material fracture toughness. Where a theoretically safe design is not possible, then it is still better to use a material with the greatest possible plane strain fracture toughness. This will ensure that the sub-critical crack growth rate is at a minimum (Miller (1968), Evans et al (1971)) and critical crack length is at a maximum. The allowable time interval between inspections of the vessel for cracking is therefore increased. In reality, it is better to inspect at frequencies based on the worst possible expected crack growth rate. The calculated maximum inspection interval being merely indicative of some factor of safety.

In any proposed design code for monoblock vessels subject to static

internal pressure, the author feels that specifying a minimum material fracture toughness is not a sufficient requirement. On the basis of the arguments presented above, it would seem more logical to categorise designs according to probable failure mode. Separate design requirements and, more importantly, operational and maintenance procedures could then be drafted suitable for each class of vessel.

6.3 DESIGN FOR FLUCTUATING PRESSURE CONTAINMENT

The major difference in design consideration with vessels intended for static pressure containment and those subjected to fluctuating pressures is the possibility of fatigue failure.

In contrast to vessels subjected only to static internal pressure, vessels intended for fatigue service are often geometrically symmetrical. A minimum of section change in the body of the vessel leads to fewer stress concentrations and hence fewer potential fatigue crack initiation sites. Whilst this simplicity of design reduces the complexity of elastic analysis, fatigue design is still largely empirical.

6.3.1 Low Cycle Fatigue

A large proportion of pressure vessels operate within a batch process scheme. According to the frequency of cycling, a vessel may be required to withstand anywhere between 10,000 and 100,000 pressure cycles during an expected operational life. Dependent on the pressure level in the process, it is not always possible to design such a vessel for an infinite fatigue life.

No generally applicable design procedure exists for such a situation but it is suggested that where no practical data exist for a high strain, low cycle fatigue situation, the methods of A.D. Merkblatter

are adopted. In essence, this design formulation involves calculating an equivalent hypothetical elastic stress from an analysis of the strain range at the worst geometric discontinuity in the vessel. This imaginary stress range is then compared with a standard strain controlled fatigue curve for the particular class of material envisaged. A factor of five on endurance is then used to reduce the theoretical endurance to give an expected endurance at the particular stress range.

Whilst not making any concessions for the effect of auto-frettage, either deliberate or self-induced through a variable peak pressure cycle, this procedure leads to safe design. It has the further advantage that for existent vessels, it is possible to measure the strain change at some critical point and interpolate an expected endurance. This then determines the minimum inspection interval or number of cycles.

The procedure has the attraction of utilising material properties measured under a constant strain range. In a low cycle fatigue situation, there is every reason to expect that the range of strain is the controlling parameter. Failing a more complete understanding of the mechanisms of low cycle fatigue, the adoption of the procedure described gives safe but not over-cautious fatigue life design.

6.3.2 High Cycle Fatigue

For any pressure vessel which is to be subjected to more than 250,000 operational cycles during its life, an infinite fatigue life design is preferable.

Very little practical data exist in the open literature for pressure vessels containing discontinuities such as cross-holes. What little data that does exist have been shown to be overly pessimistic.

It is therefore suggested that for pressure vessels made from modern steels, a ratio of allowable shear stress range divided by tensile strength of 0.25 be taken as a design criterion. Whist this only applies to well radiused cross-bores under conditions of a repeated pressure cycle, the effect of mean pressure can be judged from the data given in Figure 5.2. Similarly, the strengthening effect of autofrettage can be judged from a comparison of Figures 4.10 and 5.3. Bearing in mind the effects of temperature on residual stress stability, it would appear that autofrettage can increase the allowable shear stress range by at least 50% for an indefinite fatigue life.

From the failure mode aspect, the comments made in the preceding section with reference to sub-critical crack growth apply equally well here. Vessels should be classified at the design stage according to their expected mode of failure. The existence of a fatigue crack at a cross-hole intersection can never be completely eliminated and should therefore be assumed. Appropriate recommendations can then be made to minimise the danger in the event of failure.

In the more commonly encountered plain pressure vessel operating under fluctuating pressure conditions, the proposals of Ford et al are adequate in most respects. A danger exists, however, in the use of the empirically derived ratio of allowable shear stress range to material tensile strength.

The steel designated B in this investigation complies with all the requirements of ductility and fracture toughness as recommended by Ford et al (1978) when tested in one of the two transverse axes. The measured repeated pressure fatigue limit is, however, 18% less than that predicted by the shear stress range/UTS criterion. Hence, the factor of safety of 1.25 on fatigue limit is reduced to an unacceptably low level of 1.07.

It is therefore suggested that steels with a coefficient variation of over 25% in reduction of area property either be rejected or are used only with repeated tension fatigue data from the transverse direction. This proviso will effectively eliminate the possibility of material anisotropy contributing to an expensive fatigue failure. Similarly, steels exhibiting large variation in ductility as a function of orientation should be assumed to have anisotropic crack growth properties. The majority of literature values of crack growth rate data (stress dependence and intercept in the Paris law) are for the resistant orientations. Where no experimental values are available, data such as those shown in Figures 4.34 and 4.35 should be utilised to calculate minimum inspection intervals. It is particularly important with anisotropic steels to realise that mean stress effects are often exaggerated. Therefore, if a vessel is to operate at high mean pressure with a superimposed fluctuating pressure load, inspection intervals should be calculated using the appropriate stress ratio base data.

Having established a provisional design, it is essential, as in the previous instances, to calculate the critical crack size for a low energy mode failure. If with the particular section size and assumed material fracture toughness, a leak before burst mode of failure is marginal, there are always two options. Dependent on the relative importance of the various design criteria, the material tensile strength may be slightly reduced to increase the plane strain fracture toughness or the absolute wall thickness may be reduced. Both provisions lead to an increase in the ratio of working to allowable stress, but this is often preferable if a safe mode of failure can be ensured as a result.

Finally, it is suggested that in any proposed design code for monoblock pressure vessels, the orientation of test pieces can be specified

more precisely than is customary at present. As has been shown in this work, large variations in mechanical properties can exist in the three orthogonal directions of a block forging. Merely because a block forging is finished as an axisymmetric pressure vessel does not mean that properties are uniform circumferentially. The failure to appreciate this point at the design stage could lead to fundamentally unsafe designs being produced.

CHAPTER 7

CONCLUSIONS AND RECOMMENDATIONS

7.1 CONCLUSIONS

The objectives of this research have all been achieved to a greater or lesser extent. Experimental evidence has been provided to show that a modern steel does not exhibit a significantly higher repeated pressure fatigue strength than steels produced between 1950 and 1970.

However, the following positive conclusions can be drawn:

1) The repeated pressure fatigue strength of cross-bored radiused intersection cylinders is considerably higher than that reported for unradiused intersection cylinders. A shear stress range to ultimate tensile strength ratio of 0.25 is suggested as a design criterion.
2) The effect of mean pressure on fatigue strength of radiused cross-bored cylinders is much less than that found for plain cylinders.
3) Steel composition does not appear to influence the fatigue limit of cross-bored cylinders for the range of steels tested.
4) The fatigue limit of cross-bored cylinders with a radiused intersection is found to be most dependent on material tensile strength.
5) The failure mode of cross-bored cylinders is shown theoretically to be a function of absolute size with material fracture toughness exhibiting a secondary influence. However, the theoretical model used may have shortcomings. These limitations have been pointed out in the text.
6) A technique has been developed which allows measurement of crack growth rate in the radial direction for semi-elliptic cracks growing

from the bore of an internally pressurised thick-walled cylinder. The results obtained are shown to be reproducible and of the expected order.

7) Forged steels with anisotropic mechanical properties are shown to have similarly anisotropic fatigue properties. This effect is more marked for direct stress fatigue tests than for triaxially stressed thick cylinder repeated pressure fatigue tests.

8) Evidence is presented to show that some inclusions or defects of the same scale can initiate fatigue cracks in plain specimens and thick-walled cylinders subjected to repeated pressurisation.
Based on this evidence, a physically realistic fatigue failure criterion for low alloy steels has been developed to show that a mode I crack propagation limit is the controlling parameter within limits of surface finish and tensile strength.
Previous repeated pressure thick cylinder data have been re-analysed according to this criterion and the agreement shown to be good.

9) The fatigue criterion based on propagation limit under mode I stressing is shown to apply to all orientations of plain cylinder and repeated direct stress specimens cut from low alloy steel forgings.

10) The type of inclusion initiating fatigue failure in low alloy steels is found to be a function of its mechanical properties relative to the matrix steel during processing.

11) The shape of a fatigue crack growing from a point defect is found to remain the same during propagation in an internally pressurised thick-walled cylinder. It is shown qualitatively that this shape is a function of crack growth resistance in two orthogonal directions in the crack plane.

12) Some indirect experimental evidence is presented which may indicate that the pressurising medium in a thick-walled cylinder can enhance fatigue crack growth rate in certain orientations for inhomogeneous steels. The pressurising medium can advance the crack front locally by penetrating along suitable orientated elongated inclusions.

13) A steel with a large volume fraction of inclusion is found to have higher absolute crack growth rates for a given value of stress intensity. Elongated MnS inclusions are demonstrated to be the major reason for this behaviour.

14) Linear elastic fracture mechanics analysis of the fatigue crack initiation behaviour of low alloy steels appears to give a satisfactory, if limited, model of actual behaviour.

15) The prediction of repeated pressure thick cylinder endurance in the mortal region using crack growth data derived in air is dubious.

16) Suggestions are made concerning a possible design code for pressure vessels. The importance of mode of failure classification rather than material fracture toughness is demonstrated. Similarly, the dangers of using a reversed shear stress fatigue criterion for thick-walled cylinders are pointed out.

7.2 RECOMMENDATIONS FOR FUTURE WORK

7.2.1 Cross-Bored Cylinders

The fatigue strength reduction for a thick-walled cylinder containing a cross-bore is not easily predicted. In particular, it is recommended that the effect of a radius at the intersection of the main and cross-bores be investigated numerically. Computer solutions for various intersection geometries could then be checked by model cylinder fatigue tests to establish the magnitude and range of fatigue strength

reduction factor.

For designers of pressure vessels containing cross-holes, there is an area of great uncertainty associated with the failure mode of these vessels. Practical tests should be carried out to establish the validity of the design curves proposed in this work. Whilst by no means easy, the basic applicability of the approach could be verified by bursting pre-fatigue cracked cross-bored cylinders of varying wall thickness at high tensile strength levels.

7.2.2 Fatigue Crack Growth in Pressurised Components

The method of fatigue crack growth measurement demonstrated here should be refined in two areas. A more accurate numerical prediction would remove the necessity of establishing a calibration curve. Secondly, the instrumentation could be improved by the use of on-line data reduction using a micro-processor based system. When both these objectives have been achieved, fatigue crack growth in thick cylinders could be investigated as a function of orientation, crack shape, pressurising medium and residual stress level. Of these variables, the latter two are of most immediate practical interest.

Differences in crack growth rate as a function of environment cannot be extrapolated from tests in air. The effect of pressurisation may cause a nominally inert medium to behave aggressively at a crack tip. This behaviour might not be apparent with ambient pressure tests.

Similarly, it is of interest to be able to predict residual life of a cracked pressurised component. The existence of residual stresses induced, for example, by autofrettage can only be estimated. Their influence on crack growth rate is uncertain. Therefore, it is of immense practical interest to measure absolute crack growth rates in the

thick cylinder geometry to quantify or make comparisons of crack growth with and without residual stress.

7.2.3 Plain Cylinders

From the work reported here, recommendations for further work can be made on two levels. Of immediate practical interest to designers, it is relevant to conduct fatigue tests on low alloy steels at varying mean stress levels. The fatigue failure criterion suggested here should logically be capable of predicting the fatigue limit of internally pressurised cylinders for pressure regimes other than repeated pressure. Secondly, a range of materials other than steels should be tested in the form of thick cylinders and plain specimens to establish the applicability of the fatigue limit criterion. Having determined which materials other than steels can be correlated using a mode I propagation limit criterion, it is relevant to determine over what range of tensile strength this criterion applies. This could be most easily achieved by testing plain specimens of materials at varying strength level and examining the initiation sites using a scanning electron microscope.

A further area of immediate interest to designers of pressure vessels is the prediction of mode of failure of cracked vessels. There is an urgent need for a conclusive test programme to demonstrate the applicability or otherwise of the simple critical crack length approach.

It is recommended that plain cylinders of the same diameter ratio and plane strain fracture toughness material, but varying wall thickness, be fatigue cracked to a known depth and then pressurised to burst. The adoption of this procedure will determine whether or not a size effect exists and may indicate that the radial pressure cannot be neglected.

At a more fundamental level, it is the long-term objective of all materials research to predict mechanical properties from material parameters. For the steels tested in this research work, fatigue properties have received most attention. Qualitative and quantitative prediction of the fatigue limit of a steel which exhibits a propagation limit is determined by the inclusion or defect population.

The limitation of the fracture mechanics based approach lies in the unique geometry of inclusions where they intersect a free surface. Two areas where more work is therefore needed are in the characterisation of defect type and classification of inclusion type such that an automatic assessment can be carried out. (A similar problem exists for the case of low energy mode monotonic failure from short cracks. It is to be hoped that work in the fracture field will be applicable to the case of repeated loading.) The use of automatic imaging techniques has considerable promise in this respect, but will only have practical application when a more discriminating classification and summation system is developed. It is therefore recommended that more effort is devoted to the statistical description of inclusion or defect populations.

REFERENCES

ANDERSON, R.B., HOLMS, A.G., & ORANGE, T.W. (1970)
NASA TN.D-6054.

ATKINSON, M. (1960)
J. Iron & Steel Inst., 195, 64.

AUGER, J.P., & FRANCOIS, D. (1974)
Revue de Physique Appliquée, 9,

BACKOFEN, W.A. (1959)
in Fracture, Technology Press, Wiley & Sons, New York.

BAKER, T.J., & CHARLES, J.A. (1972)
J. Iron & Steel Inst., 210, 680.

BAKER, T.J. GROVE, K.B., & CHARLES, J.A. (1976)
Metals Technology, April 1976, 183.

BARSOM, J.M. (1974)
WRC Bulletin, 194, 1.

BEILBY, G. (1921)*

BOWIE, O.L. (1956)
J. Maths. & Phys., 35, 60.

BROOKSBANK, D., & ANDREWS, K.W. (1968)
J. Iron & Steel Inst., 206, 595.

BROOKSBANK, D., & ANDREWS, K.W. (1969)
J. Iron & Steel Inst., 207, 474.

BROOKSBANK, D., & ANDREWS, K.W. (1970)
J. Iron & Steel Inst., 208, 495.

BROOKSBANK, D., & ANDREWS, K.W. (1970)
J. Iron & Steel Inst., 208, 582.

---

* Widely held theory at the time.

BROOKSBANK, D., & ANDREWS, K.W. (1972)

Proc. Int. Conf. on Production & Application of Clean Steels, Balatonfüred, Hungary, 1970, 186. Published 1972.

BROWN, W.F., & SRAWLEY, J.E. (1966)

ASTM STP410.

BUCH, A., & CHODOROWSKI, J. (1964)

in Fatigue Resistance of Materials and Metal Structural Parts, (ed. A. Buch), Pergamon Press, 161.

BUECKNER, H.F. (1960)

in Boundary Problems in Differential Equations, University of Wisconsin Press, Madison, Wisconsin, 216.

BURNS, D.J., & PARRY, J.S.C. (1967-68)

Proc. Inst. Mech. Engrs., 182, Part 3C,

CHODOROWSKI, W.T. (1956)

Proc. Int. Conf. on Fatigue of Metals, I.Mech.E., London.

CINA, B. (1960)

J. Iron & Steel Inst., 194, 324.

CLARK, W.G., & WESSEL, E.T. (1970)

ASTM STP463, 160.

COOK, W.T. (1970)

J. Iron & Steel Inst., 43, 363.

COOKE, R.J., IRVING, P.E., BOOTH, G.S., & BEEVERS, C.J. (1975)

Eng. Fract. Mechs., 7,

COTTRELL, A.H., & HULL, D. (1957)

Proc. R. Soc. Lond., A242, 211.

COX, T.B., & LOW, J.R. (1973)

NASA Technical Report No. 5, May 1973.

CROFTON, P.S.J. (1972)

M.Sc. Thesis, Imperial College, University of London.

CROSSLAND, B. (1956)

Proc. Int. Conf. on Fatigue of Metals, I.Mech.E., London, 138.

CROSSLAND, B. (1976)

Paper presented at Int. Conf. on

Boulder, Colorado, Paper H-4-A.

CROSSLAND, B., & SKELTON, W.J. (1967)

Proc. Inst. Mech. Engrs., 182, Part 3C.

CRYMBLE, T.G., GOLDTHORPE, B.D., & AUSTIN, B.A. (1975)

Proc. 2nd Int. Conf. on High Pressure Engineering, I.Mech.E., 341.

CUMMINGS, H.N., STULEN, F.B., & SCHULTE, W.C. (1958)

Proc. ASTM, 58, 505.

DEHOFF, R.T. (1968)

Techniques for the Direct Observation of Structure and Imperfections,

John Wiley & Sons, New York, Vol. 2, Part 1.

DOREY, S.F., & SMEDLEY, G.P. (1956)

Proc. Int. Conf. on Fatigue of Metals, I.Mech.E., 247.

DUGGAN, T.V. (1977)

Eng. Fract. Mechs., 4, 22.

ELBER, W. (1970)

Eng. Fract. Mechs., 2, 37.

EVANS, P.R.V., OWEN, N.B., & HOPKINS, B.E. (1971)

Eng. Fract. Mechs., 3,

EWING, J.A., & HUMFREY, J.C.W. (1903)

Phil. Trans. R. Soc., A200, 241.

FIEGE, N.C., & MURPHY, T. (1967)

Metals Eng. Quarterly, 7, 53.

FELTNER, C.E., & MORROW, J.D. (1961)

J. Basic Eng., 83, 15.

FESSLER, H., & LEWIN, B.H. (1956)

Brit. J. Appl. Physics, 7, 76.

FORD, H., CROSSLAND, B., & WATSON, E.H. (1978)

Proc. Conf. on Pressure Vessels & Piping, Montreal, Canada.

FORMAN, R.G. (1968)

Air Force Flight Dynamics Laboratory Technical Report AFFDL-TR-68-100.

FORMAN, R.G., KEARNEY, V.E., & ENGLE, R.M. (1966)

ASME Paper No. 66-WA/Met-4.

FORSYTH, P.J.E. (1957)

Proc. R. Soc. Lond., A242, 198.

FRITH, P.H. (1954)

Iron & Steel Inst. Special Report No. 50.

FRITH, P.H. (1955)

J. Iron & Steel Inst.,

FRITH, P.H. (1956)

Paper presented at Int. Conf. on Fatigue of Metals, I.Mech.E./ASME, 462.

FROST, W.J., & BURNS, D.J. (1967)

Proc. Inst. Mech. Engrs., 182, Part 3C.

FROST, N.E., MARSH, K.J., & POOK, L.P. (1974)

in Metal Fatigue, Clarendon Press, Oxford.

FROST, N.E., POOK, L.P., & DENTON, K. (1971)

Eng. Fract. Mechs., 3, 109.

FROST, N.E., & SHARPLES, J.K. (1978)

Eng. Fract. Mechs., 10, 371.

GERBER, W. (1874)

Z. bayer. Archit. Ing. Ver., 6, 101.

GERDEEN, J.C. (1972)

Trans. ASME, J. Eng. for Industry, Series B, 94, 815.

GERDEEN, J.C., & SMITH, R.E. (1972)

Experimental Mechanics, 530.

GOLDTHORPE, B.D. (1973)

Paper 17, British Steel Corporation Conf. on Mechanics & Mechanisms of Crack Growth, Cambridge, UK.

GOODMAN, J. (1899)

Mechanics Applied to Engineering, Longman, Green & Company, London.

GOUGH, H.J. (1933)

Proc. ASTM, 33, 3.

GOUGH, H.J., & HANSON, D. (1923)

Proc. R. Soc. Lond., A104, 539.

GREEN, G., & KNOTT, J.F. (1975)

Metals Technology, September 1975, 422.

GREGOR, V. (1960)

Proc. Int. Conf. on Fatigue Resistance of Materials & Metal Structural Parts, (ed. A. Buch), 299.

GRIFFITH, A.A. (1920)

Phil. Trans. R. Soc., A221, 163.

GROSSKREUTZ, J.C. (1963)

J. Appl. Physics, 34, 372.

GROVER, H.J., HYLER, W.S., & JACKSON, L.R. (1959)

NASA Technical Note D111.

HADDAD, M.H.El., TOPPER, T.H., & SMITH, K.N. (1979)

Eng. Fract. Mechs., 11,

HAHN, G.T., & ROSENFIELD, . (1973)

Paper presented at 3rd Int. Conf. on Fracture (ICF3), Plenary Lecture.

HASLAM, G.H. (1969)

High Temperatures: High Pressures, 1, 705.

HASLAM, G.H. (1971)

J. Mech. Eng. Sci., 13,

HASLAM, G.H. (1972)

Trans. ASME, J. Eng. for Industry, February 1972, 284.

HASLAM, G.H., & MARSH, K.J. (1969)

NEL Report No. 381.

HAUSER, J.J., & WELLS, M.G.H. (1970)

Technical Report AFML-TR-69-339.

HEISER, F.A., & HERTZBERG, R.W. (1971)

Trans. ASME, J. Basic Eng., June 1971,

HEWITT, J., & MURRAY, J.D. (1968)

Brit. Weld. J., 15, 151.

HOPPER, C.D., & MILLER, K.J. (1977)

J. Strain Anal., 12,

INGLIS, C.E. (1913)

Trans. Inst. Nav. Archit., LV, 1, 219.

IRWIN, G.R. (1957)

Paper 101(II), 9th Int. Congr. on Applied Mechanics, University of Brussels, 254.

IRWIN, G.R. (1962)

J. Appl. Mechs., 29, 651.

JACK, A.R., & PRICE, A.T. (1970)

Int. J. Fract. Mechs., 6,

JACOB, L. (1920)

Résistance et Construction des Bouches à Feu, Dain et Fils, Paris, 157.

JAGANNADHAM, K. (1977)

Eng. Fract. Mechs., 9,

KENDALL, C.T. (1972)

M.Phil. Thesis, Imperial College, University of London.

KIESSLING, R. (1968)

Non-Metallic Inclusions in Steel, Part III, Iron & Steel Inst., London.

KIESSLING, R. (1969)

Jernkon. Ann., 153,

KIESSLING, R., & LANGE, N. (1966)

Non-Metallic Inclusions in Steel, Part II, Iron & Steel Inst., London.

KIESSLING, R., & NORDBERG, H. (1972)

Proc. Int. Conf. on Production & Application of Clean Steels,

Balatonfüred, Hungary, 1970. Published by Iron & Steel Inst., 1972.

KIKUWA, M., JONO, M., & TANAKA, K. (1976)

Paper presented at 2nd Int. Conf. on Mechanical Behaviour of Materials,

Boston, USA.

KLESNIL, M., & LUKAS, P. (1972)

Mater. Sci. Eng., 9, 231.

KLESNIL, M., & LUKAS, P. (1972)

Eng. Fract. Mechs., 4, 22.

KLINTWORTH, G.C. (1977)

M.Sc. Thesis, Imperial College, University of London.

KNOTT, J.F. (1973)

Fundamentals of Fracture Mechanics, Butterworths, London.

KOBAYASHI, A.S. (1965)

ASTM STP381.

KÖRNER, J.P. (1974)

Chemie-Ingenieur-Technik, 10 (reprinted in English).

KUTTER, M.K. (1970)

Int. J. Fract. Mechs., 6, 233.

LAMÉ, G., & CLAPEYRON, B.P.E. (1833)

Mem. Acad. Sci., 4, 465.

LANKFORD, J. (1977)

Eng. Fract. Mechs., 9, 617.

LASZLO, F. (1943)

J. Iron & Steel Inst., 147, 173.

LIBERTINY, G.Z. (1967)

Proc. Inst. Mech. Engrs., 182, Part 3C.

LITTLE, R.E. (1965)

Machine Design, 37, 133.

LONGRIDGE, J.A. (1860)

Proc. Inst. Civil Engrs., 19, 283.

LYNE, C.M., & KASAK, A. (1963)

Trans. ASM, 56, 803.

MAY, A.N. (1960)

Nature, 185, 303.

McEVILY, A.J., & GROEGER, J. (1977)

Proc. 4th Int. Conf. on Fracture (ICF4), Waterloo, Canada, 2, 1293.

MILLER, G.A. (1968)

Trans. QASM, 61,

MORRISON, J.L.M., CROSSLAND, B., & PARRY, J.S.C. (1956)

Proc. Inst. Mech. Engrs., 170, 697.

MORRISON, J.L.M., CROSSLAND, B., & PARRY, J.S.C. (1959)

J. Mech. Eng. Sci., 1, 207.

MORRISON, J.L.M., CROSSLAND, B., & PARRY, J.S.C. (1960)

Proc. Inst. Mech. Engrs., 174, 95.

MOSTOVOY, S., CROSLEY, P.B., & RIPLING, E.J. (1967)

J. Materials, 2, 661.

MOTT, N.F. (1958)

Acta Met., 6, 195.

NISHIOKA, K., & HIRAKAWA, K. (1975)

Proc. 2nd Int. Conf. on High Pressure Engineering, I.Mech.E., 325.

ORANGE, T.W. (1975)

NASA Technical Memorandum, NASA TM X-71772.

OROWAN, E. (1945)

Trans. Inst. Engrs. Shipbuilders, Scotland, 89, 165.

PARIS, P.C., & ERDOGAN, F. (1963)

Trans. ASME, J. Basic Eng., 85, 528.

PARIS, P.C., & SIH, G.C. (1965)

ASTM STP381, 30.

PARRY, J.S.C. (1956)

Proc. Int. Conf. on Fatigue of Metals, I.Mech.E., 132.

PARRY, J.S.C. (1965)

Proc. Inst. Mech. Engrs., 180, 387.

PARRY, J.S.C., & SHANNON, R.W.E. (1977)

Proc. 2nd Int. Conf. on High Pressure Engineering, I.Mech.E.

PEREIRA, M.F.S. (1977)

Ph.D. Thesis, Imperial College, University of London.

POOK, L.P. (1972)

ASTM STP513.

POOK, L.P., & HOLMES, R. (1976)

NEL Report 82/5, Presented at Int. Conf. on Fatigue Testing & Pressure, City University, London, April 1976.

PRIDDLE, E.K. (1977)

Proc. 4th Int. Conf. on Fracture (ICF4), Waterloo, Canada.

PRIEST, A.H. (1971)

BSC Report MG/6/(1971).

PUGH, H.Ll.D. (1977)

Proc. 2nd Int. Conf. on High Pressure Engineering, I.Mech.E.

RANKINE, W.J.M. (1843)

Proc. Inst. Civil Engrs., 2, 105.

RANSON, J.T. (1954)

Trans. ASM, 46, 1254.

RANSON, J.T., & MEHL, R.F. (1952)

Proc. ASTM, 52, 779.

RICHARDS, C.E., & LINDLEY, T.C. (1972)

Eng. Fract. Mechs., 4, 951.

RITCHIE, R.O. (1977)

Proc. 4th Int. Conf. on Fracture, Waterloo, Canada, 2, 1325.

RITCHIE, R.O., & KNOTT, J.F. (1973)

Acta Met., 21, 639.

RODMAN, T.J. (1861)

Reports of Experiments on the Properties of Metals for Cannon, Boston, USA.

ROGAN, J. (1975)

Proc. 2nd Int. Conf. on High Pressure Engineering, I.Mech.E., 287.

ROGAN, J. (1975)

Proc. 2nd Int. Conf. on High Pressure Engineering, I.Mech.E., 281.

SCHMIDT, R.A., & PARIS, P.C. (1973)

ASTM STP536, 79.

SCHÜTZ, W. (1979)

Eng. Fract. Mechs., 11, 405.

SHANNON, R.W.E. (1970)

Ph.D. Thesis, The Queen's University of Belfast, Northern Ireland.

SHANNON, R.W.E. (1973)

Press. Vess. & Piping, 1,

SHIH, T., & ARAKI, T. (1973)

Trans. Iron & Steel Inst. Japan, 13, 11.

SMITH, R.W., HIRSCHBERG, M.H., & MANSON, S.S. (1963)

NASA Technical Note D-1574.

SODERBURG, . (1930)

Trans. ASME, 52, APM-52-2.

SRAWLEY, J.E., & GROSS, B. (1967)

NASA Technical Note, NASA-TN-D-3820.

STULEN, F.B., CUMMINGS, H.N., & SCHULTE, W.C. (1956)

Proc. Int. Conf. on Fatigue of Metals, I.Mech.E.

TAN, C.L., & FENNER, R.T. (1978)

J. Strain Anal., 13,

TAN, C.L., & FENNER, R.T. (1980)

Int. J. Fracture, 16, 233.

THOMPSON, N., & WADSWORTH, N.J. (1958)

Advanced Physics, 7, 72.

THORNTON, P.A. (1971)

J. Mat. Sci., 6, 347.

THORNTON, P.A. (1972)

Technical Report WVT-7215, Wateruliet Arsenal, New York, May 1972.

THROOP, J.F. (1970)

Technical Report WVT-7035, Wateruliet Arsenal, New York.

TIFFANY, C.F., LORENZ, P.M., & HALL, L.R. (1966)

NASA CR-54837, Boeing Report D2-20478-1.

TIFFANY, C.F., & MASTERS, J.N. (1965)

ASTM STP381.

TOMKINS, B. (1973)

Press. Vess. & Piping, 1, 37.

UNDERWOOD, J.H. (1972)

ASTM STP513, 59.

UNDERWOOD, J.H., LASELLE, R.R., SCANLON, R.D., & HUSSAIN, M.A. (1970)
Technical Report WVT-7026, Wateruliet Arsenal, New York.

WALKER, E.F., WATSON, E.H., JAMES, D.B., McINTYRE, P., & MAY, M.J. (1977)
Proc. 2nd Int. Conf. on High Pressure Engineering, I.Mech.E.

WESTERGAARD, H.M. (1939)
J. Appl. Mechs., 49,

WILLIAMS, J.G. (1980)
Int. J. Fracture, 16, R127.

WITKIN, D.E., & MRAZ, G.J. (1977)
Paper presented at Symp. on Safety in the High Pressure Polyethylene Process, 83rd Nat. Meeting of the Am. Inst. Chem. Eng., Houston, USA.

WÖHLER, A. (1871)
Engineering, 11, 199.

WOOD, W.A. (1956)
Paper presented at Int. Conf. on Fatigue, I.Mech.E., 531.

WOOD, W.A. (1959)
in Fracture, Technology Press, Wiley & Sons, New York, 412.

ZACKY, V.F., GERBERICH, W.W., & PARKER, E.R. (1968)
in Fracture: An Advanced Treatise, (ed. H. Liebowitz), Vol. 1, Chapter 6, publisher?

LIST OF TABLES

TABLE 3.1

Dimensions of Specimens Used to Measure Crack Growth Rates in Air

Steel	Specimen and Orientation	B (mm)	W (mm)	H (mm)	Comments
B	LQ - 3	25.7	120.0	75-50	Reversed constant K 66% side grooved DCB
B	TQ	25.6	120.0	75-50	
B	LQ - 1	44.5	89.0	107.0	Compact tension
B	QT	44.5	89.0	107.0	Compact tension
G	LQ	25.7	192.1	81.5	66% side grooved DCB
G	TQ	25.8	163.3	81.3	
G	QT	25.7	201.3	81.5	60% side grooved DCB
G	QL	21.6	81.0	49.6	50% side grooved DCB
G	TL - 3 and 5	21.6	81.0	49.6	

TABLE 4.1

Chemical Analysis

Steel	Element (wt%)														
	C	Si	S	P	Mn	Ni	Cr	Mo	Ti	Cu	Co	Sn	N	Al	V
J	0.35	0.20	0.010	0.008	0.45	3.52	1.42	0.65	<0.02	0.12	<0.01	0.012	<0.02	<0.005	0.12
Y	0.34	0.24	0.010	0.010	0.65	2.00	0.60	0.23	<0.02	0.09	<0.01	0.012	<0.02	0.034	<0.02
M	0.12	0.34	0.010	0.012	0.58	4.88	0.64	0.50	<0.02	0.12	0.09	0.012	<0.02	0.034	0.05
BO	0.23	0.20	0.008	0.011	0.46	2.18	1.80	0.32	<0.02	0.18	0.02	0.018	<0.02	0.040	<0.02
OES	0.39	0.25	0.022	0.014	0.73	2.00	0.62	0.26	<0.02	0.07	<0.01	0.012	<0.02	0.020	<0.02

Analysis Source: Waleswood Stainless Steel Company
Error (Relative): 3% estimated

Steel	Element (wt%)														
	C	Si	S	P	Mn	Ni	Cr	Mo	Ti	Cu	Co	Sn	N	Al	V
M	0.16	0.33	0.007	0.020	0.68	4.67	0.73	0.53	-	-	-	-	-	-	0.11

Analysis Source: Manufacturer
Error (Relative): 3% estimated

TABLE 4.1 (continued)

Steel	Element (wt%)														
	C	Si	S	P	Mn	Ni	Cr	Mo	Ti	Cu	Co	Sn	N	Al	V
CH	0.30	0.35	0.033	0.017	0.58	3.47	1.06	0.06	-	0.23	-	0.033	-	0.044	-

Analysis Source: Waleswood Stainless Steel Company
Error (Relative): 3% estimated

Steel	Element (wt%)														
	C	Si	S	P	Mn	Ni	Cr	Mo	Ti	Cu	Co	Sn	N	Al	V
B	0.47	0.32	0.026	0.009	0.73	1.77	0.91	0.26	-	0.13	-	0.014	-	0.007	-
G	0.47	0.31	0.003	0.006	0.87	1.77	0.83	0.28	-	0.18	-	0.019	-	0.063	-

Analysis Source: Waleswood Stainless Steel Company
Error (Relative): 3% estimated

Steel	Element (wt%)														
	C	Si	S	P	Mn	Ni	Cr	Mo	Ti	Cu	Co	Sn	N	Al	V
B	0.41	0.29	0.015	0.005	0.70	1.80	0.89	0.22	-	-	-	-	-	-	0.031
G	0.41	0.29	0.004	0.007	0.79	1.80	0.82	0.26	-	-	-	-	-	-	-

Analysis Source: Manufacturer
Error (Relative): 3% estimated

TABLE 4.2

Chemical Analysis

Steel	Element in ppm			
	Ca	Cs	Ce	O
B	< 20	ND	ND	39 (average of two results)
G	< 20	ND	ND	23 (average of two results)

TABLE 4.3

Mechanical and Physical Properties

Steel	Orientation: Direction of Specimen Axis	Yield Stress or Offset Yield (N/mm^2)	Ultimate Tensile Strength (N/mm^2)	% Reduction Area	% Elongation on 5D	Hardness HV (50 kgs)
J	L	1020	1111	41	14	369
Y	L	839	925	58	21	307
M	L	906	992	62	22	312
BO	L	787	926	70	19	308
OES	L	665	852	58	18	275
CH	L	749	869	56	13	300
B	L	843	946	64	20	320
	Q	830	945	21	11	
	T	850	945	43	15	
	Radial i.e. Oblique			24	11	
G	L	741	893	65	22	305
	Q	759	896	54	19	All values average of ten results
	T	742	889	60	20	

TABLE 4.4

Fracture Toughness and Charpy Impact Properties

Steel	Orientation of Test Specimen	K_Q* (MPa.m$^{\frac{1}{2}}$) at Room Temperature	Charpy Impact (Joules)	
			Room Temperature (+20°C)	-20°C
B	LQ	258.7†	93	L 54-47
	LT	-	92	
	QL	-	28	Q 17-13
	TQ	121.6	36	
	TL	-	38	Radial 19-26
	QT	130.2	32	
G	LQ	-	135	119
	LT	-	134	125
	QL	-	125	119
	TQ	-	122	118
	TL	-	125	123
	QT	-	122	126

* Fracture toughness values quoted are from tests failing to meet the validity criterion associated with ASTM E399-72 and BS5447:1977.

† Value derived from a J integral test assuming the equivalence of J with the strain energy release rate, G.

TABLE 4.5

Results of Quantimet Analysis

Steel	Volume Fraction of Inclusions (%)		Mean Inclusion Spacing (μm)		Number of Inclusions per Square mm		Mean Inclusion Diameter (μm)	
	Automatic	Visual	Automatic	Visual	Automatic	Visual	Automatic	Visual
J	0.033	0.046	295	-	11	-	3.43	-
Y	0.045	0.056	173	-	33	-	3.27	-
M	0.055	0.054	183	-	29	0.52	3.57	-
BO	0.023	0.031	302	-	11	-	3.87	-
OES	0.099	0.142	133	-	56	-	3.06	-
B	0.135	0.128 to 0.140	139	200	51.7	18.0	3.89	7.20
G	0.0214	0.014	493	553	4.1	7.4	6.59	5.98

TABLE 4.6

Inclusion Types Observed

Steel	Inclusion Type					
	MnS	FeO	Fe Silicate	MnS/Mn Silicate	Al_2O_3	Duplex Aluminates
J	O	O	O	O	O	X
Y	O	O	O	X	O	O
M	O	O	O	X	O	X
BO	O	X	O	X	O	X
OES	O	O	O	O	O	O
CH	O	X	X	X	O	O
B	O	X	X	O	O	O
G	O	X	X	X	X	O

O = Yes

X = No

TABLE 4.7

Proportions of "Hard" and "Soft" Inclusions

Steel	Hard (%)	Soft (%)
J	35	65
Y	76	24
M	75	25
BO	20	80
OES	49	51

TABLE 4.8

Crack Orientation	Semi-Minor to Major Axis Ratio	
	Steel B	Steel G
LT	0.92	0.96
TL	0.98	0.96
LT/TL	0.99	0.97
cl. LT	0.92	-
cl. TL	0.92	-
LQ	0.94	0.95
QL	1.04	0.96
LQ/QL	0.94	0.98
cl. LQ	0.92	-
cl. QL	0.92	-
QT	0.74	0.95
TQ	0.82	0.96
QT/TQ	0.73	0.97
cl. QT	0.83	-
cl. TQ	0.83	-

TABLE 4.9

Summary of Fatigue Crack Growth Rate Tests in Air

Steel	Specimen and Orientation	Stress Ratio	Exponent, n	Intercept, C_o	Range of Applicability ($MPa.m^{\frac{1}{2}}$)	Specimen Crack Width and Type (mm)	
B	LQ - 3	0.05	2.5	2.9×10^{-11}	14 - 45	8.8	Reversed constant K 66% side grooved DCB
B	LQ - 1	0.05	3.0	5.2×10^{-12}	14 - 40	44.5	Compact tension
B	LQ - 1	0.05	3.2	6.4×10^{-12}	15 - 35		
B	TQ	0.05	4.1	8.7×10^{-14}	22 - 50	8.7	Reversed constant K 66% side grooved DCB
B	QT	0.05	4.0	1.1×10^{-13}	15 - 30	44.5	Compact tension
B	QT	0.05	5.5	1.0×10^{-11}	20 - 35		
G	LQ	0.05	2.5 - 4.0	-	20 - 55	8.7	66% side grooved DCB
G	TQ	0.05	3.8	1.1×10^{-13}	25 - 65	8.8	66% side grooved DCB
G	QT	0.05	3.3	1.0×10^{-12}	20 - 40	9.75	60% side grooved DCB
G	QT	0.05	3.1	4.1×10^{-12}	25 - 40	9.75	
G	QL	0.05	4.2	-	25 - 45	11.5	50% side grooved DCB
G	TL - 3 & TL - 5	0.05	4.0	-	25 - 45	11.0	

TABLE 5.1

Summary of Fatigue Crack Initiation Orientations for Plain Cylinders of Steels B and G

Steel	Axis of Cylinder: Direction of Forging	Number of Cylinders Tested to Failure	Orientation of Failures	Preferred Orientation
B	L	7	4 QT 3 QT/TQ	QT
	Q	5	5 TL	TL
	T	5	3 QL 2 cl. QL	QL
G	L	4	2 TQ 2 QT	-
	Q	6	3 TL 3 LT	-
	T	5	2 QL 2 LQ 1 QL/LQ	-

TABLE 5.2

Summary of Fatigue Results for Steels B and G

Steel	Axis of Specimen	Plain Cylinders $D = 3$			Repeated Tension	Reversed Torsion
	Range of: at Fatigue Limit	P (MPa)	τ (MPa)	σ_θ (MPa)	$\Delta\sigma_1$ (MPa)	$\Delta\tau/2$ (MPa)
B	L	233	262	291	698	≃ 268
	Q	282	317	352	518	
	T	282	317	352	502	
G	L	289	325	361	717	290
	Q	318	358	397	679	
	T	318	358	397	673	

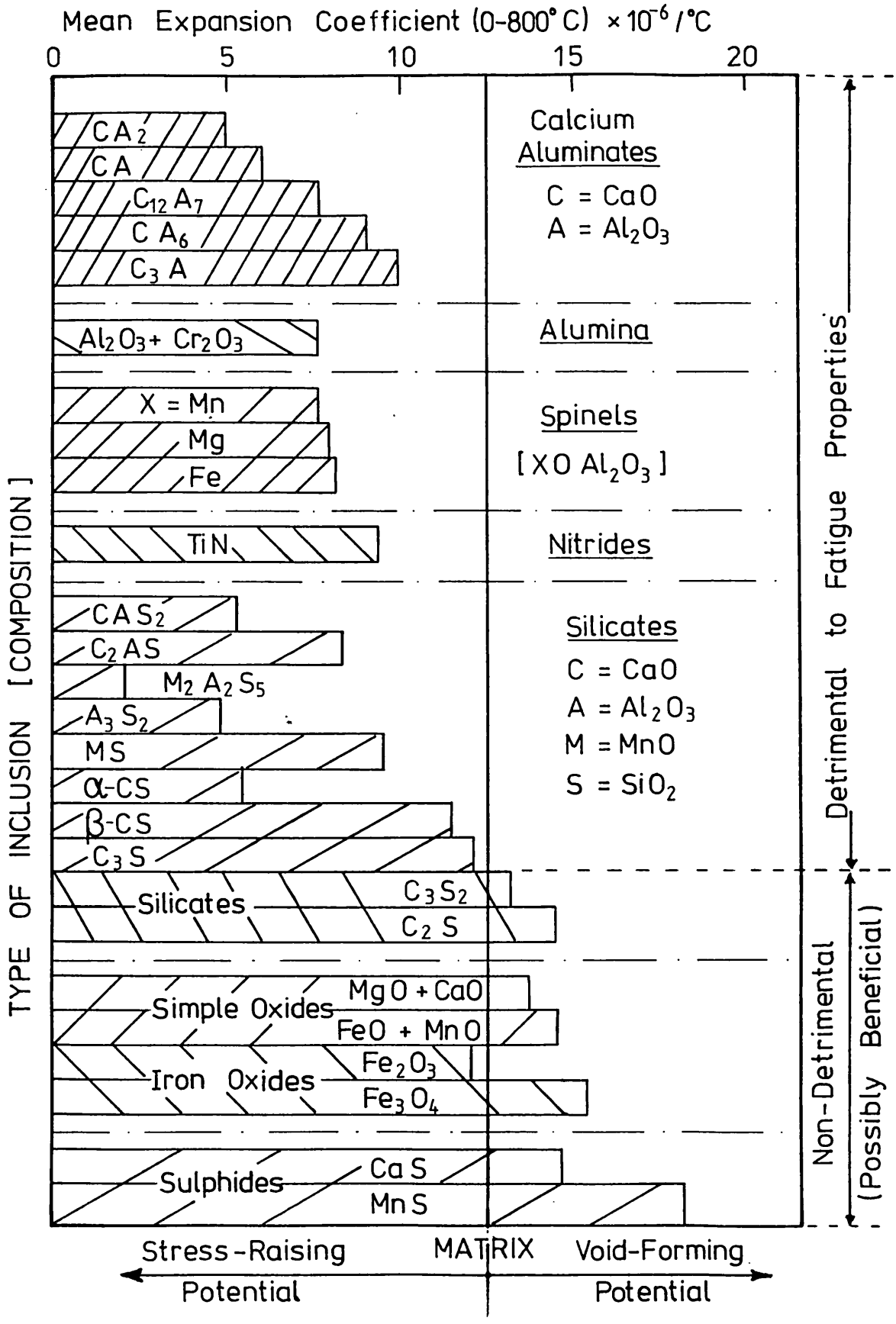

TABLE 5.3 Stress-Raising Properties of Inclusions in 1%C-Cr Bearing Steel.
[Taken from Brooksbank and Andrews (1972)]

TABLE 5.4

Material	Effective Hoop Stress Criterion. Predicted Fatigue Limit in Thick Cylinders, $\Delta\sigma_\theta$ (MPa)	Semi Range of Reversed Shear Stress Criterion. Predicted Fatigue Limit, $\Delta\tau$ (MPa)	Experimental Fatigue Limit in Thick Cylinders		Fatigue Limit % Difference in Predicted		
			$\Delta\tau$ (MPa)	$\Delta\sigma_\theta$ (MPa)	$\Delta\tau$	$\Delta\sigma_\theta$	Reference
Vibrac (soft)	572	300	287	574	+ 4.5	-0.3	Morrison et al (1960)
Vibrac (hard)	678	365	363	726	+ 0.6	-6.6	
Hykro (EN40S)	544	287	297	594	- 3.3	-8.4	
0.15% C Steel	255	136	134	268	+ 1.5	-4.8	
Al Alloy (DTD364)	270*	96*	140*	280*	-31.0	-3.5	
Titanium	334*	174*	180*	360*	- 3.3	-6.7	
EN56C	493	234	255	510	- 8.2	-3.3	Parry (1965)
Austenitic Stainless	462	184	167	334	+10.0	+38	
EN31	715	510	347	694	+46.9	+3.0	
EN25	578	284	287	574	- 1.0	+0.7	Parry (1956)
EN25	562	301	278	556	+ 7.6	+1.0	Morrison et al (1956)

* Endurance limit at 10^7 cycles

LIST OF FIGURES

(d) Volume fraction of inclusions

(e) Mean inclusion diameter (equivalent circle diameter - Quantimet)

(f) Mean inclusion spacing

5.5 : Critical pressure and crack depths for double cross-bored cylinders as a function of wall thickness

5.6 : (a) Schematic representation of the inclusion population in steel B

(b) Schematic representation of the inclusion population in steel G

5.7 : Comparison of experimental and predicted fatigue limits for steels B and G

5.8 : Comparison of previous results of repeated internal pressure fatigue tests using the effective stress range criterion

5.9 : Comparison of crack growth rates for various orientations of specimen measured in air. Steel B

5.10 : Comparison of crack growth rates for various orientations of specimen measured in air. Steel G

5.11 : Comparison of crack growth rates measured in air for steels B and G

5.12 : Comparison of actual and predicted endurances of thick cylinders (longitudinal axis in L direction) of steel B

5.13 : Comparison of actual and predicted endurances of thick cylinders (longitudinal axis in L direction) of steel G

5.14 : Variation of stress intensity factor with crack length for a double cantilever beam specimen predicted by analytical expressions and found by experiment

5.15 : Approximate stress intensity factor versus crack depth for varying crack shapes in internally pressurised thick cylinders

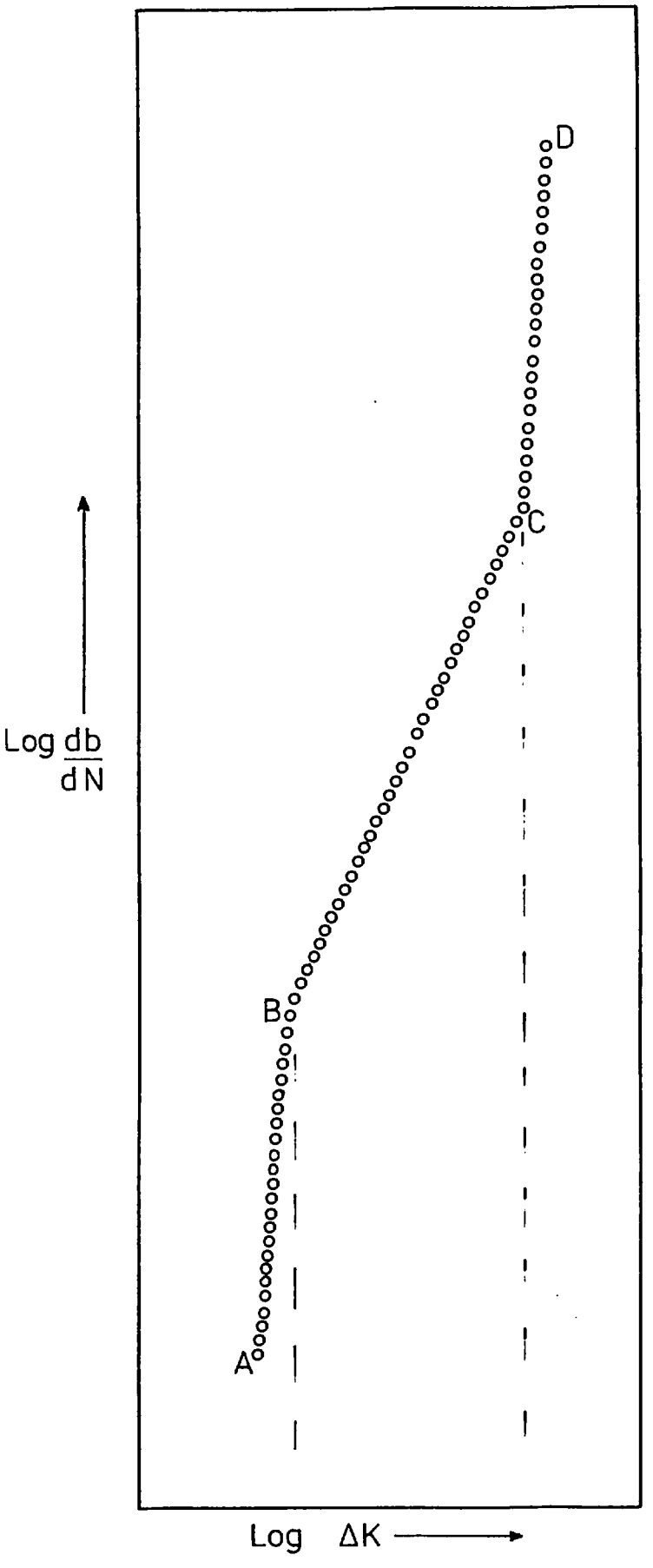

FIGURE 2.1 Typical Crack Growth Rate Versus Stress Intensity Plot

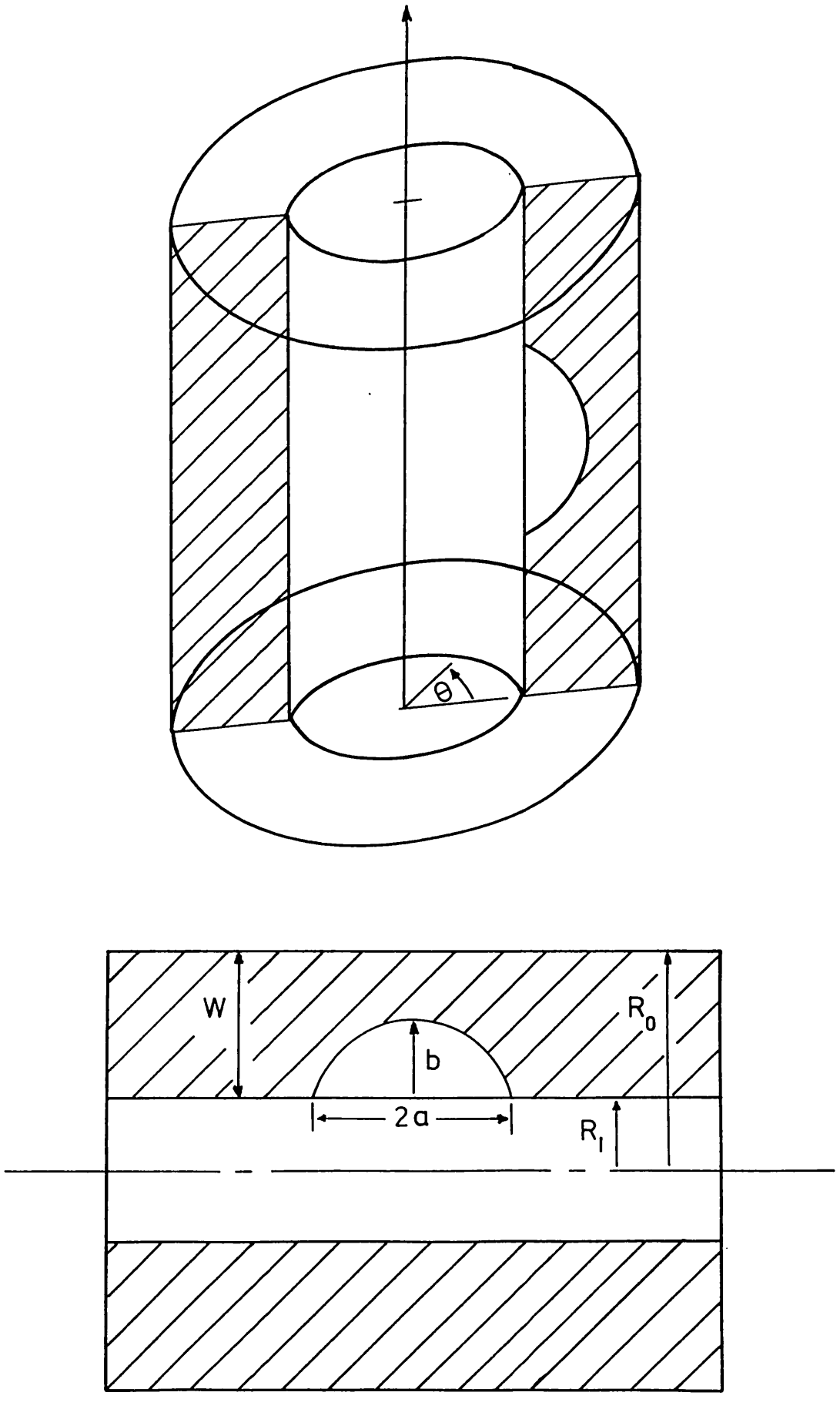

FIGURE 2.2 NOTATION FOR CRACKS IN CYLINDERS

FIGURE 2.3 Variation of Stress Intensity Factor with Crack Depth for Straight Fronted Cracks in Internally Pressurised Cylinders. [Taken from Bowie (1956)]

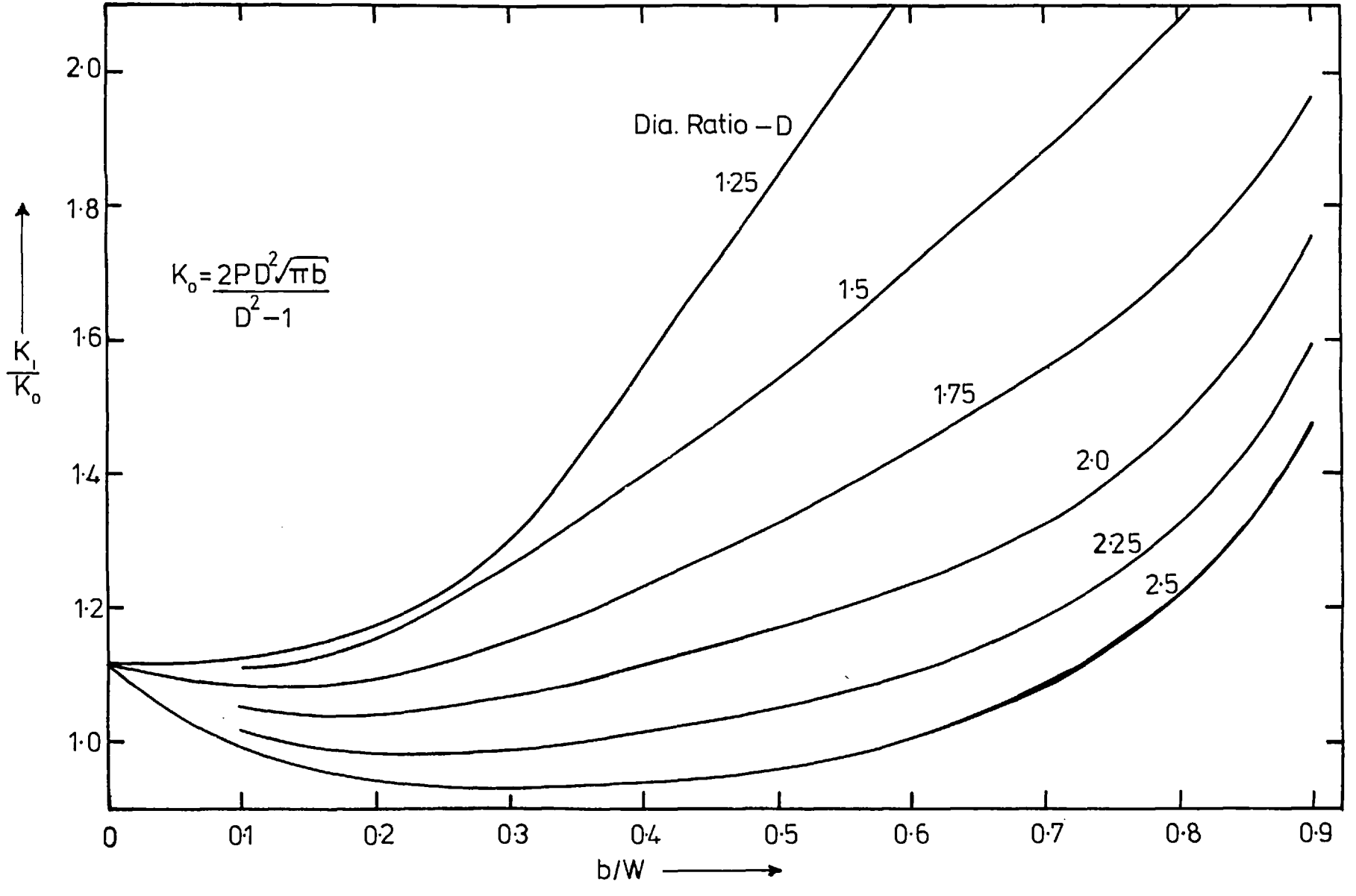

FIGURE 2.4

Comparison of Stress Intensity Factors for Semi-Elliptic Cracks in Cylinders.

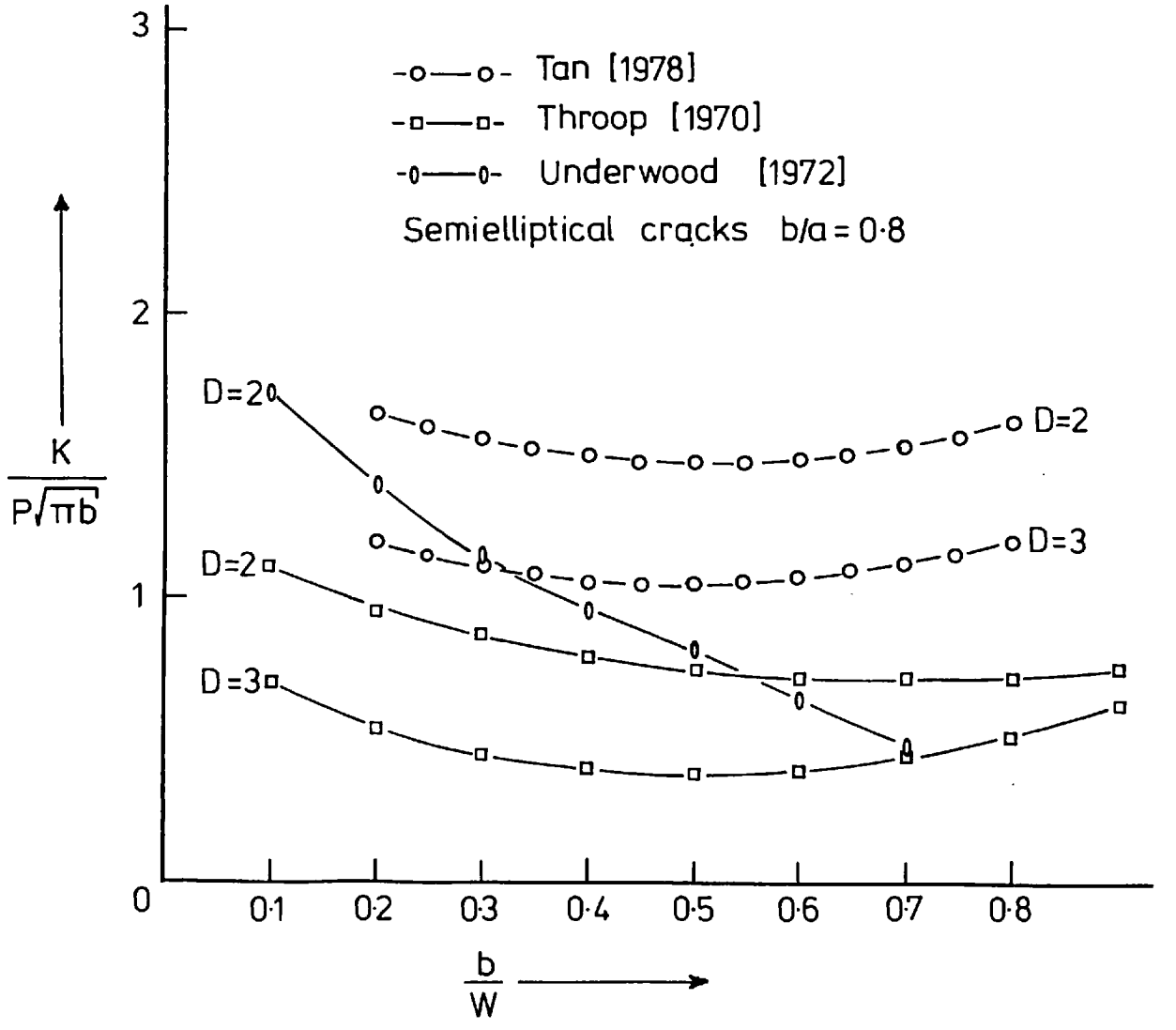

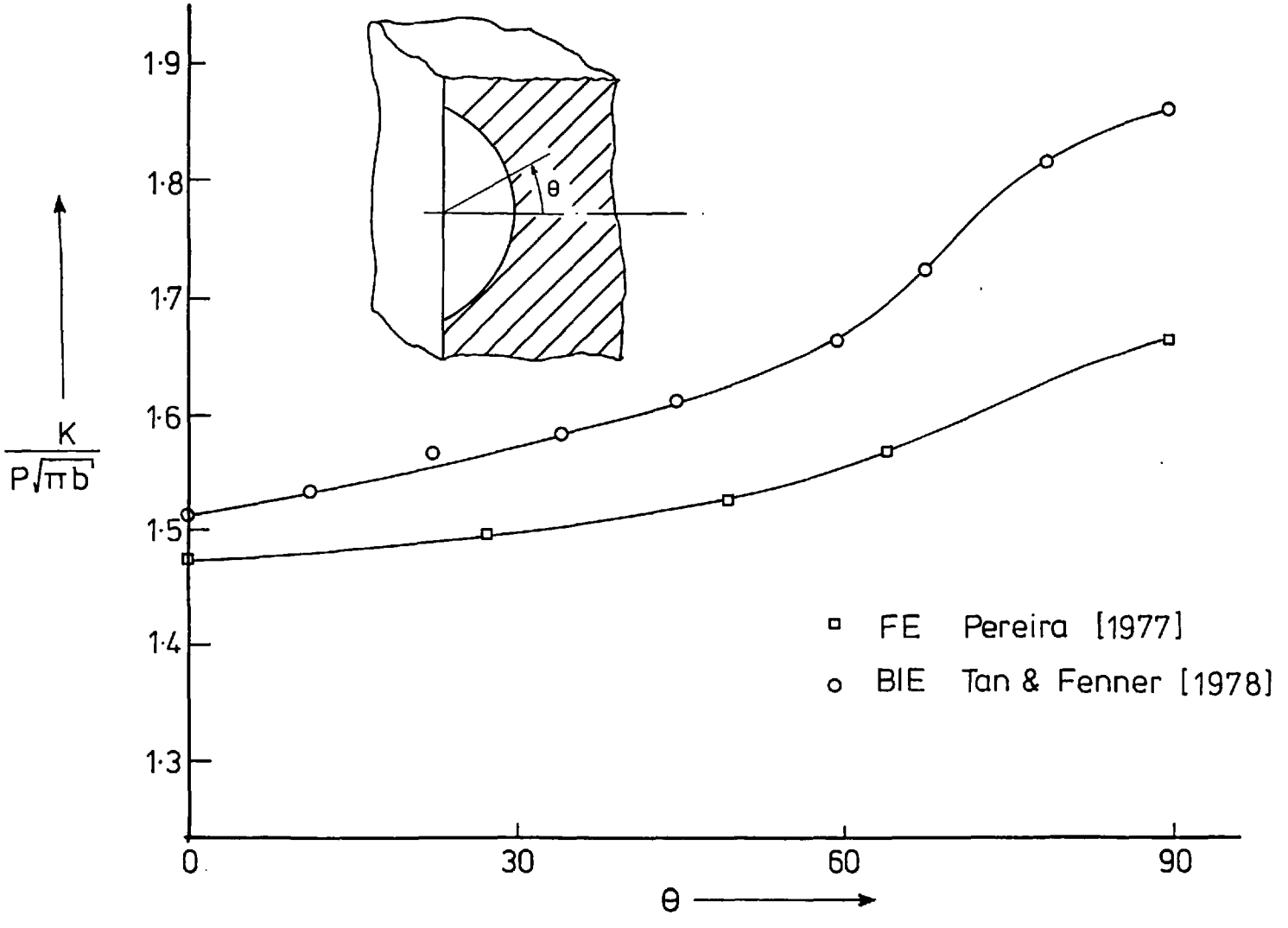

FIGURE 2.5 Variation of Stress Intensity Factor at the Periphery of a Semi-Elliptic Crack in a Cylinder

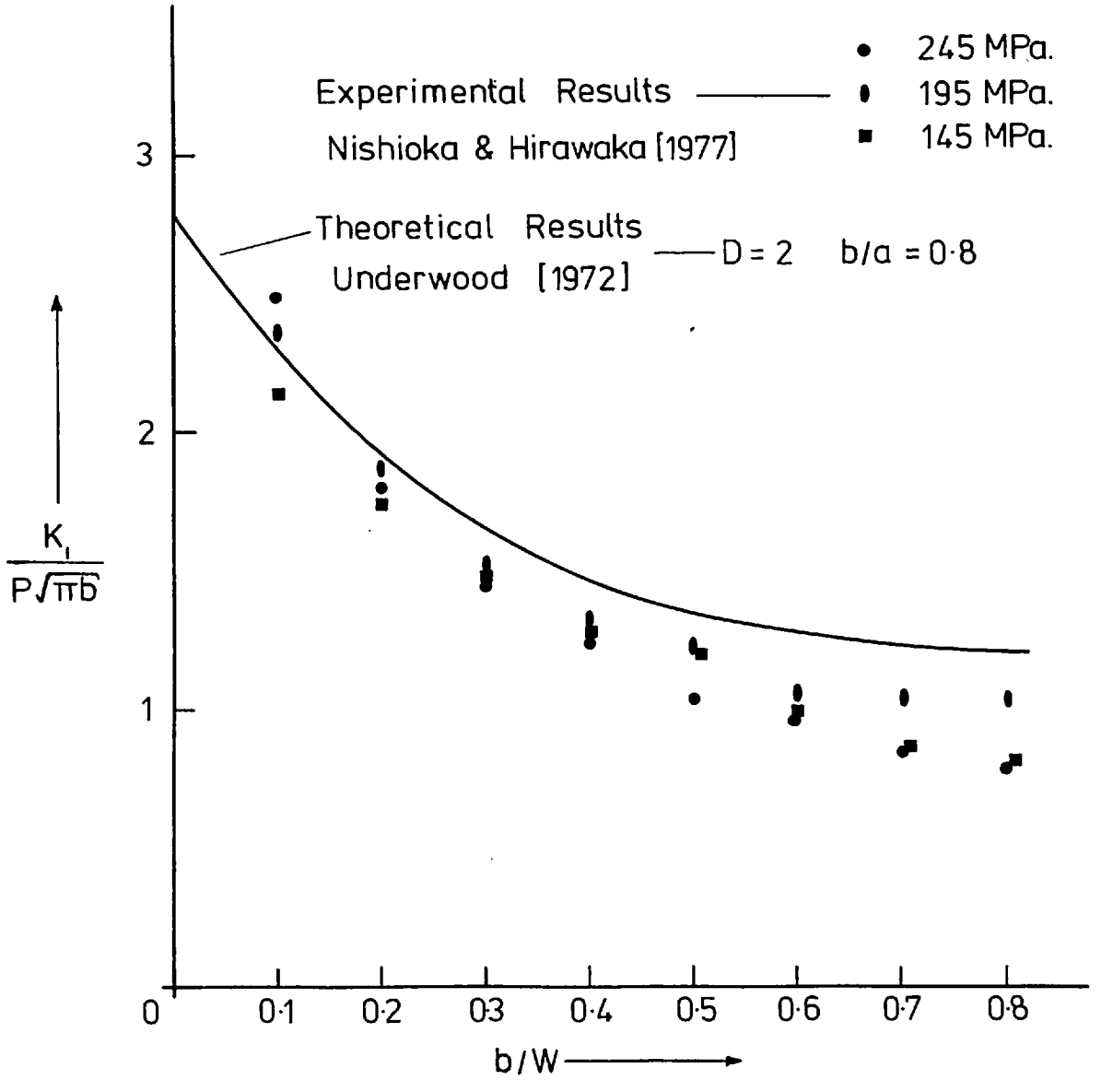

FIGURE 2.6 Variation of Stress Intensity with Crack Depth

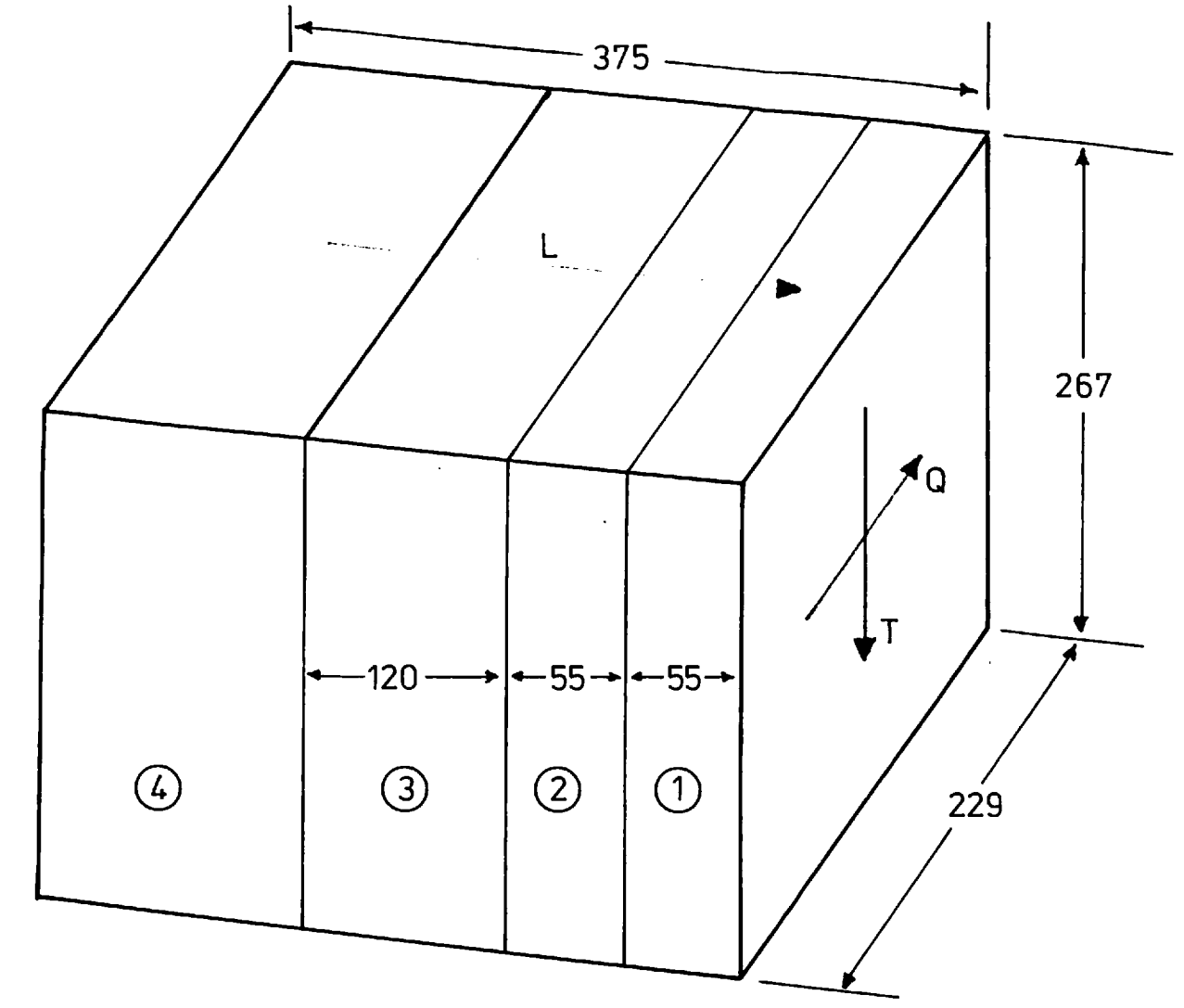

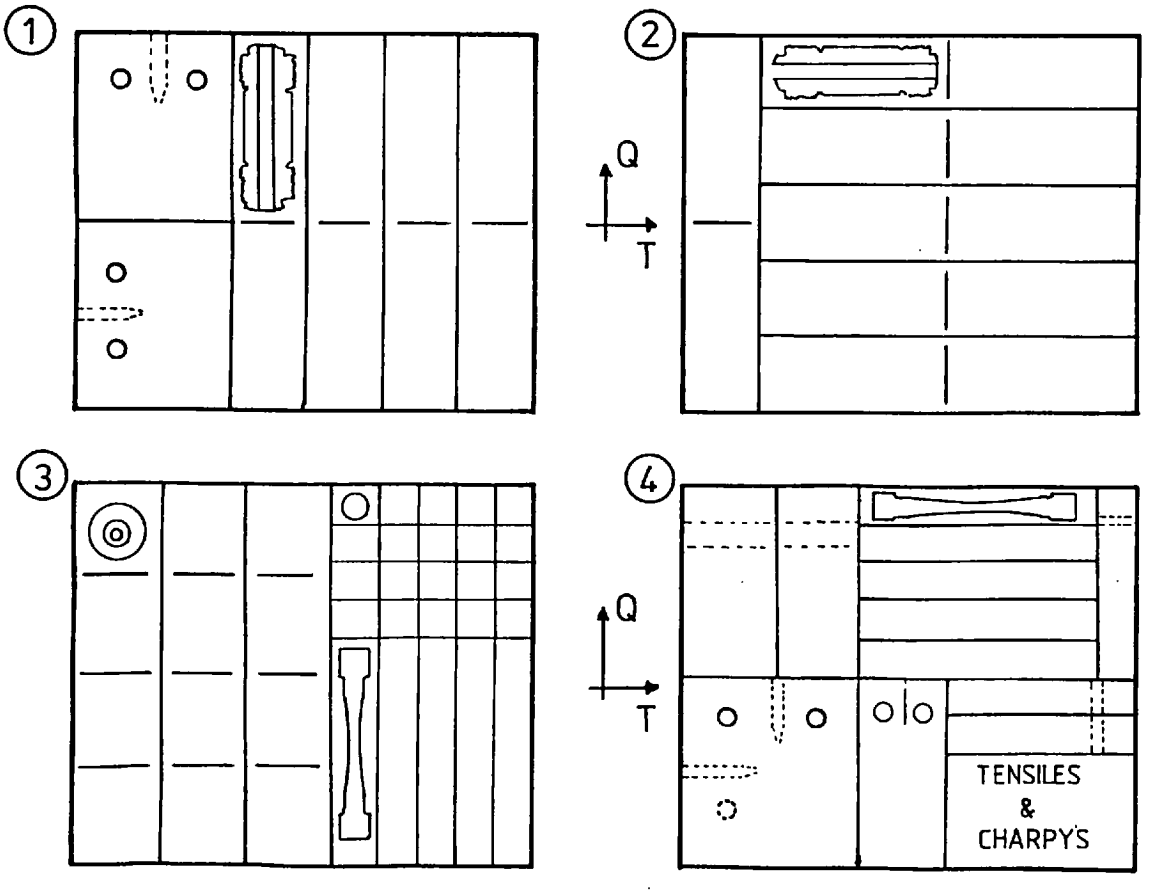

FIGURE 3.1 CUTTING PLAN — STEEL B

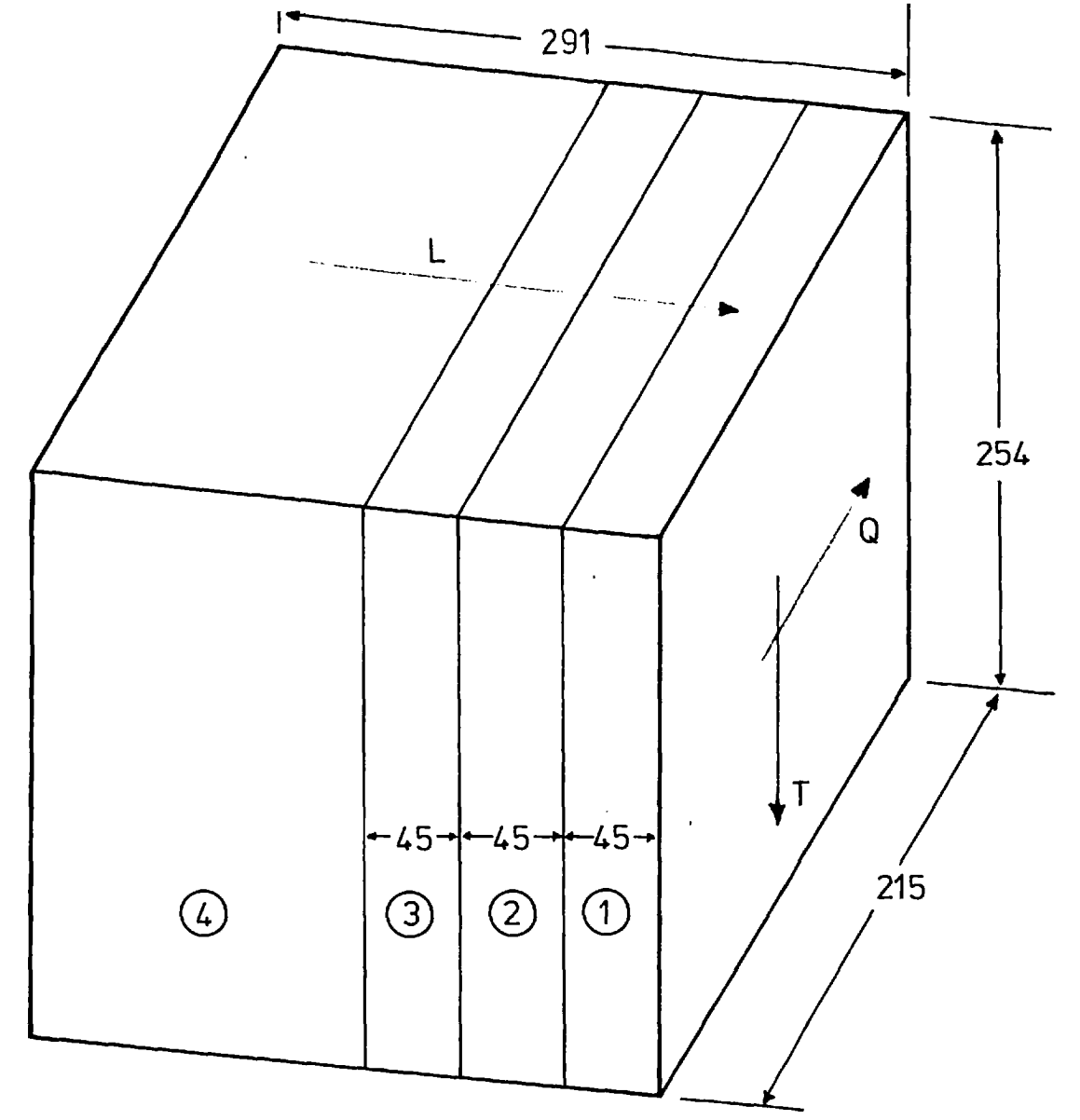

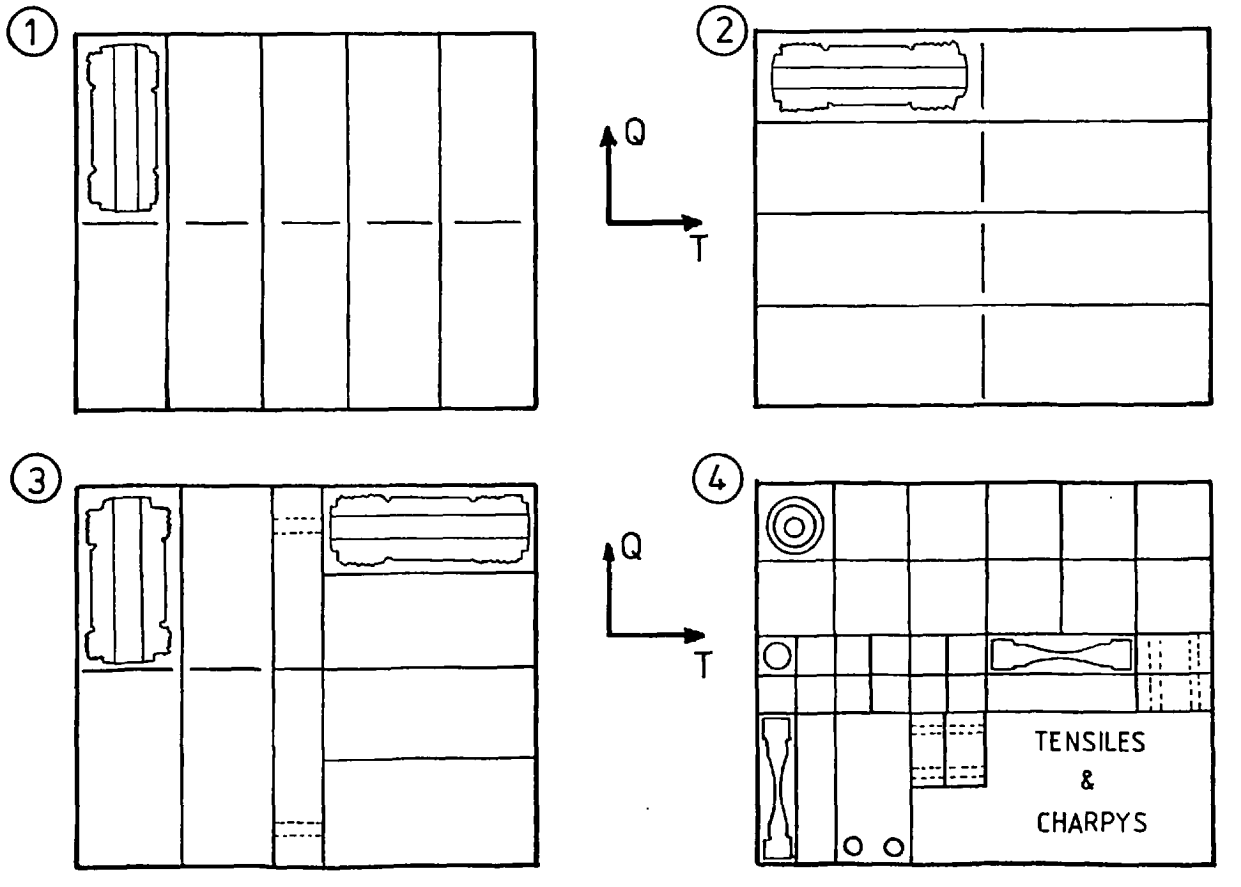

FIGURE 3.2 CUTTING PLAN — STEEL G

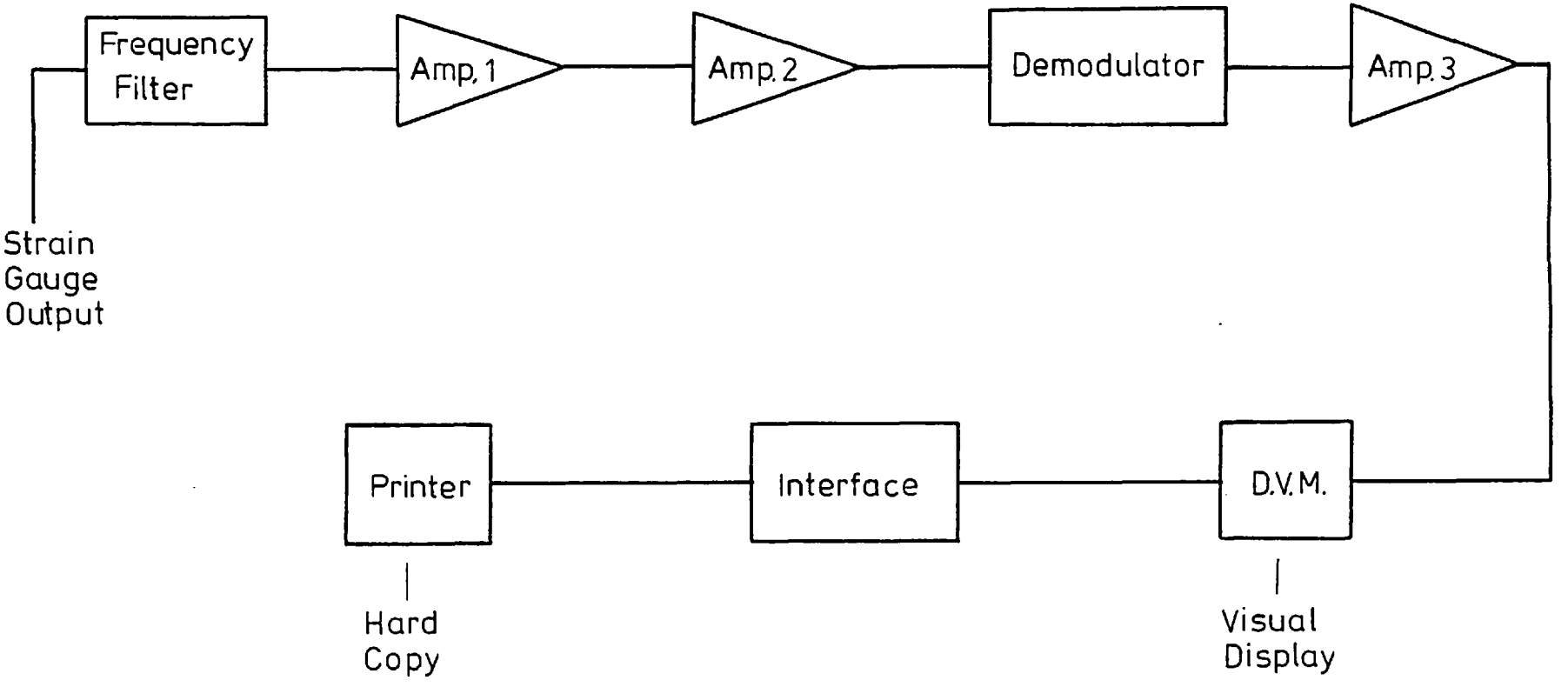

FIGURE 3.3
Schematic Outline Of Strain Gauge Signal Processing

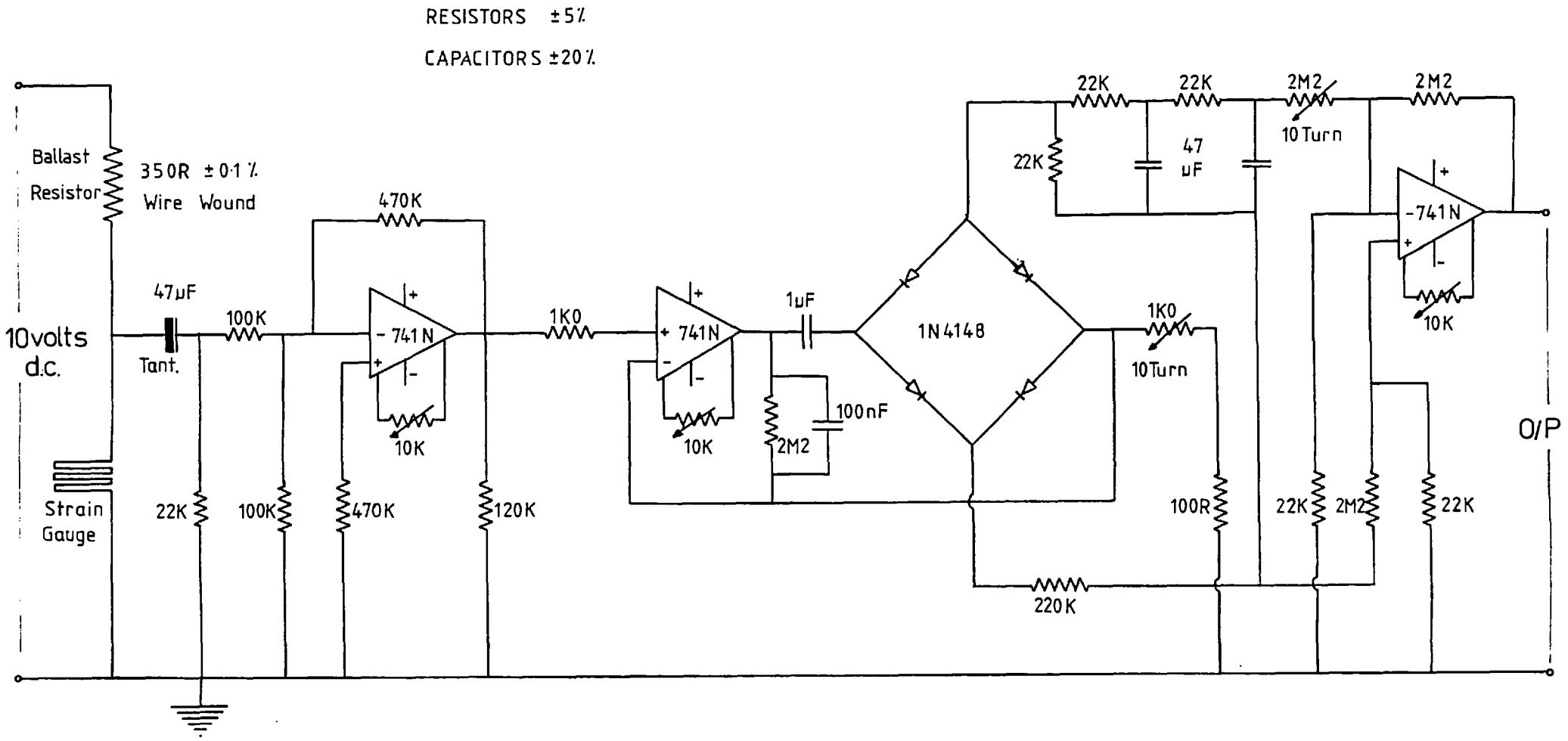

FIGURE 3.4 CIRCUIT DETAILS - STRAIN GAUGE AMPLIFIER

FIGURE 3.5

CIRCUIT DETAILS — POWER SUPPLIES

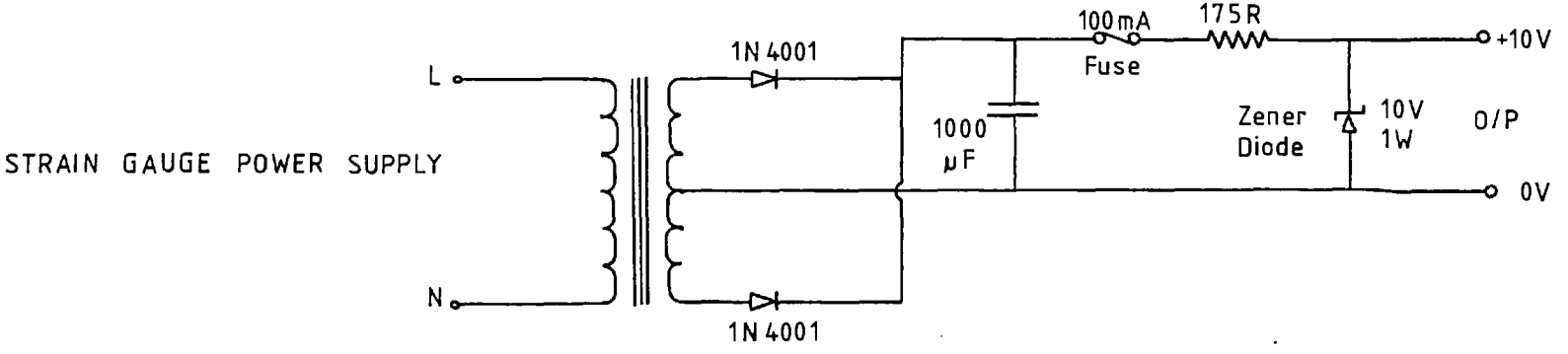

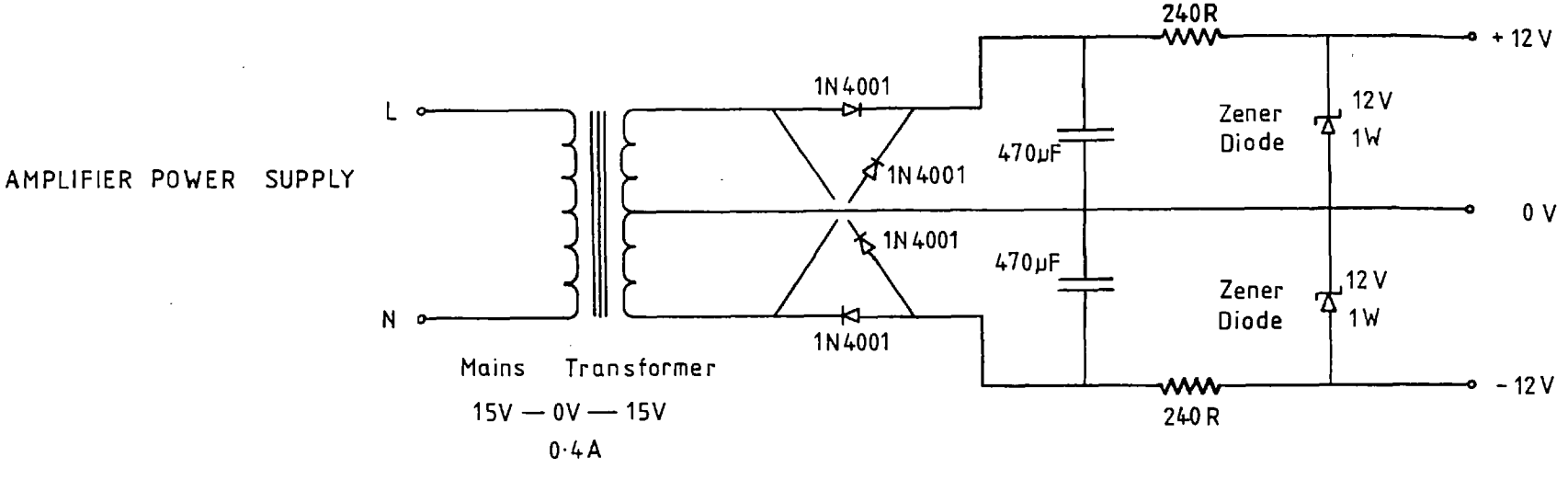

FIGURE 4.1 Inclusion Size Analysis

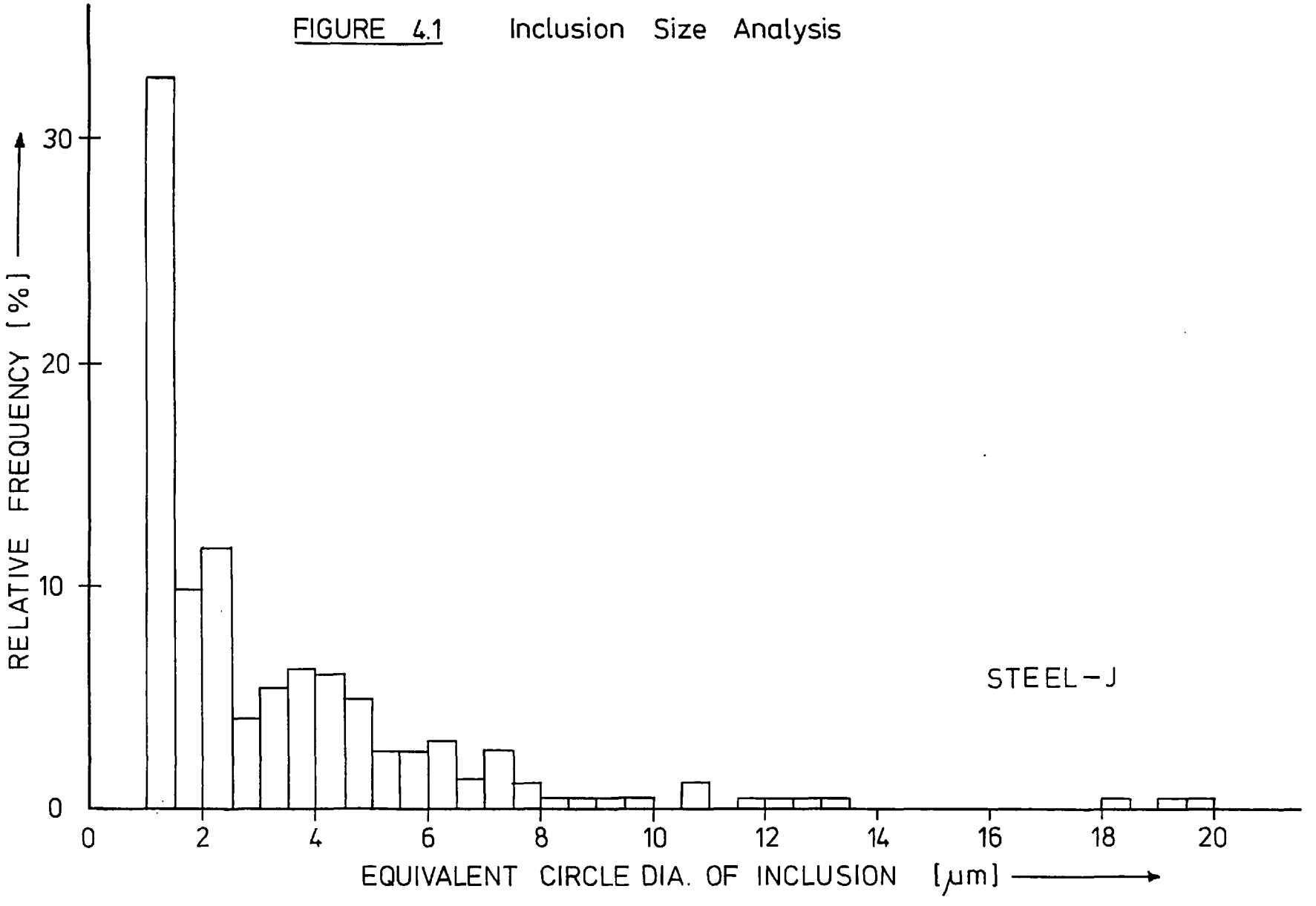

FIGURE 4.2 Inclusion Size Analysis

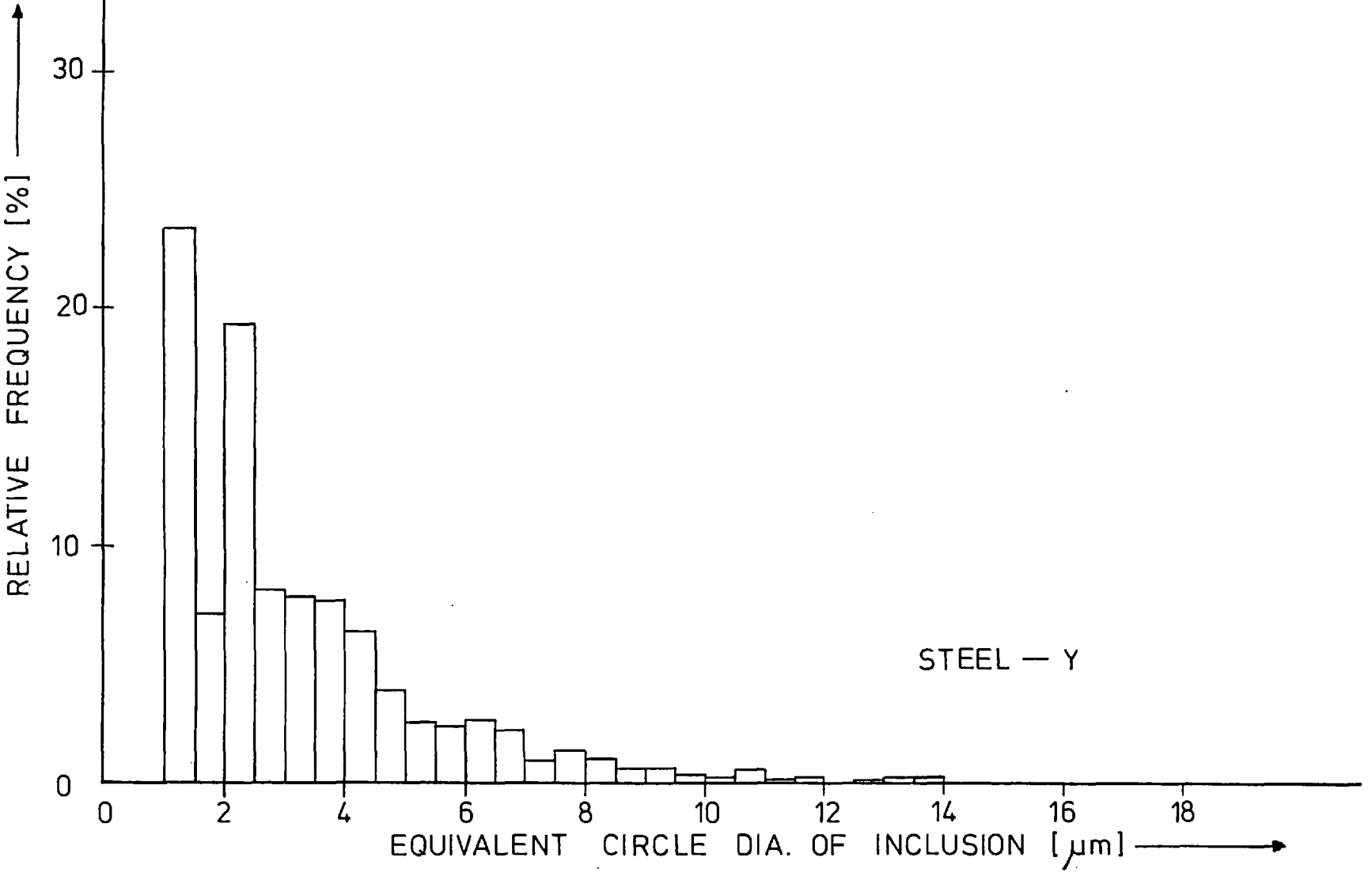

FIGURE 4.3 Inclusion Size Analysis

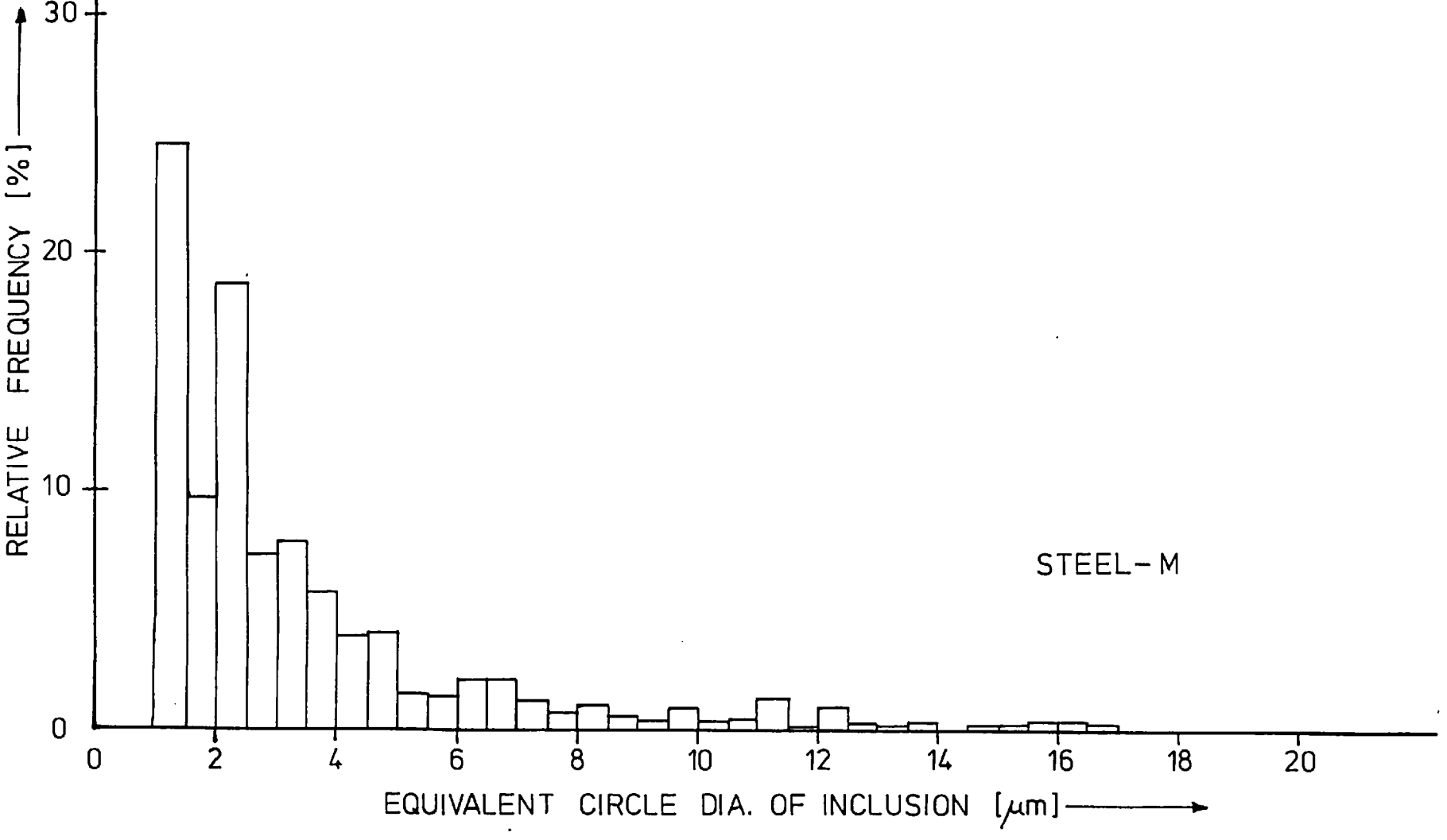

FIGURE 4.4 Inclusion Size Analysis

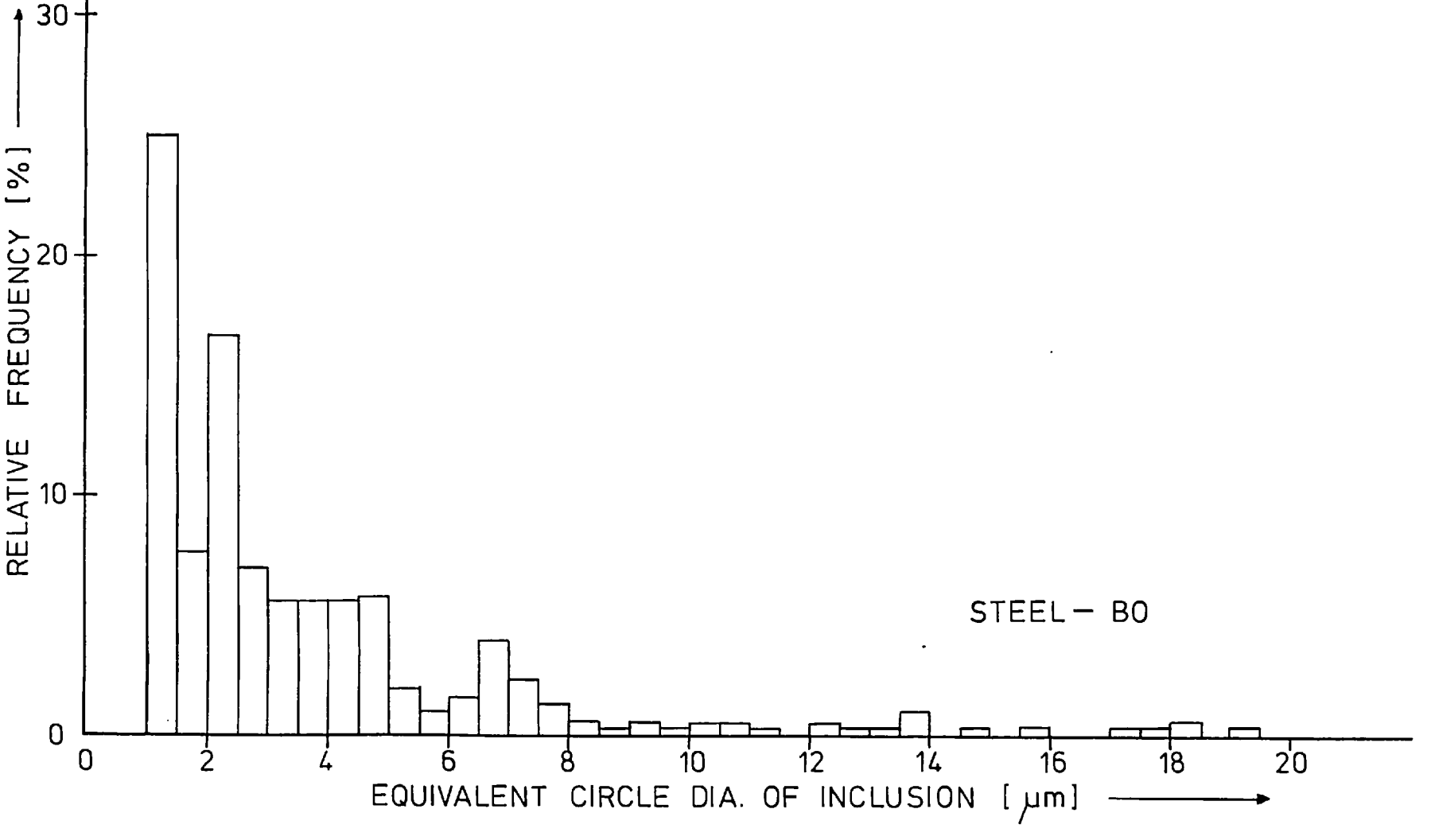

FIGURE 4.5 Inclusion Size Analysis

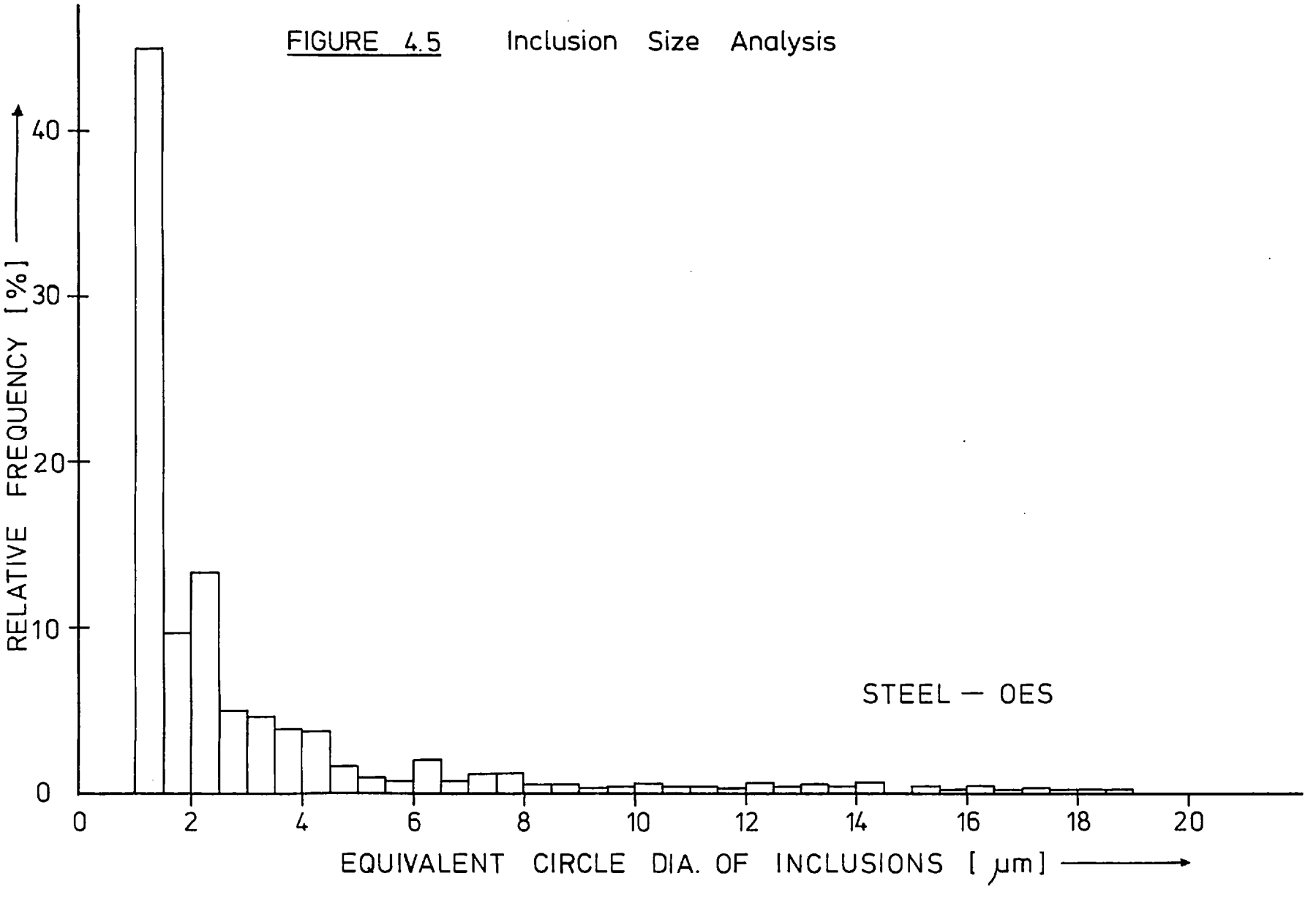

FIGURE 4.6 Comparison of Inclusion Size Analyses [Quantimet]

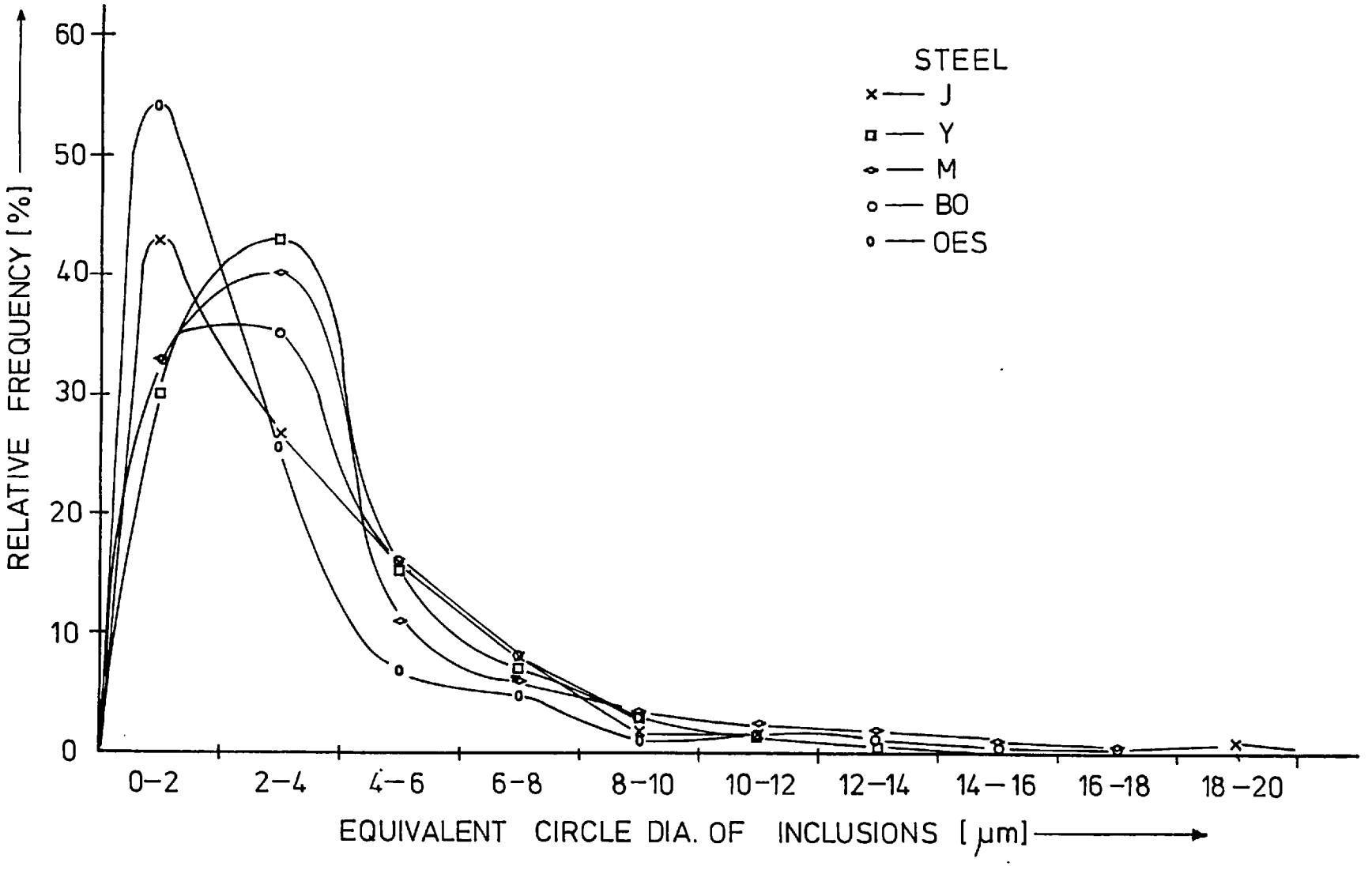

FIGURE 4.7 Inclusion Size Analyses [Quantimet]

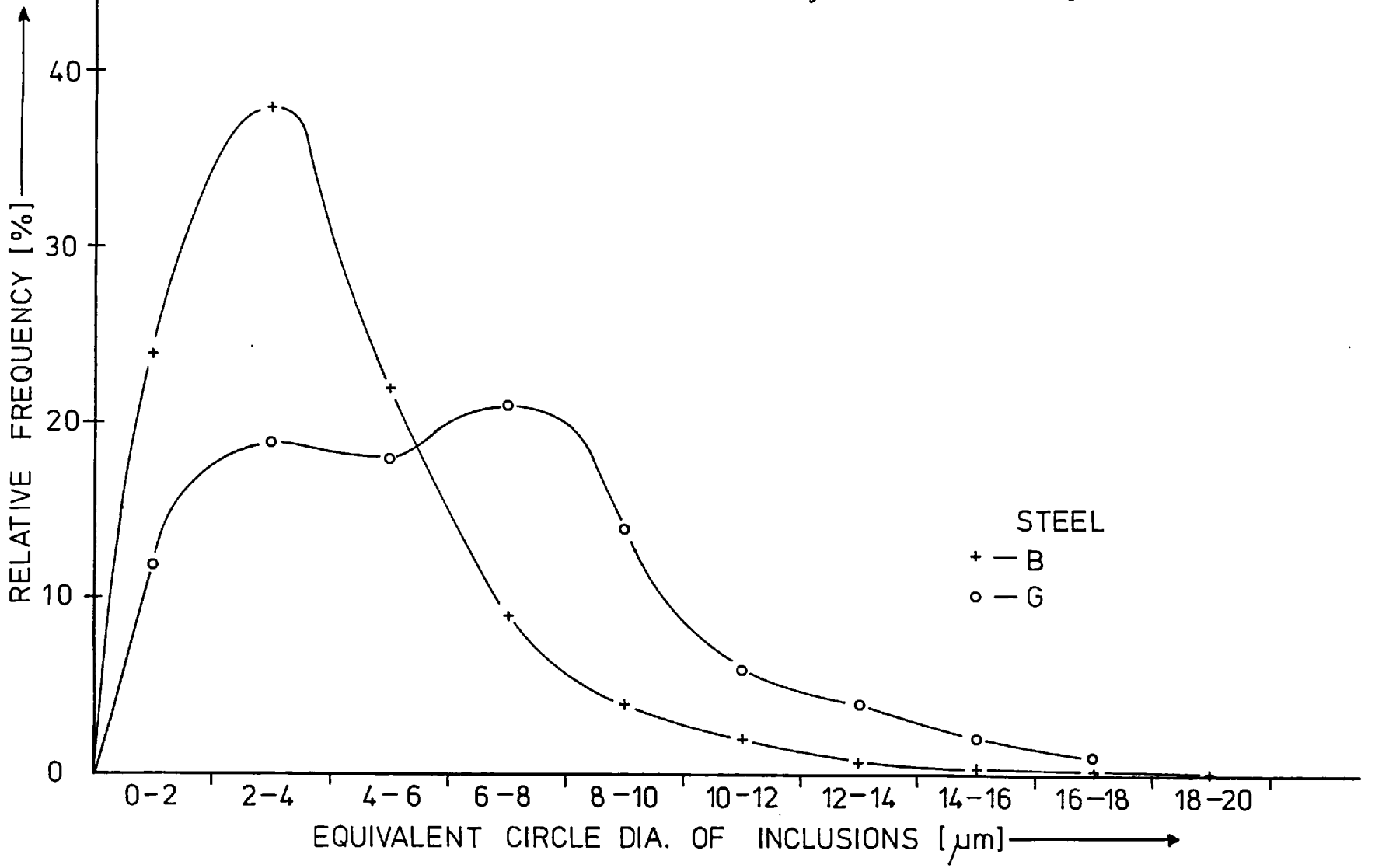

FIGURE 4.8 Inclusion Size Analyses [Visual]

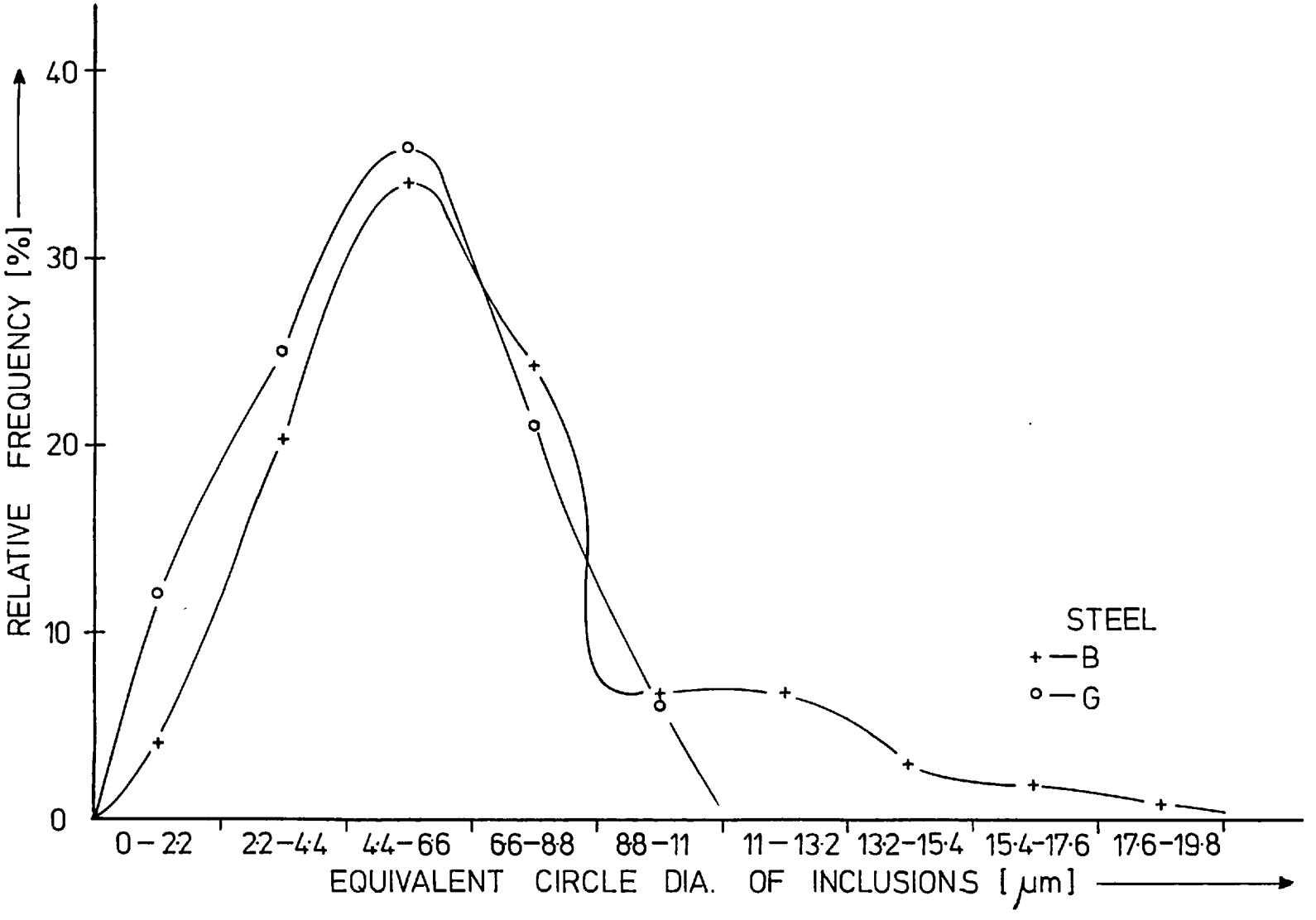

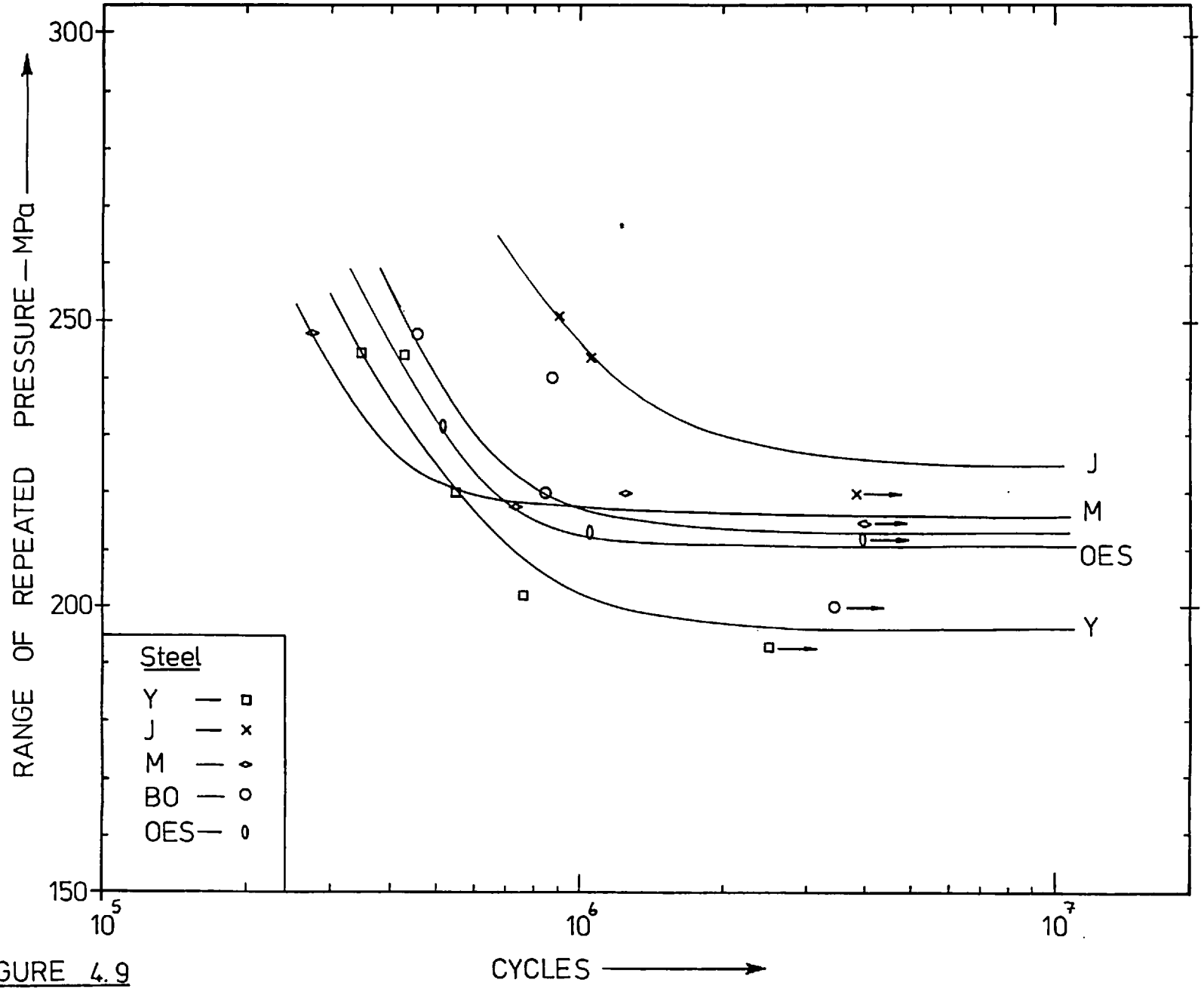
300
250
200
150
RANGE OF REPEATED PRESSURE — MPa
10^5
10^6
10^7
CYCLES
J
M
OES
Y
Steel
Y
J
M
BO
OES

FIGURE 4.9

FIGURE 4.10

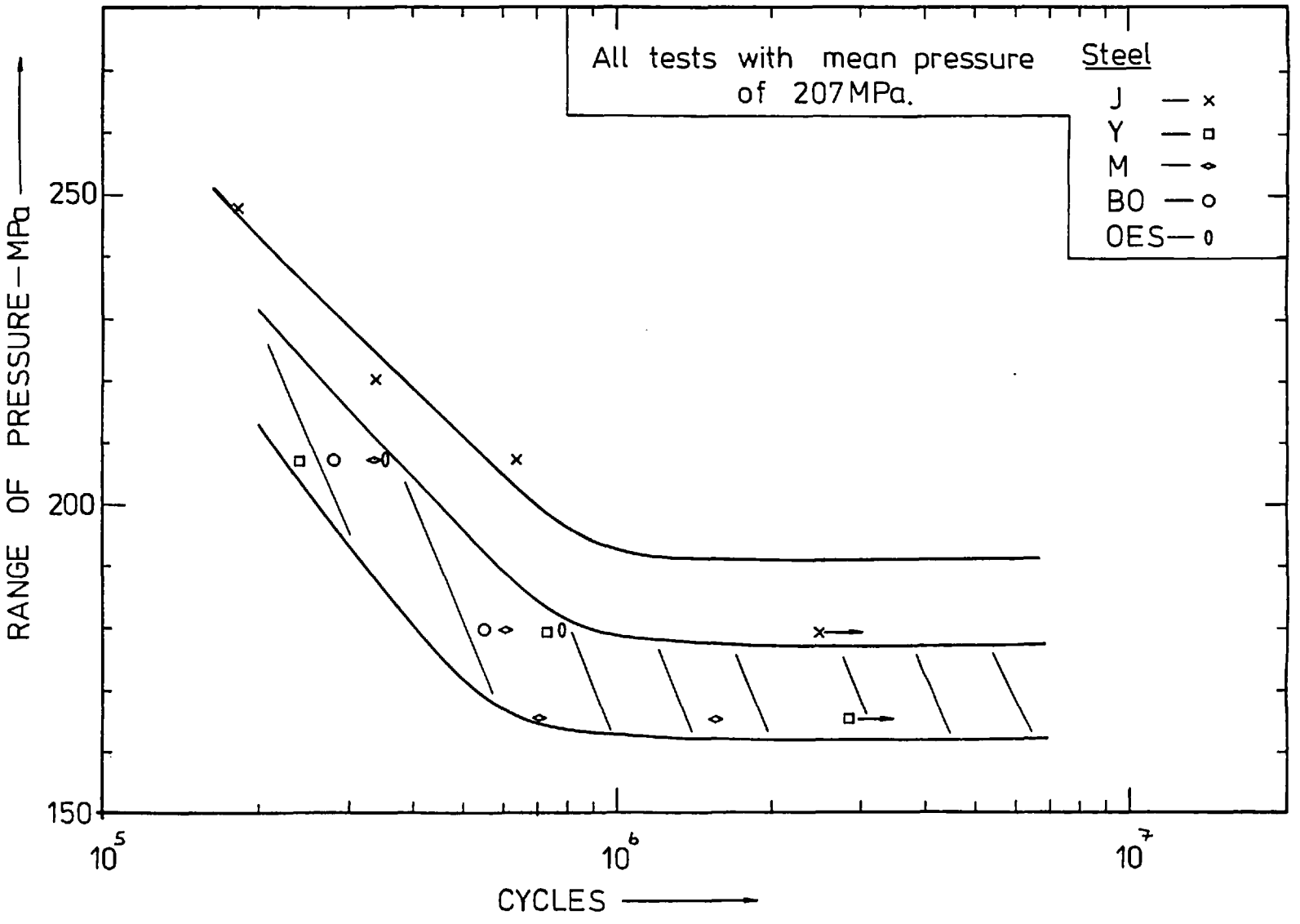
All tests with mean pressure of 207MPa.
Steel
J — ×
Y — □
M — ◇
BO — ○
OES — ◊
RANGE OF PRESSURE — MPa
250
200
150
10^5
10^6
10^7
CYCLES

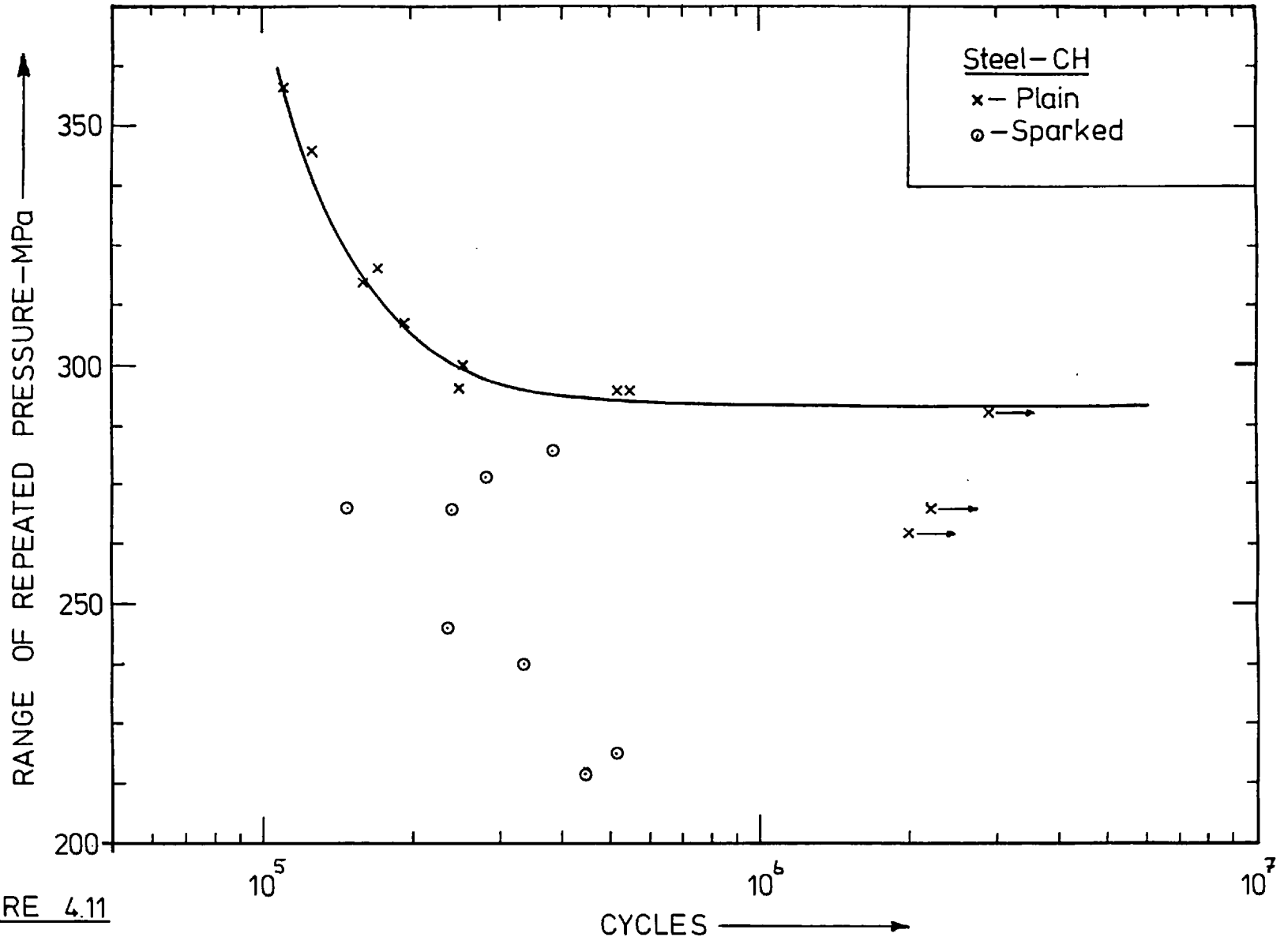
Steel – CH
× – Plain
⊙ – Sparked
RANGE OF REPEATED PRESSURE – MPa
350
300
250
200
10^5
10^6
10^7
CYCLES

FIGURE 4.11

FIGURE 4.12

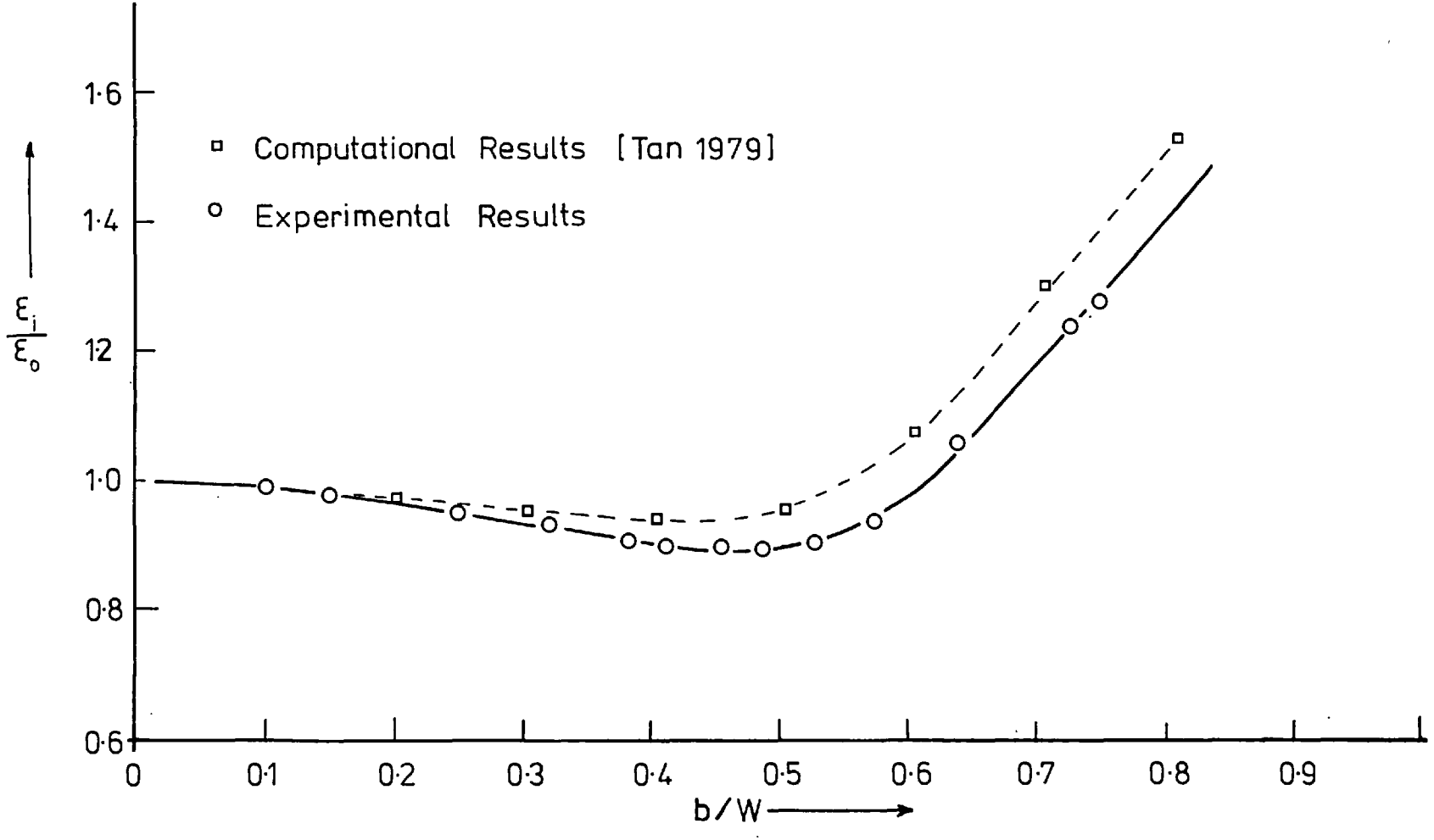
Computational Results [Tan 1979]
Experimental Results
$\frac{\varepsilon_i}{\varepsilon_o}$
1·6
1·4
1·2
1·0
0·8
0·6
0
0·1
0·2
0·3
0·4
0·5
0·6
0·7
0·8
0·9
b/W

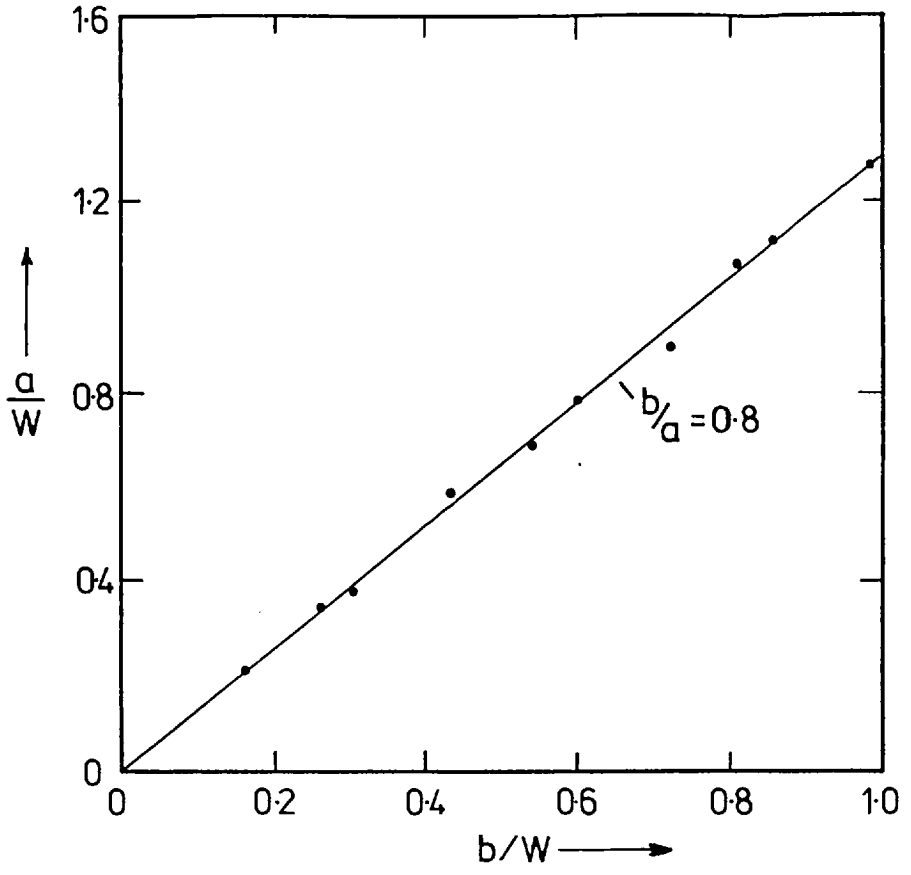

FIGURE 4.13

FIGURE 4.14

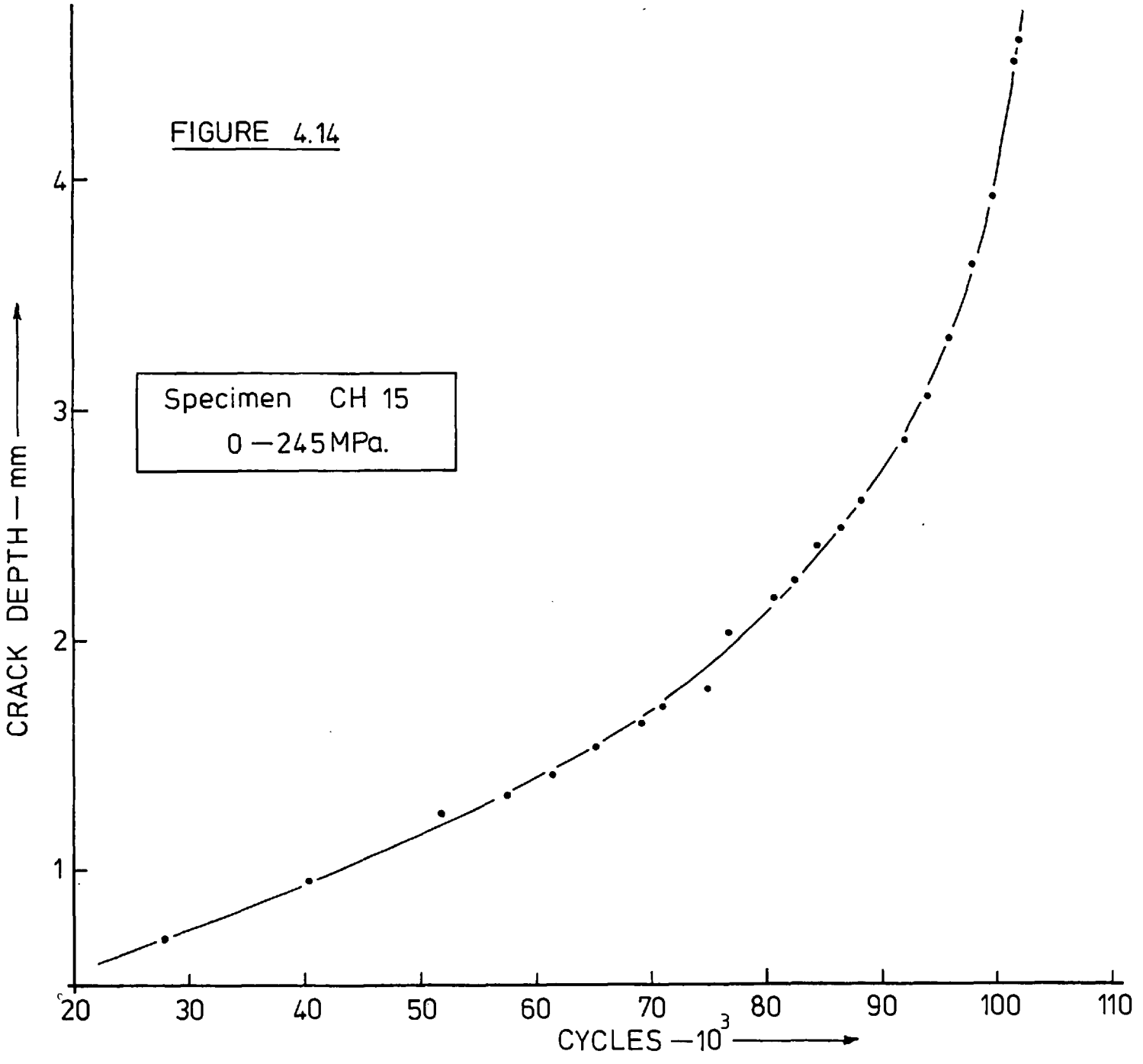
Specimen CH 15
0 — 245 MPa.
CRACK DEPTH — mm
1
2
3
4
20
30
40
50
60
70
80
90
100
110
CYCLES — 10³

FIGURE 4.15

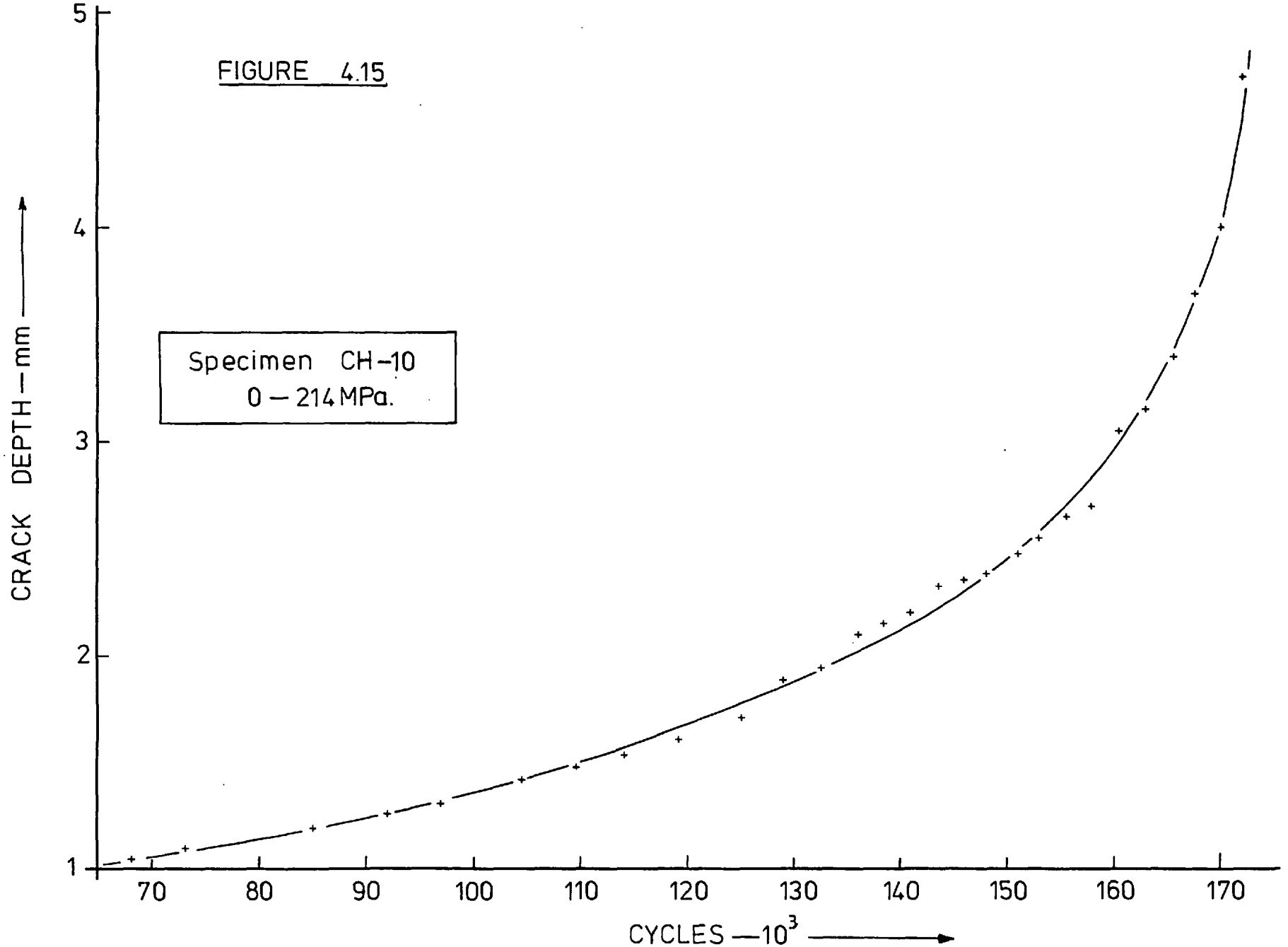
Specimen CH-10
0 — 214 MPa.
CRACK DEPTH — mm
CYCLES — 10^3
1
2
3
4
5
70
80
90
100
110
120
130
140
150
160
170

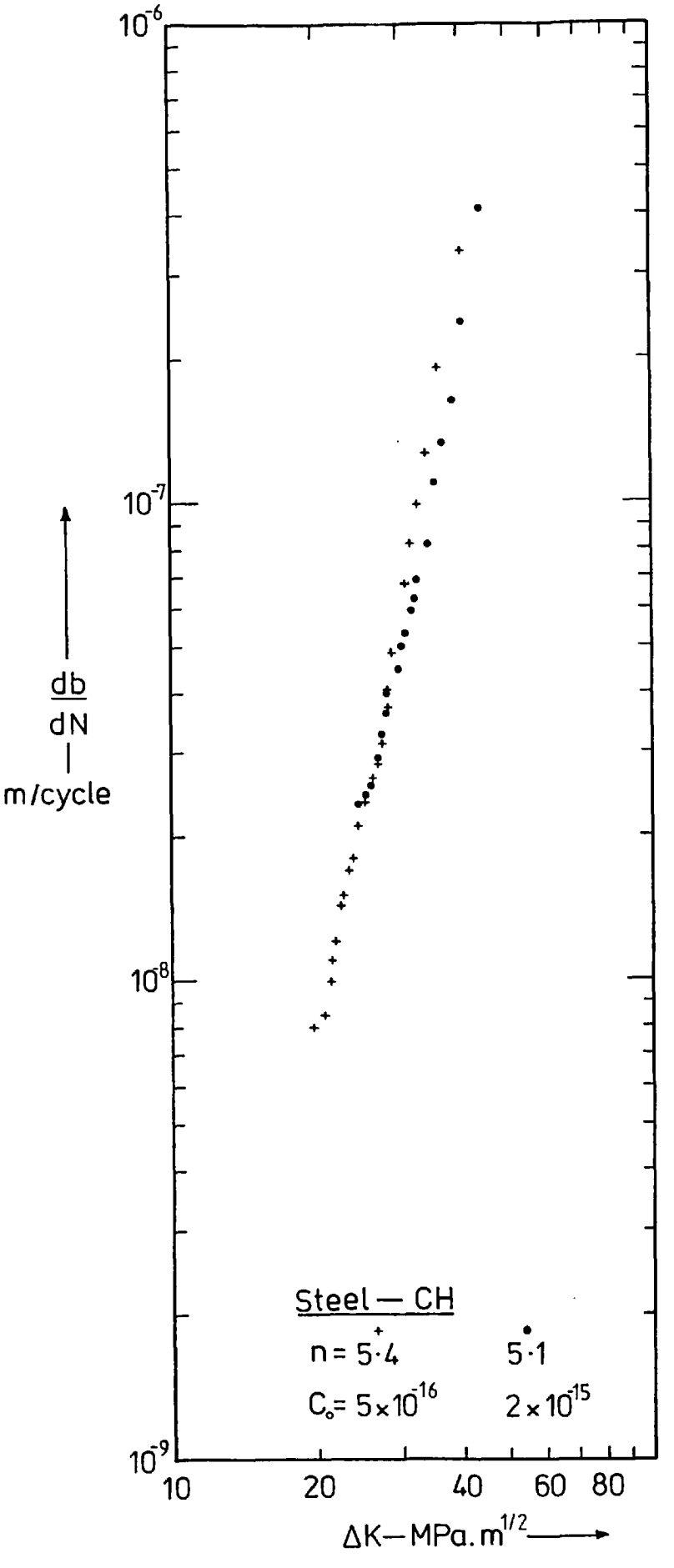
10^{-6}
10^{-7}
10^{-8}
10^{-9}
db/dN
m/cycle
Steel — CH
n = 5·4
5·1
$C_o = 5 \times 10^{-16}$
2×10^{-15}
10
20
40
60
80
ΔK — MPa.m$^{1/2}$

FIGURE 4.16

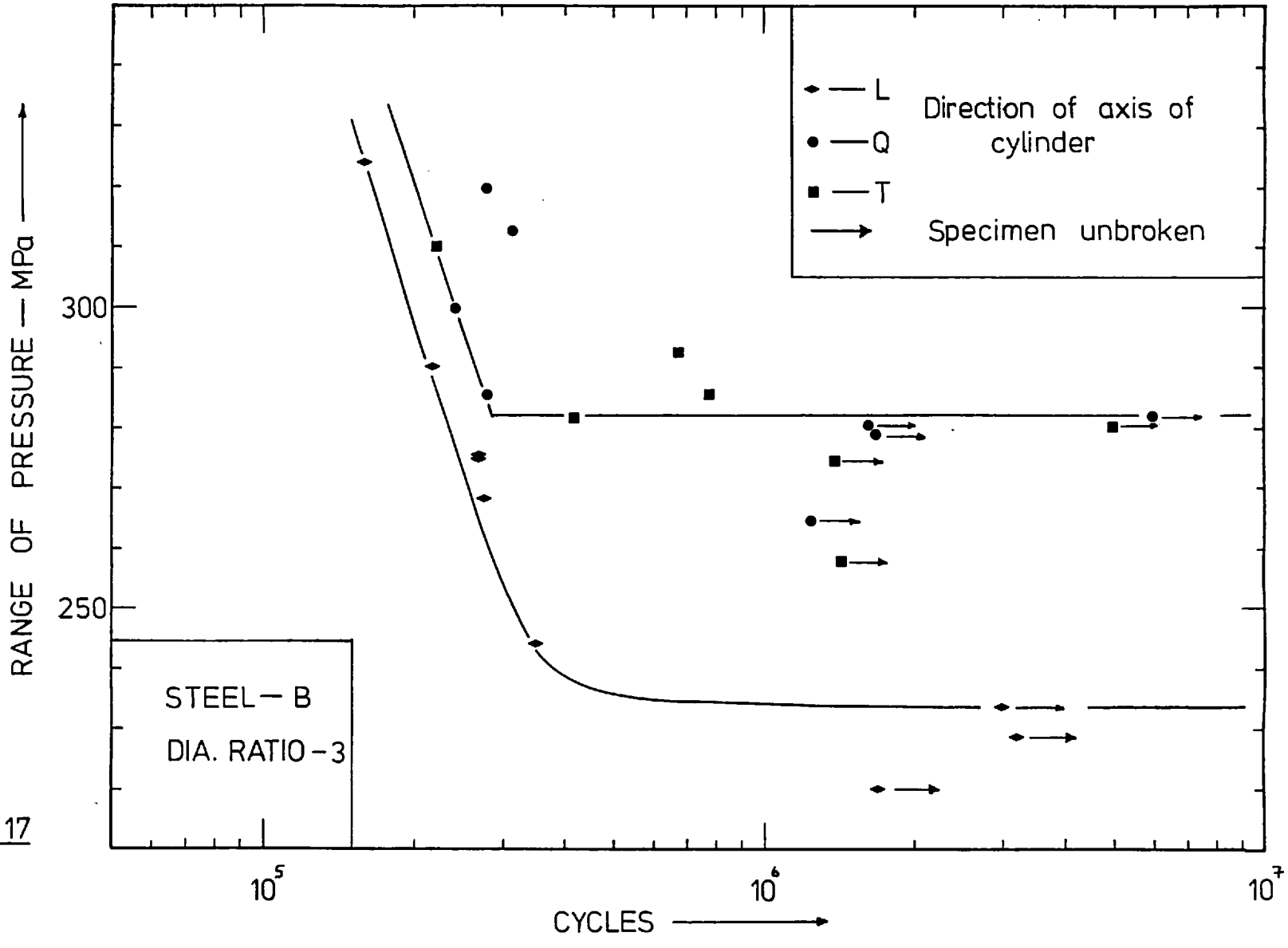
L
Q
T
Direction of axis of cylinder
Specimen unbroken
RANGE OF PRESSURE — MPa
300
250
STEEL — B
DIA. RATIO - 3
10^5
10^6
10^7
CYCLES

FIGURE 4.17

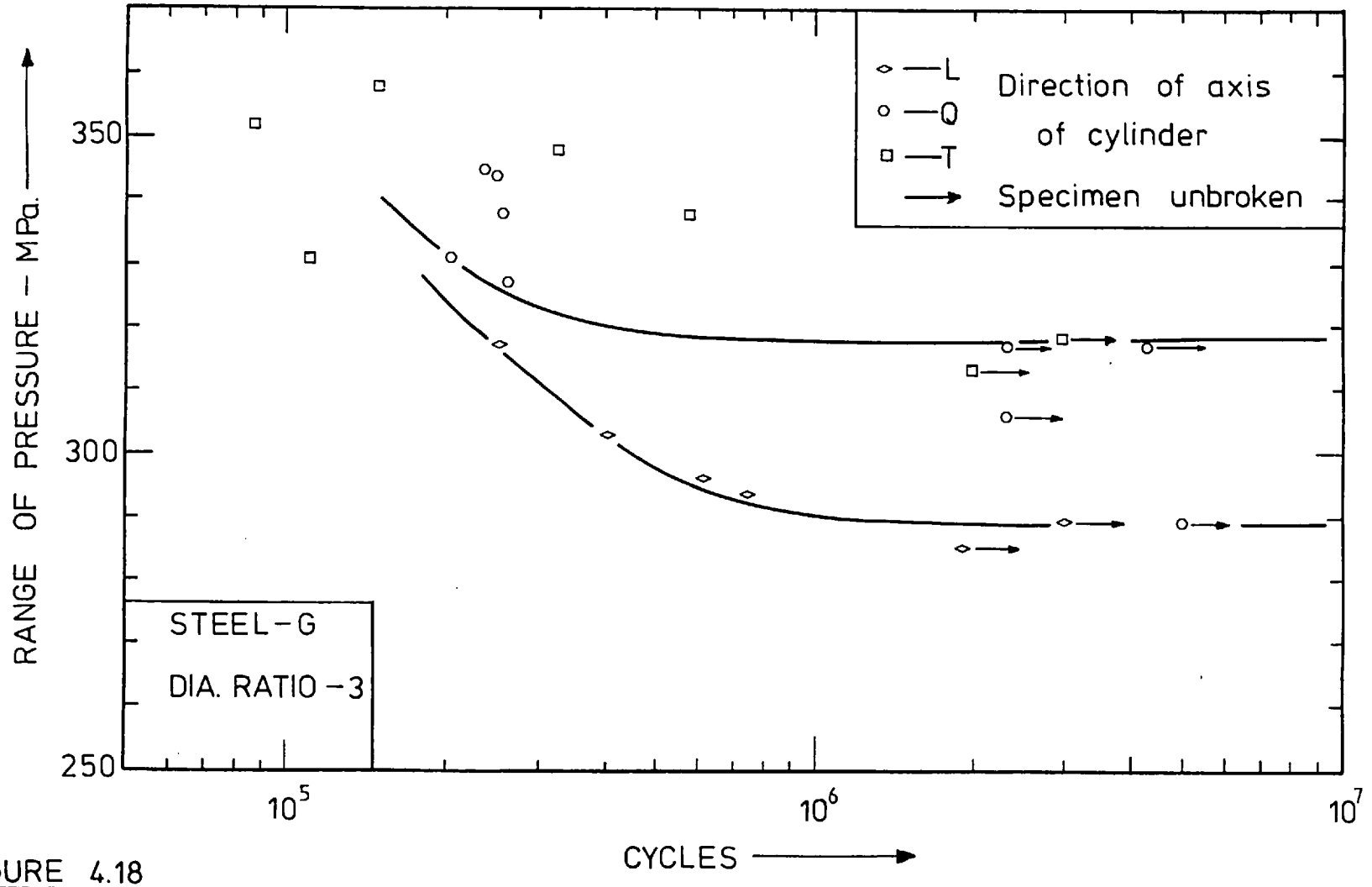
RANGE OF PRESSURE – MPa.
350
300
250
10^5
10^6
10^7
CYCLES
L
Q
T
Direction of axis of cylinder
Specimen unbroken
STEEL – G
DIA. RATIO – 3

FIGURE 4.18

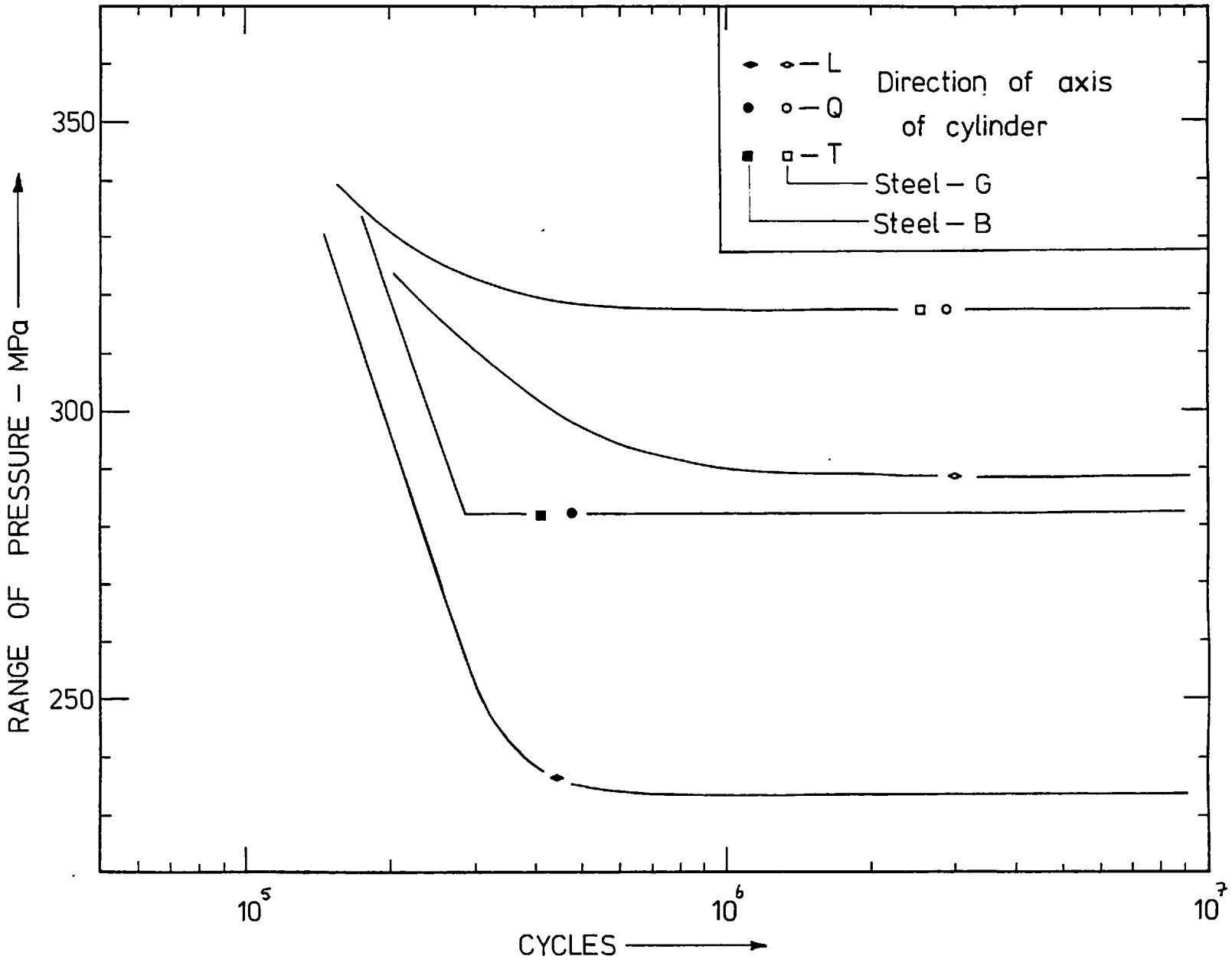
L
Q
T
Direction of axis of cylinder
Steel – G
Steel – B
350
300
250
RANGE OF PRESSURE – MPa
10^5
10^6
10^7
CYCLES

FIGURE 4.19

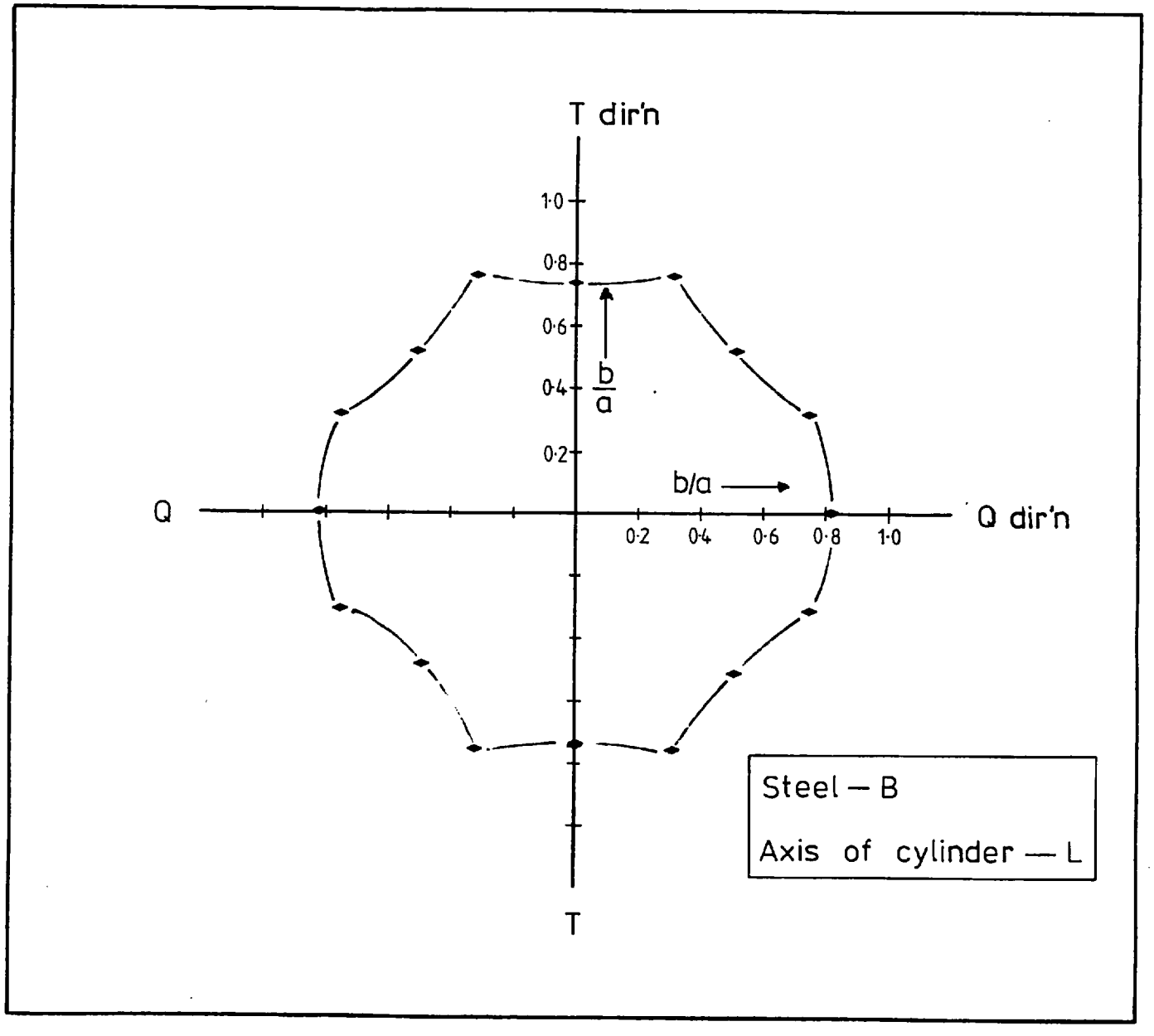
T dir'n
1·0
0·8
0·6
0·4
0·2
b/a
b/a
Q
Q dir'n
0·2
0·4
0·6
0·8
1·0
T
Steel — B
Axis of cylinder — L

FIGURE 4.20

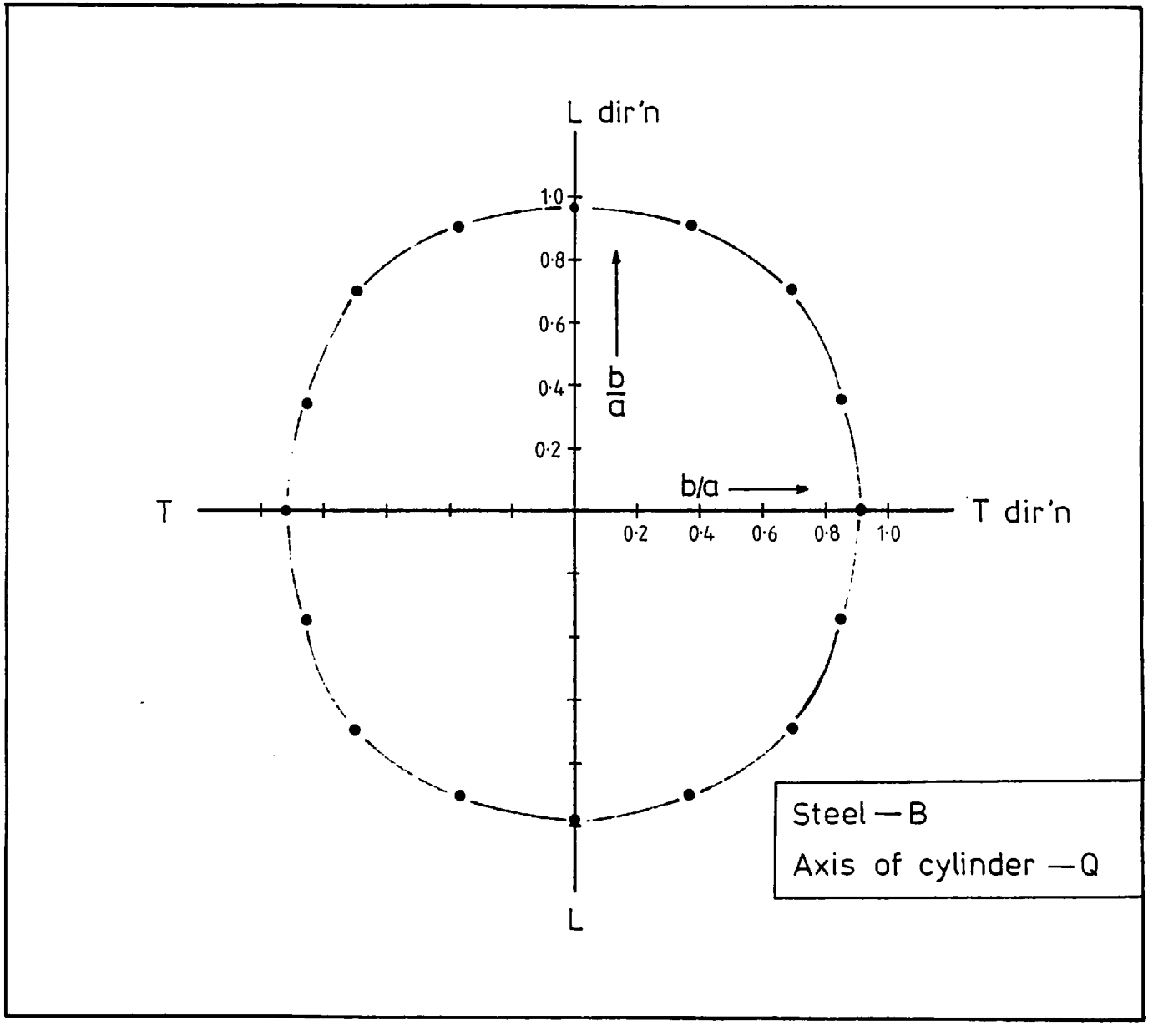
L dir'n
1·0
0·8
0·6
0·4
0·2
a/b
b/a
T
T dir'n
0·2
0·4
0·6
0·8
1·0
L
Steel — B
Axis of cylinder — Q

FIGURE 4.21

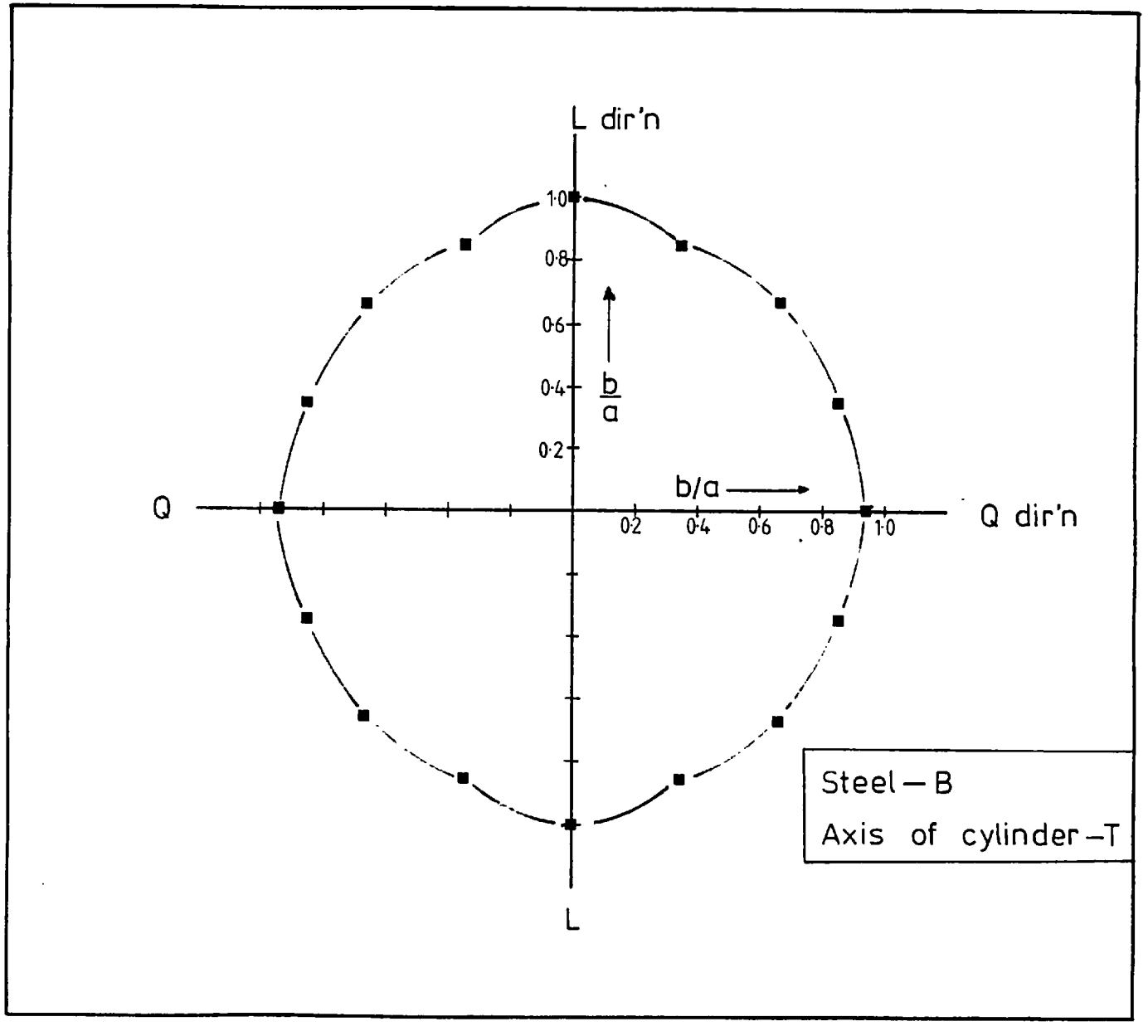
L dir'n
1·0
0·8
0·6
0·4
0·2
b/a
b/a
Q
Q dir'n
0·2
0·4
0·6
0·8
1·0
L
Steel – B
Axis of cylinder – T

FIGURE 4.22

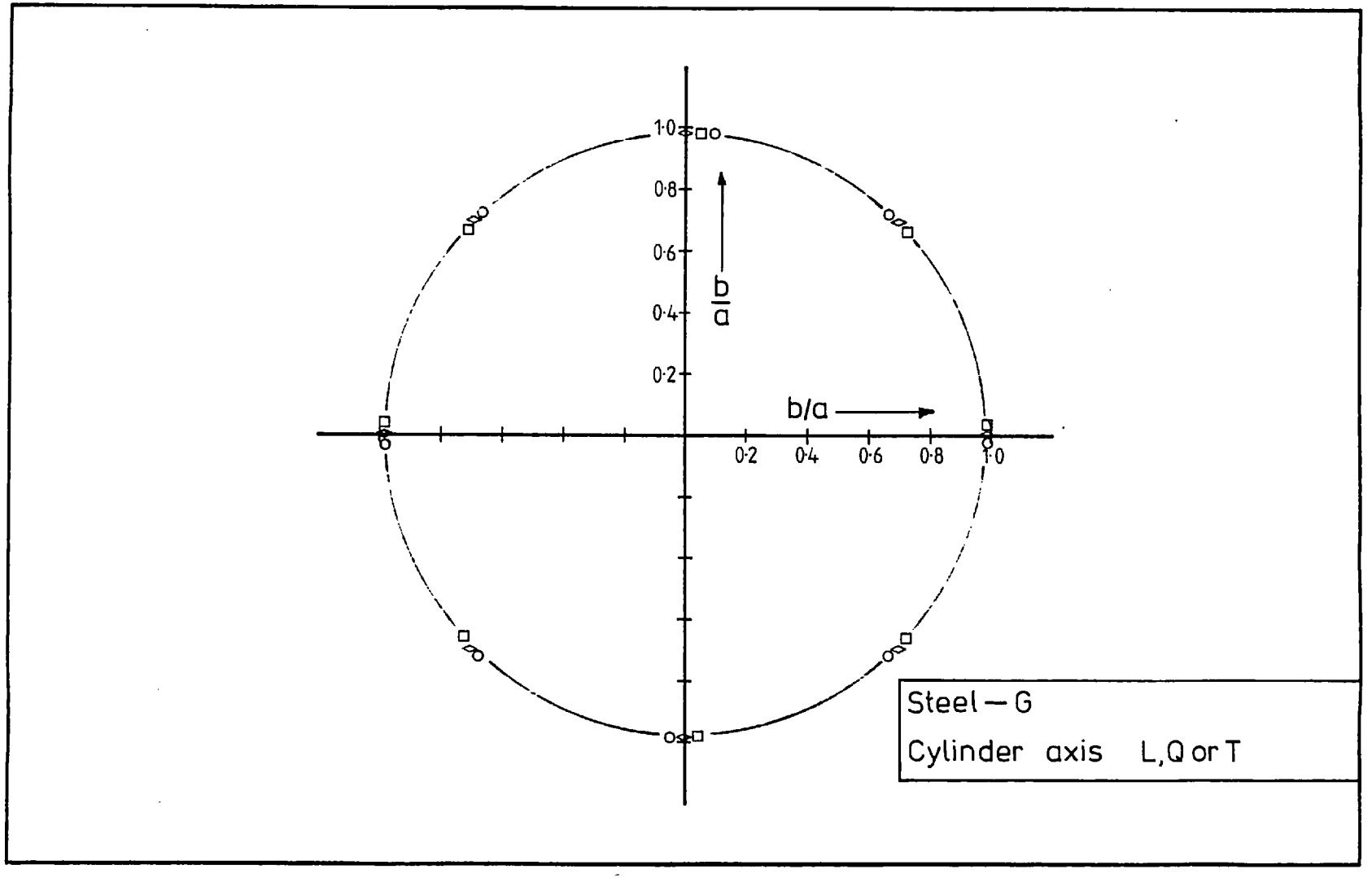

FIGURE 4.23

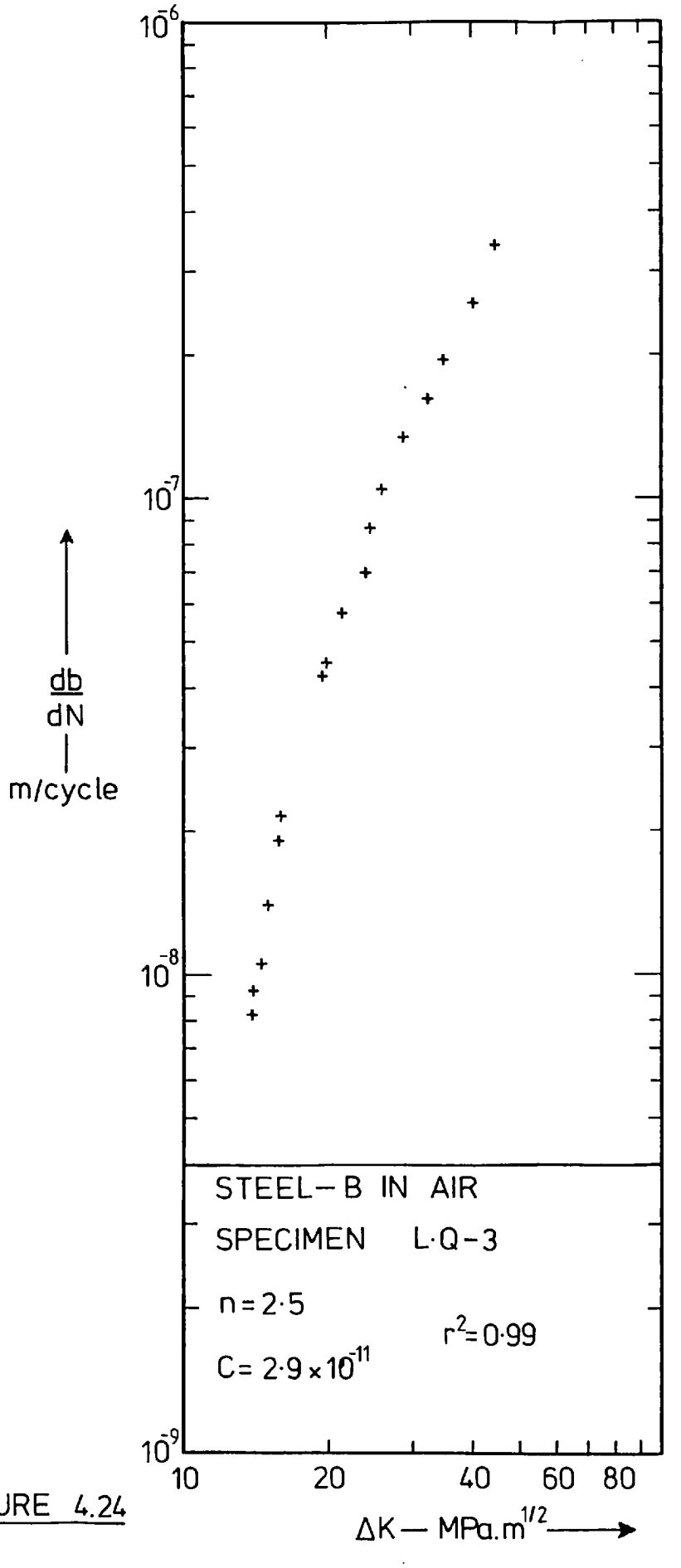
10^{-6}
10^{-7}
10^{-8}
10^{-9}
db/dN
m/cycle
STEEL – B IN AIR
SPECIMEN L·Q-3
n = 2·5
r^2 = 0·99
C = 2·9 × 10^{-11}
10
20
40
60
80
ΔK — MPa.$m^{1/2}$

FIGURE 4.24

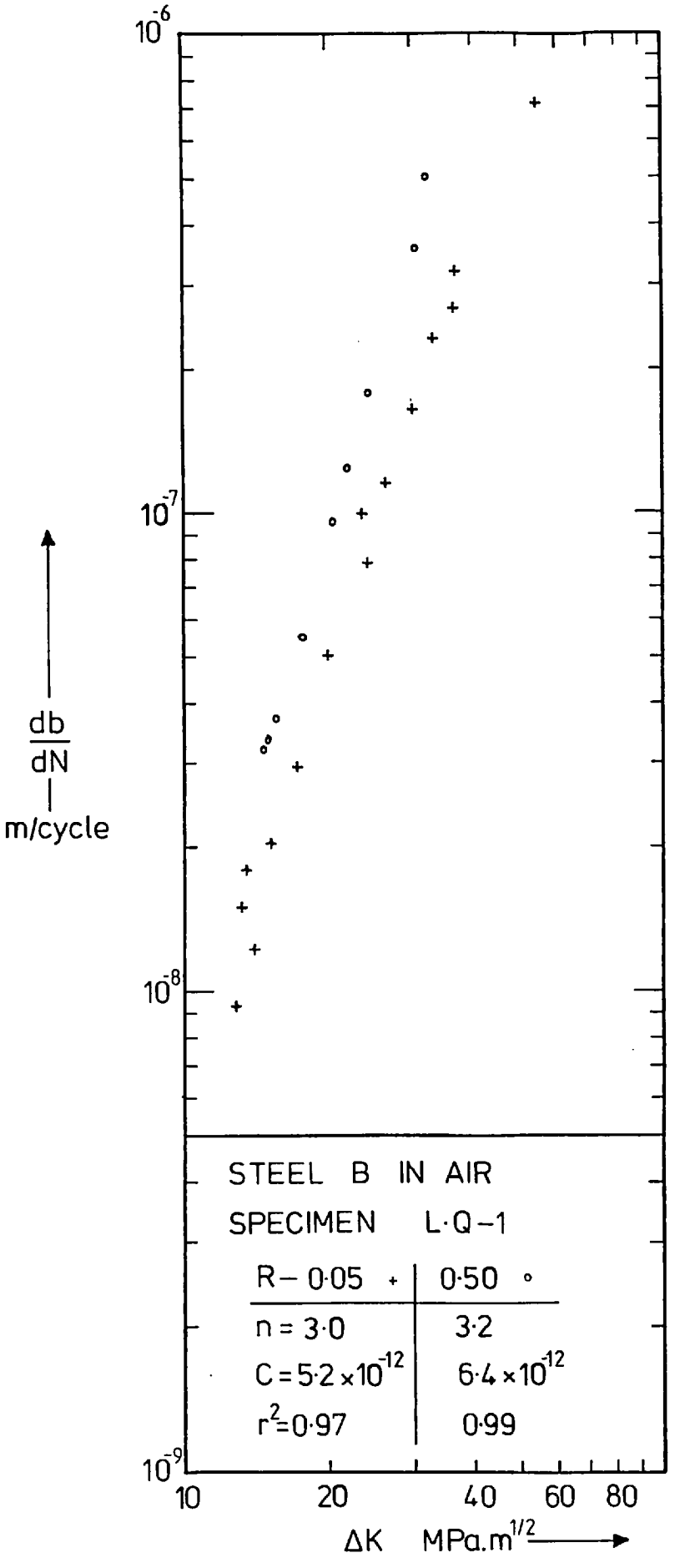
10^{-6}
10^{-7}
10^{-8}
10^{-9}
db/dN
m/cycle
STEEL B IN AIR
SPECIMEN L·Q–1
R – 0·05 + | 0·50 °
n = 3·0 | 3·2
C = 5·2 × 10^{-12} | 6·4 × 10^{-12}
r^2 = 0·97 | 0·99
10
20
40
60
80
ΔK MPa.$m^{1/2}$

FIGURE 4.25

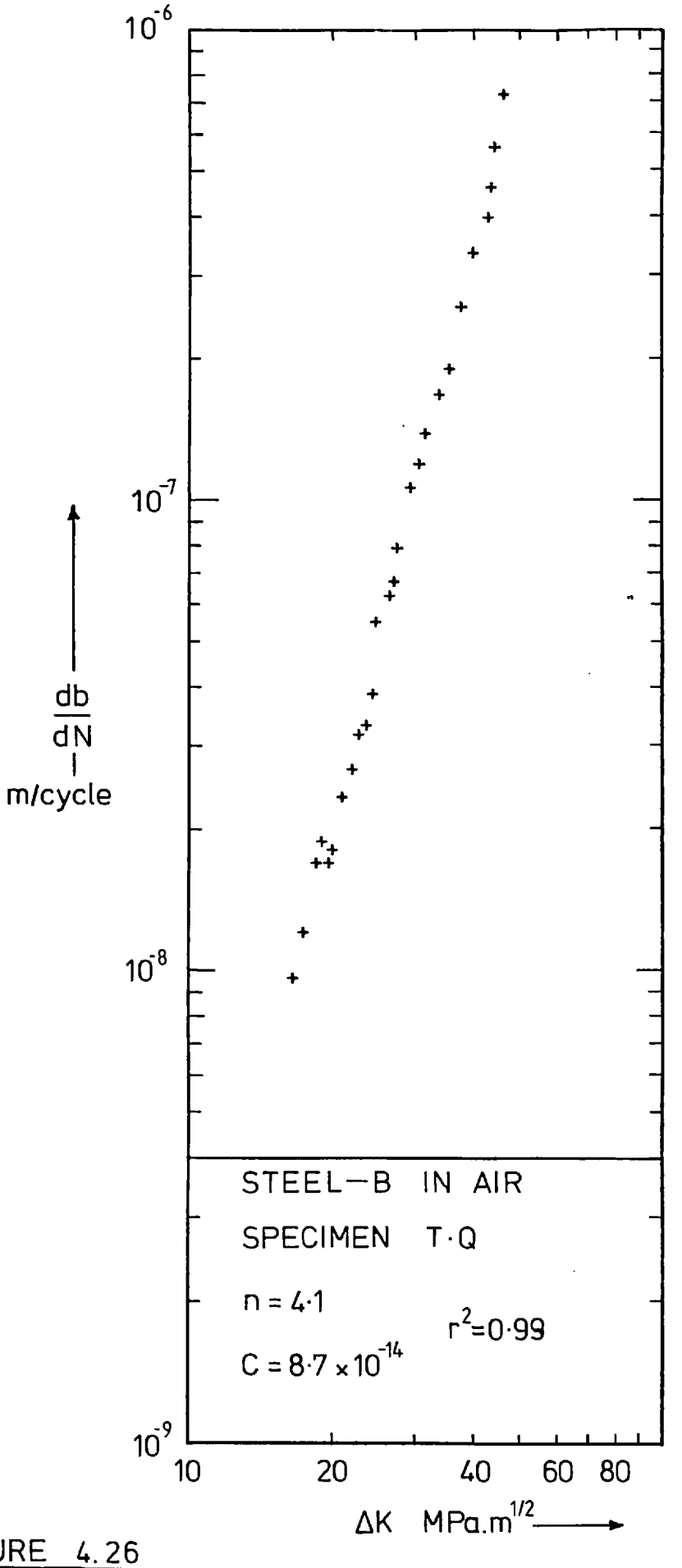
10^{-6}
10^{-7}
10^{-8}
10^{-9}
db/dN
m/cycle
STEEL—B IN AIR
SPECIMEN T·Q
n = 4·1
r^2=0·99
C = 8·7 x 10^{-14}
10
20
40
60
80
ΔK MPa.$m^{1/2}$

FIGURE 4.26

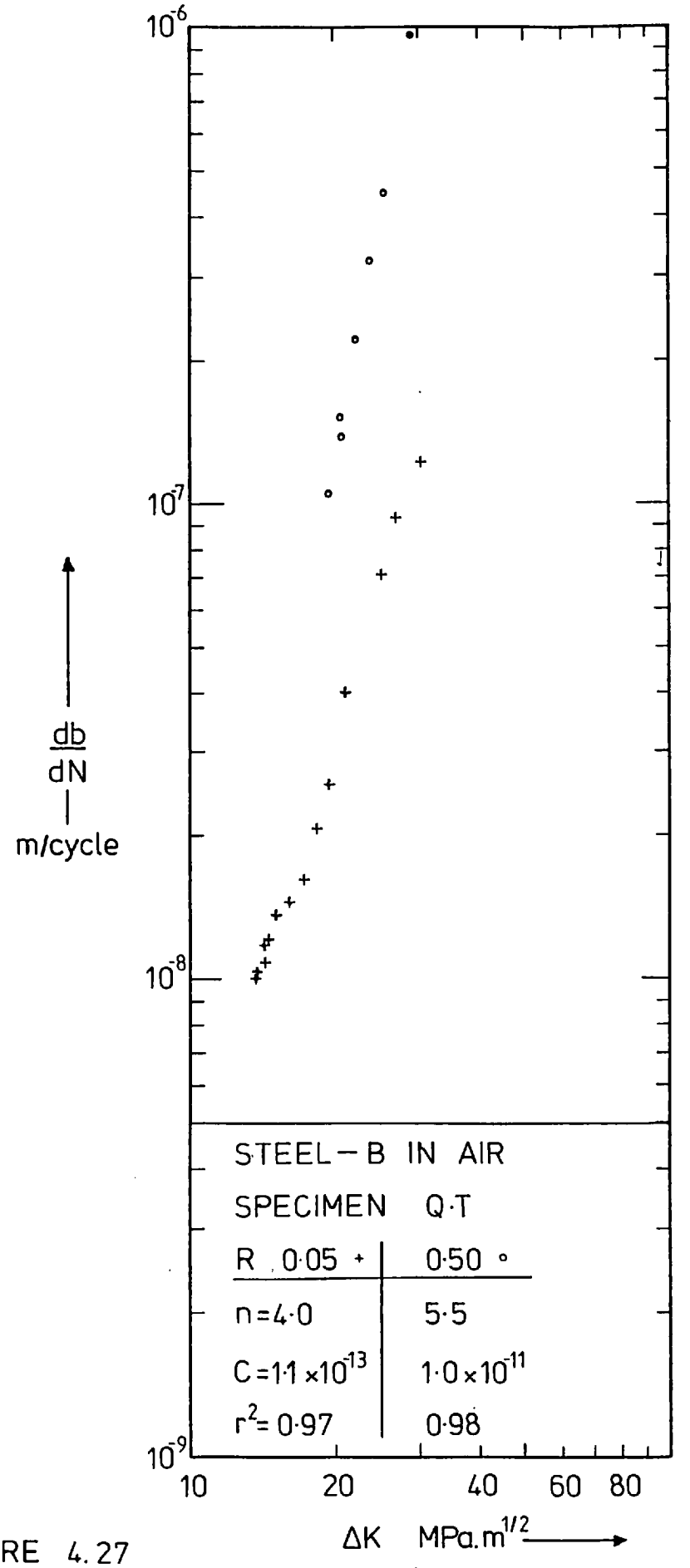
10^{-6}
10^{-7}
10^{-8}
10^{-9}
db/dN
m/cycle
STEEL – B IN AIR
SPECIMEN Q·T
R 0·05 + | 0·50 ∘
n = 4·0 | 5·5
C = 1·1 × 10^{-13} | 1·0 × 10^{-11}
r^2 = 0·97 | 0·98
10
20
40
60
80
ΔK MPa.$m^{1/2}$

FIGURE 4.27

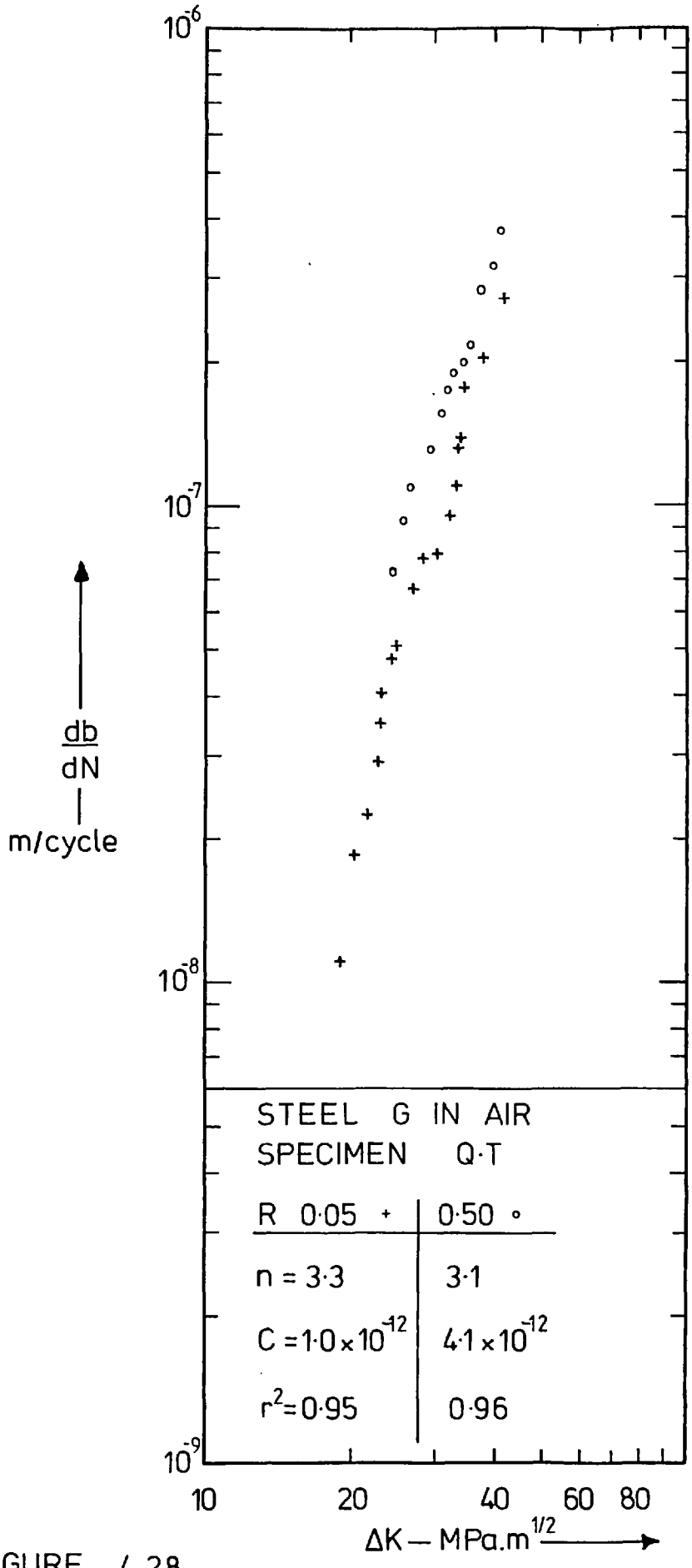
10^{-6}
10^{-7}
10^{-8}
10^{-9}
db/dN
m/cycle
STEEL G IN AIR
SPECIMEN Q·T
R 0·05 + | 0·50 ∘
n = 3·3 | 3·1
C = 1·0 × 10^{-12} | 4·1 × 10^{-12}
r^2 = 0·95 | 0·96
10
20
40
60
80
ΔK — MPa.$m^{1/2}$

FIGURE 4.28

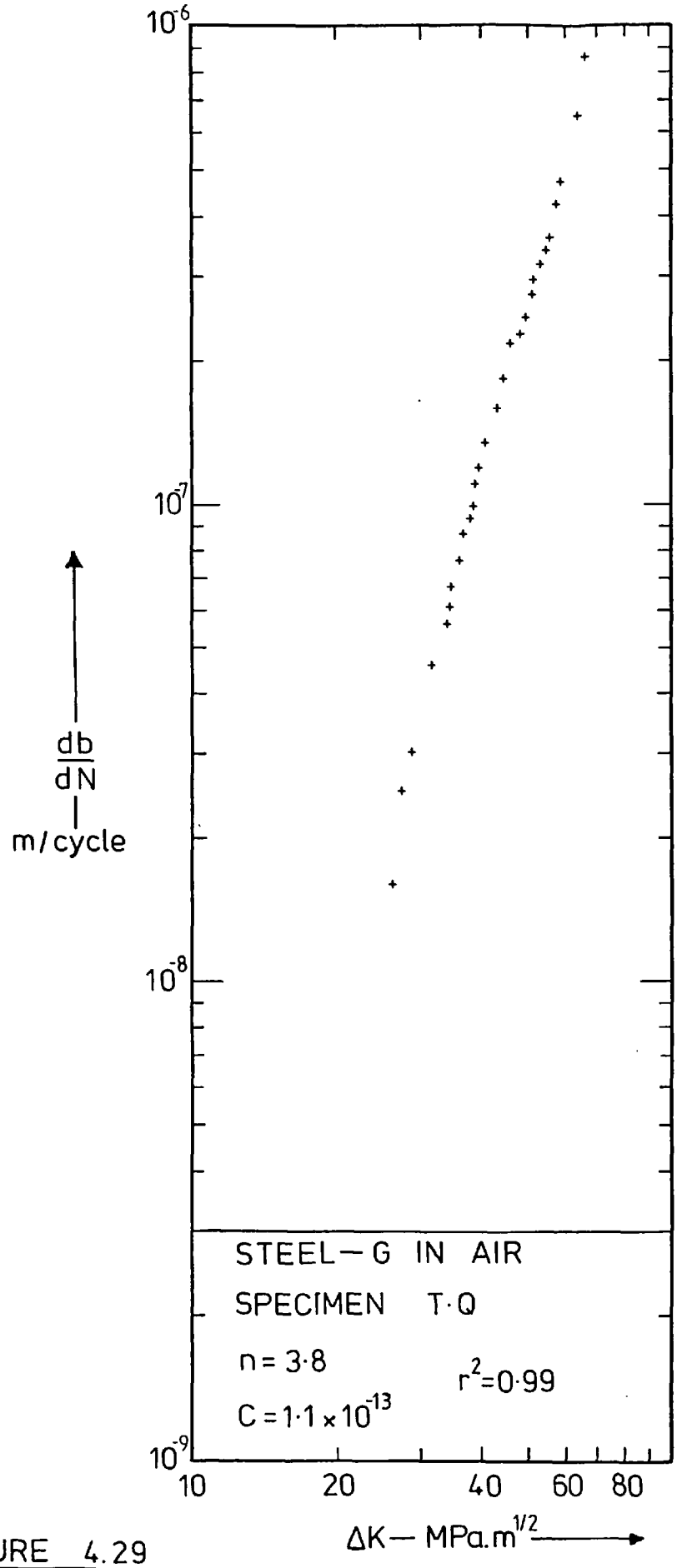
10^{-6}
10^{-7}
10^{-8}
10^{-9}
$\frac{db}{dN}$
m/cycle
STEEL—G IN AIR
SPECIMEN T·Q
n = 3·8
r^2=0·99
C = 1·1 x 10^{-13}
10
20
40
60
80
ΔK— MPa.$m^{1/2}$

FIGURE 4.29

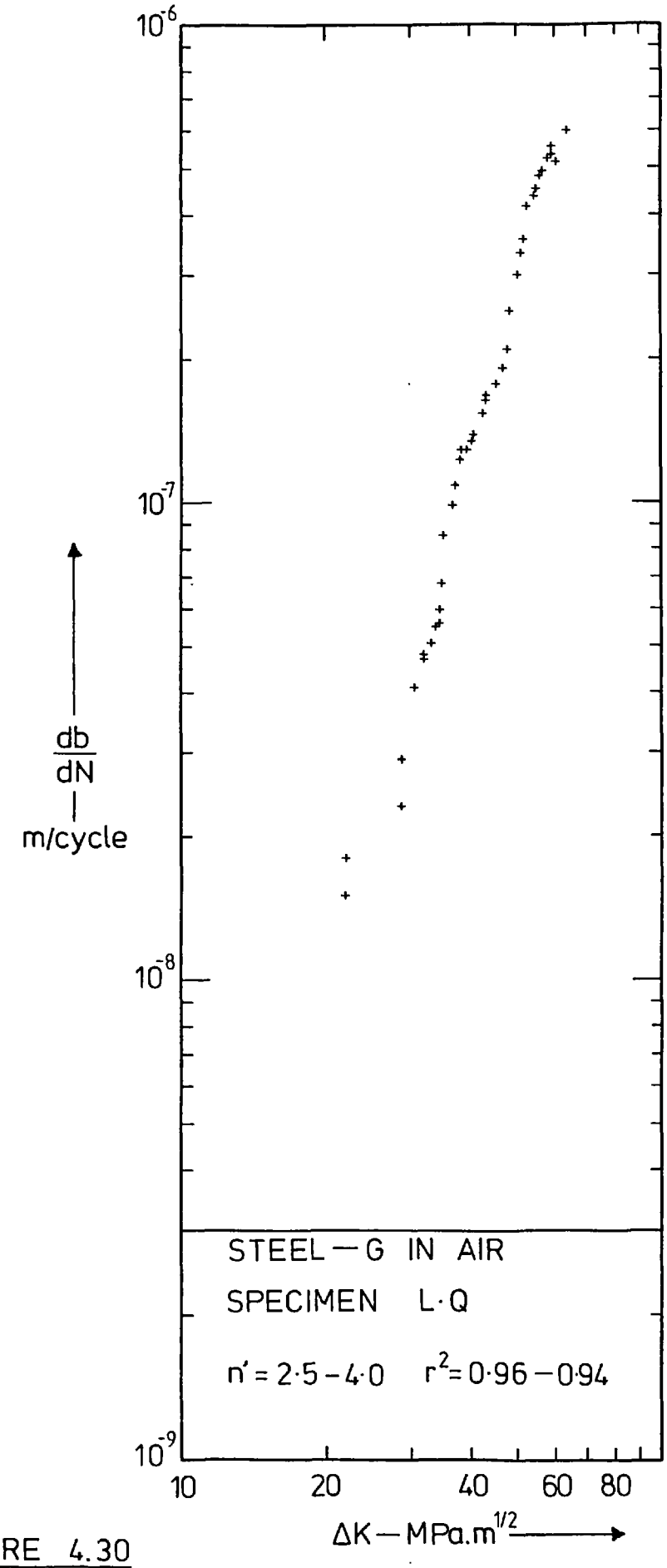
10^{-6}
10^{-7}
10^{-8}
10^{-9}
db/dN
m/cycle
STEEL — G IN AIR
SPECIMEN L·Q
n' = 2·5 – 4·0 r^2 = 0·96 – 0·94
10
20
40
60
80
ΔK — MPa.$m^{1/2}$

FIGURE 4.30

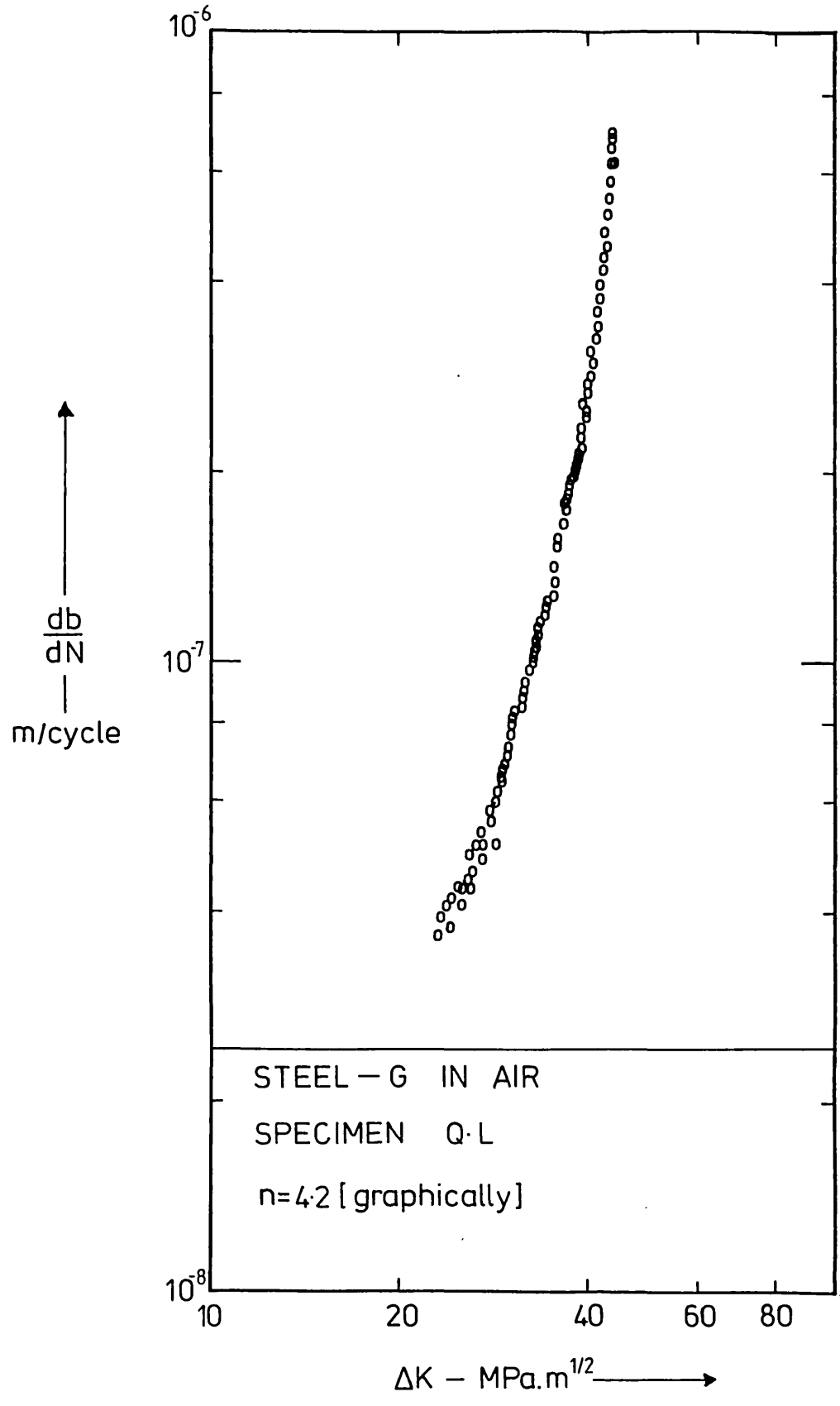
10^{-6}
10^{-7}
10^{-8}
db/dN
m/cycle
STEEL — G IN AIR
SPECIMEN Q·L
n=4·2 [graphically]
10
20
40
60
80
ΔK — MPa.m$^{1/2}$

FIGURE 4.31

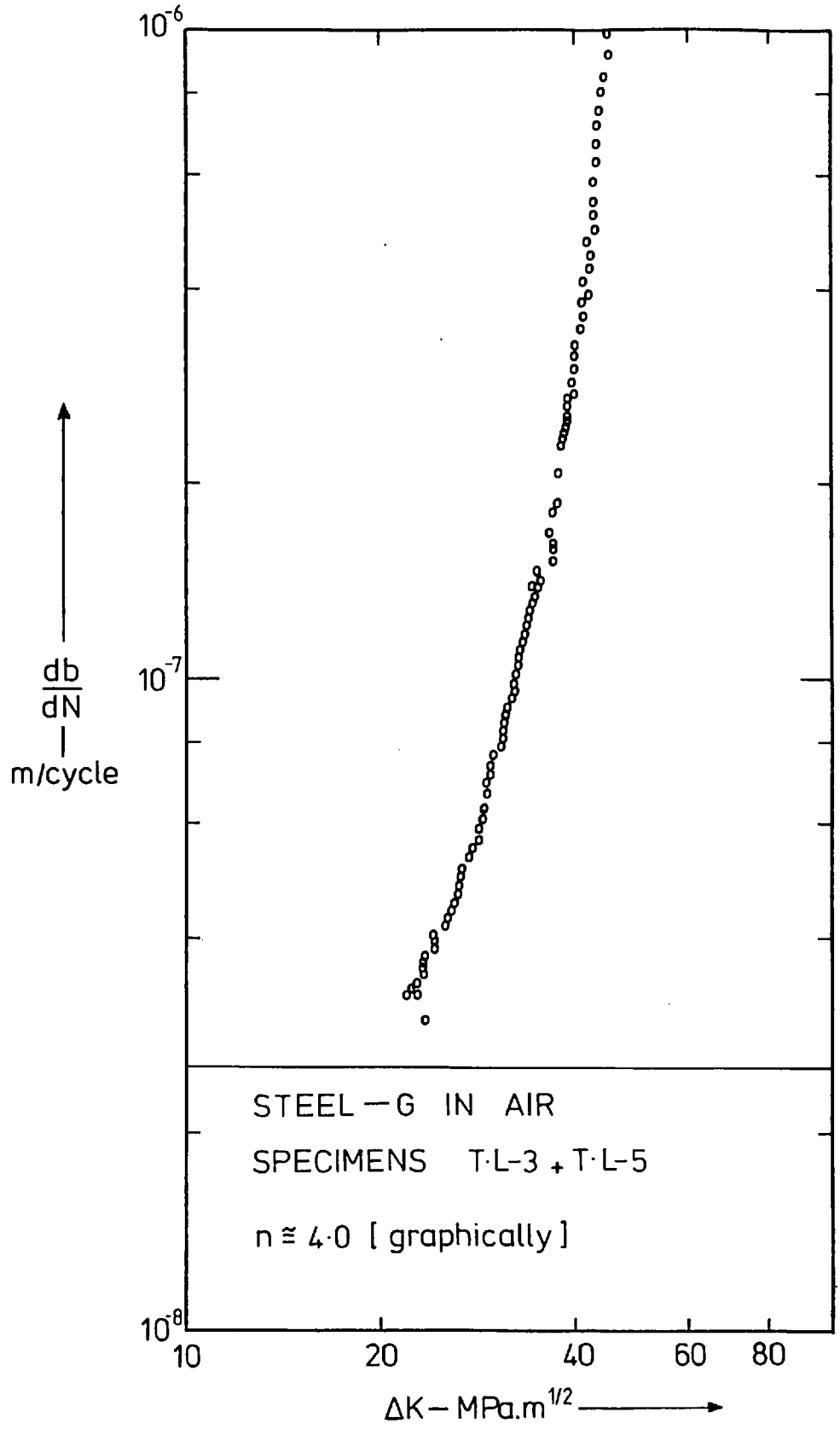
10^{-6}
10^{-7}
10^{-8}
db/dN
m/cycle
STEEL — G IN AIR
SPECIMENS T·L-3 + T·L-5
n ≅ 4·0 [graphically]
10
20
40
60
80
ΔK — MPa.m$^{1/2}$

FIGURE 4.32

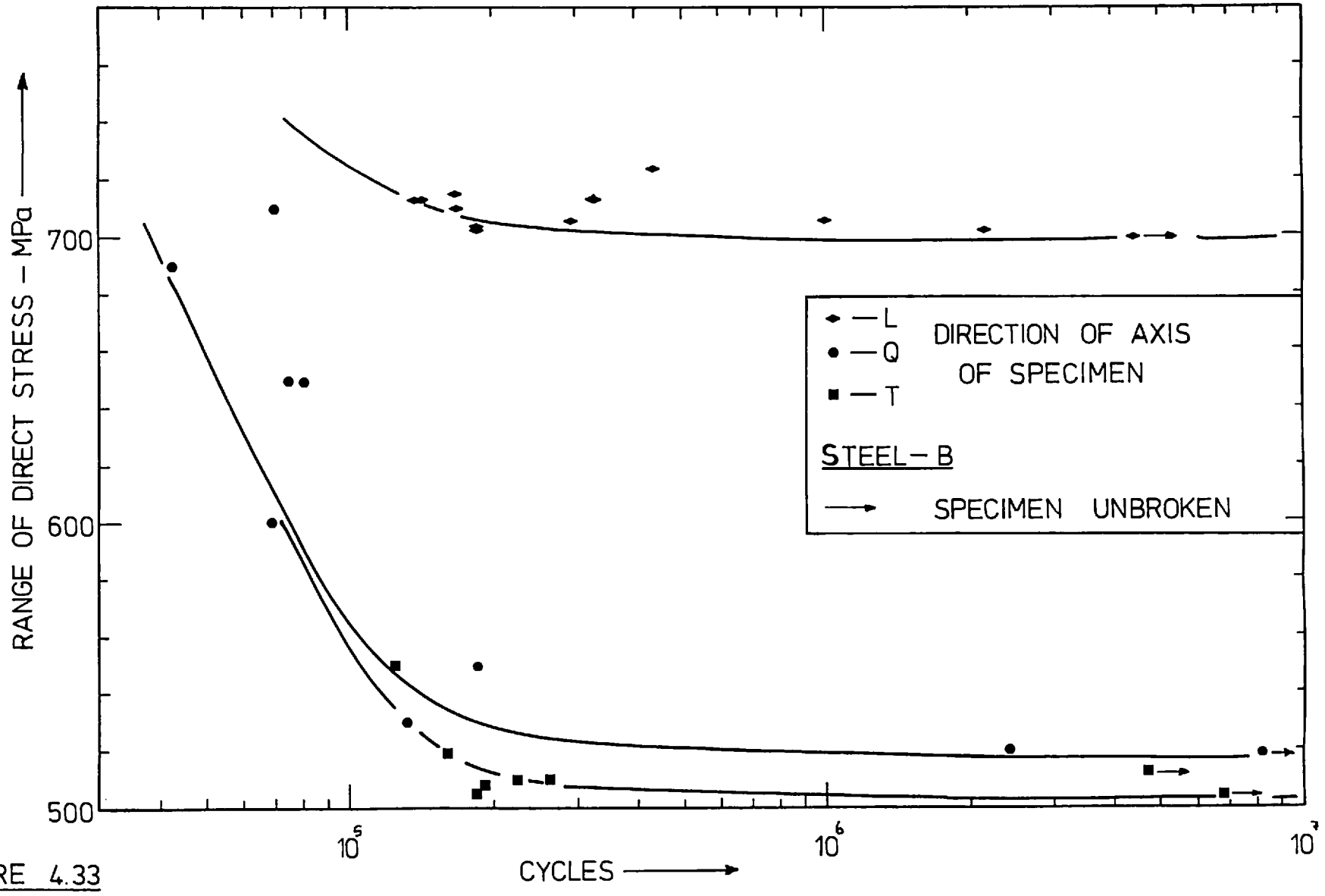
RANGE OF DIRECT STRESS – MPa
700
600
500
10^5
10^6
10^7
CYCLES
L
Q
T
DIRECTION OF AXIS OF SPECIMEN
STEEL – B
SPECIMEN UNBROKEN

FIGURE 4.33

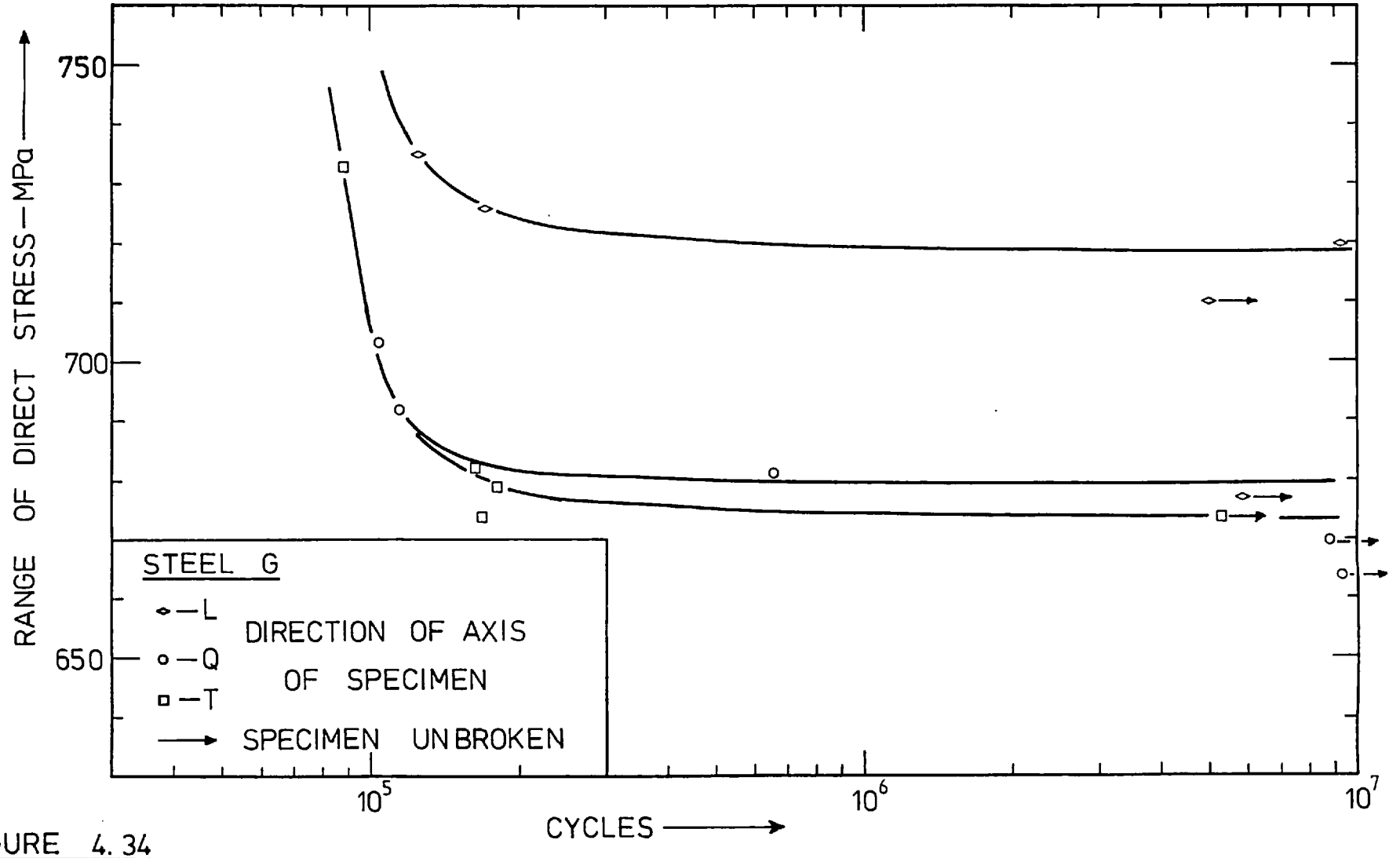
RANGE OF DIRECT STRESS—MPa
750
700
650
STEEL G
◇—L
○—Q
□—T
DIRECTION OF AXIS
OF SPECIMEN
→ SPECIMEN UNBROKEN
10^5
10^6
10^7
CYCLES

FIGURE 4.34

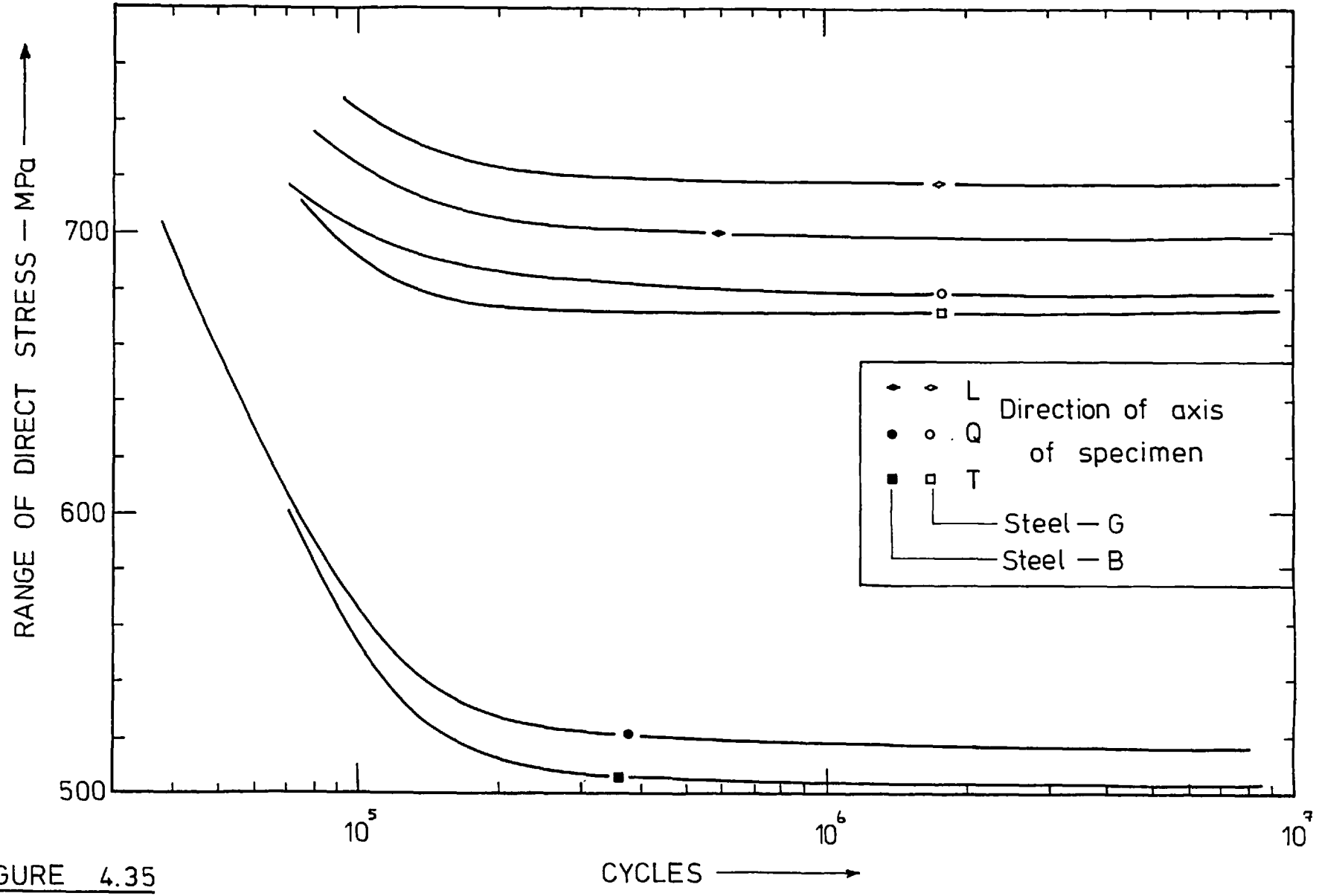
RANGE OF DIRECT STRESS — MPa
700
600
500
10^5
10^6
10^7
CYCLES
L
Q
T
Direction of axis of specimen
Steel — G
Steel — B

FIGURE 4.35

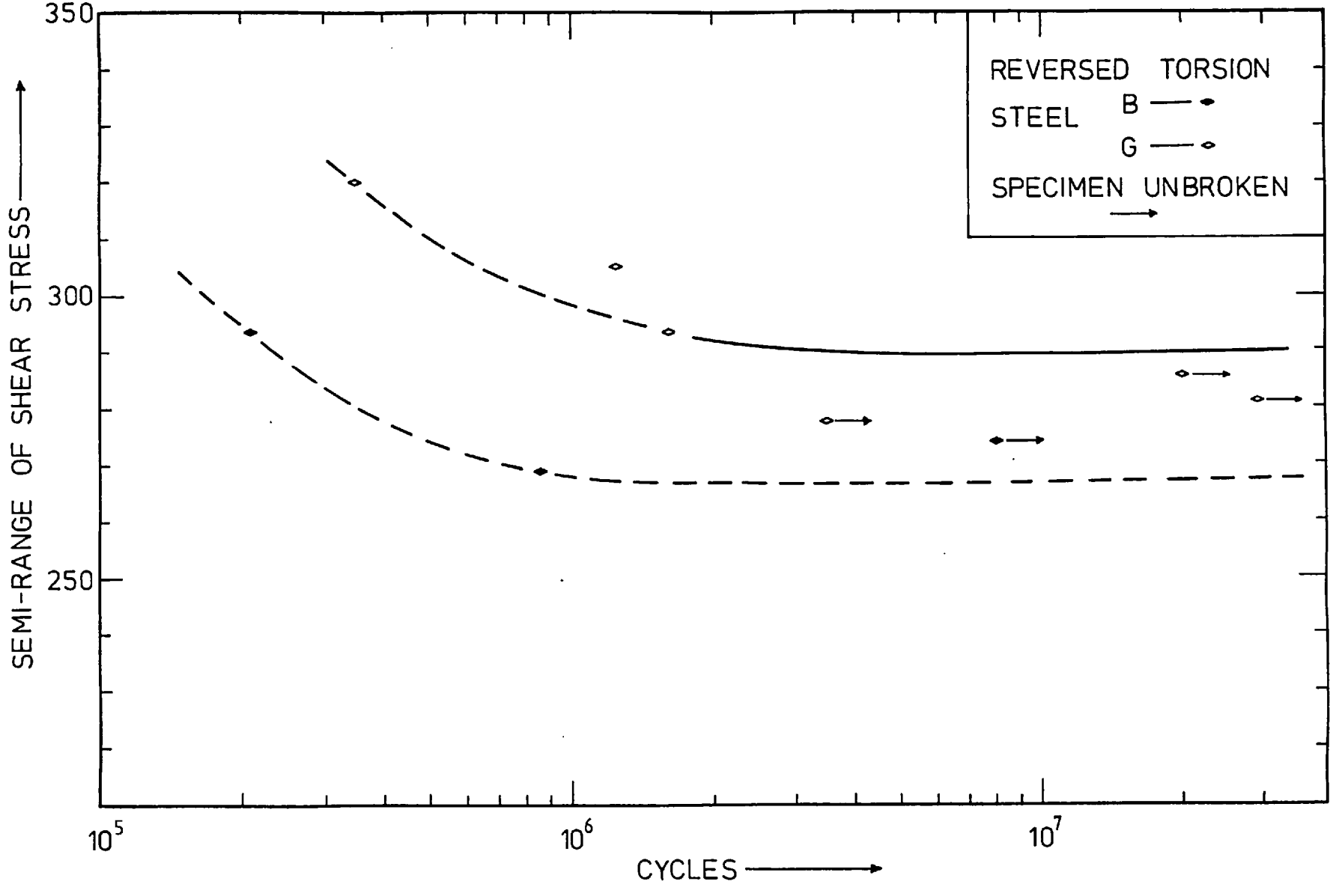
350
300
250
SEMI-RANGE OF SHEAR STRESS
REVERSED TORSION
STEEL B
G
SPECIMEN UNBROKEN
10^5
10^6
10^7
CYCLES

FIGURE 4.36

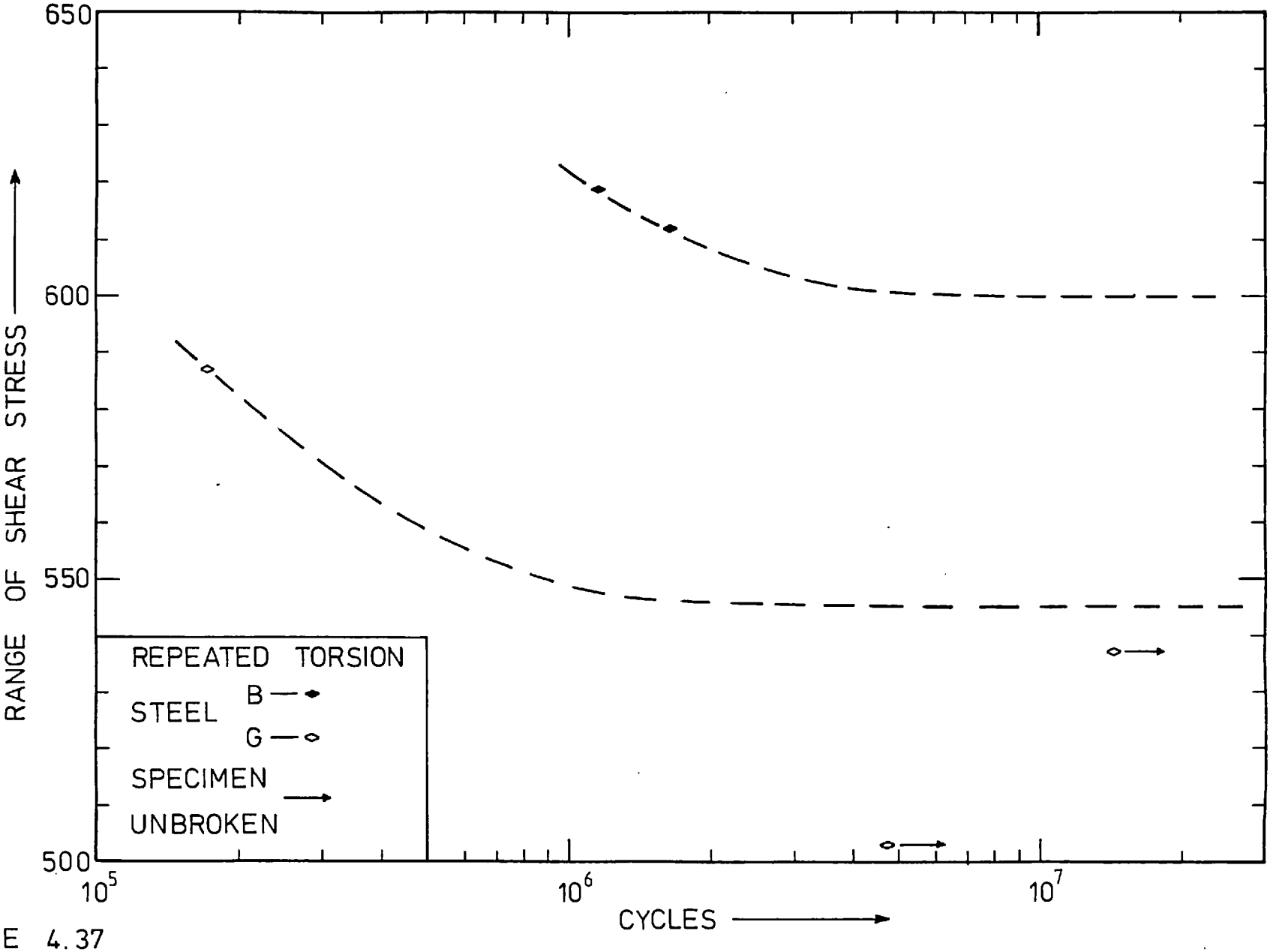
650
600
550
500
RANGE OF SHEAR STRESS
REPEATED TORSION
STEEL B
G
SPECIMEN
UNBROKEN
10^5
10^6
10^7
CYCLES

FIGURE 4.37

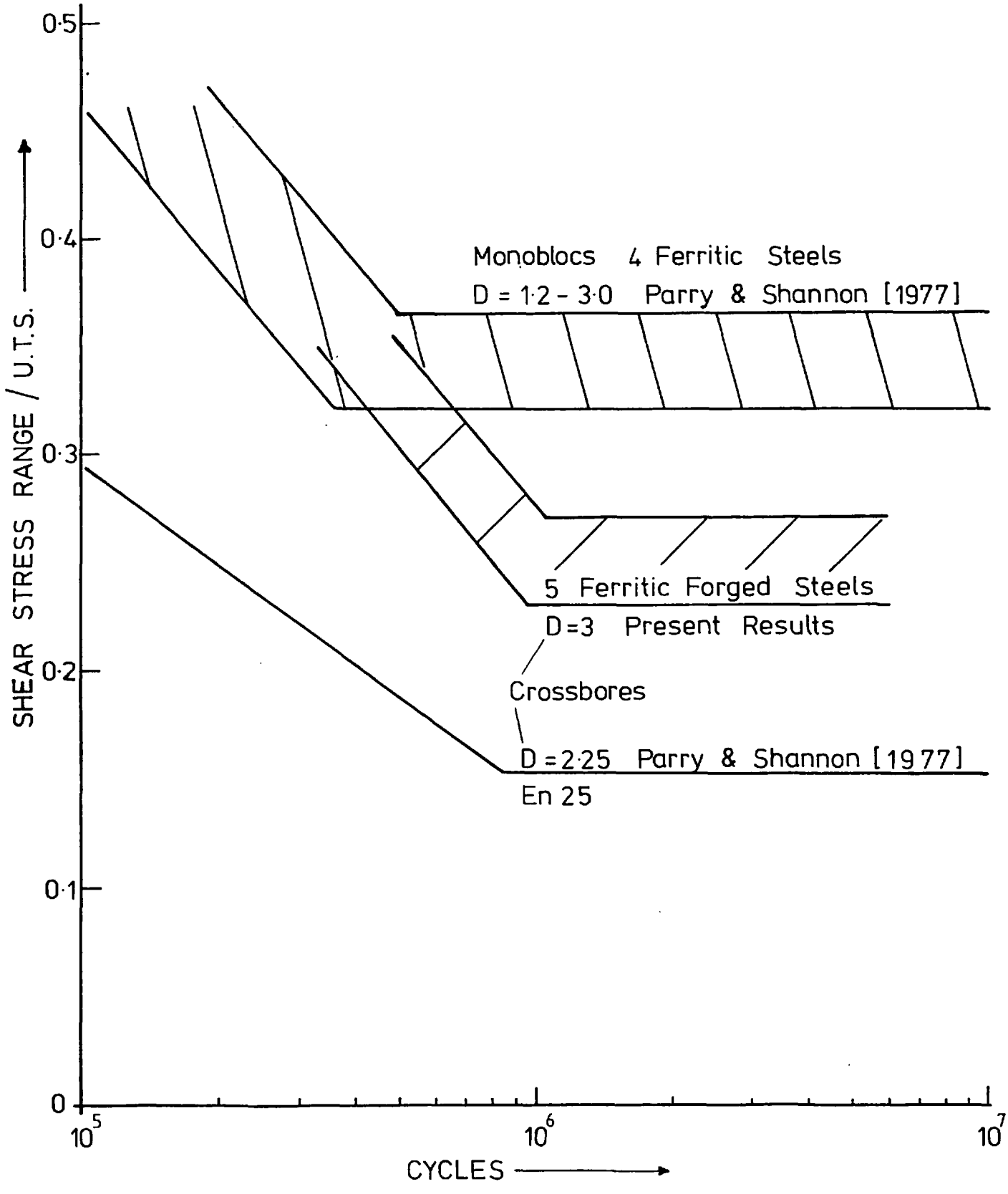
0·5
0·4
0·3
0·2
0·1
0
SHEAR STRESS RANGE / U.T.S.
Monoblocs 4 Ferritic Steels
D = 1·2 - 3·0 Parry & Shannon [1977]
5 Ferritic Forged Steels
D=3 Present Results
Crossbores
D = 2·25 Parry & Shannon [1977]
En 25
10^5
10^6
10^7
CYCLES

FIGURE 5.1

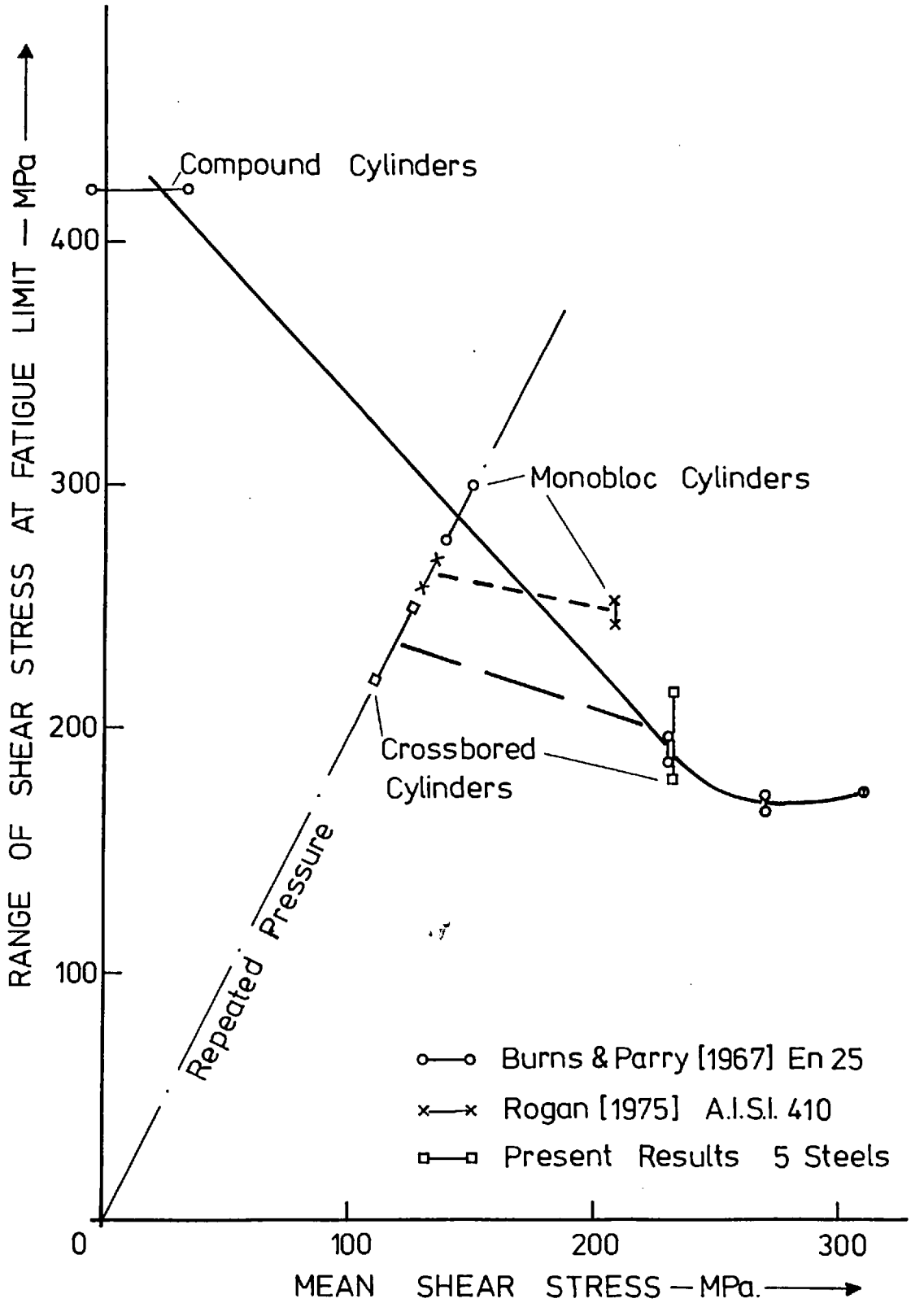
RANGE OF SHEAR STRESS AT FATIGUE LIMIT — MPa
400
300
200
100
0
100
200
300
MEAN SHEAR STRESS — MPa.
Compound Cylinders
Monobloc Cylinders
Crossbored Cylinders
Repeated Pressure
Burns & Parry [1967] En 25
Rogan [1975] A.I.S.I. 410
Present Results 5 Steels

FIGURE 5.2

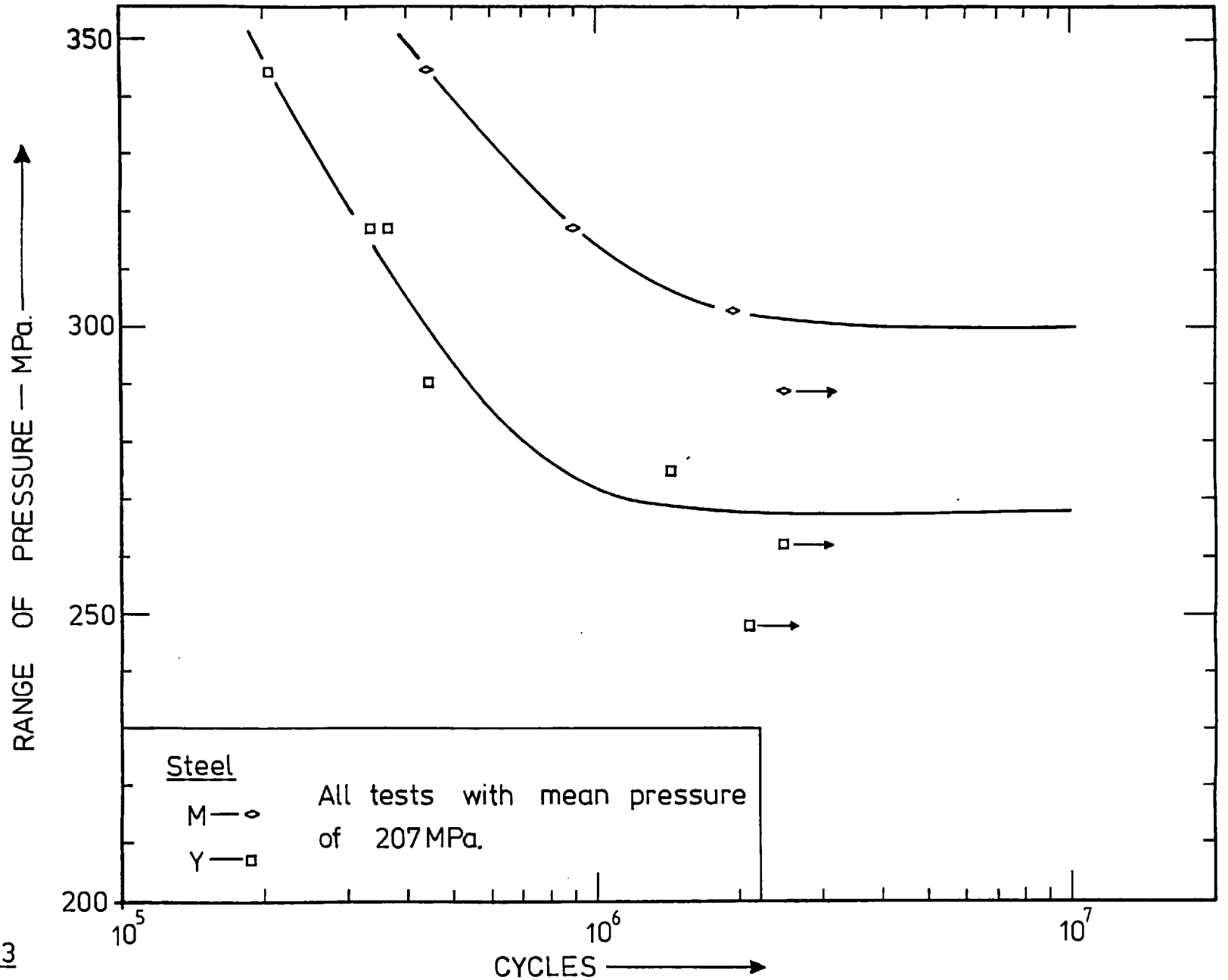
350
300
250
200
RANGE OF PRESSURE — MPa.
10^5
10^6
10^7
CYCLES
Steel
M
Y
All tests with mean pressure
of 207 MPa.

FIGURE 5.3

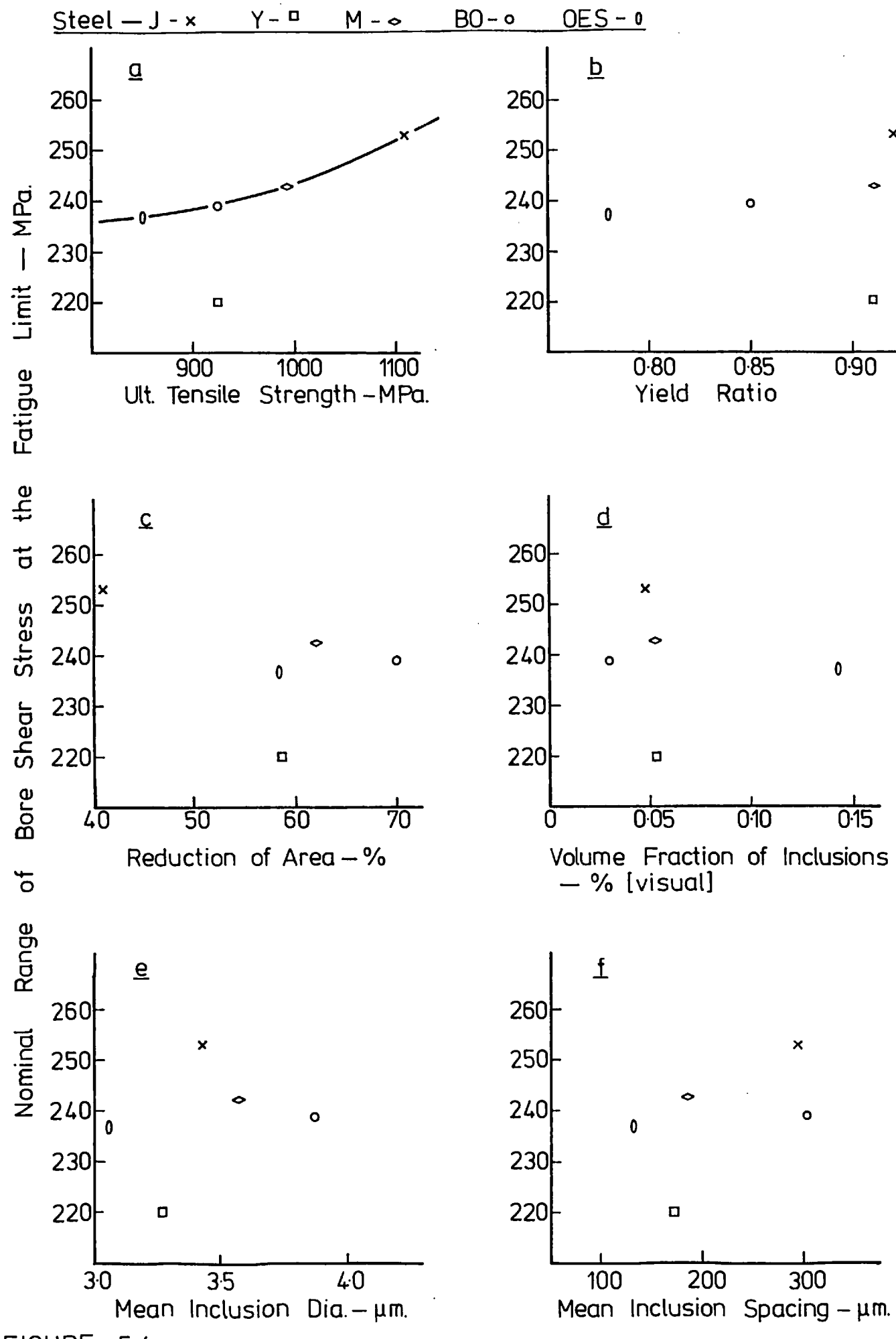
Steel — J - × Y - □ M - ◇ BO - ○ OES - 0
a
b
c
d
e
f
Nominal Range of Bore Shear Stress at the Fatigue Limit — MPa.
260
250
240
230
220
900
1000
1100
Ult. Tensile Strength – MPa.
0·80
0·85
0·90
Yield Ratio
40
50
60
70
Reduction of Area – %
0
0·05
0·10
0·15
Volume Fraction of Inclusions — % [visual]
3·0
3·5
4·0
Mean Inclusion Dia. – µm.
100
200
300
Mean Inclusion Spacing – µm.

FIGURE 5.4

FIGURE 5.5

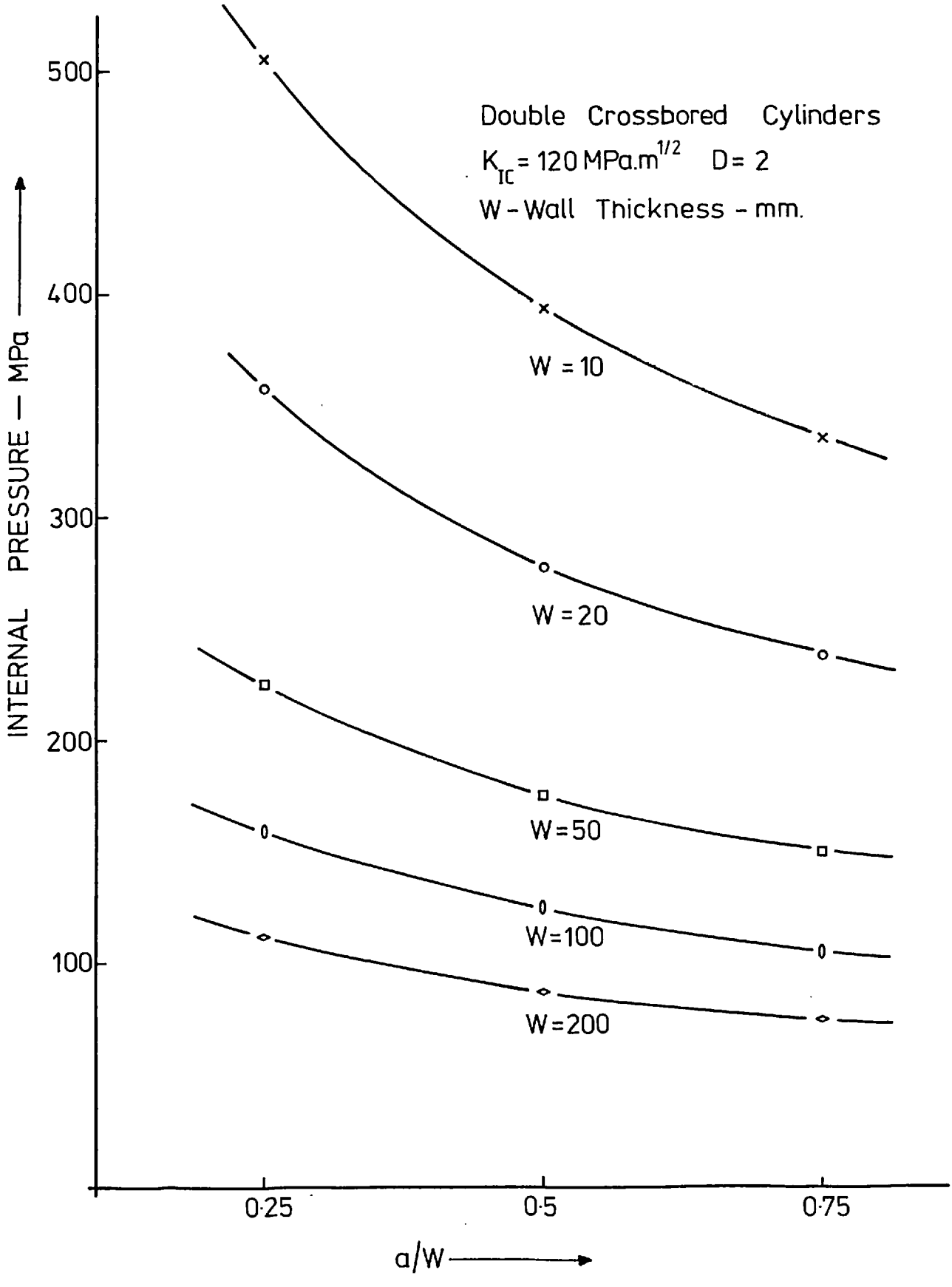
Double Crossbored Cylinders
K_{IC} = 120 MPa.m$^{1/2}$ D= 2
W - Wall Thickness - mm.
W = 10
W = 20
W = 50
W = 100
W = 200
INTERNAL PRESSURE — MPa
500
400
300
200
100
0·25
0·5
0·75
a/W

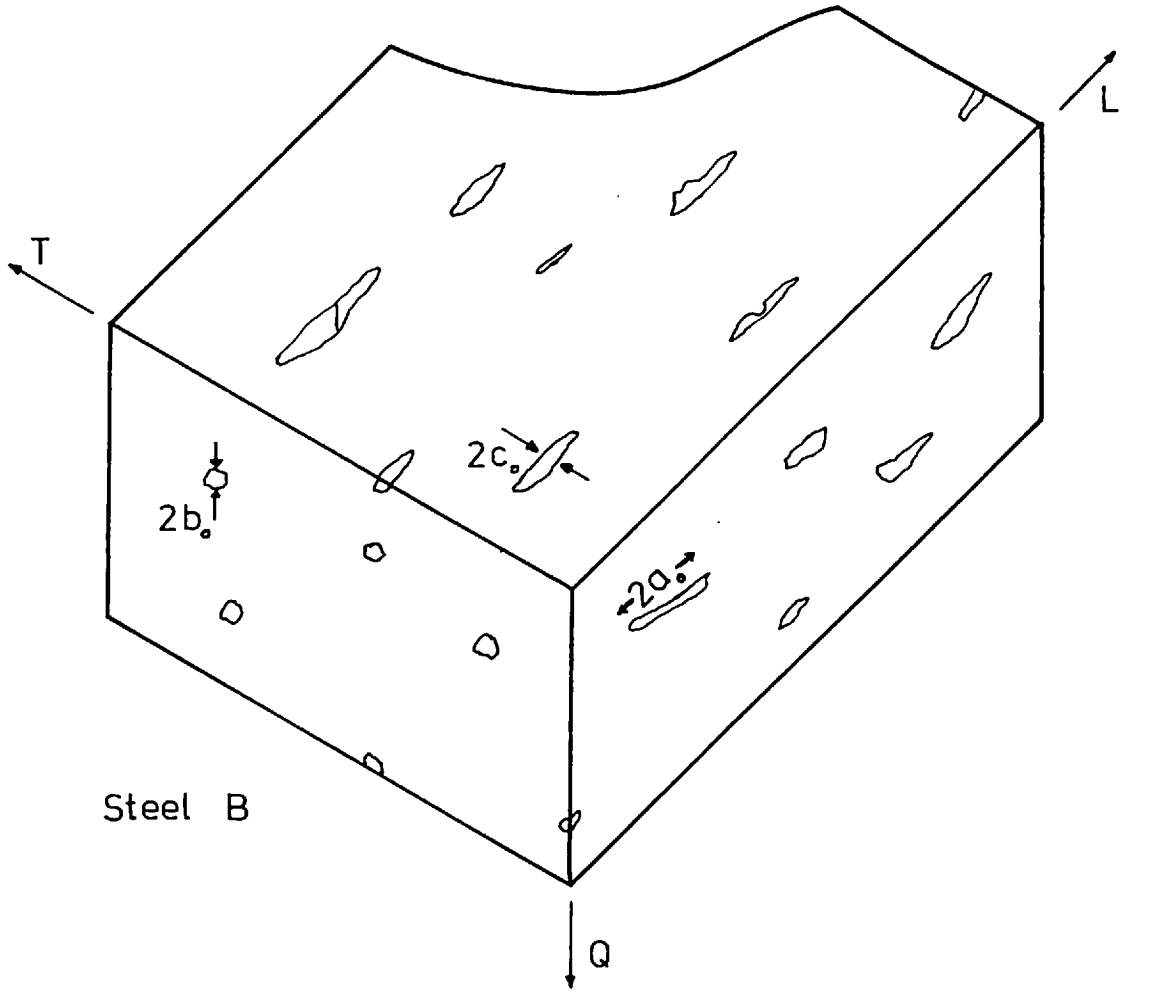

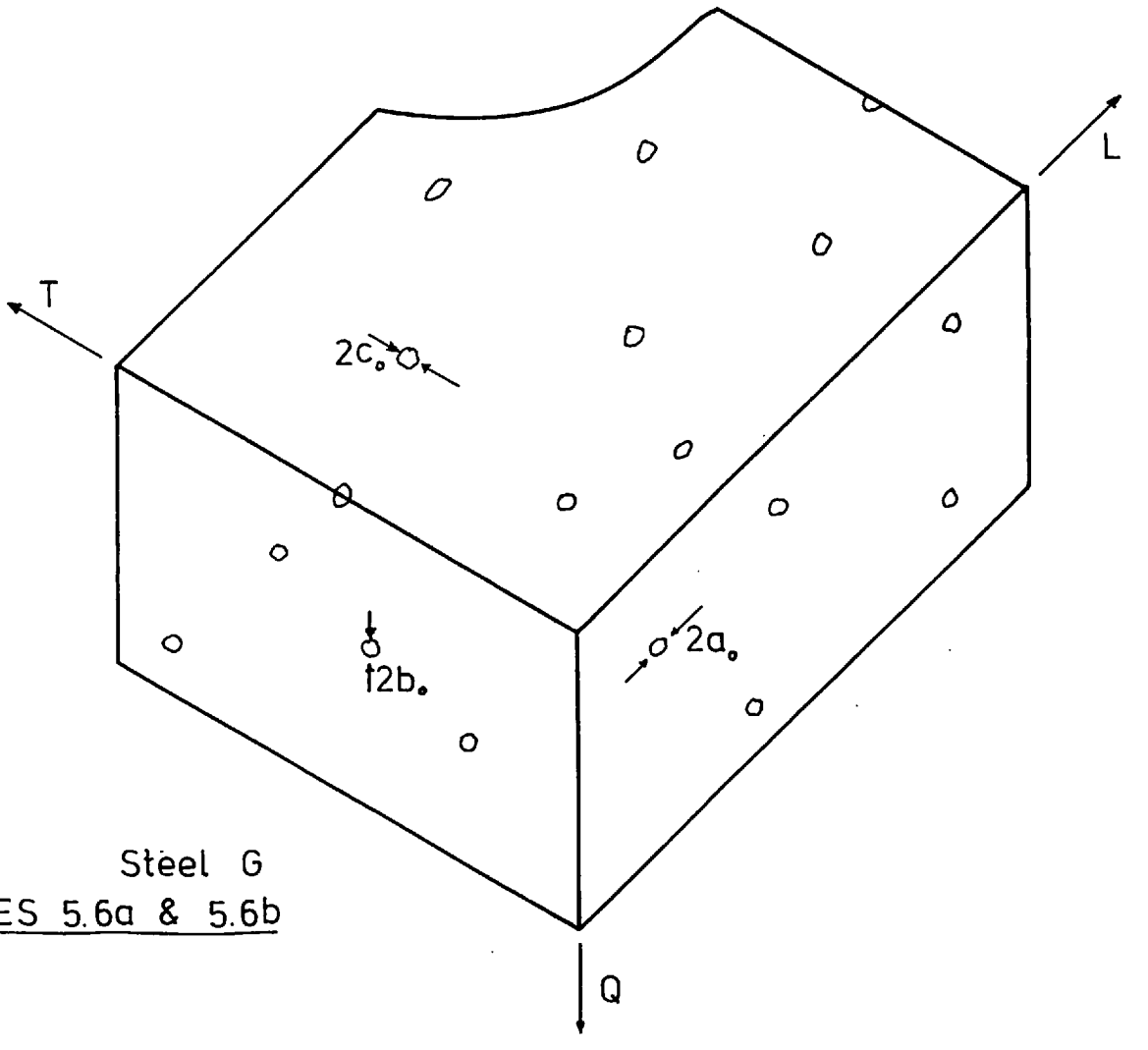

FIGURES 5.6a & 5.6b

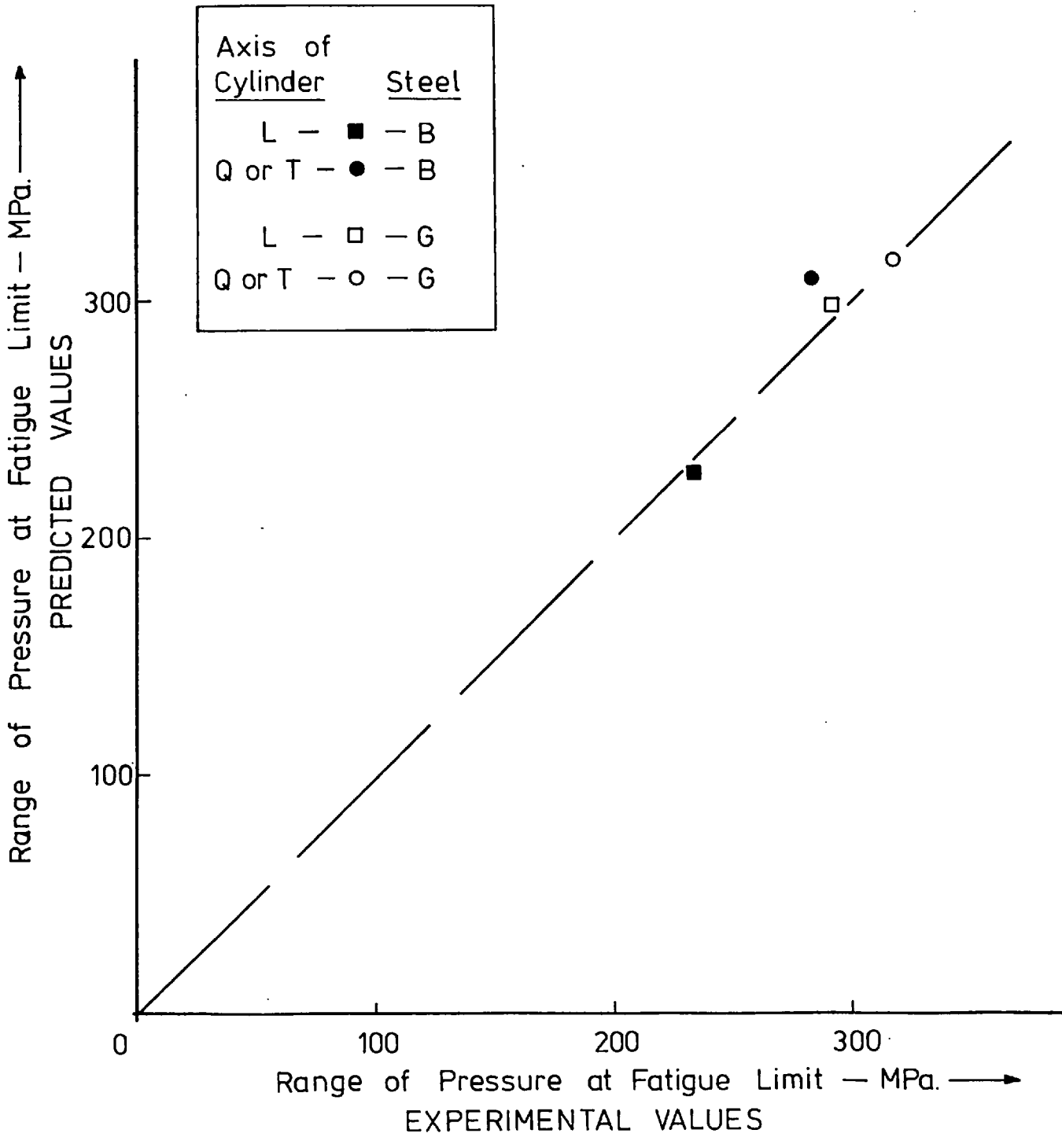
Axis of Cylinder
Steel
L — ■ — B
Q or T — ● — B
L — □ — G
Q or T — ○ — G
Range of Pressure at Fatigue Limit — MPa.
PREDICTED VALUES
300
200
100
0
100
200
300
Range of Pressure at Fatigue Limit — MPa.
EXPERIMENTAL VALUES

FIGURE 5.7

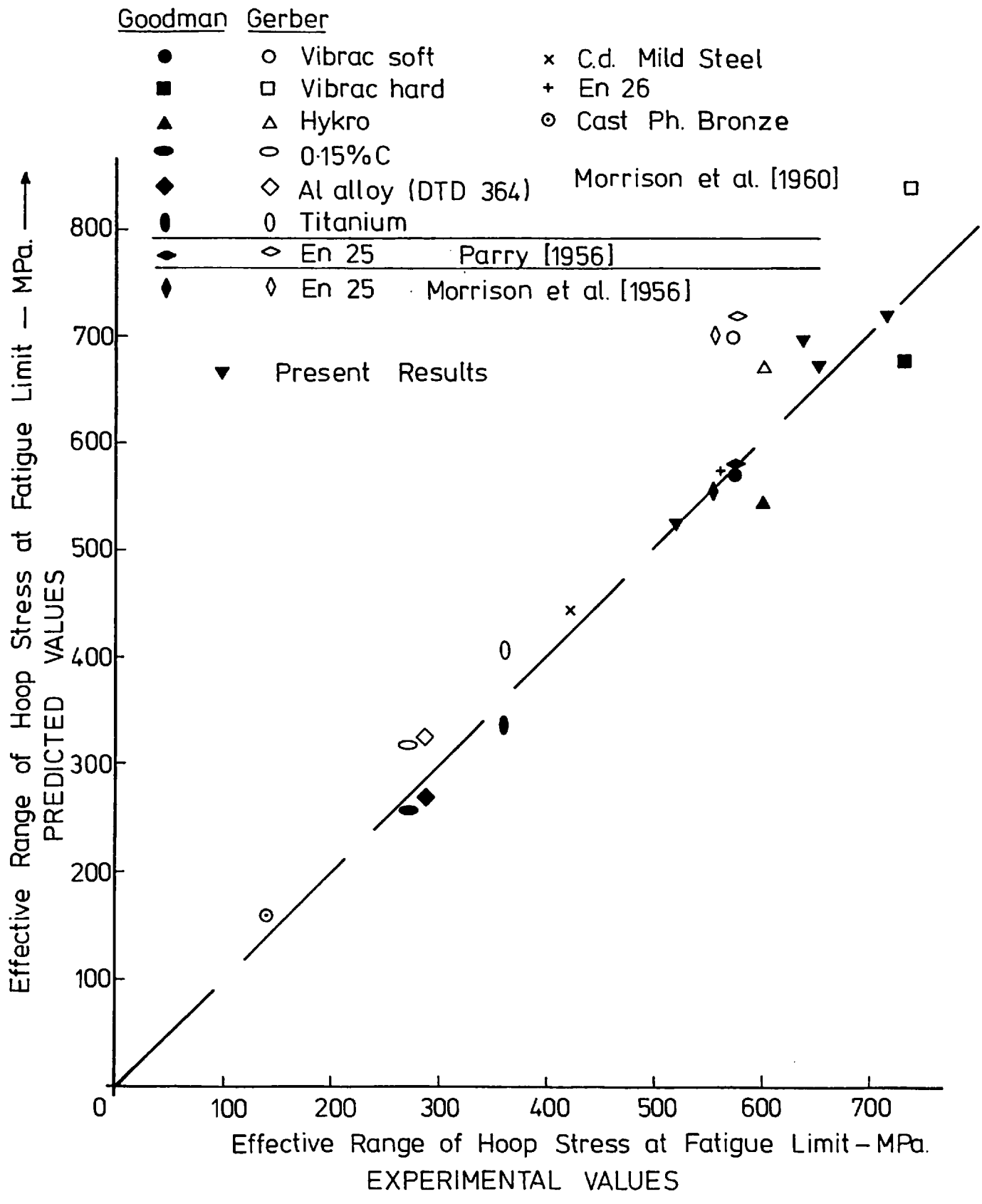
Goodman Gerber
Vibrac soft
Vibrac hard
Hykro
0·15%C
Al alloy (DTD 364)
Titanium
En 25 Parry [1956]
En 25 Morrison et al. [1956]
C.d. Mild Steel
En 26
Cast Ph. Bronze
Morrison et al. [1960]
Present Results
Effective Range of Hoop Stress at Fatigue Limit — MPa.
PREDICTED VALUES
Effective Range of Hoop Stress at Fatigue Limit – MPa.
EXPERIMENTAL VALUES
0
100
200
300
400
500
600
700
800

FIGURE 5.8

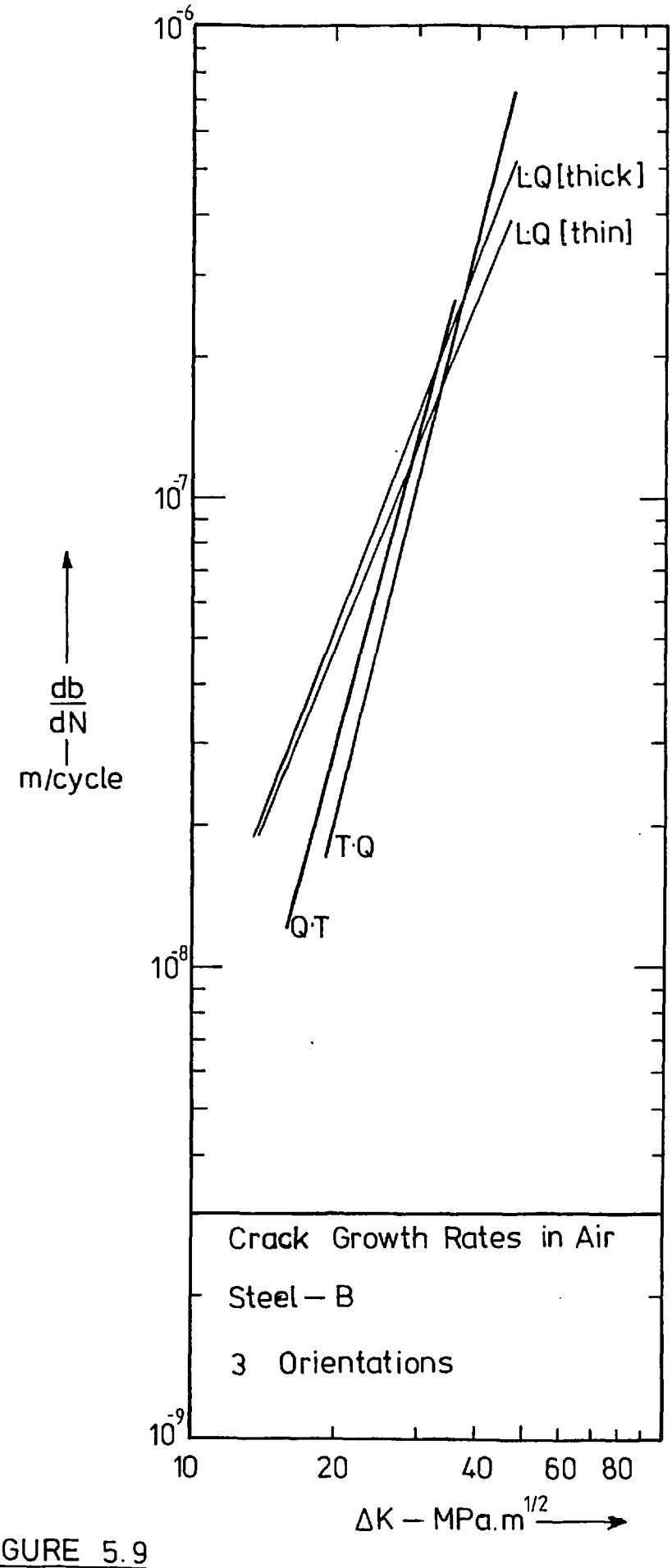
10^{-6}
10^{-7}
10^{-8}
10^{-9}
L-Q [thick]
L-Q [thin]
T-Q
Q-T
db/dN
m/cycle
Crack Growth Rates in Air
Steel – B
3 Orientations
10
20
40
60
80
ΔK – MPa.m$^{1/2}$

FIGURE 5.9

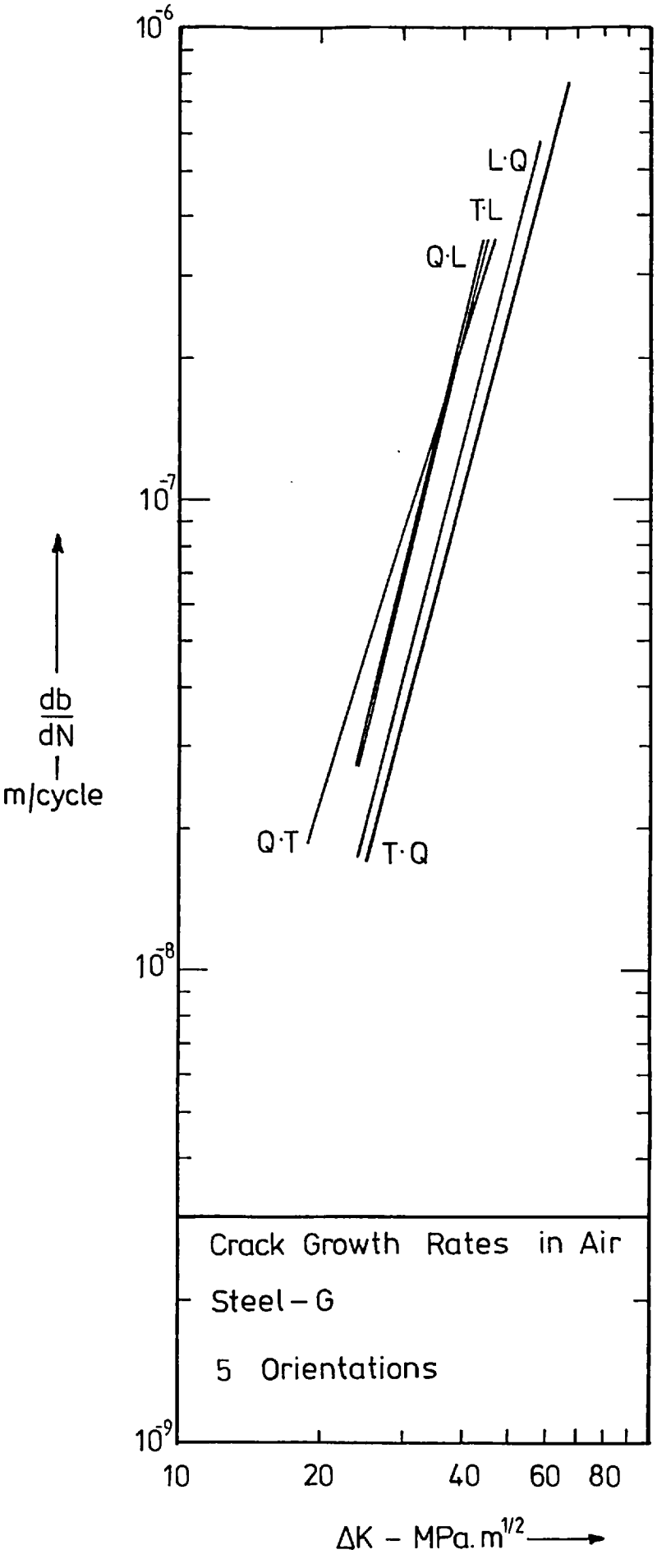
10^{-6}
10^{-7}
10^{-8}
10^{-9}
L·Q
T·L
Q·L
Q·T
T·Q
$\frac{db}{dN}$
m/cycle
Crack Growth Rates in Air
Steel – G
5 Orientations
10
20
40
60
80
ΔK – MPa. $m^{1/2}$

FIGURE 5.10

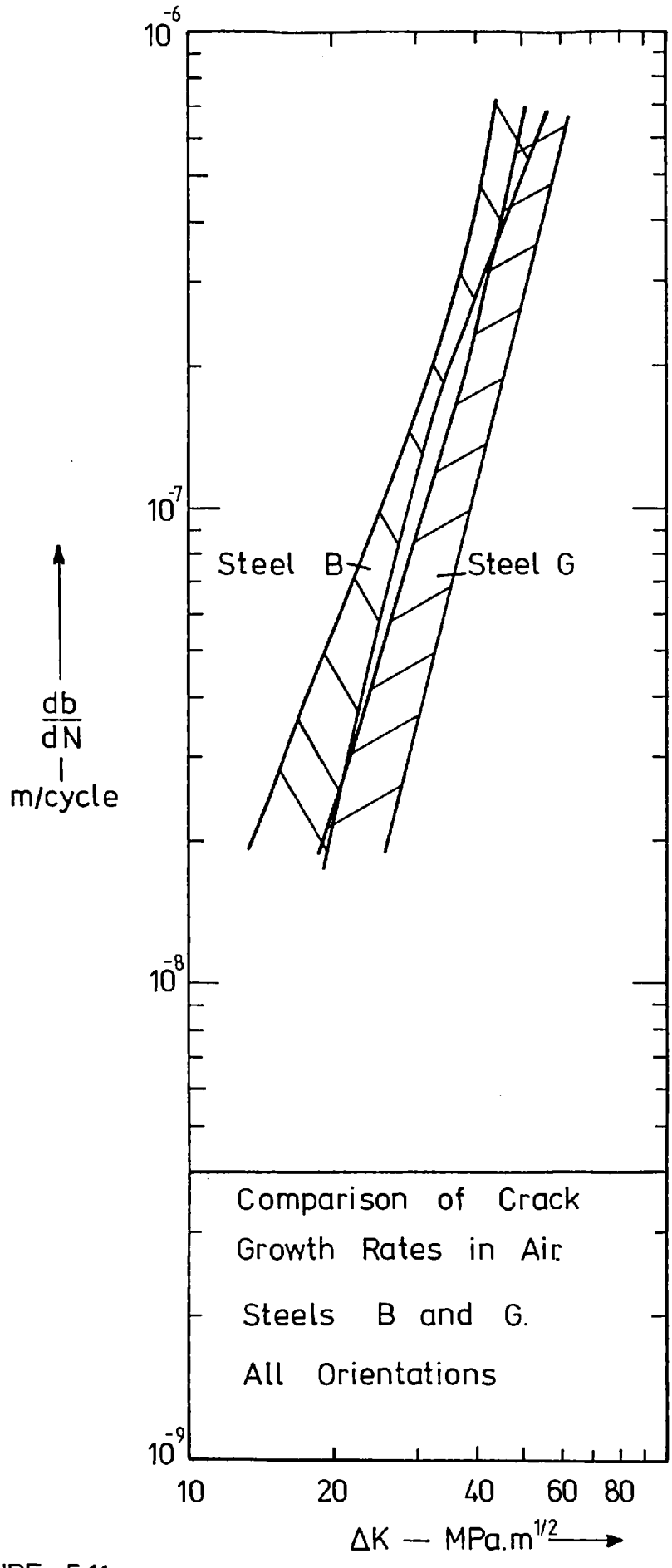
10^{-6}
10^{-7}
10^{-8}
10^{-9}
Steel B
Steel G
$\frac{db}{dN}$
m/cycle
Comparison of Crack Growth Rates in Air
Steels B and G.
All Orientations
10
20
40
60
80
ΔK — $MPa.m^{1/2}$

FIGURE 5.11

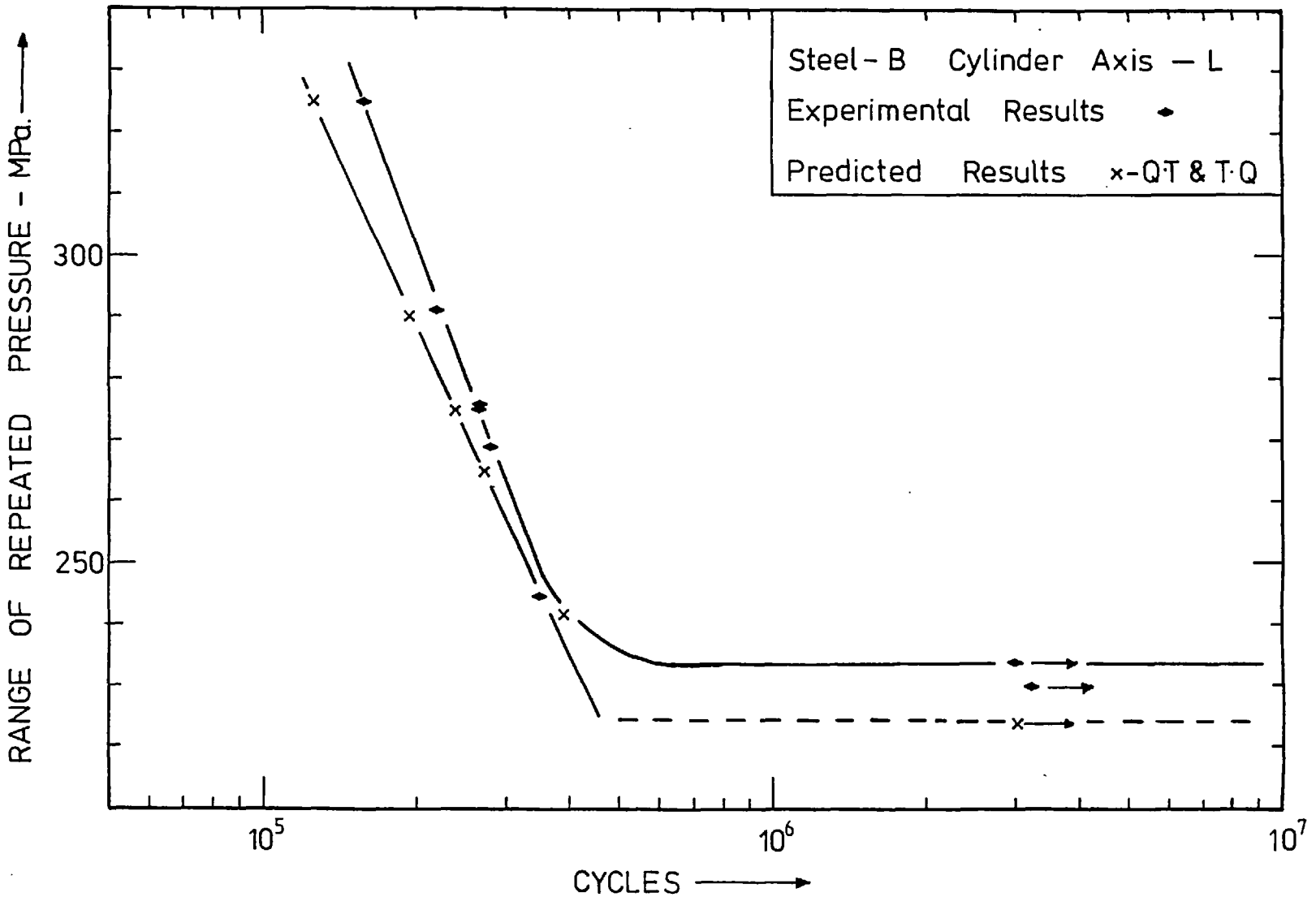

FIGURE 5.12 Comparison of Experimental and Predicted Fatigue Curves

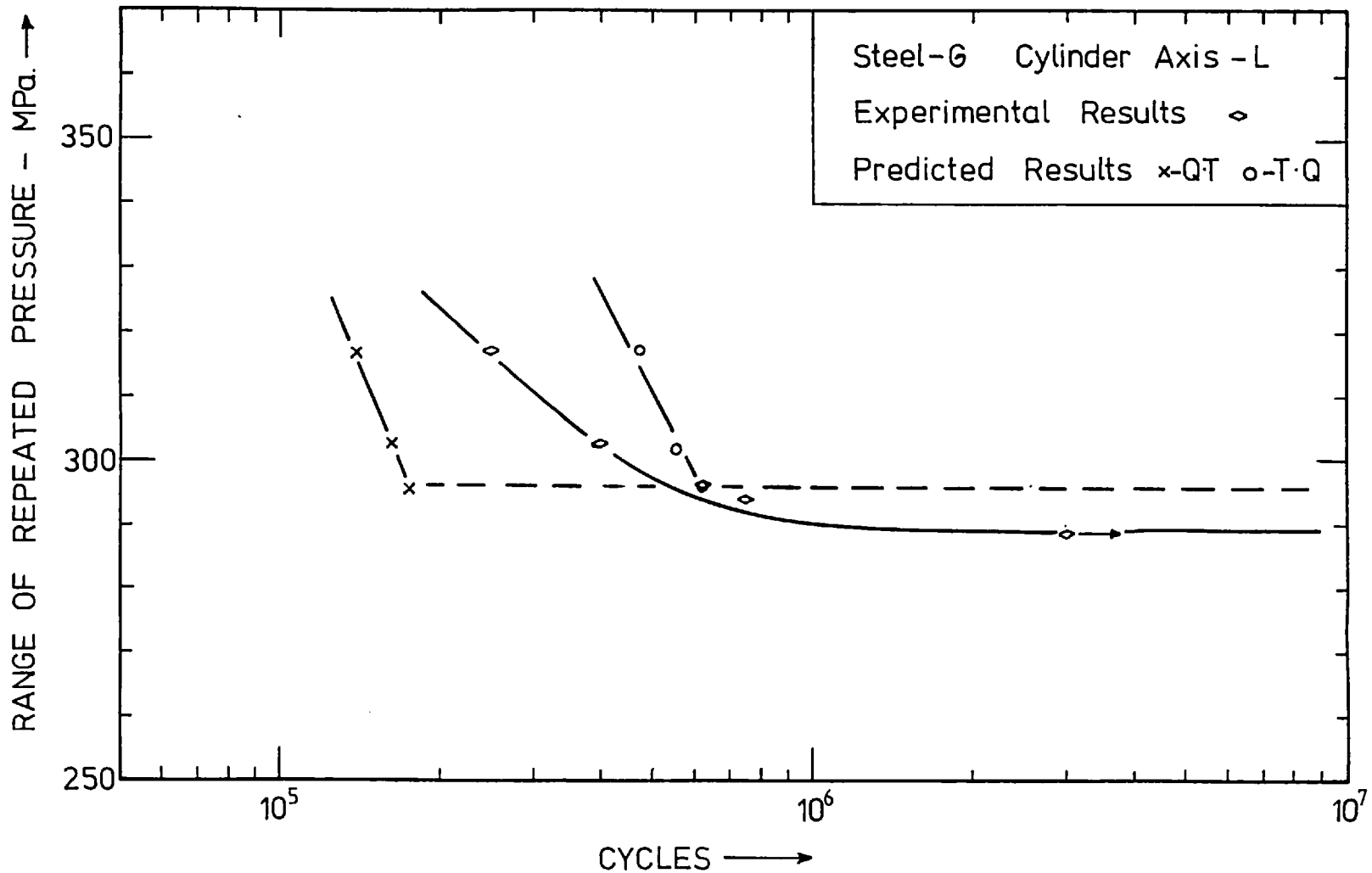

FIGURE 5.13 Comparison of Experimental and Predicted Fatigue Curves

FIGURE 5.14 Variation of Stress Intensity with Crack Length in a D.C.B. Specimen.

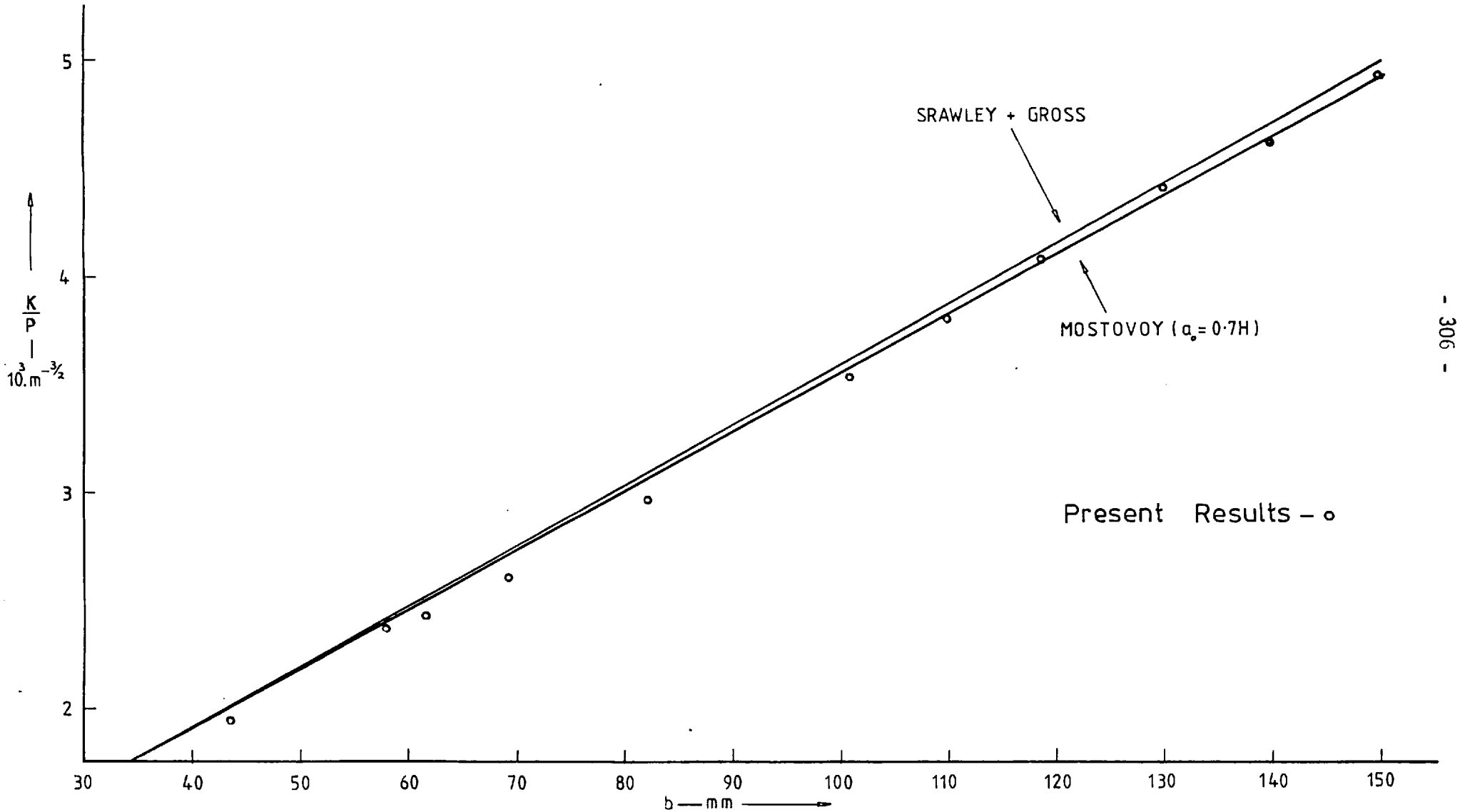

FIGURE 5.15

Variation in Stress Intensity Factor with Crack Depth for Cracks of Differing Semi Axis Ratio. Dia. Ratio = 3.

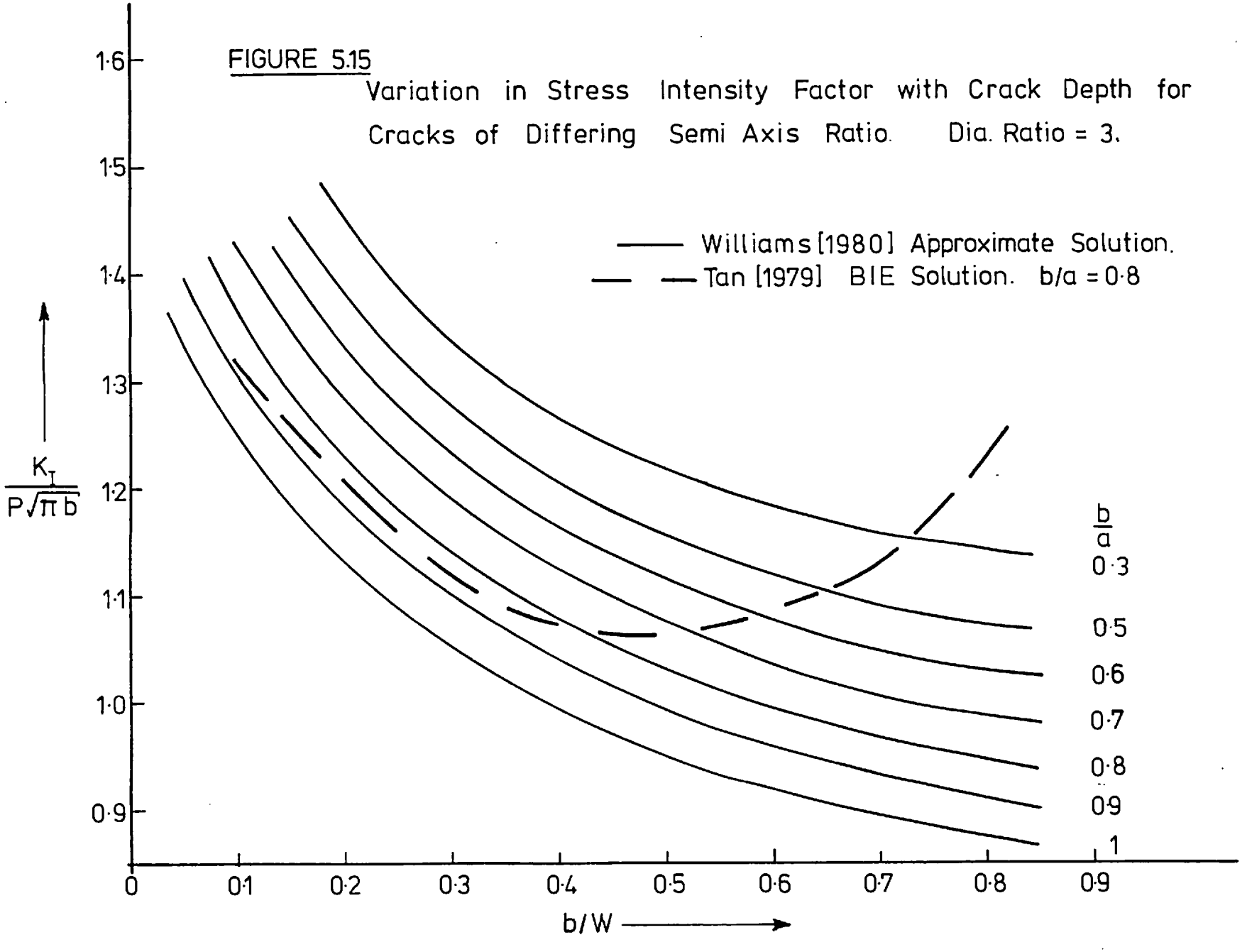

FIGURE 5.16

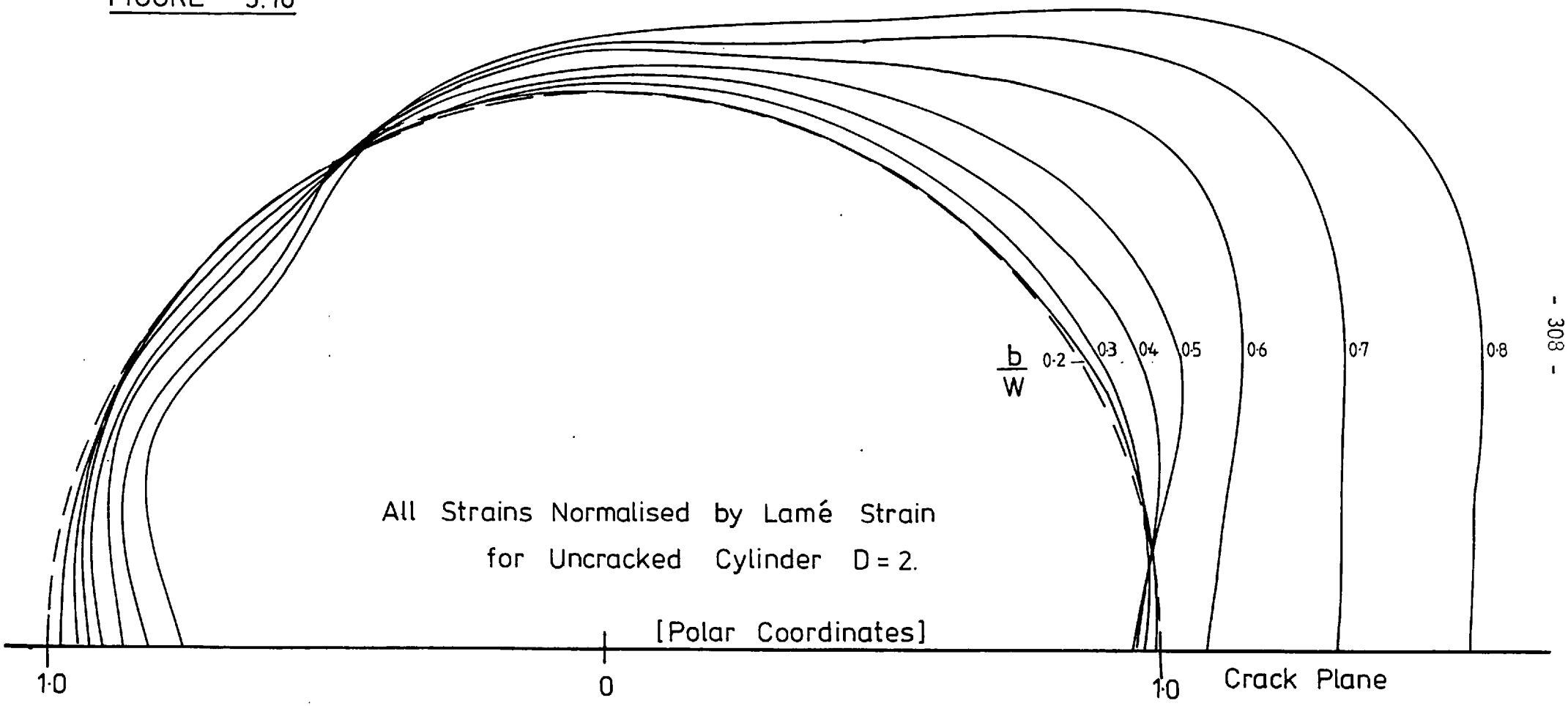

Variation of Hoop Strain at Outer Circumference [Calculated]

FIGURE 6.1

Variation in Critical Crack Depth with P/K_{Ic} for Different Wall Thickness.

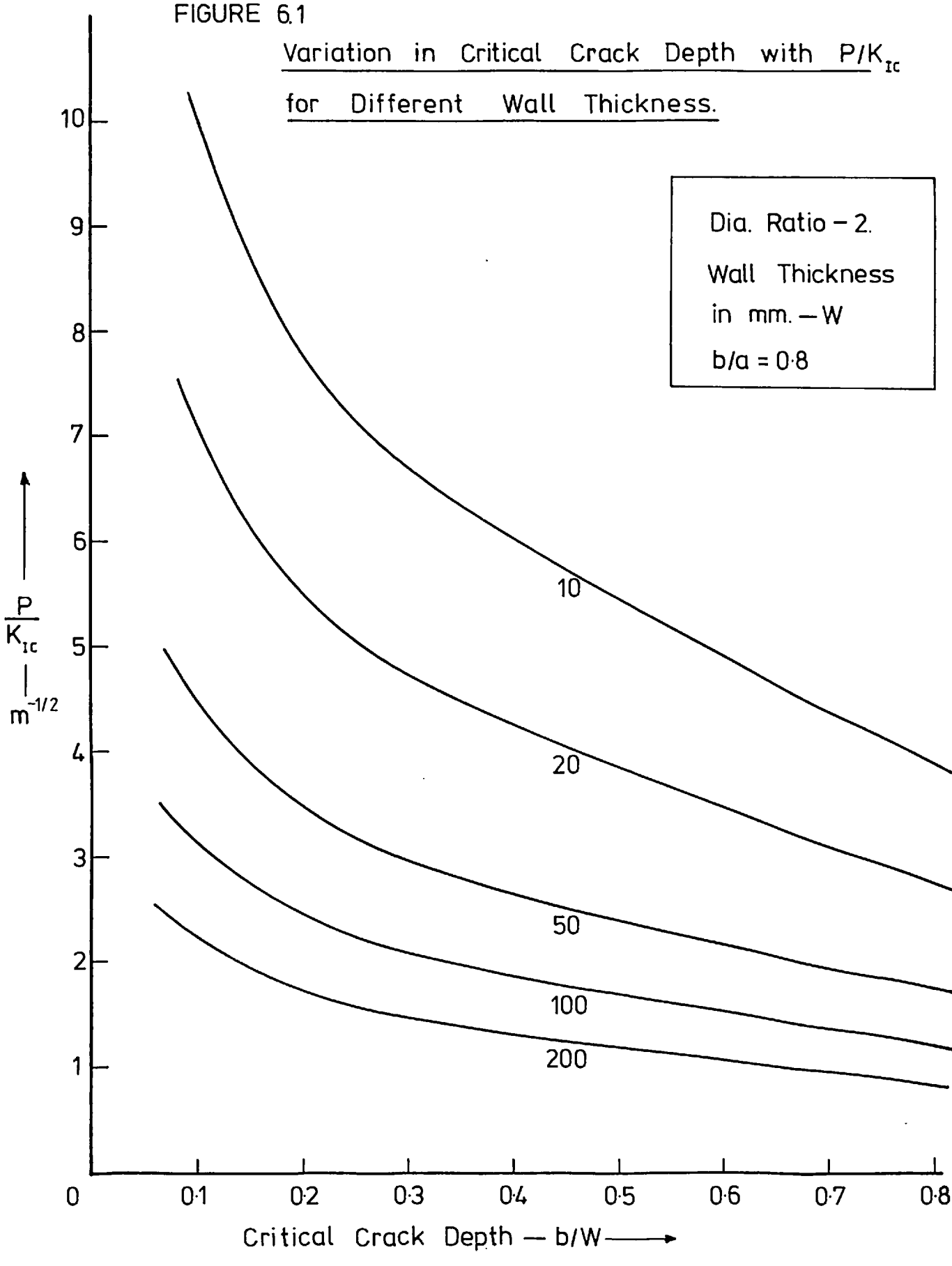

FIGURE 6.2

Variation in Critical Crack Depth with P/K_{Ic} for Different Wall Thickness.

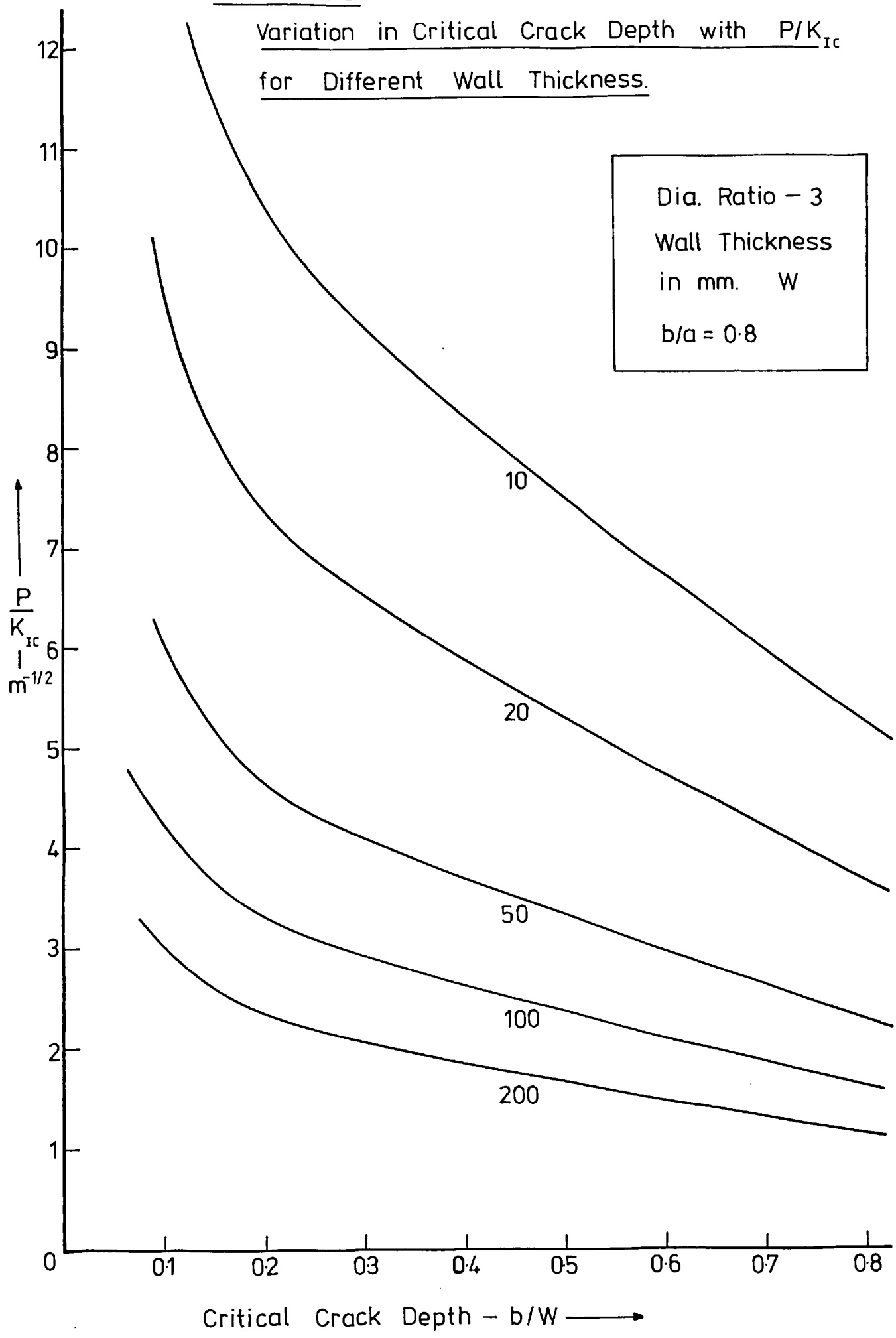

LIST OF DRAWINGS

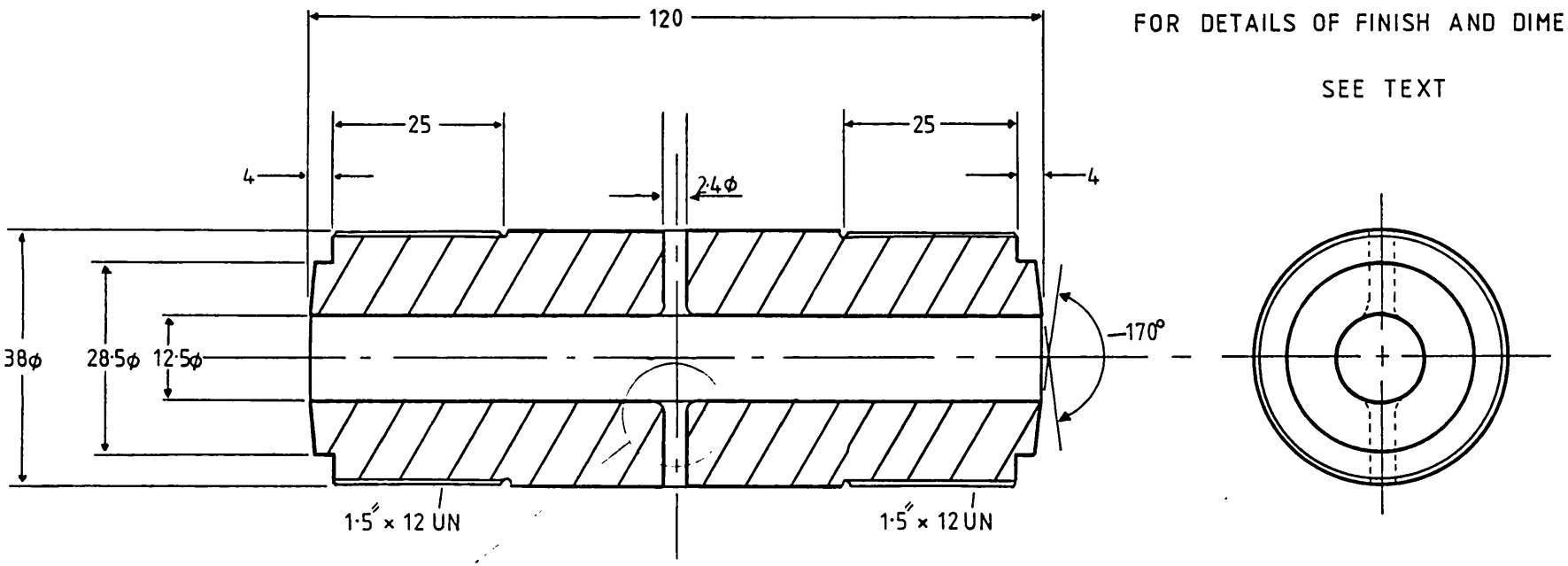

FOR DETAILS OF FINISH AND DIMENSIONS

SEE TEXT

DETAIL-'A'

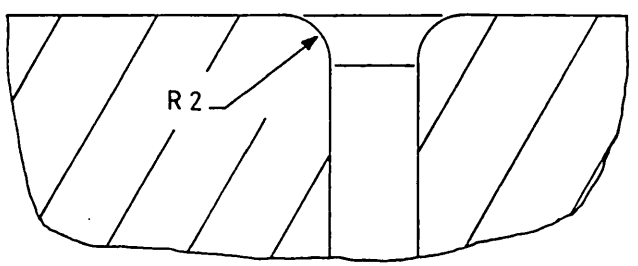

Drawings 3.1 & 3.1a.

Repeated Pressure Fatigue Specimens

Double Cross Bored Cylinders

Forgings BO, J, OES, Y

Diameter Ratio = 3

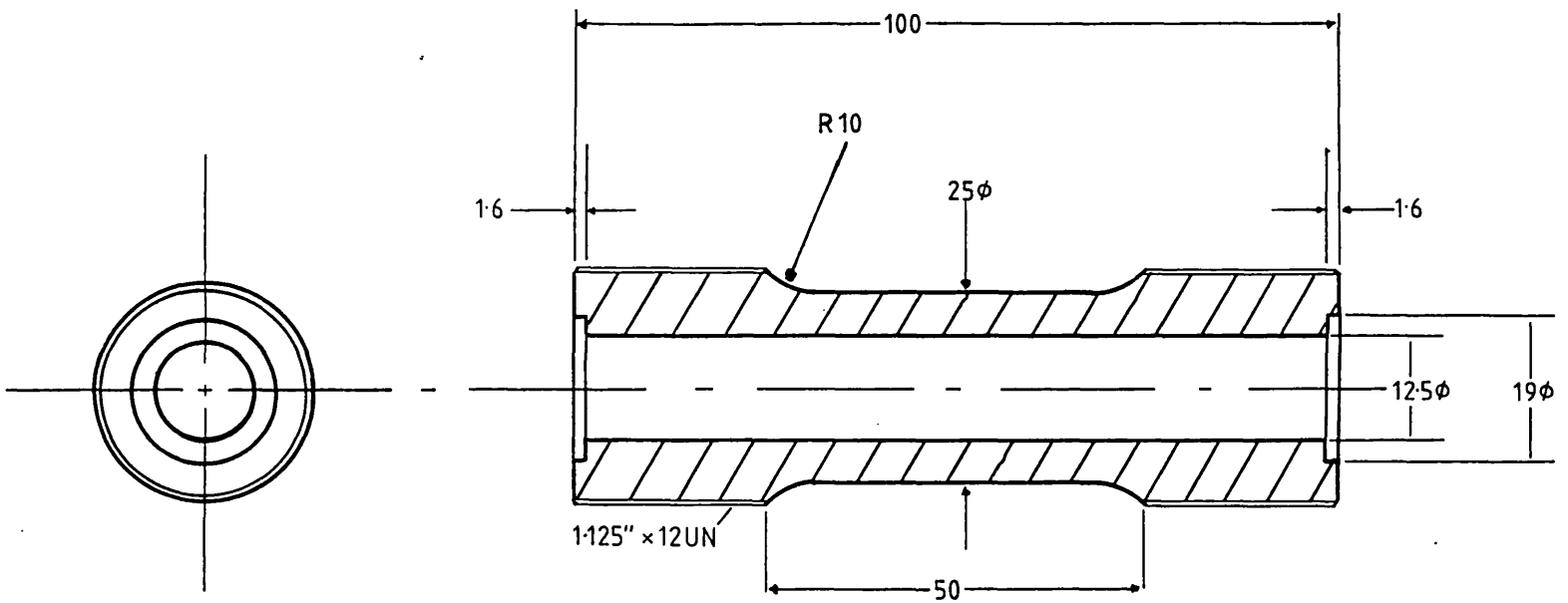

Drawing 3.3 Repeated Pressure Fatigue Specimens

Plain Cylinders For Technique Developement

Material CH. Diameter Ratio = 2

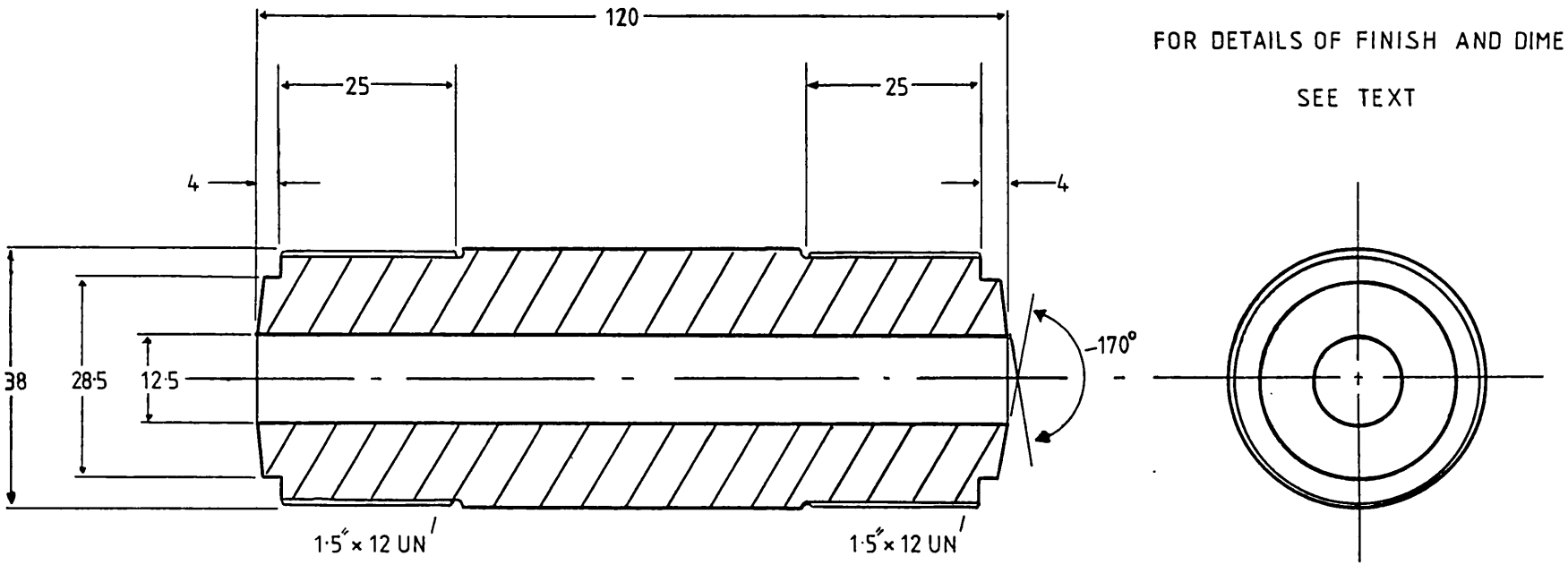

FOR DETAILS OF FINISH AND DIMENSIONS

SEE TEXT

Drawing 3.4

Repeated Pressure Fatigue Specimens

Plain Cylinders Forgings 'B' + 'G'

Diameter Ratio = 3

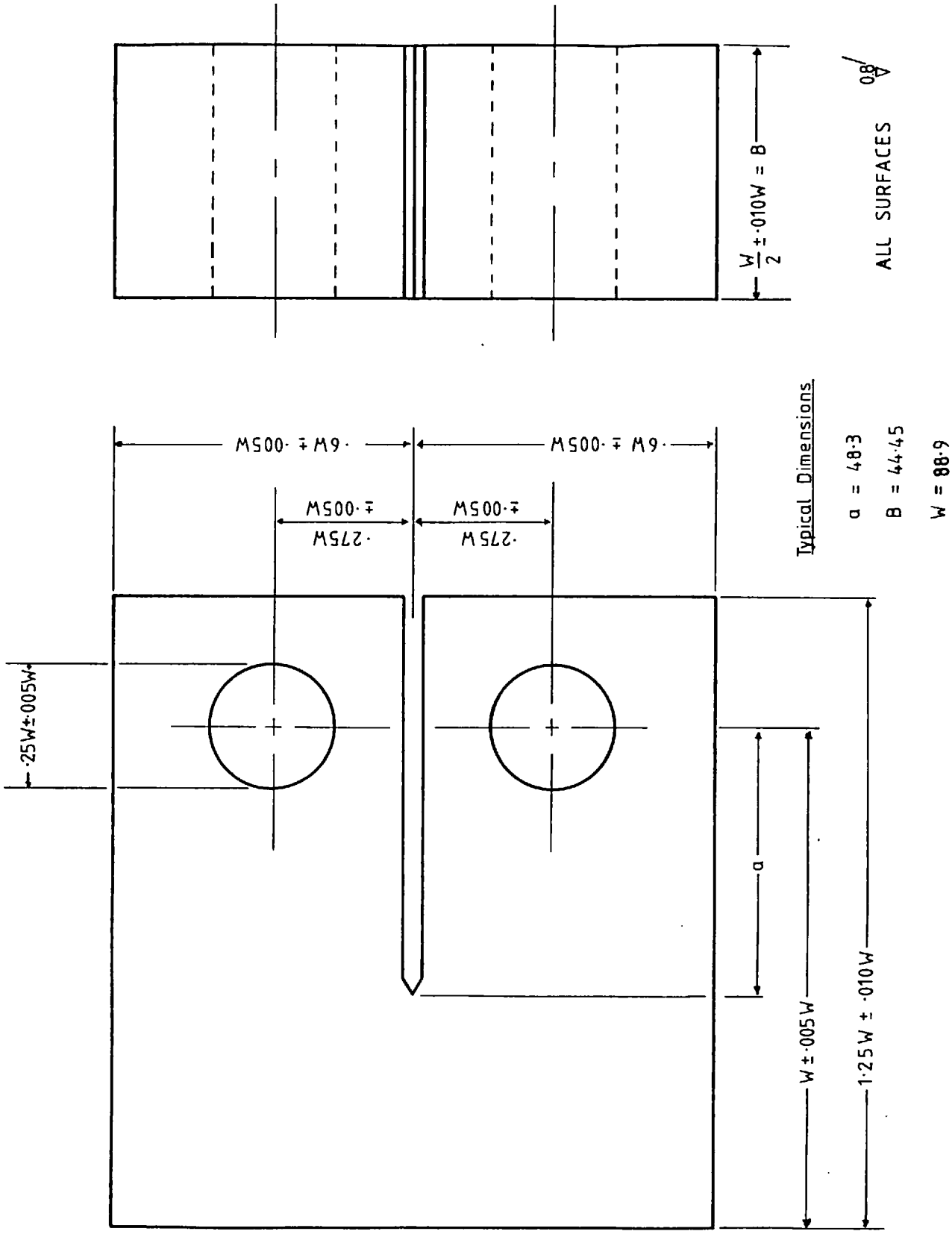

Drawing 3.5

Compact Tension Specimen Geometry — Used For Fracture Toughness And Fatigue Crack Growth Rate Tests—— Forging B

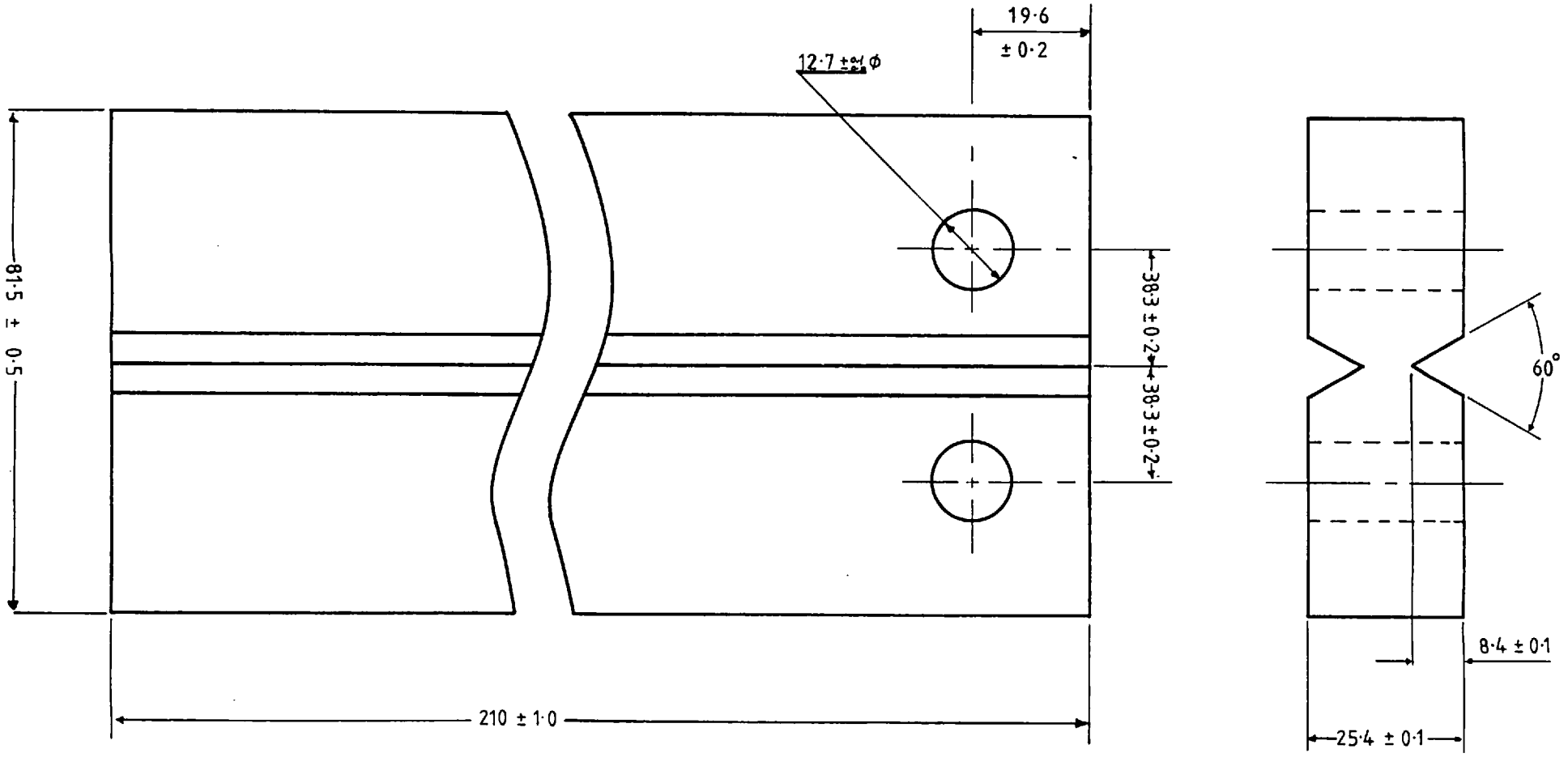

Drawing 3.6

Typical DCB Specimen Used For Forgings 'B' + 'G'

ALL SURFACES 0·8

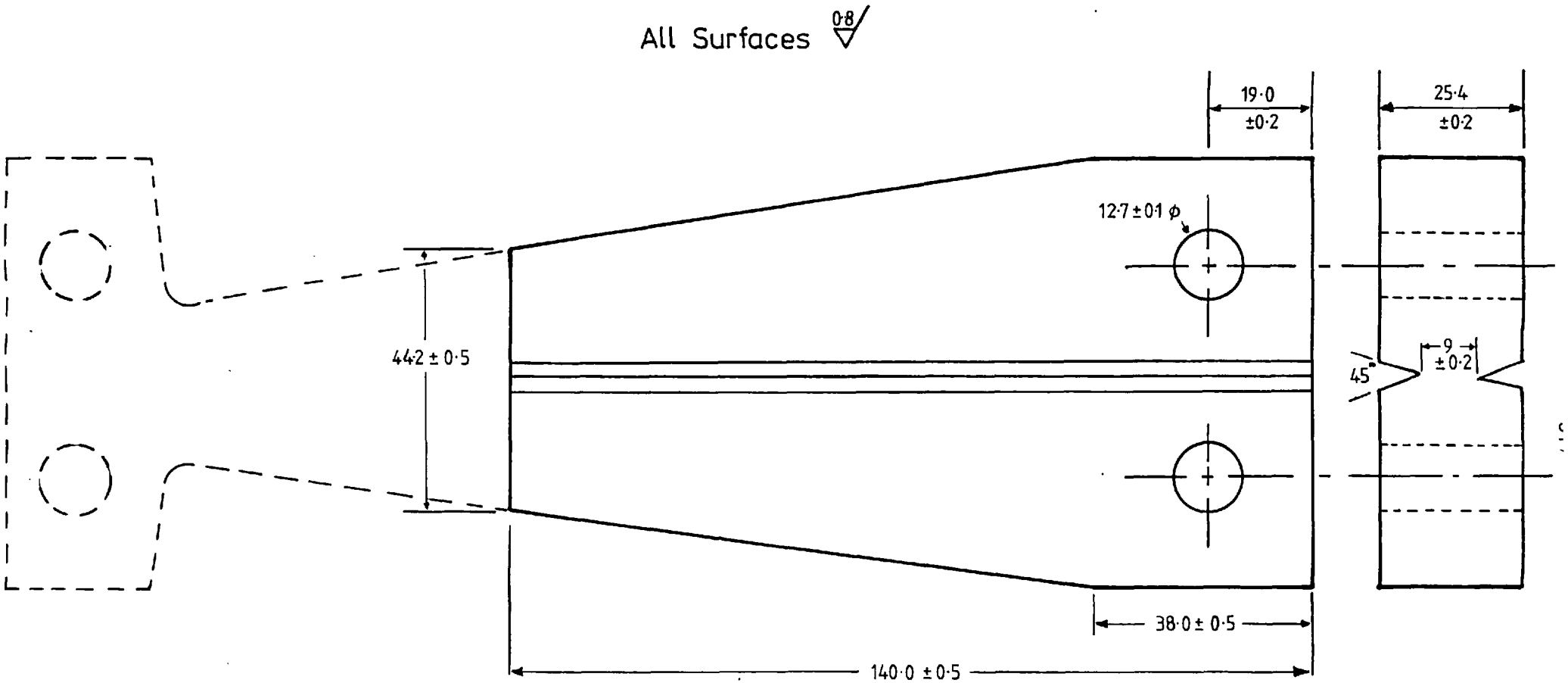

REVERSED CONSTANT 'K' DCB SPECIMEN.

DRAWING 3.7

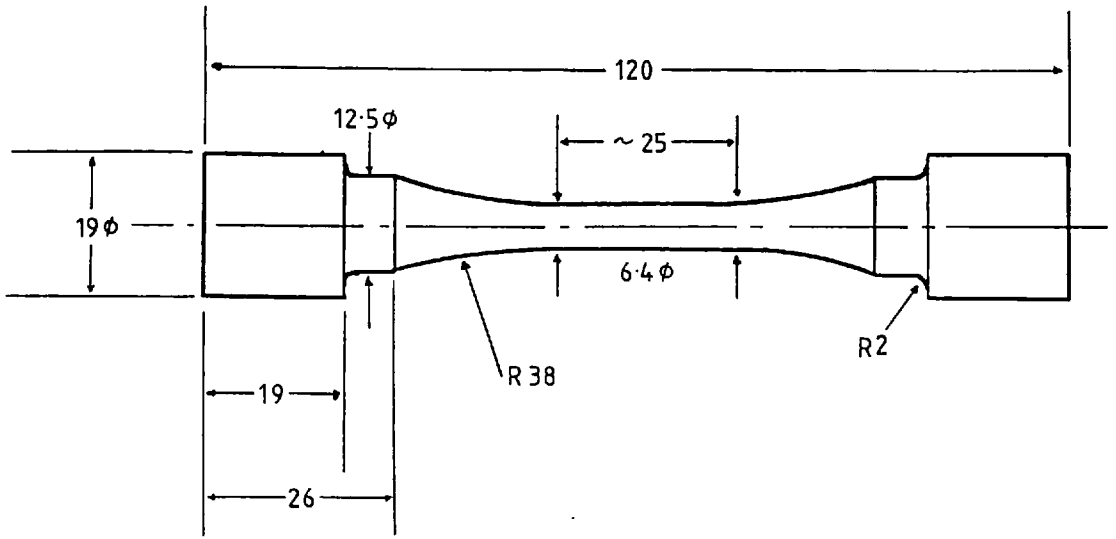

Repeated Tension

Fatigue Specimens

Drawing 3.8

FOR DETAILS OF FINISH AND DIMENSIONS — SEE TEXT.

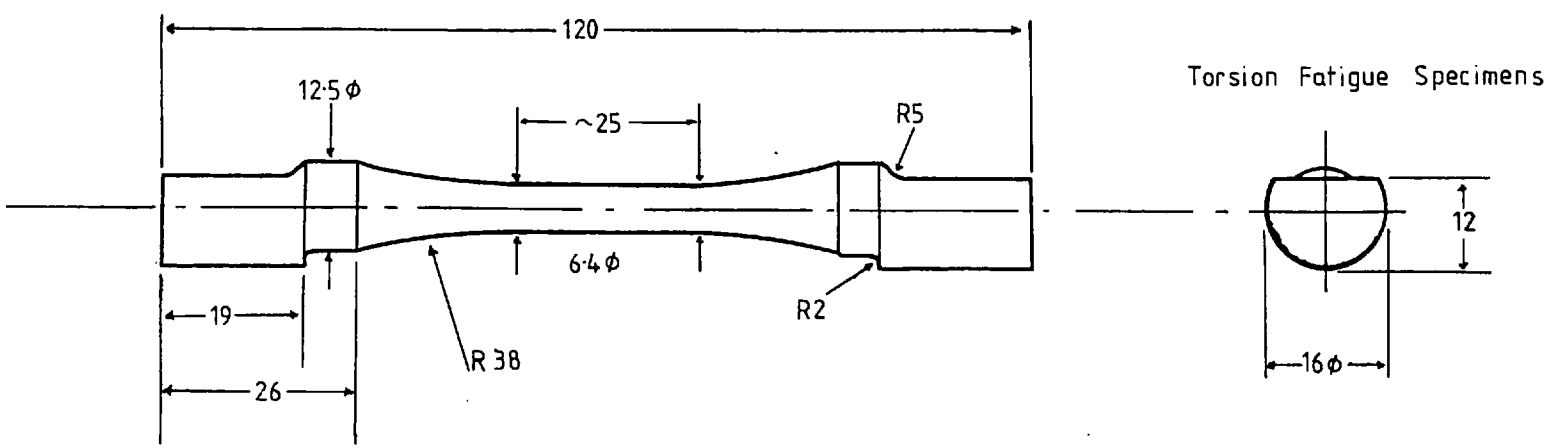

Torsion Fatigue Specimens

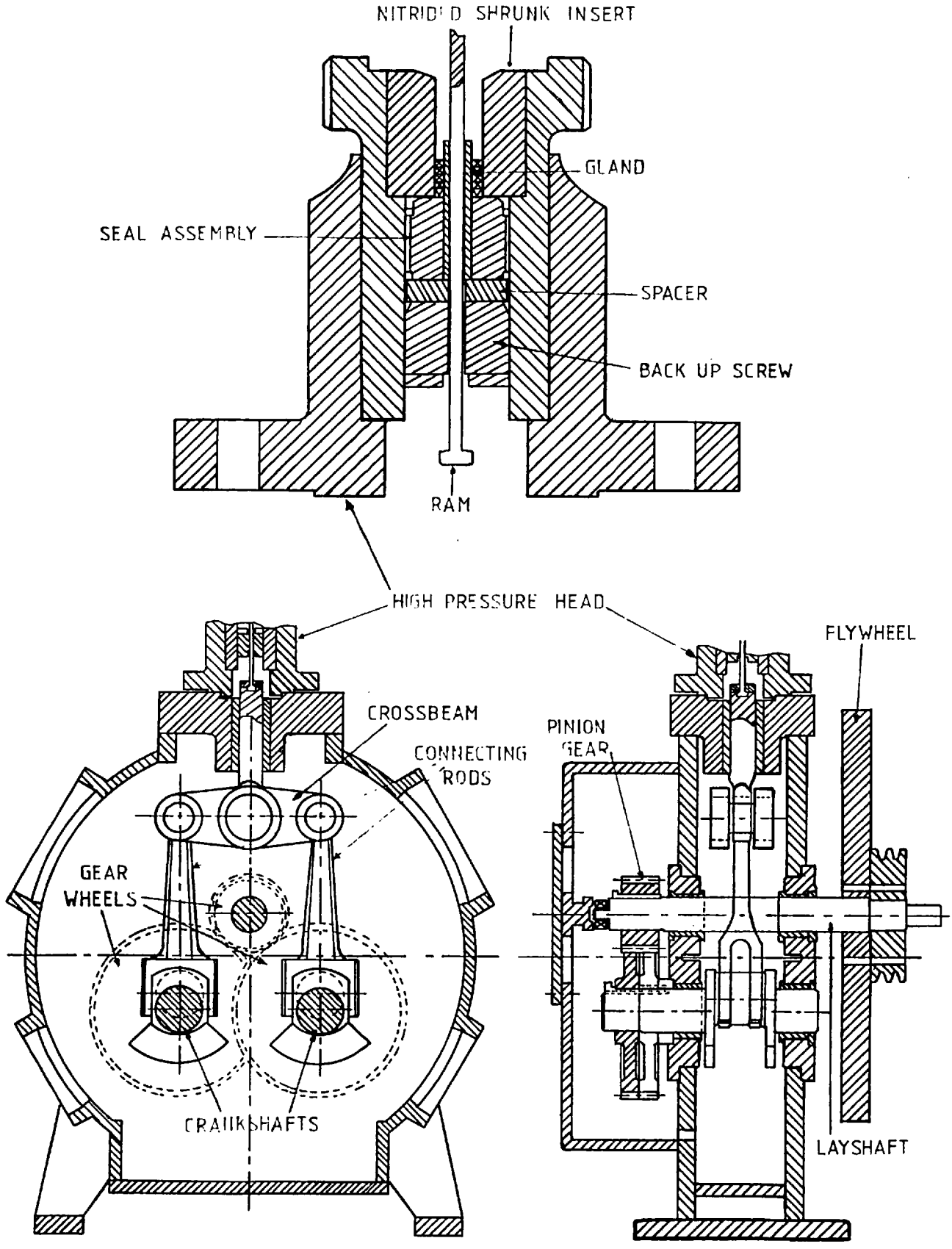

Drawing 3.9

LAYOUT OF FATIGUE TESTING MACHINE

LIST OF PHOTOGRAPHS

5.48 : Sawtooth fracture on a nickel plated fracture profile of a steel B cylinder (close to QL fracture plane)

5.49(a) to (f) : Photomicrograph series of an inclusion family lying on the surface of a TL fracture plane from a cylinder of steel B

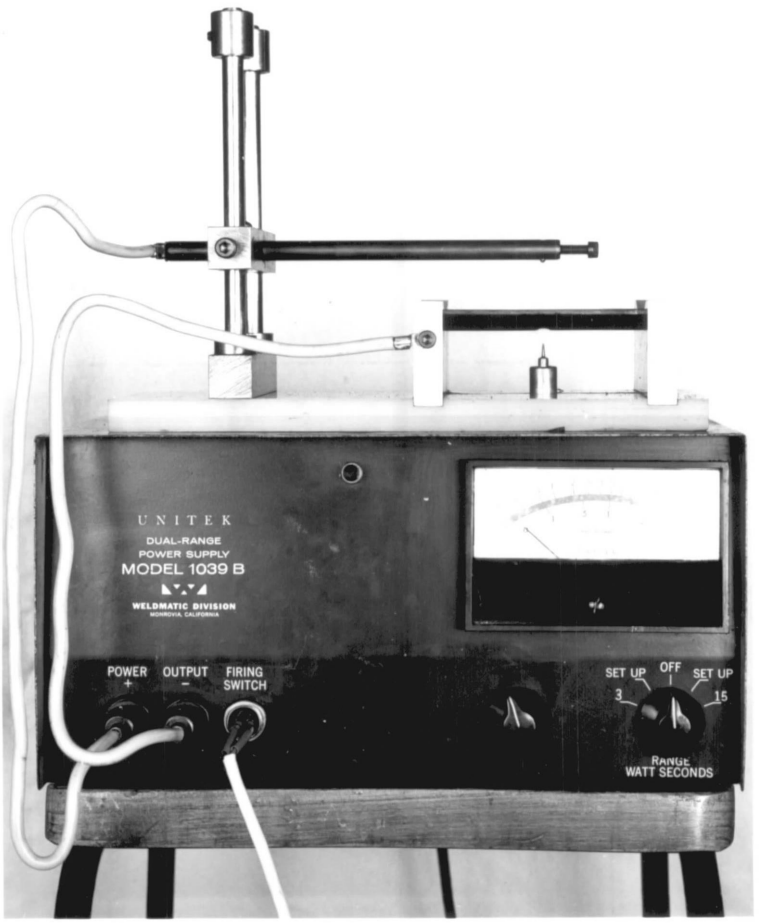

Photograph 3.1

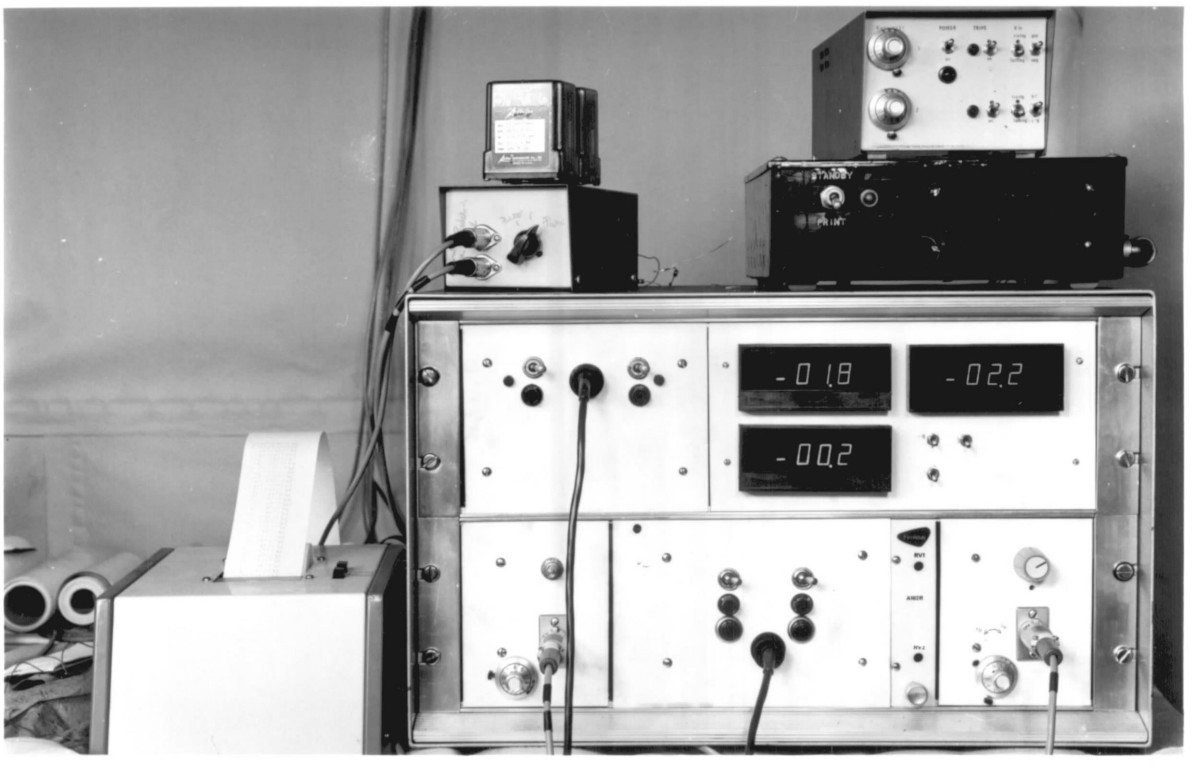

Photograph 3.2

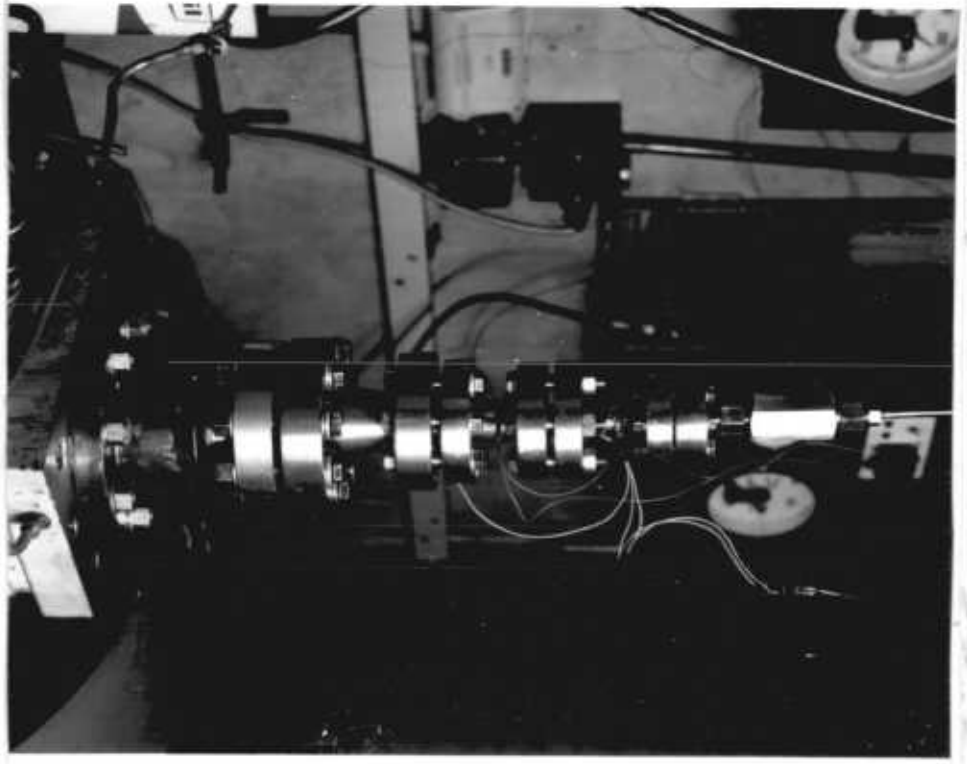

Photograph 3.4

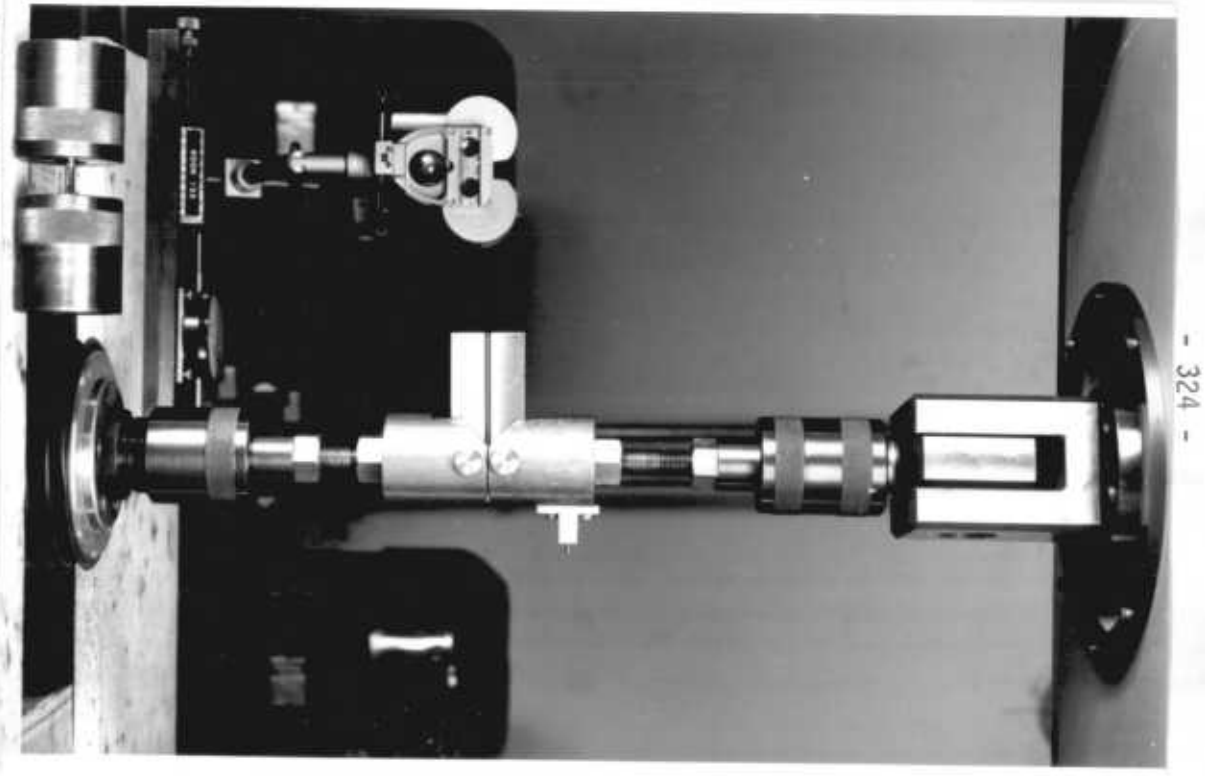

Photograph 3.3

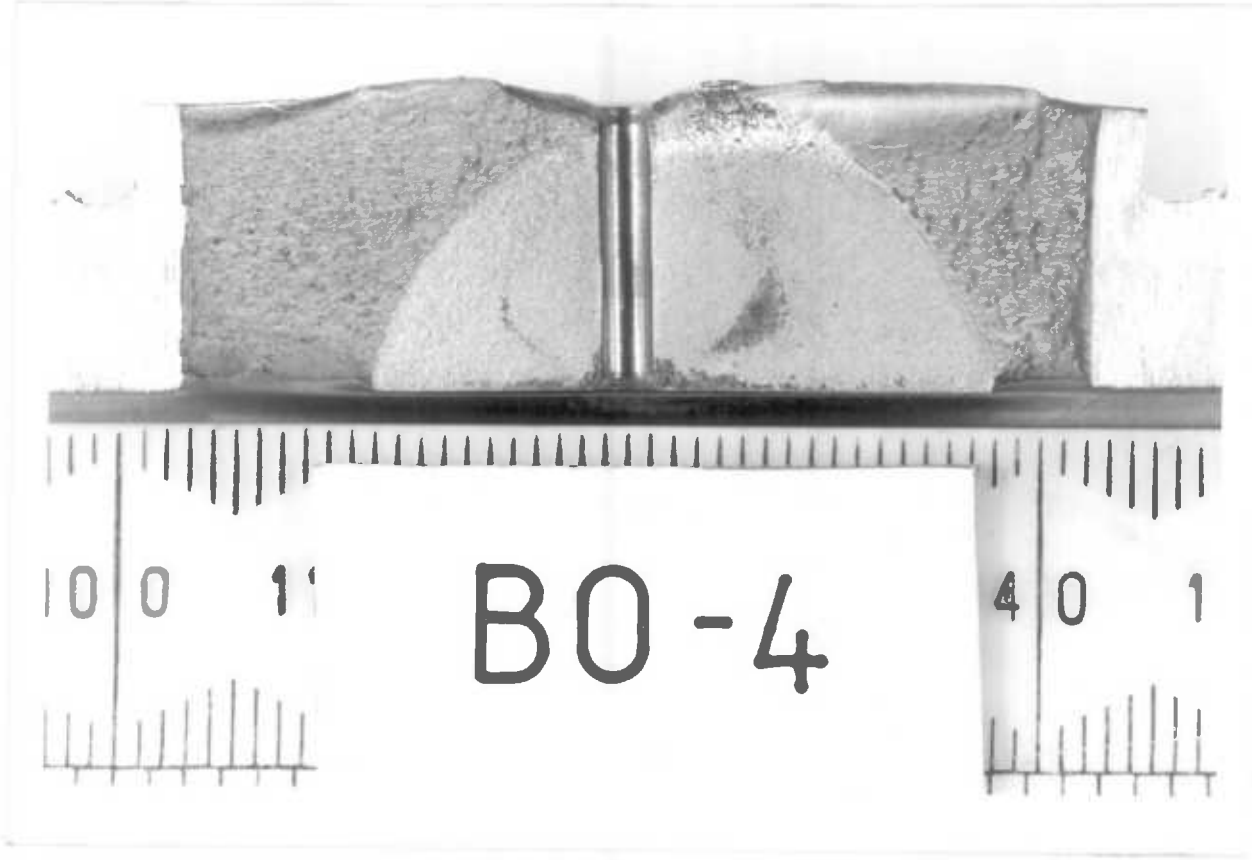

Photograph 4.1

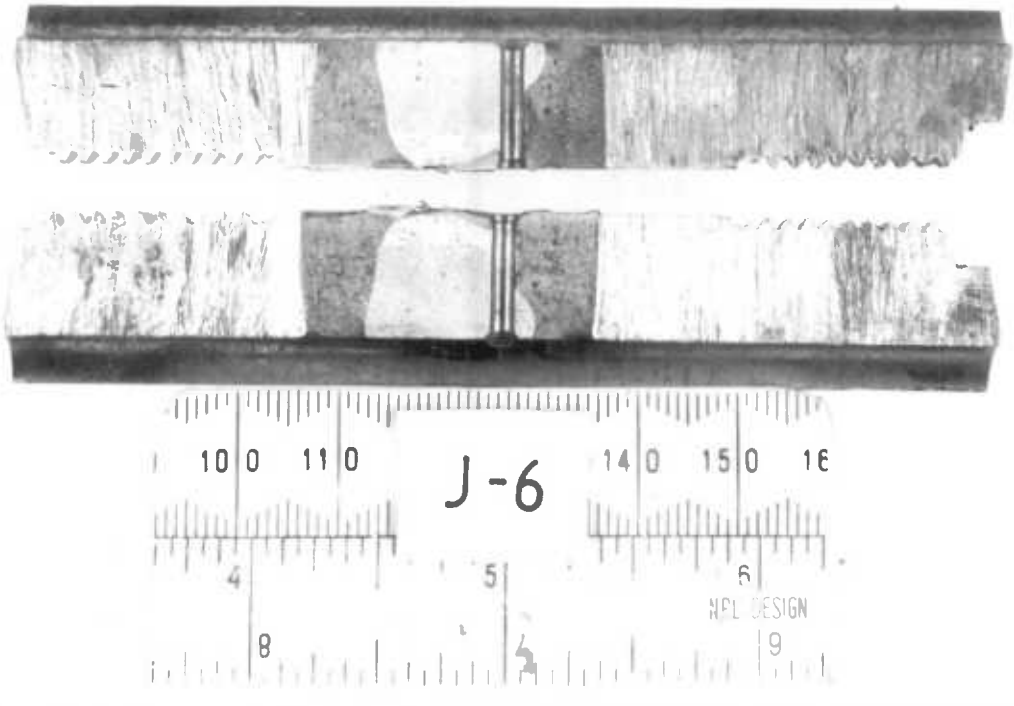

Photograph 4.2

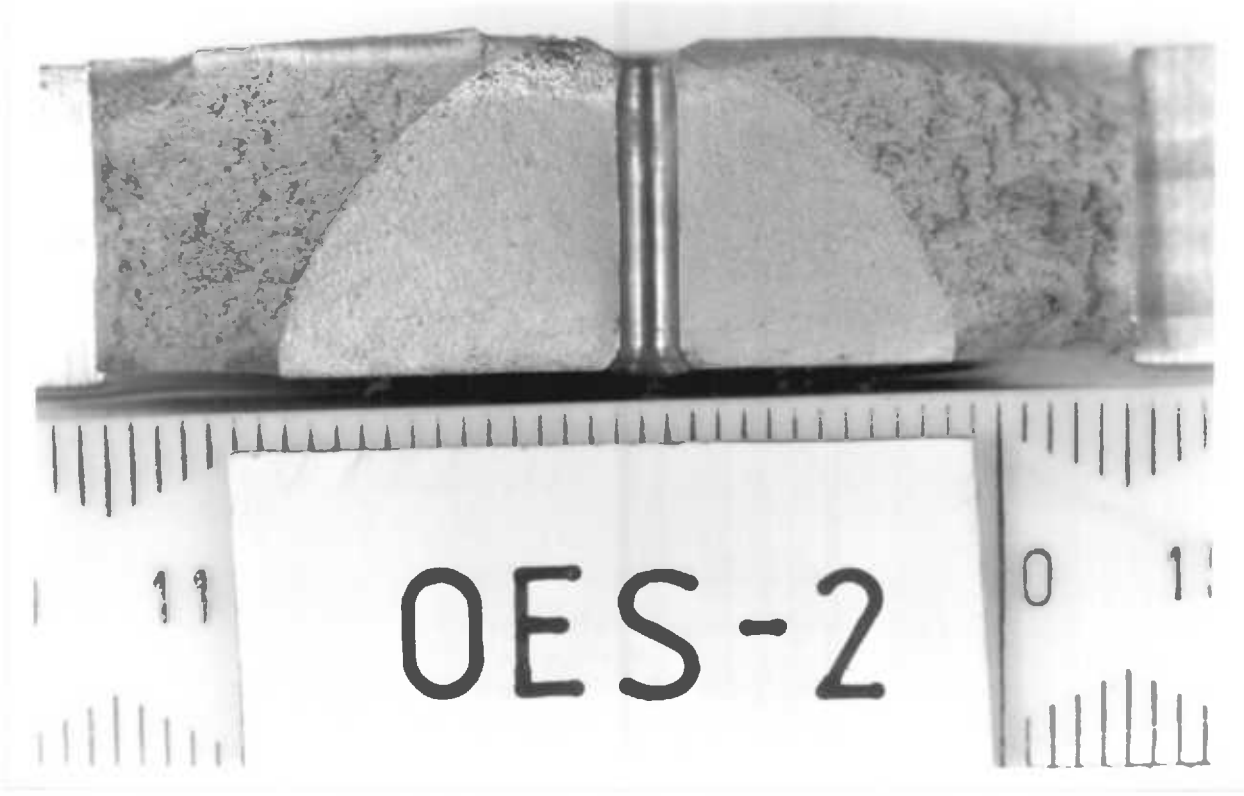

Photograph 4.3

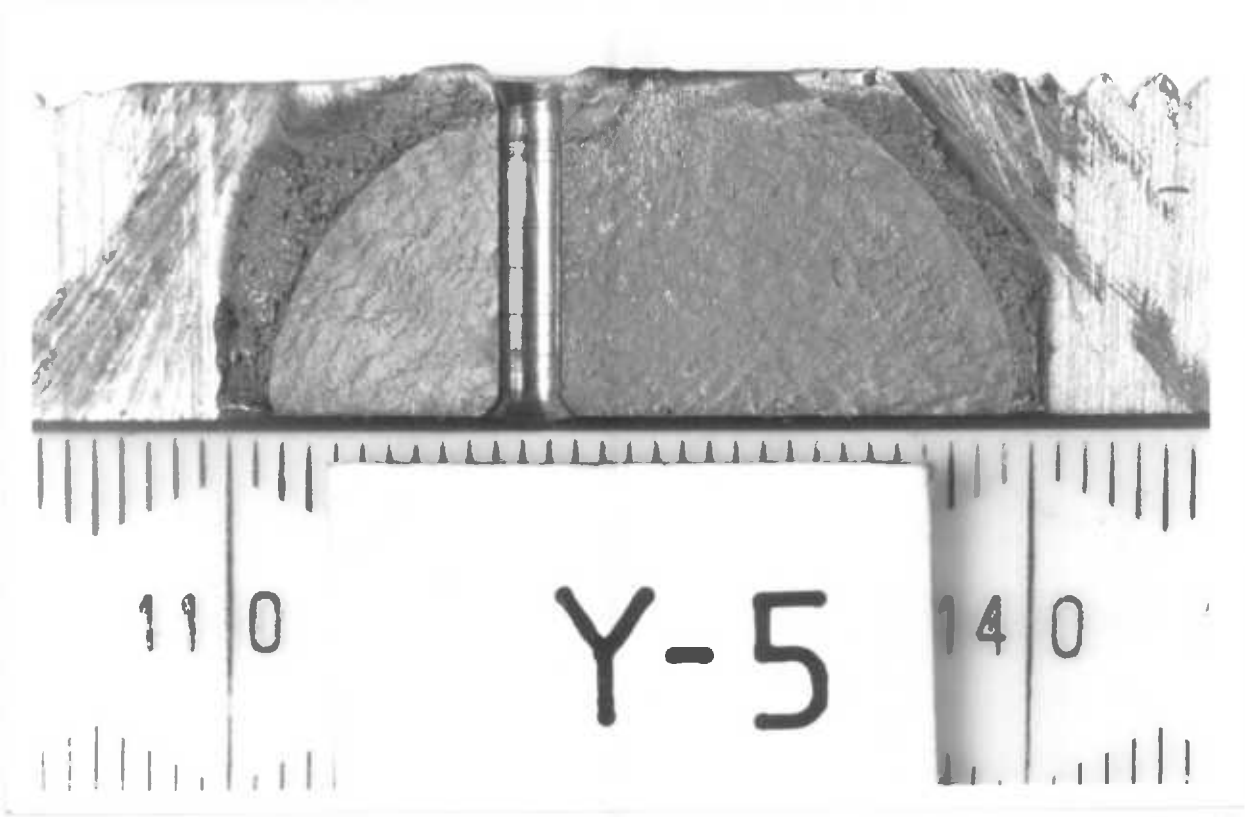

Photograph 4.4

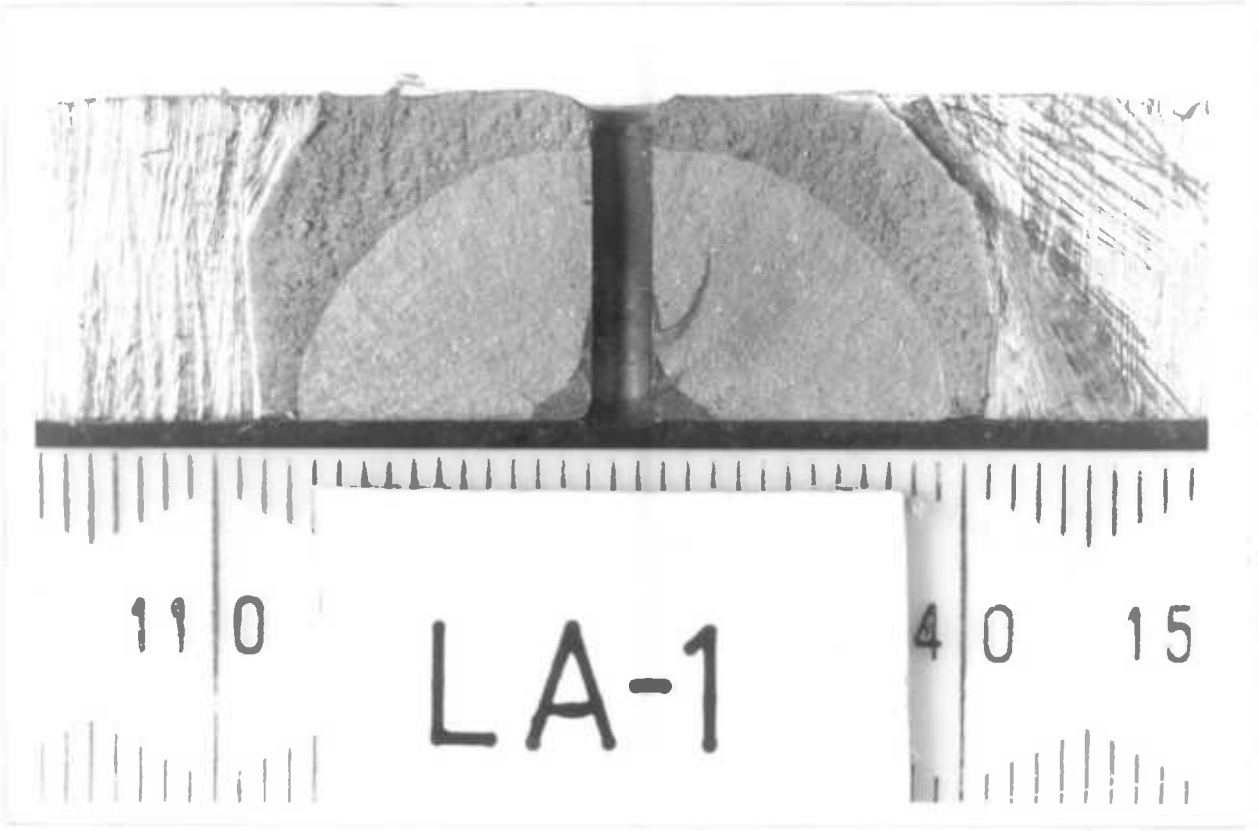

Photograph 4.5

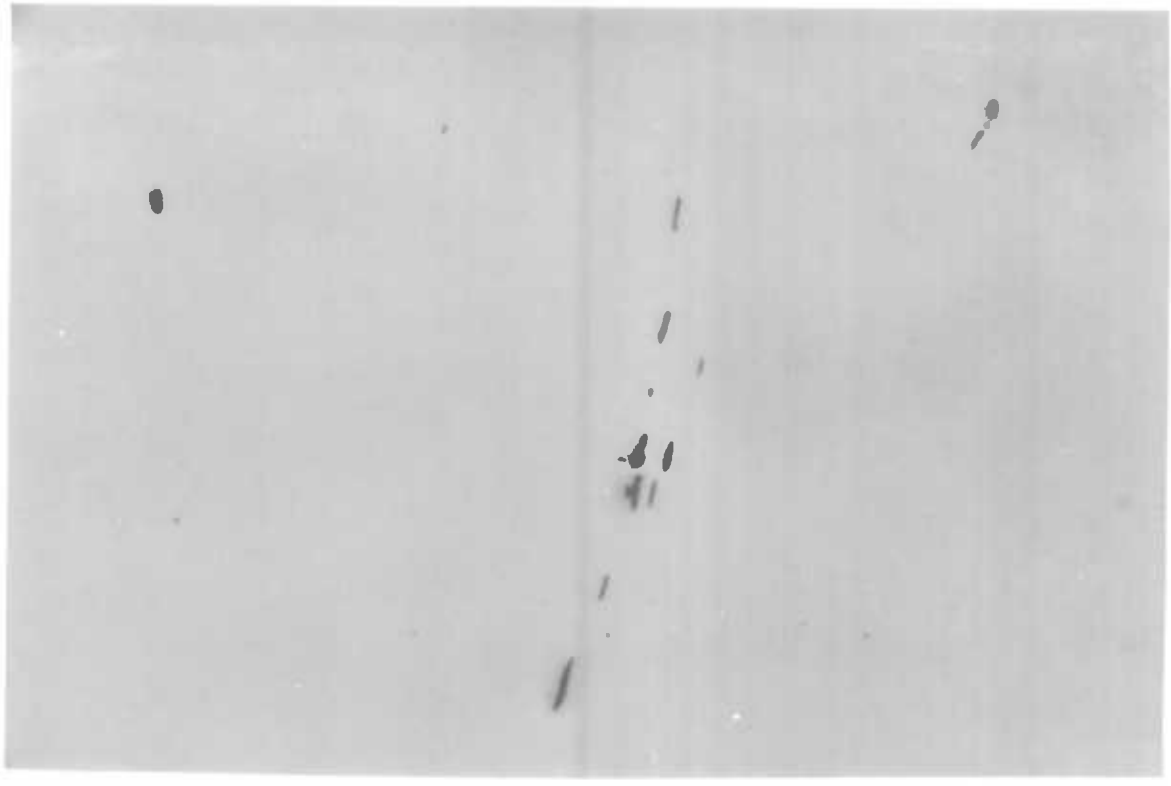

Photograph 4.6 ×50 (×4.4)

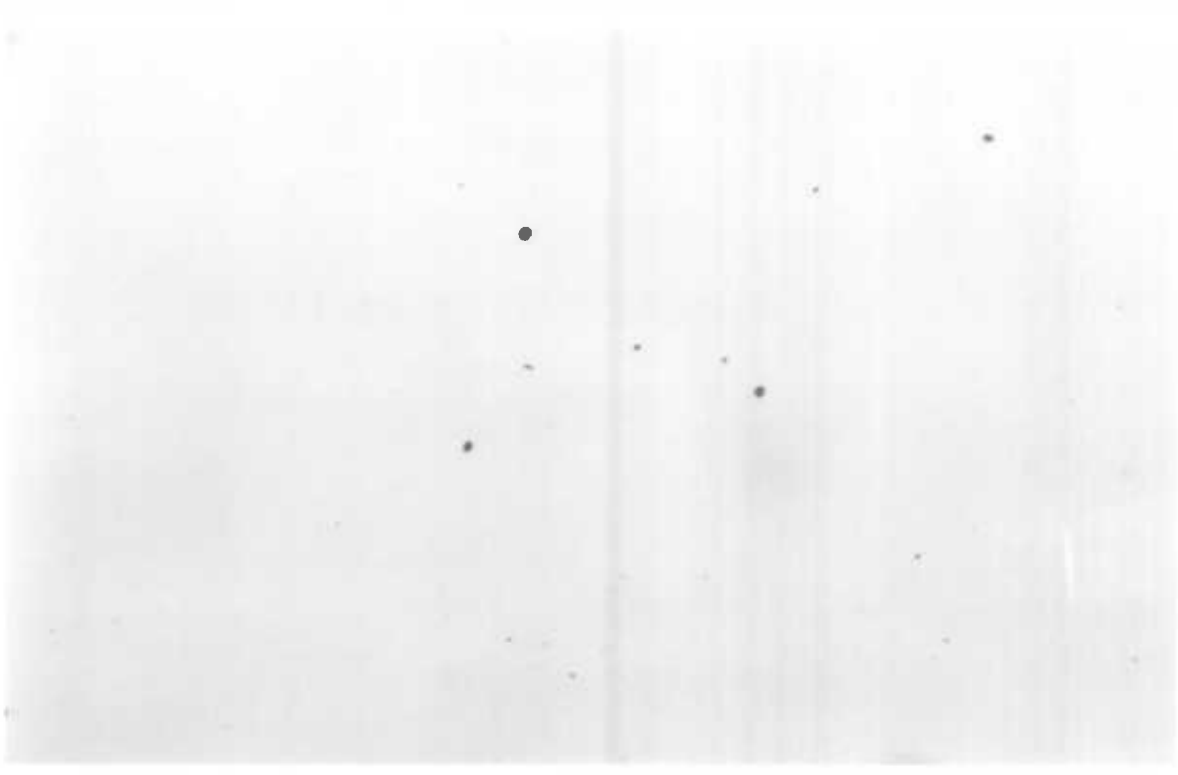

Photograph 4.7 ×50 (×4.4)

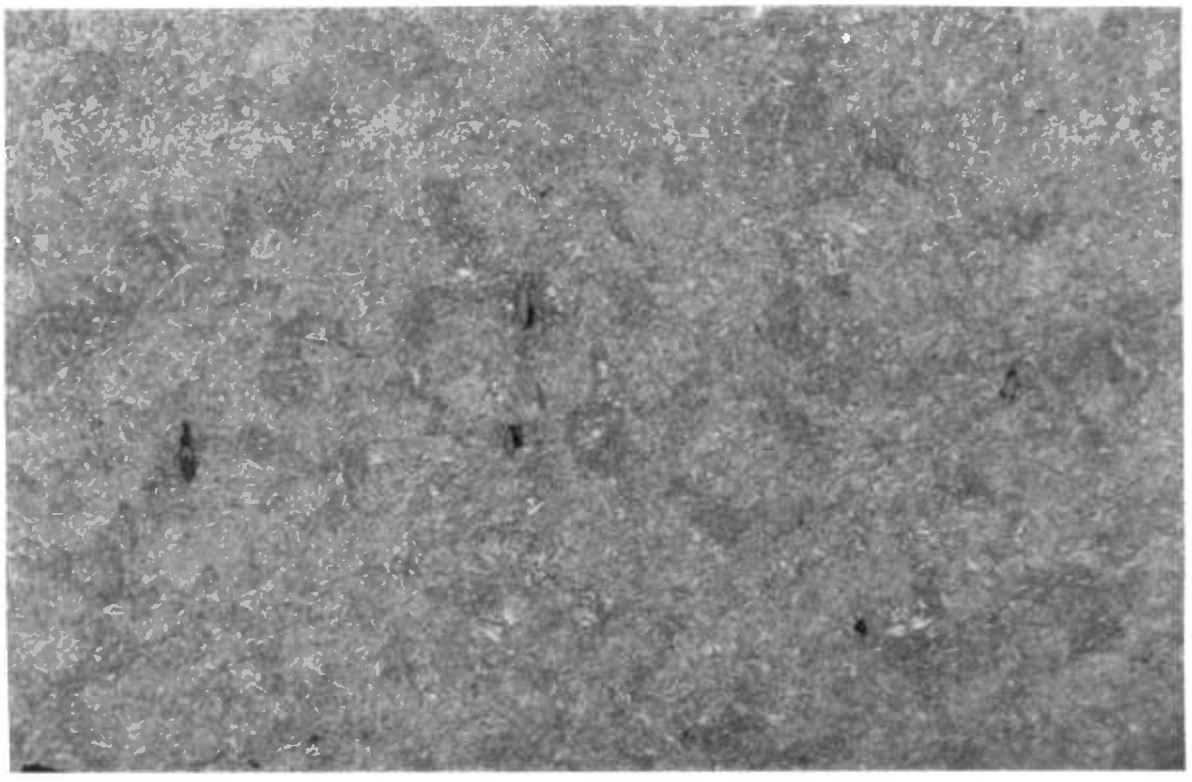

Photograph 4.8 ×50 (×4.4)

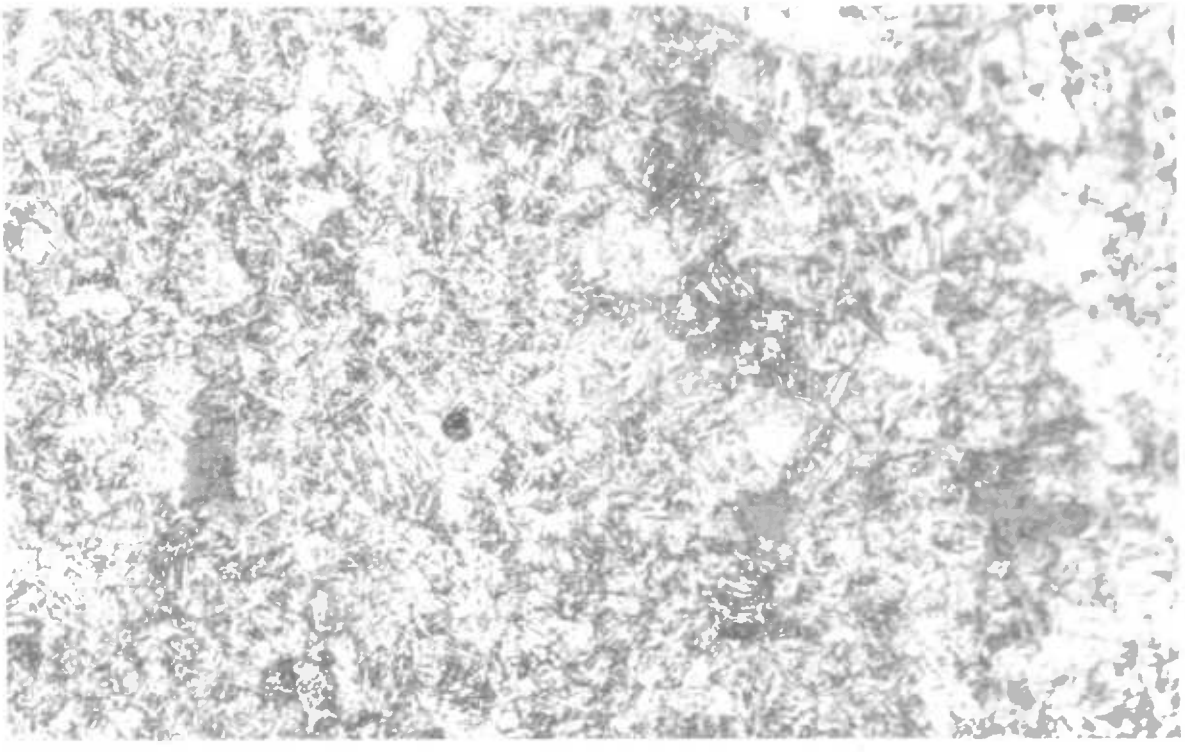

Photograph 4.9 **×50 (×4.4)**

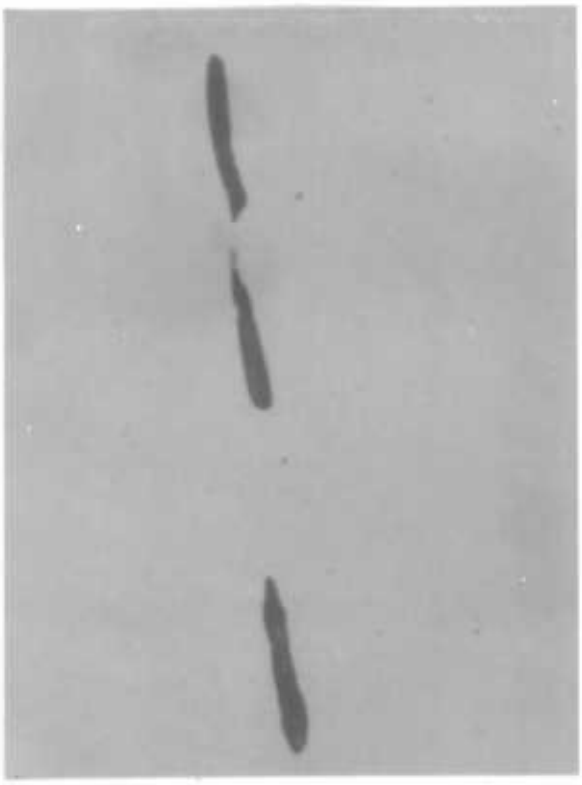

Photograph 4.10 ×200 (×4.4)

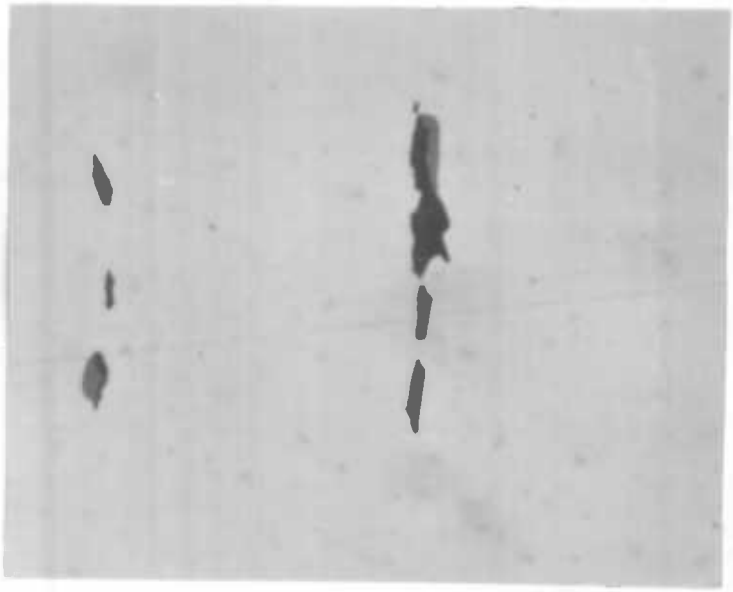

Photograph 4.11 ×200 (×4.4)

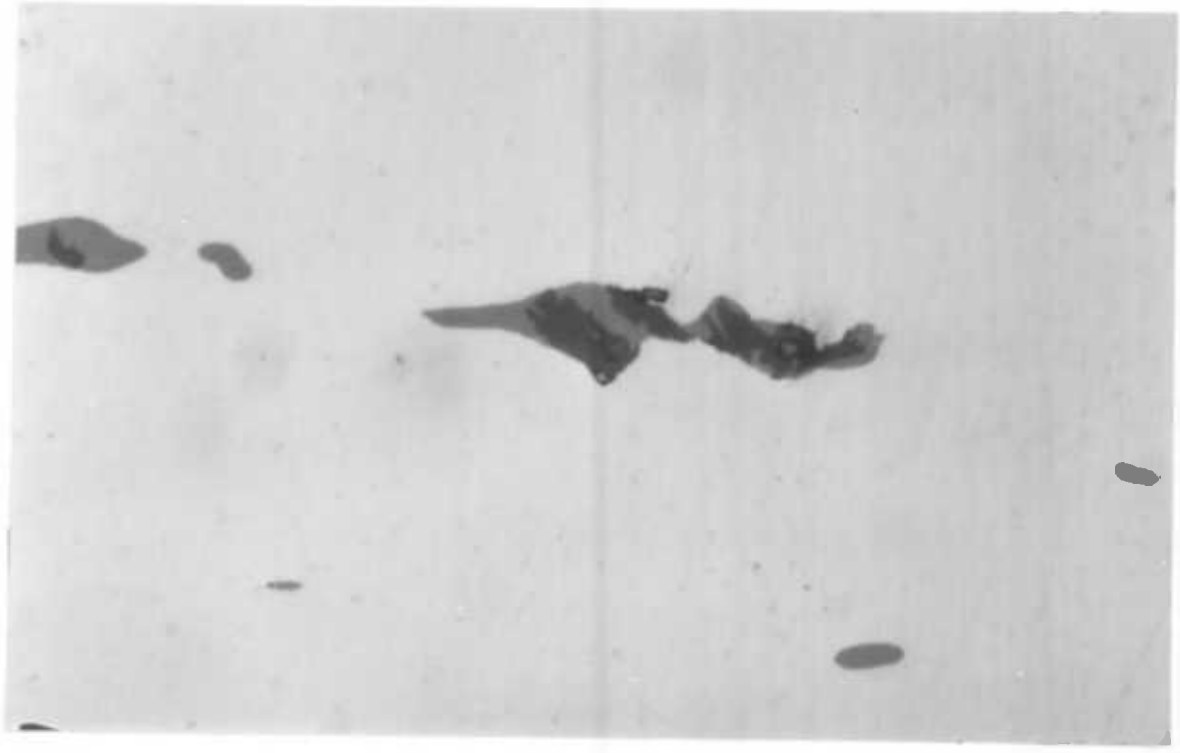

Photograph 4.12 ×200 (×4.4)

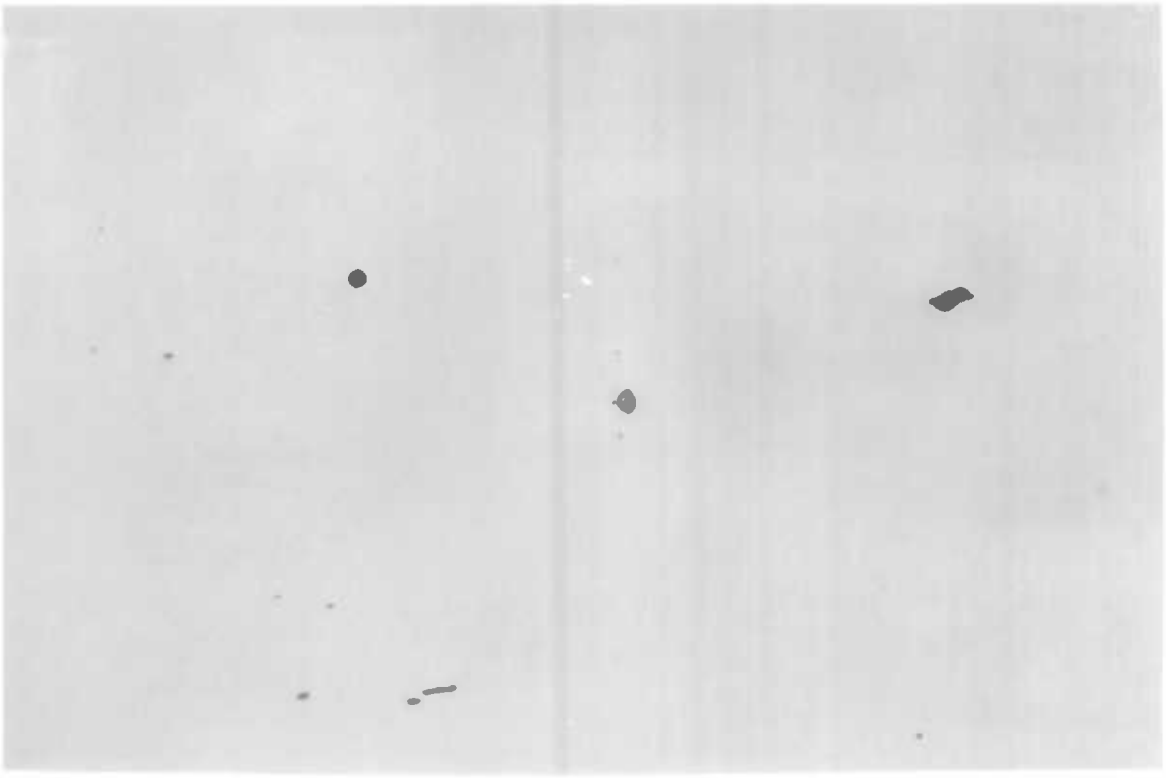

Photograph 4.13 ×50 (×4.4)

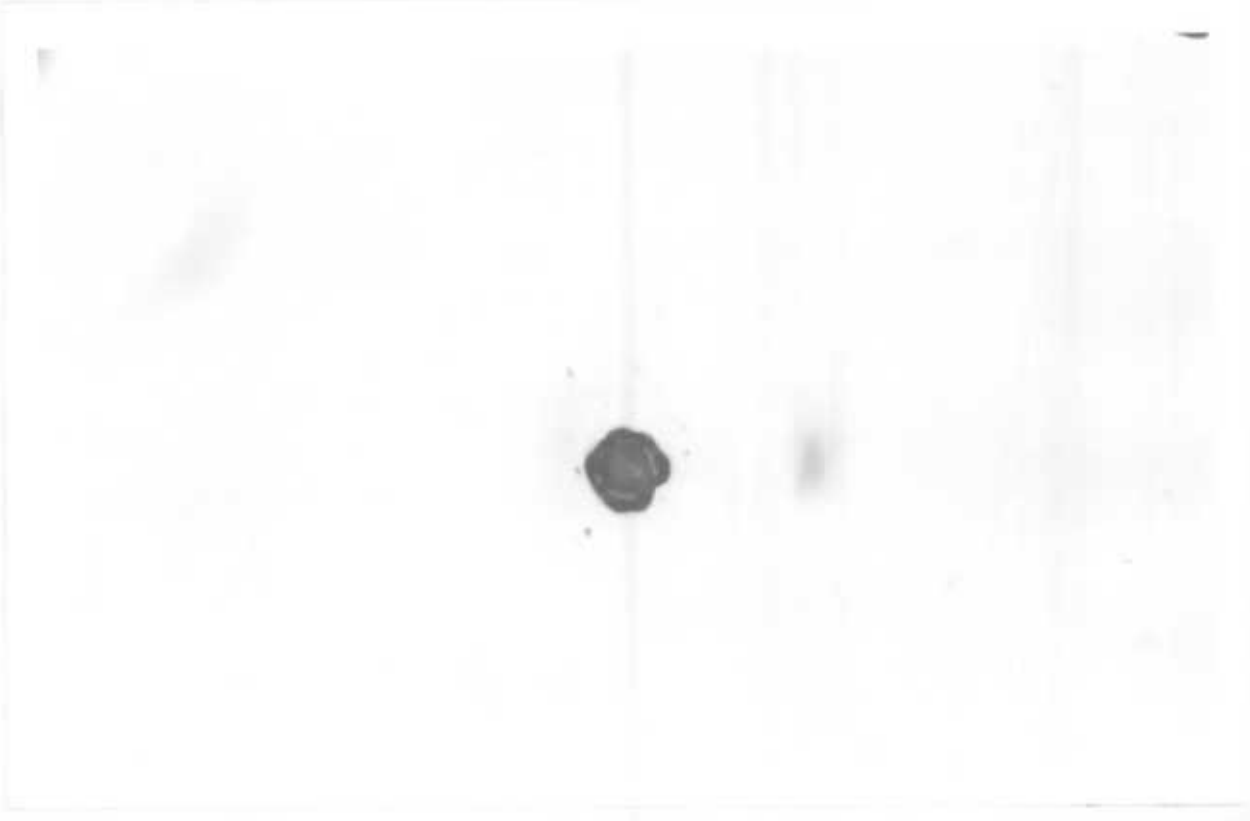

Photograph 4.14 ×200 (×4.4)

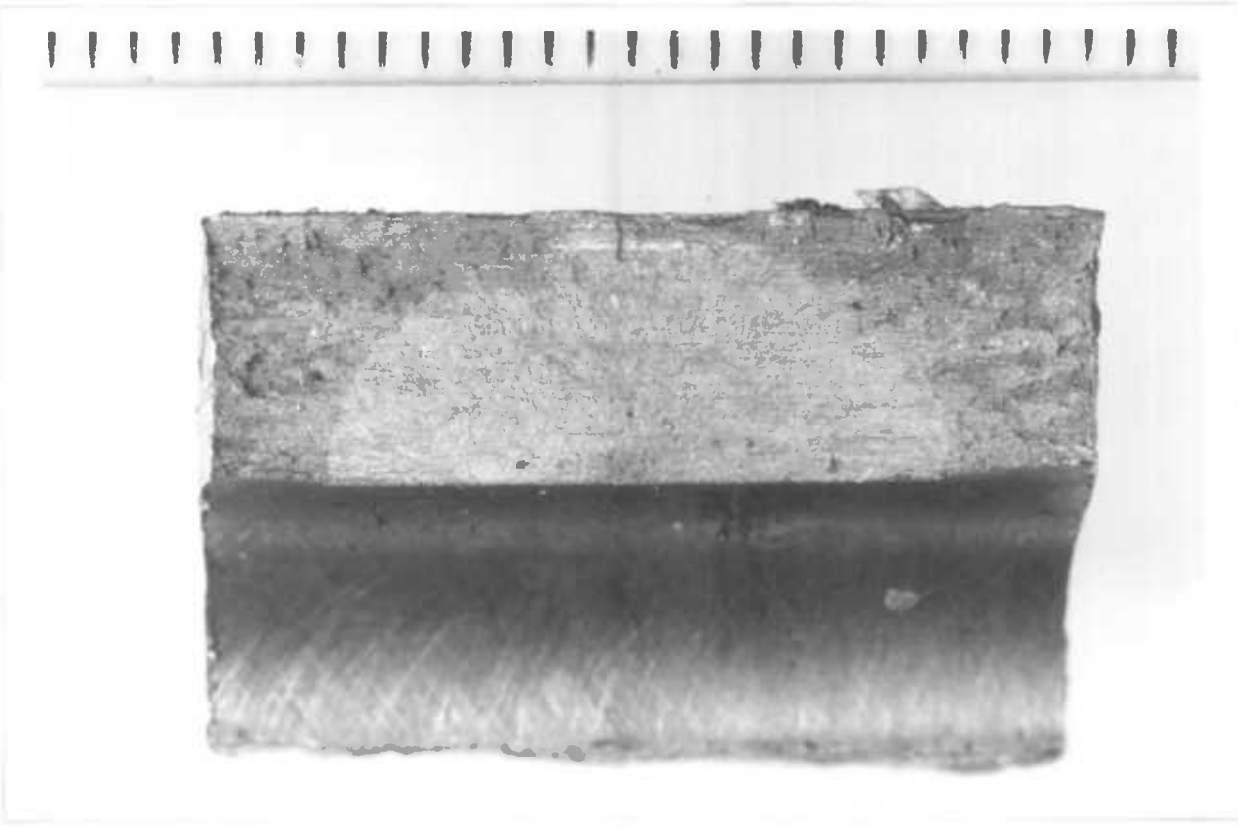

Photograph 5.1a

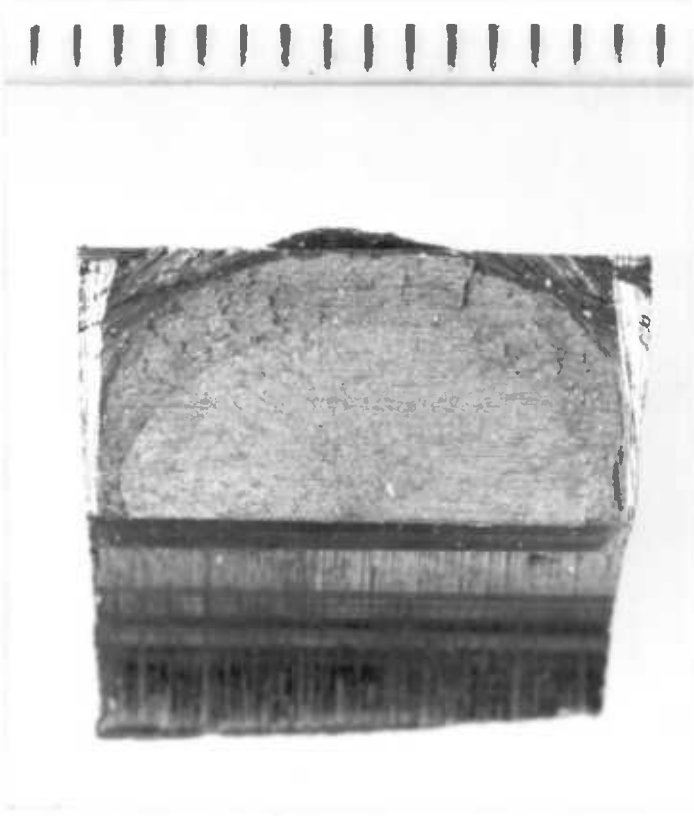

Photograph 5.1b

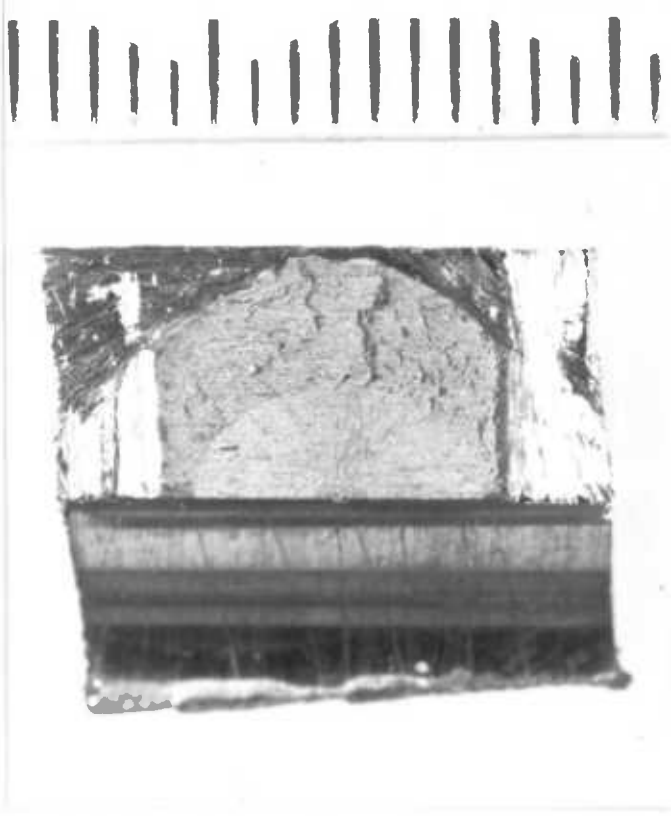

Photograph 5.1c

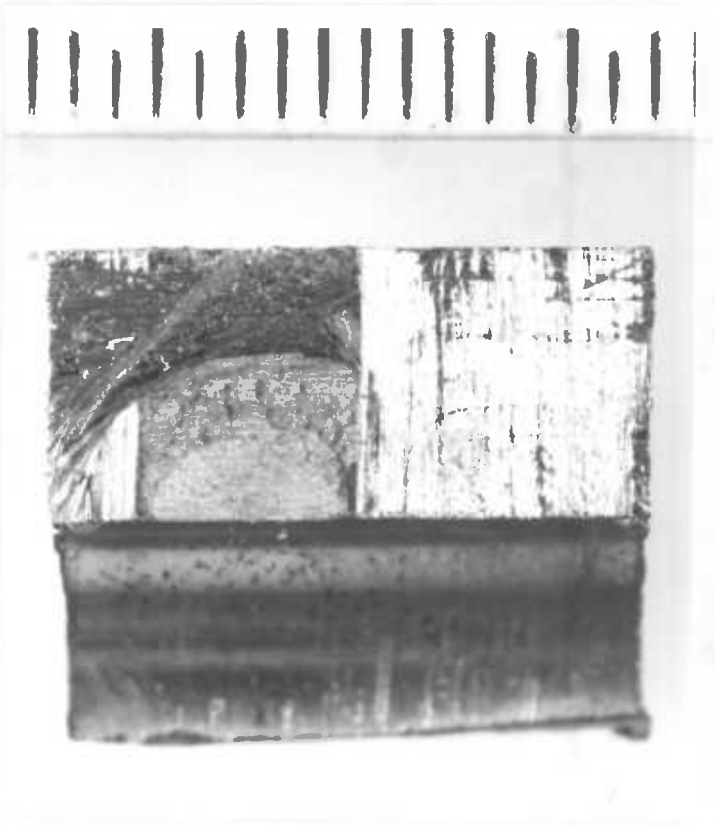

Photograph 5.1d

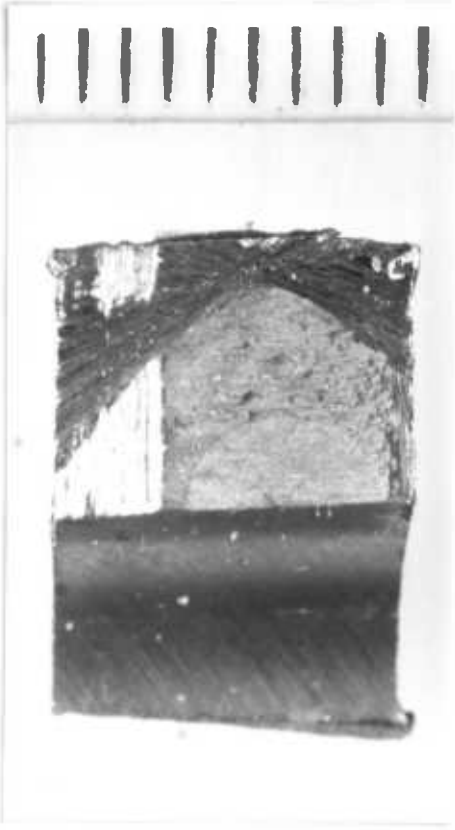

Photograph 5.1e

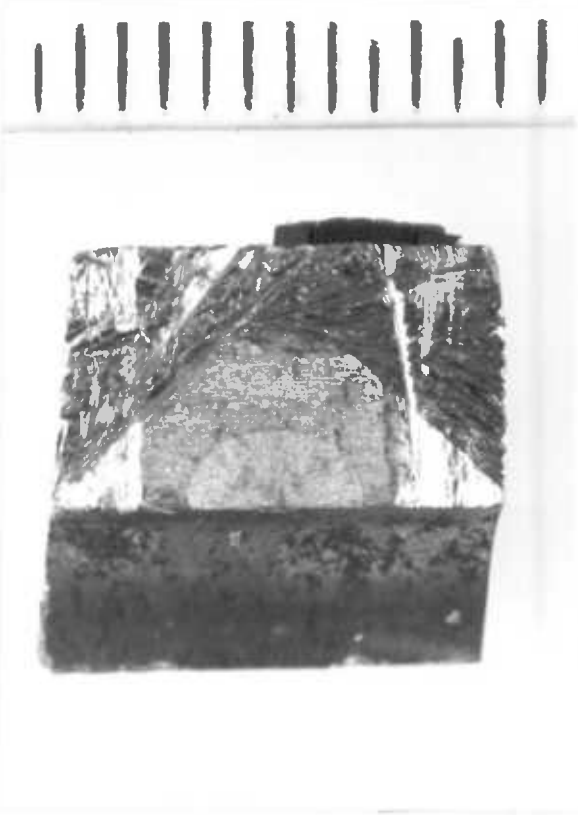

Photograph 5.1f

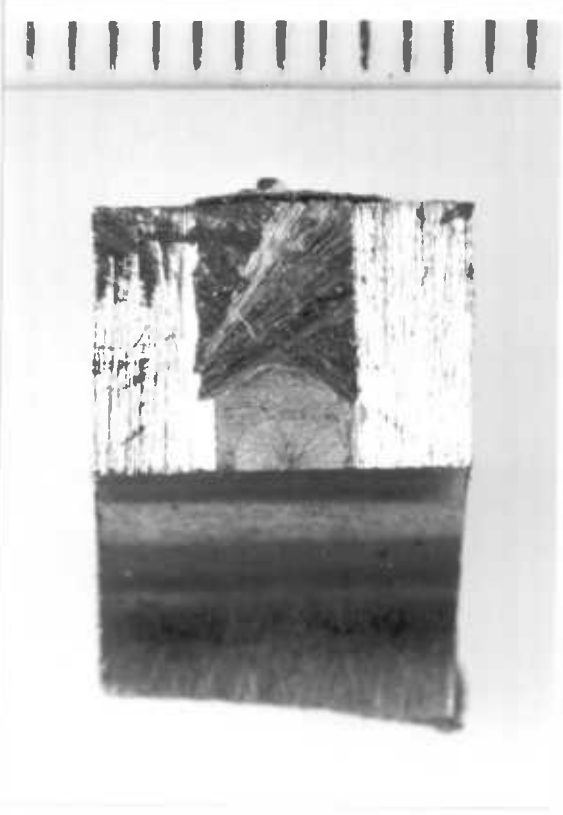

Photograph 5.1g

Photograph 5.1h

Photograph 5.1i

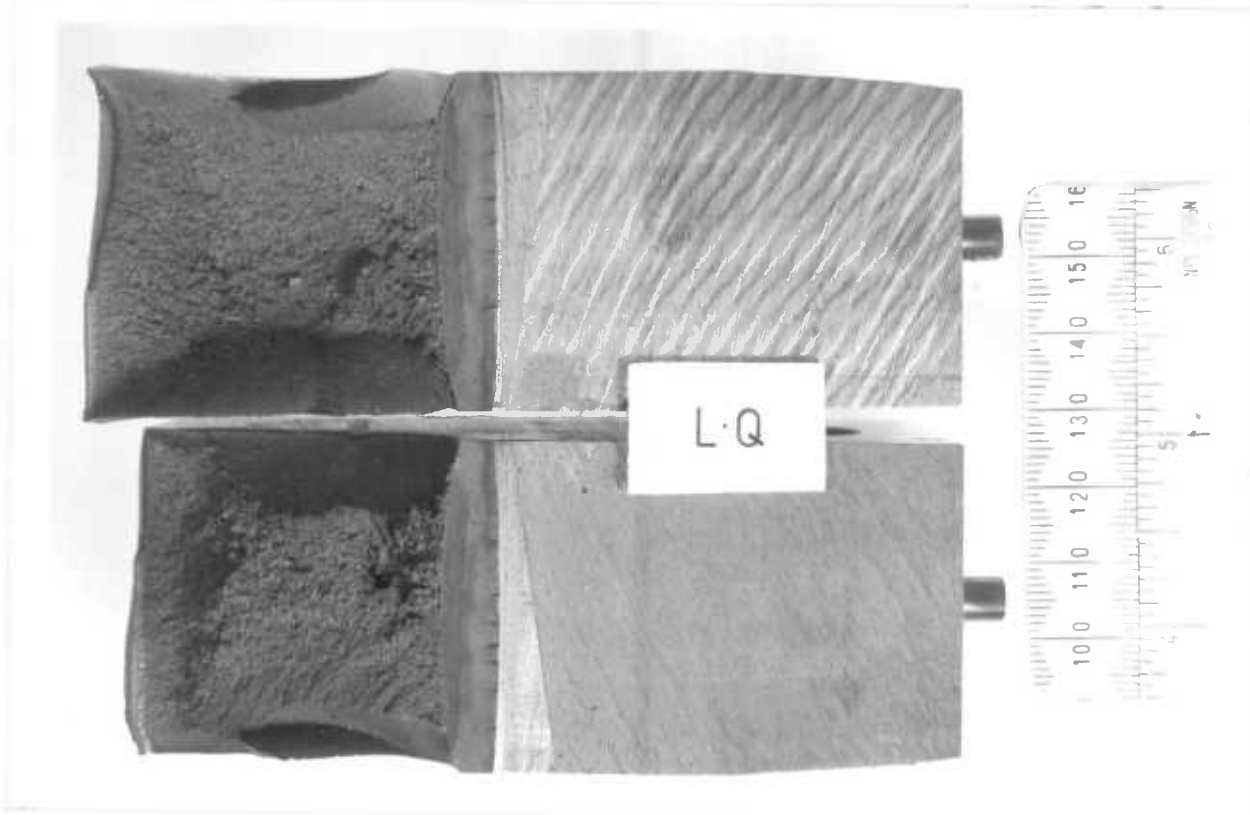

Photograph 5.2

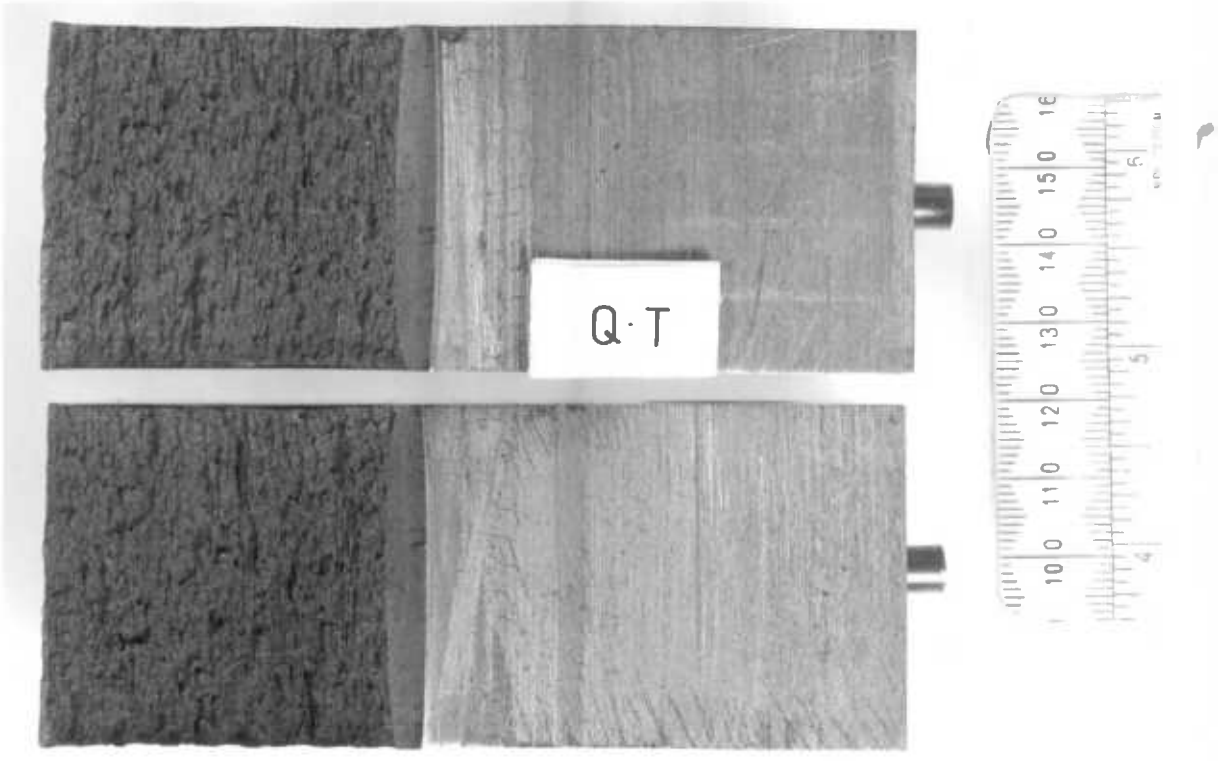

Photograph 5.3

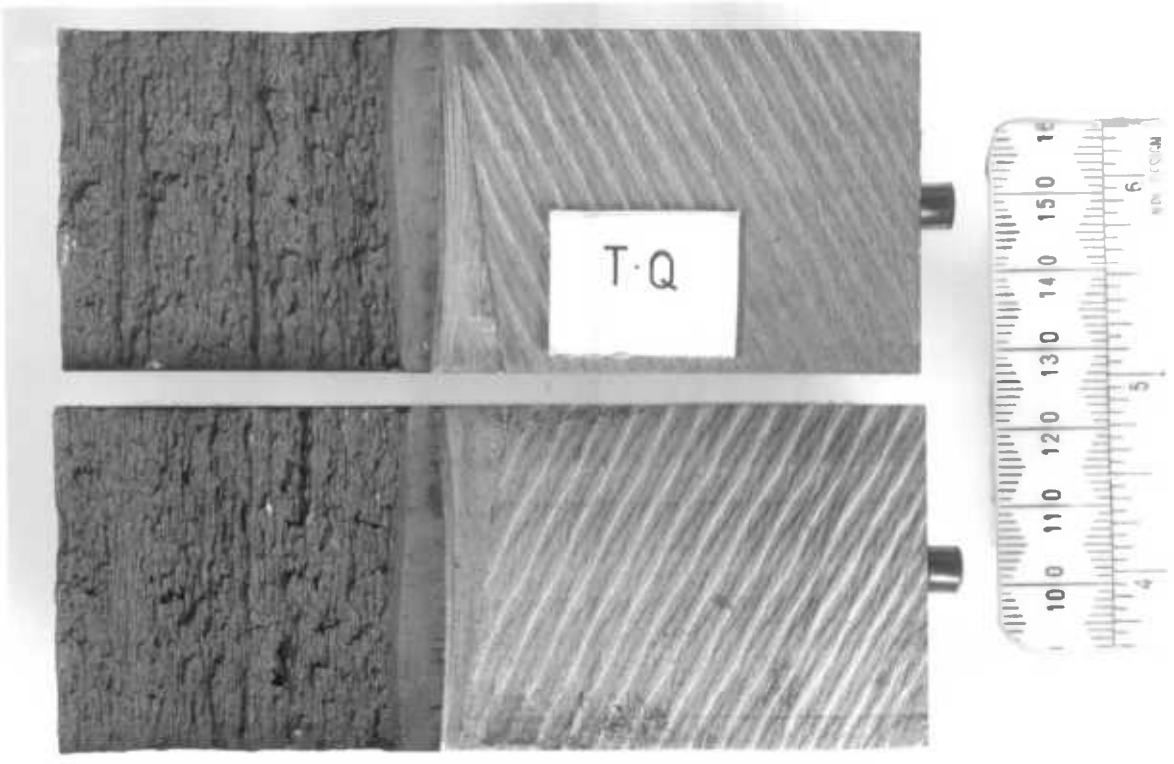

Photograph 5.4

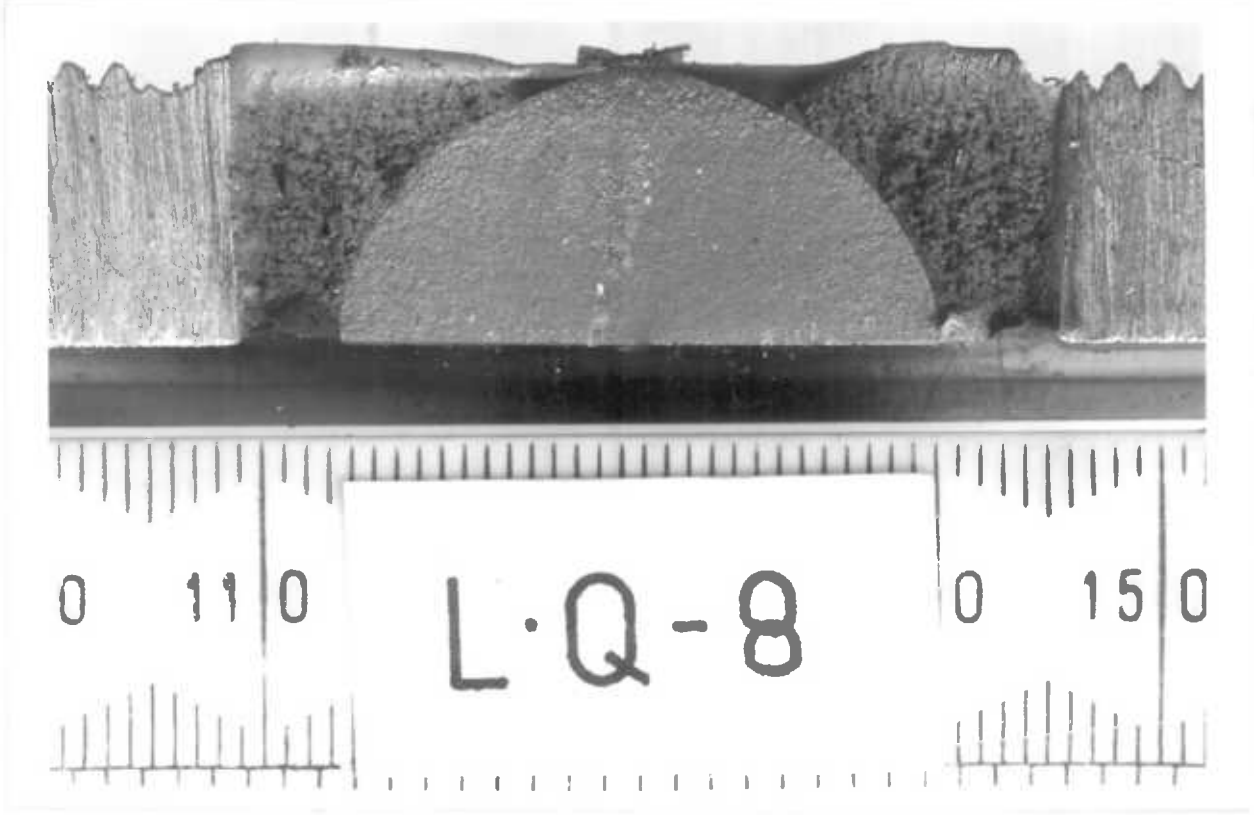

Photograph 5.5

Photograph 5.6

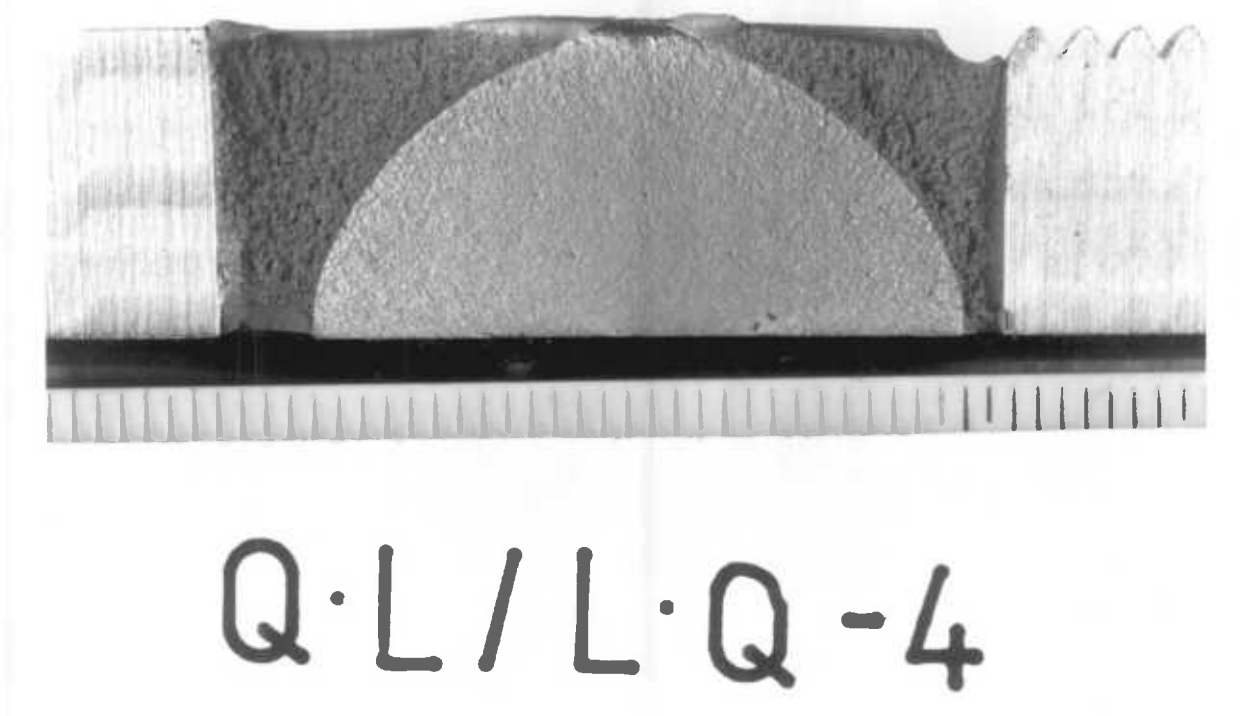

Photograph 5.7

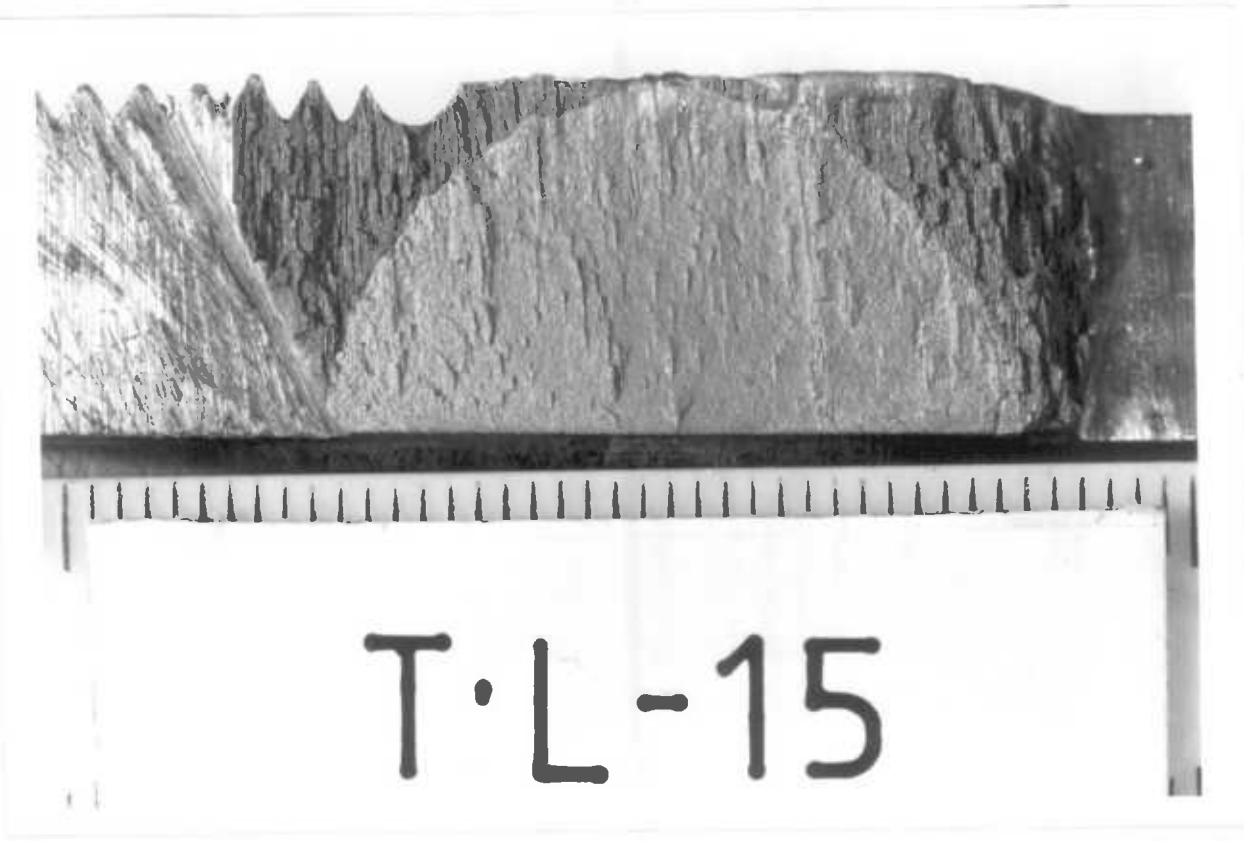

Photograph 5.8

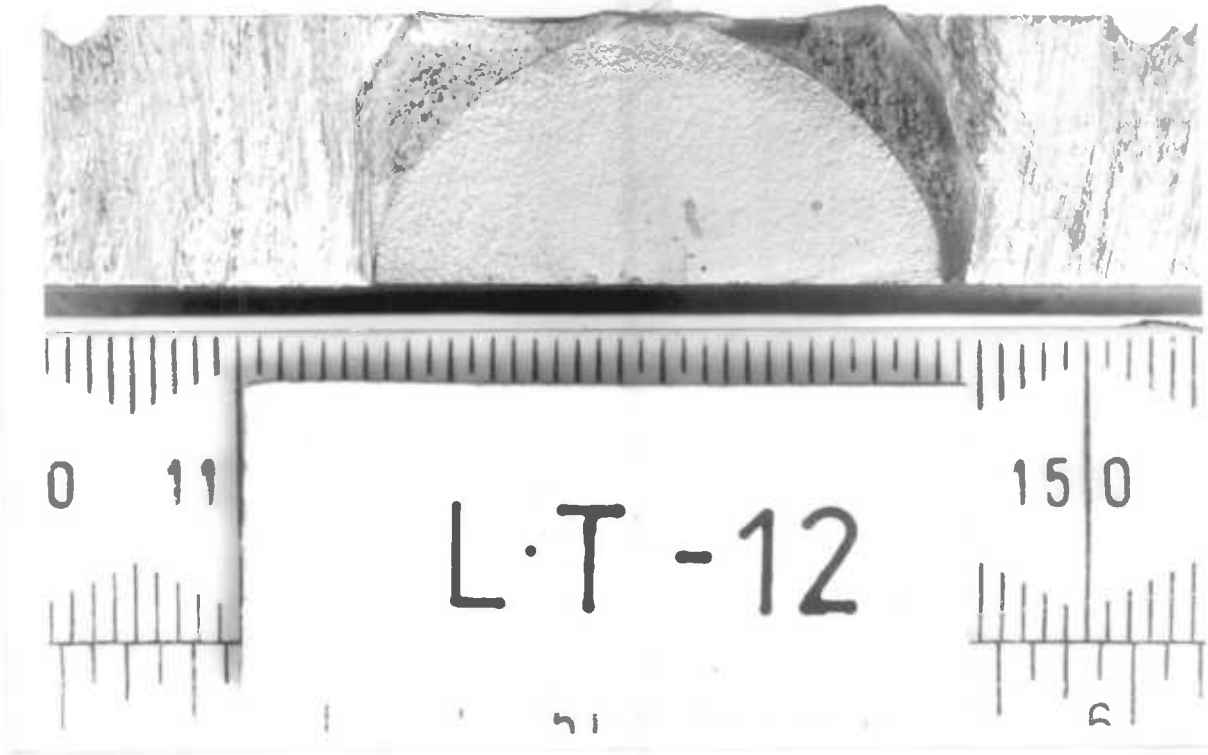

Photograph 5.9

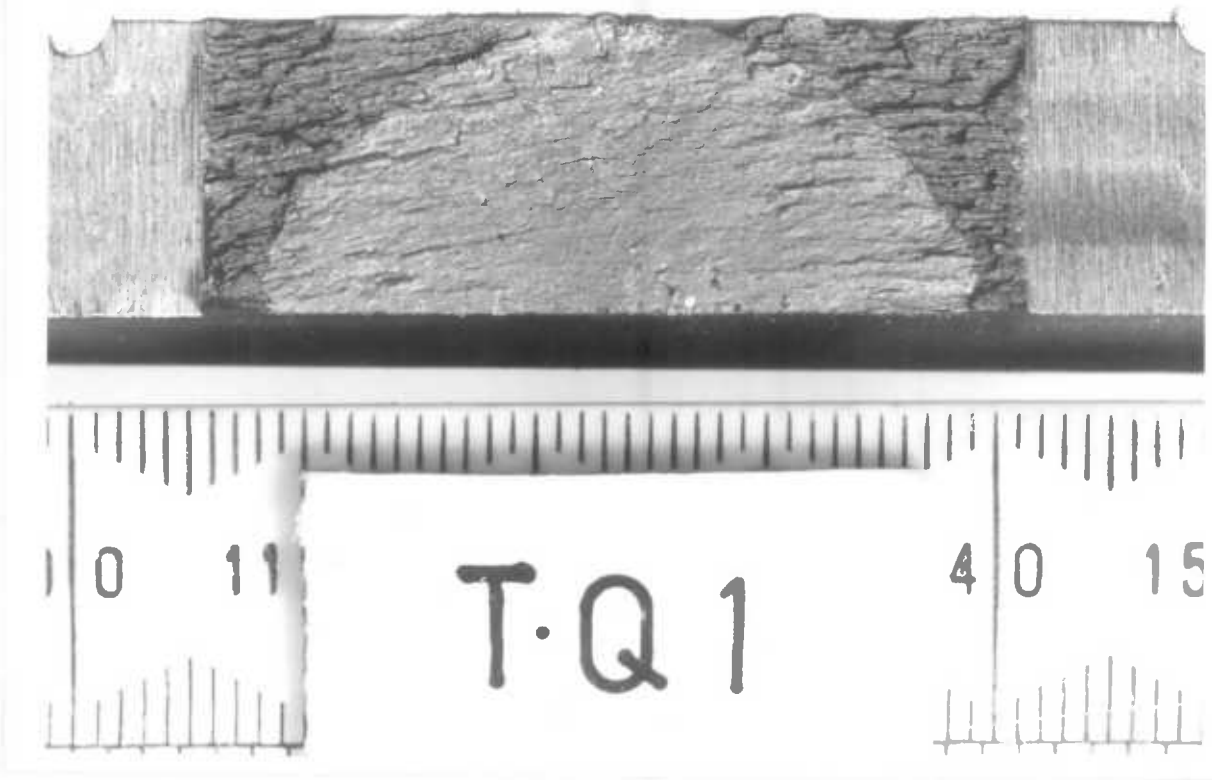

Photograph 5.10

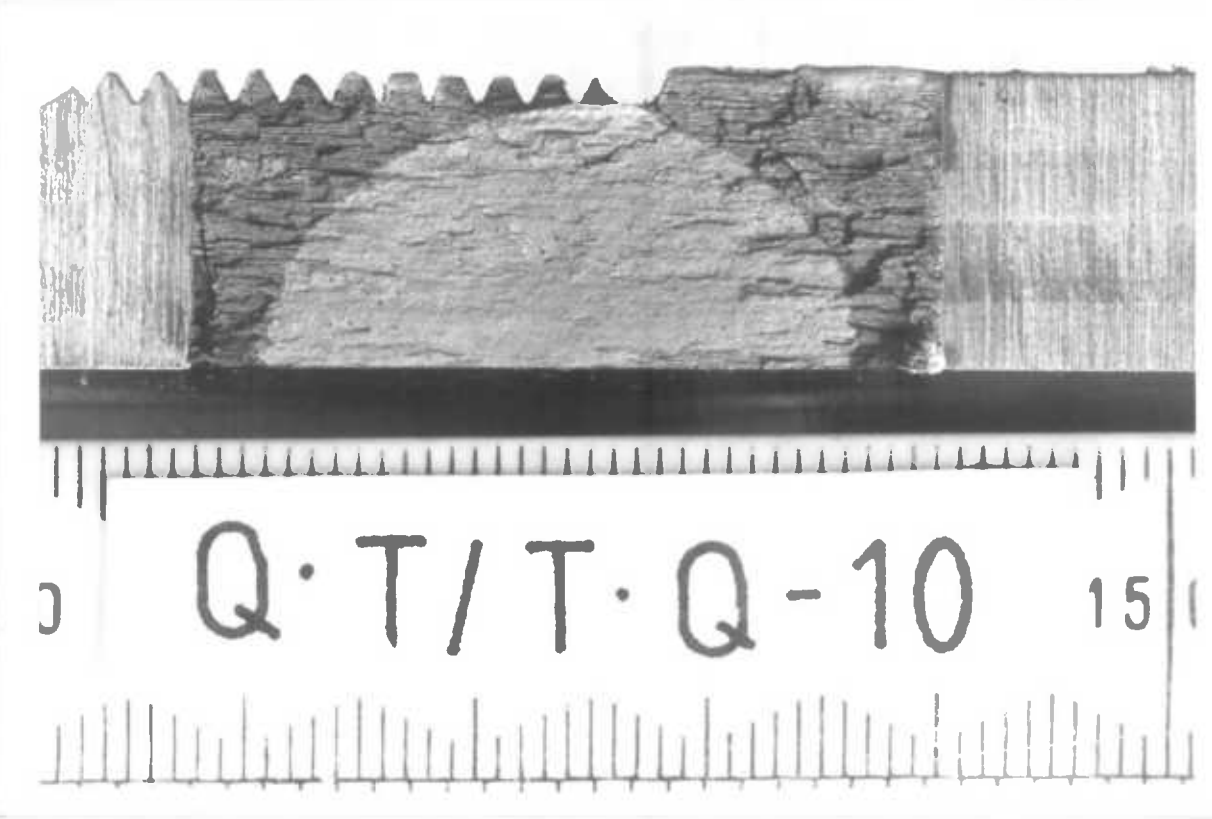

Photograph 5.11

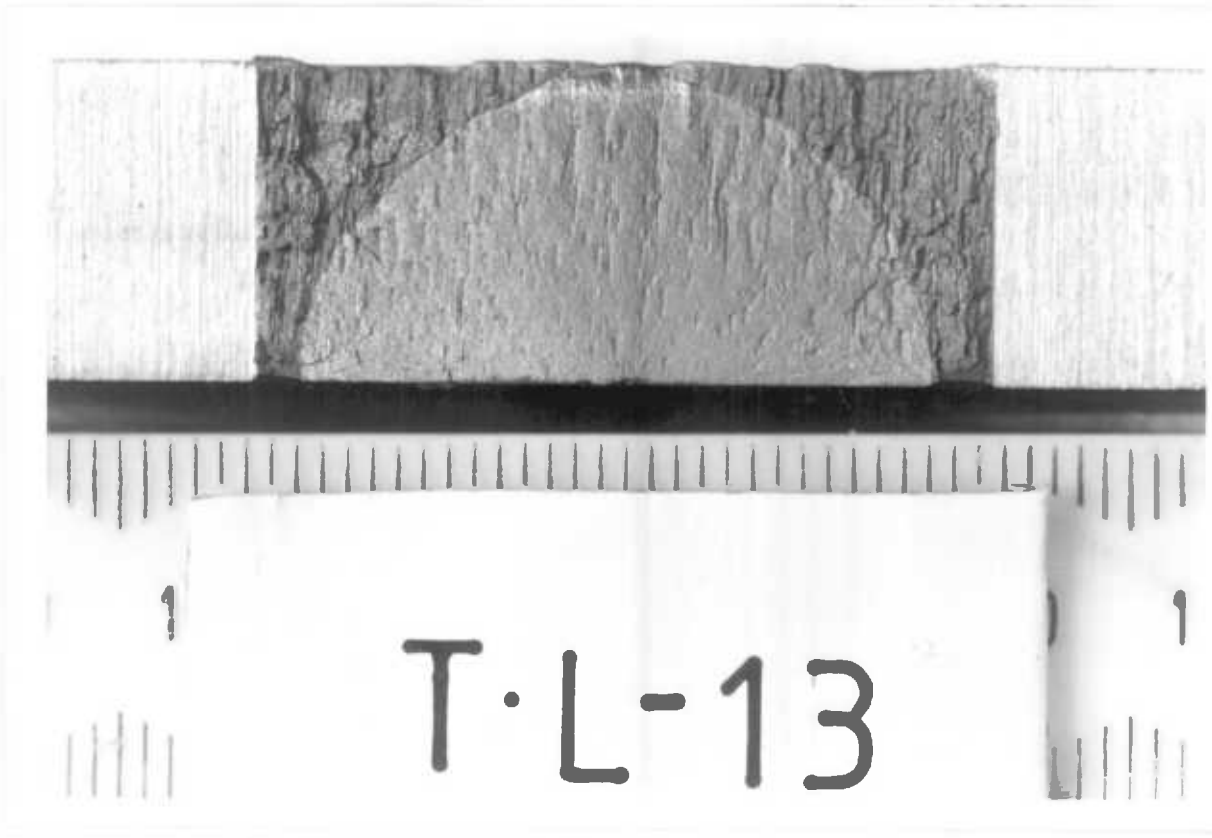

Photograph 5.12

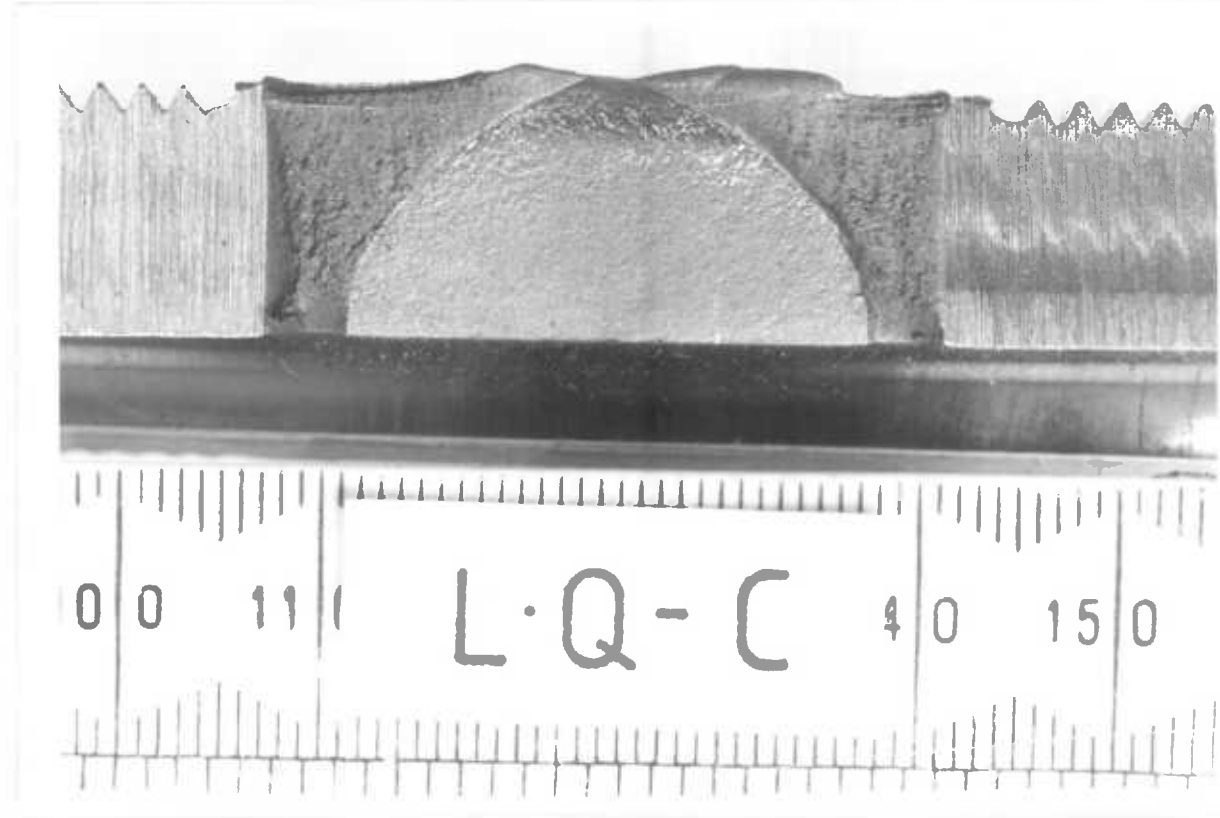

Photograph 5.13

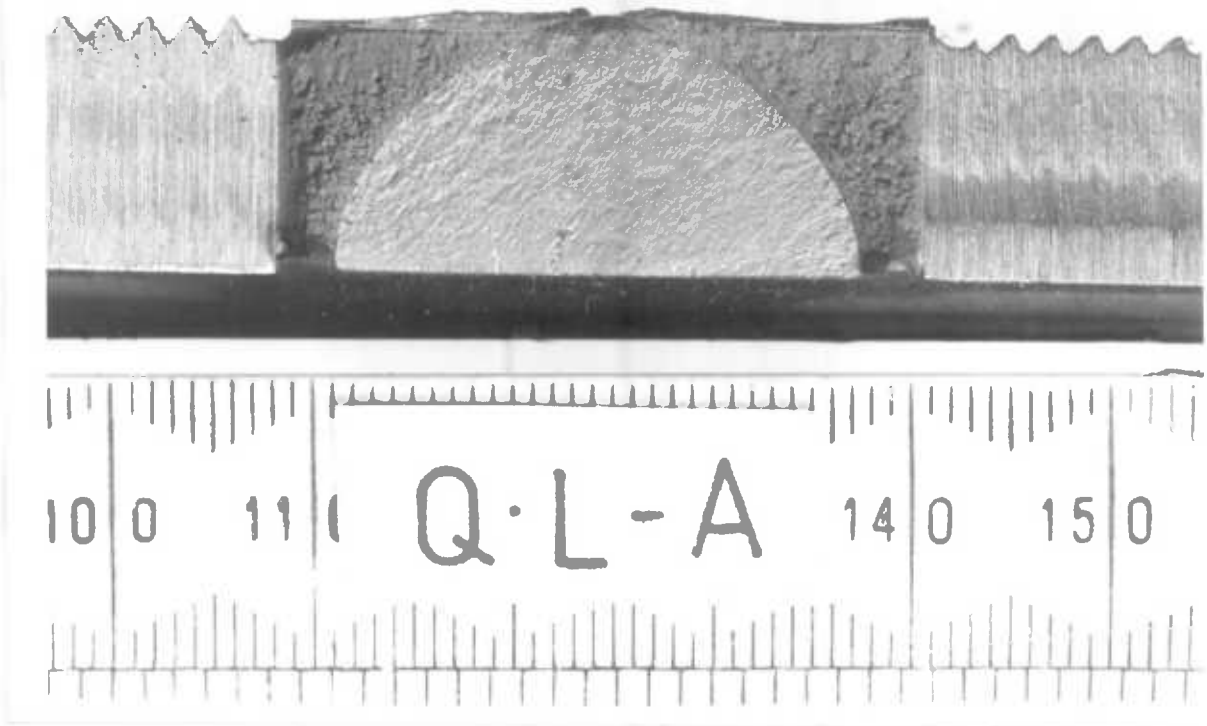

Photograph 5.14

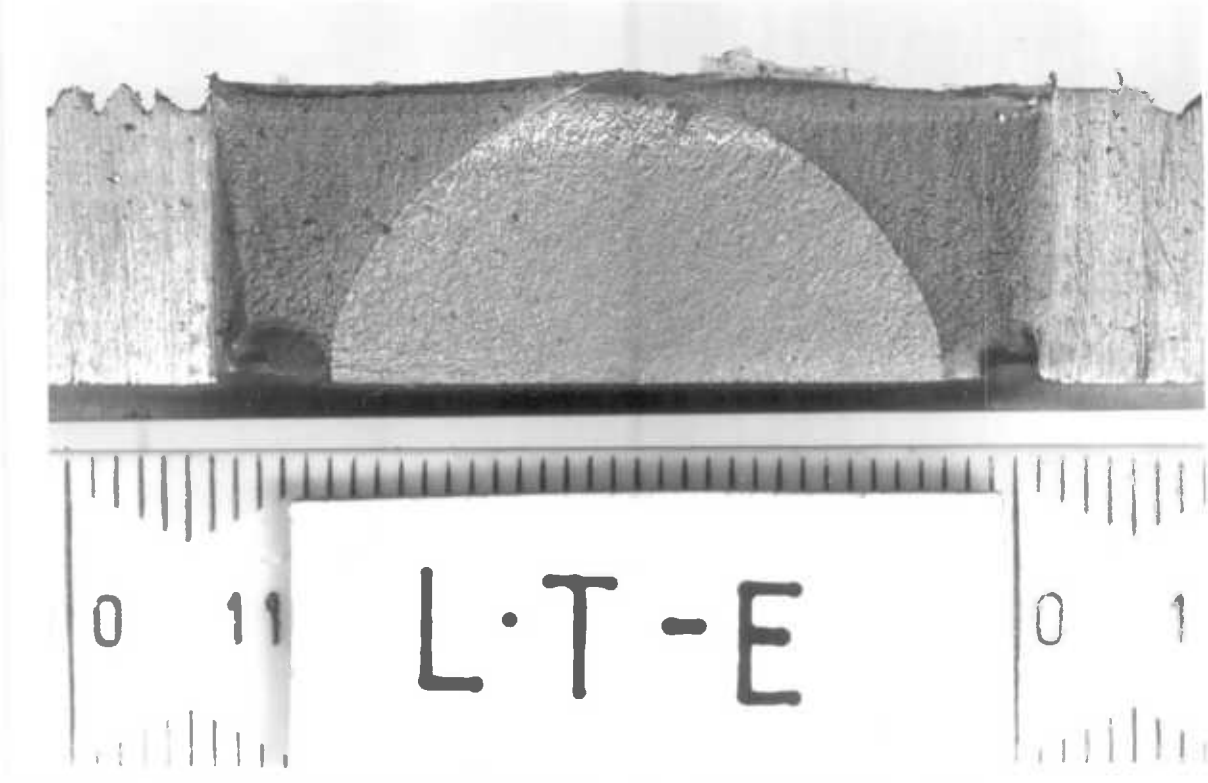

Photograph 5.15

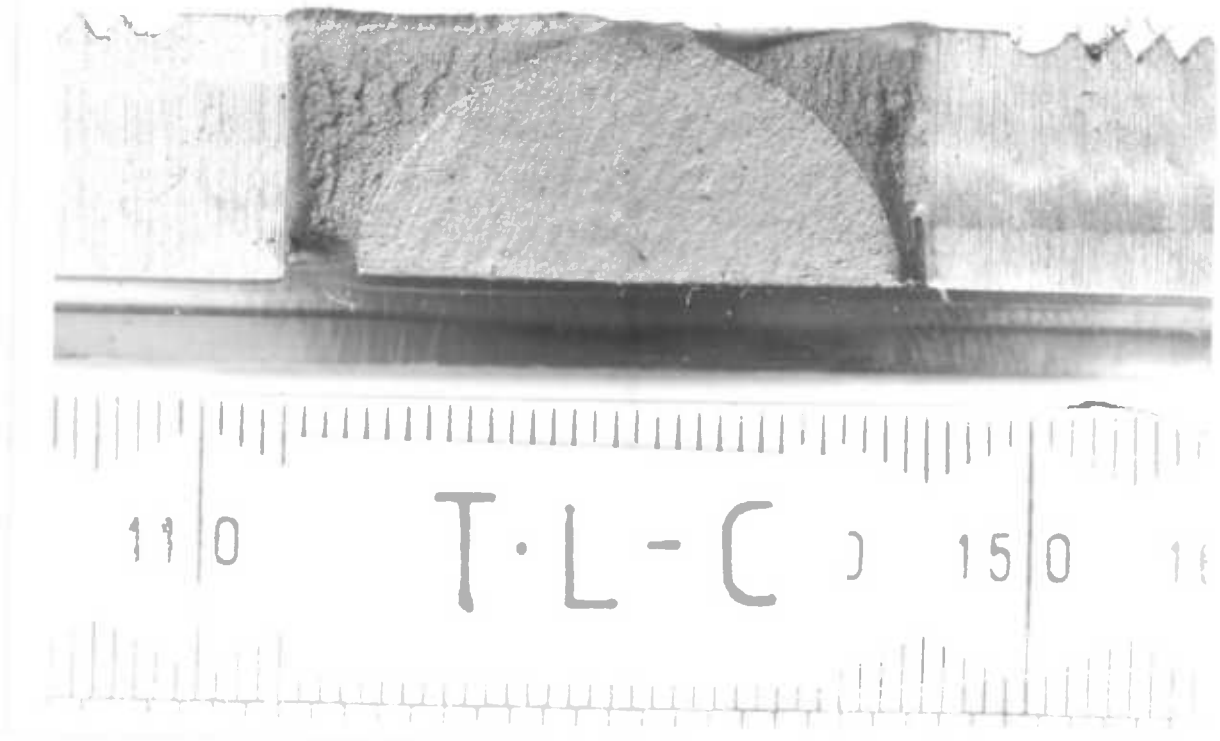

Photograph 5.16

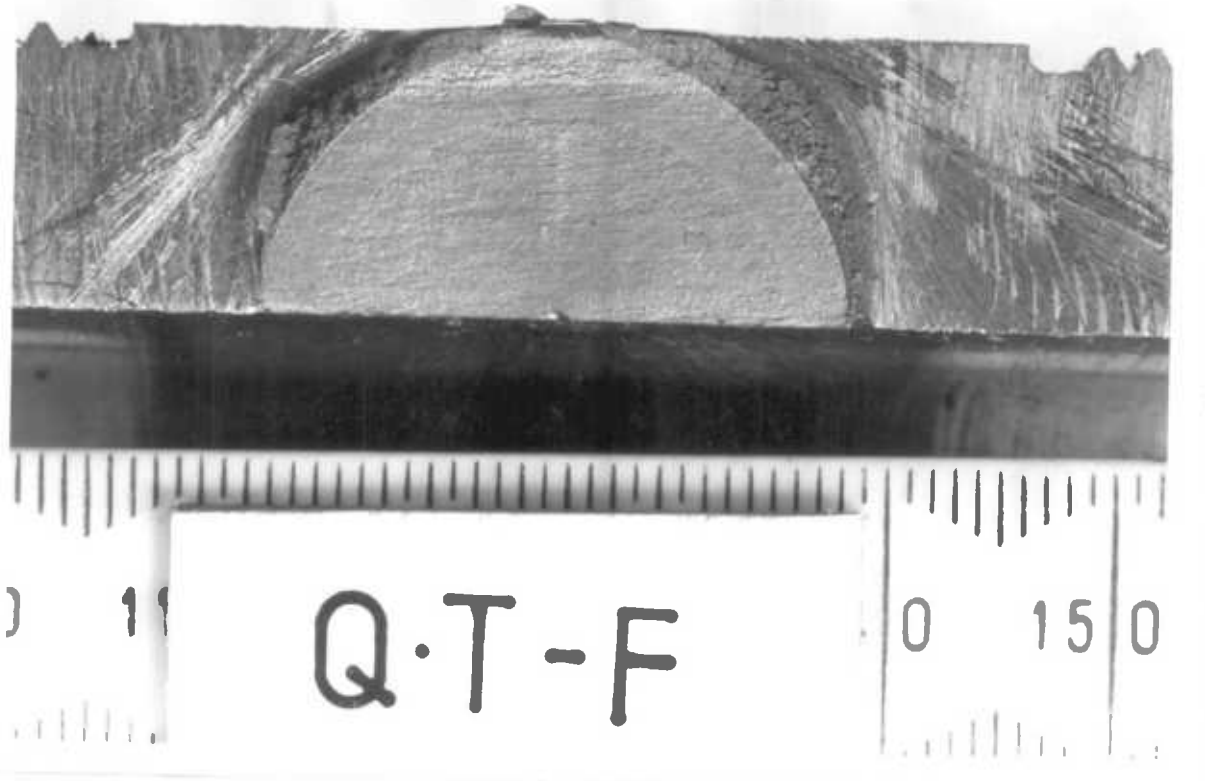

Photograph 5.17

Photograph 5.20

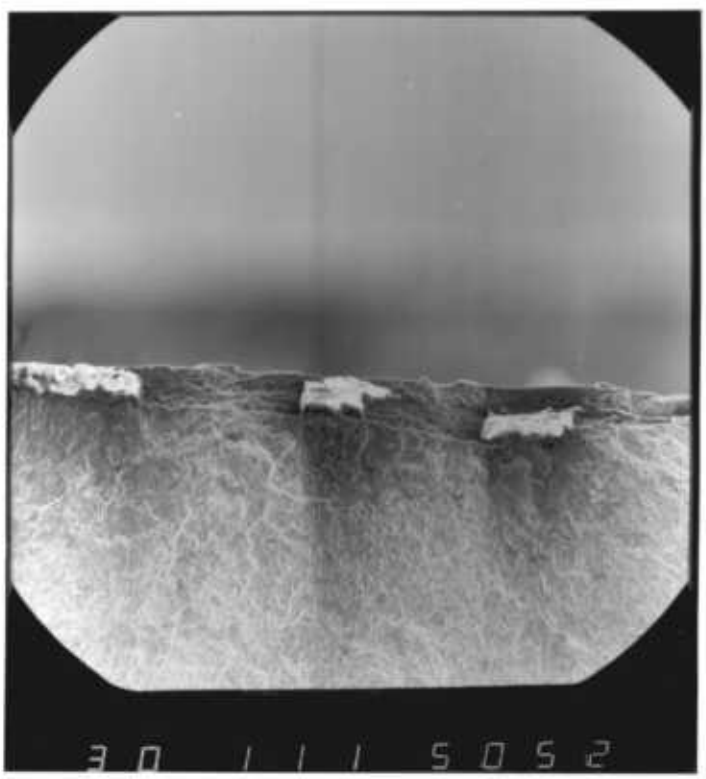

Photograph 5.21

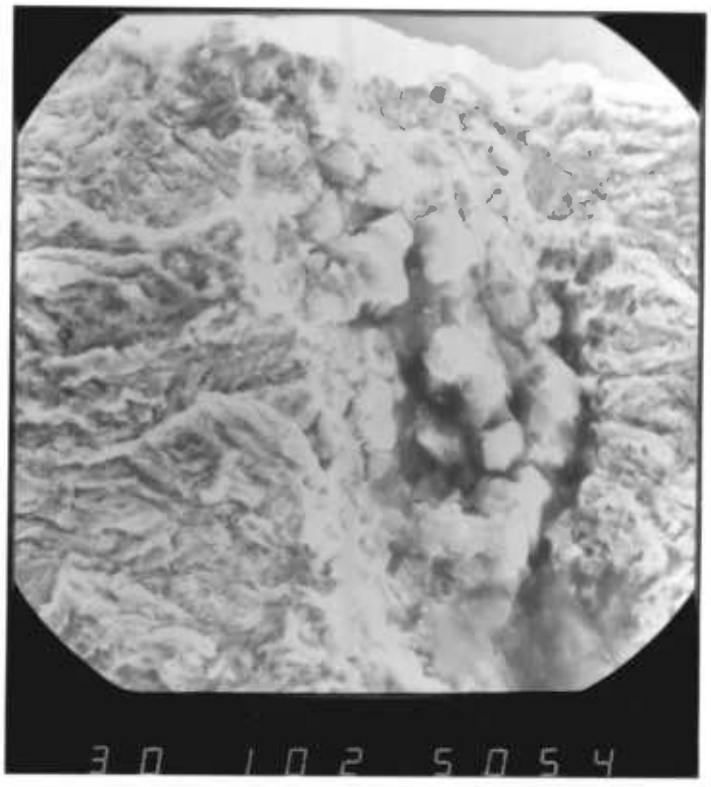

Photograph 5.22

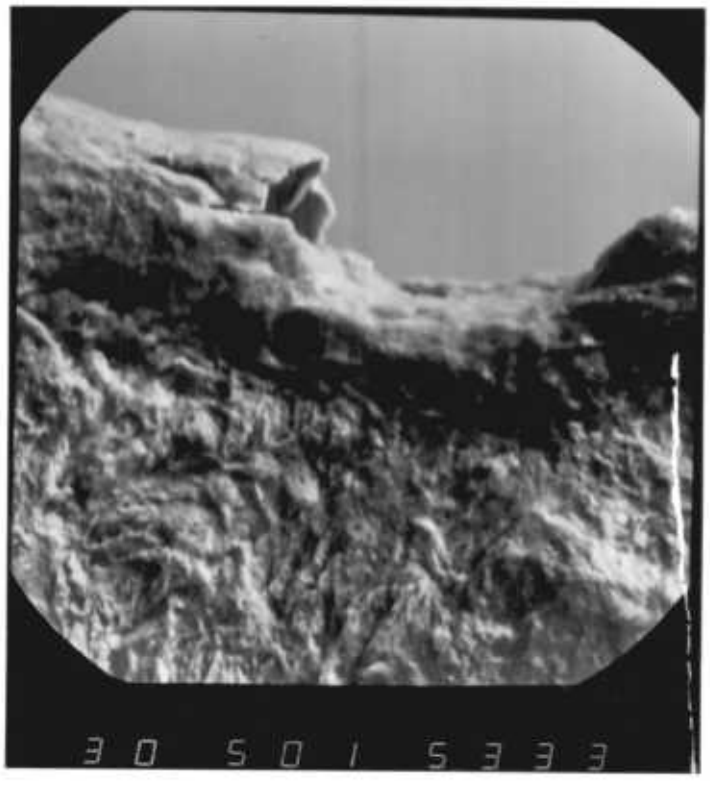

Photograph 5.23

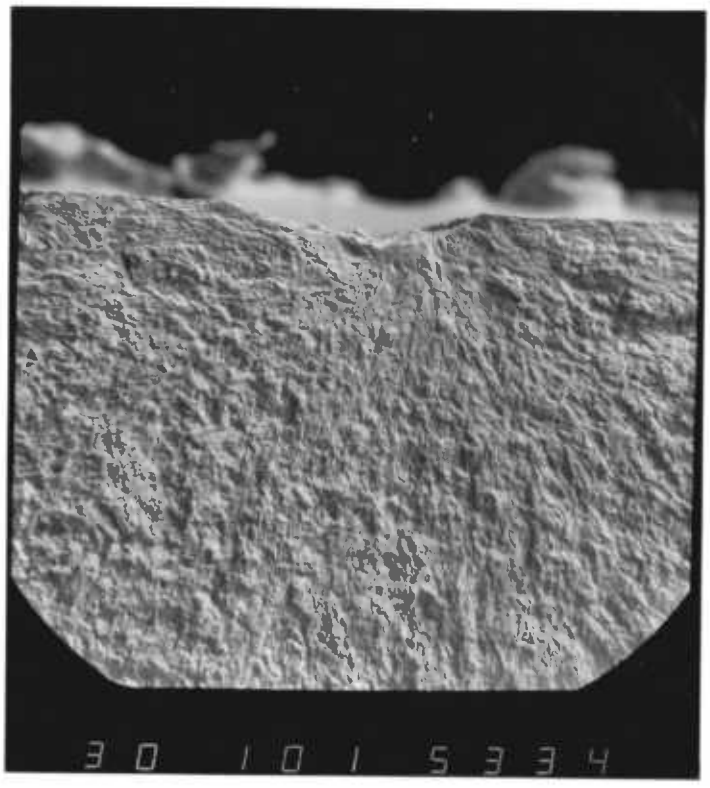

Photograph 5.24

Photograph 5.25

Photograph 5.26

Photograph 5.27

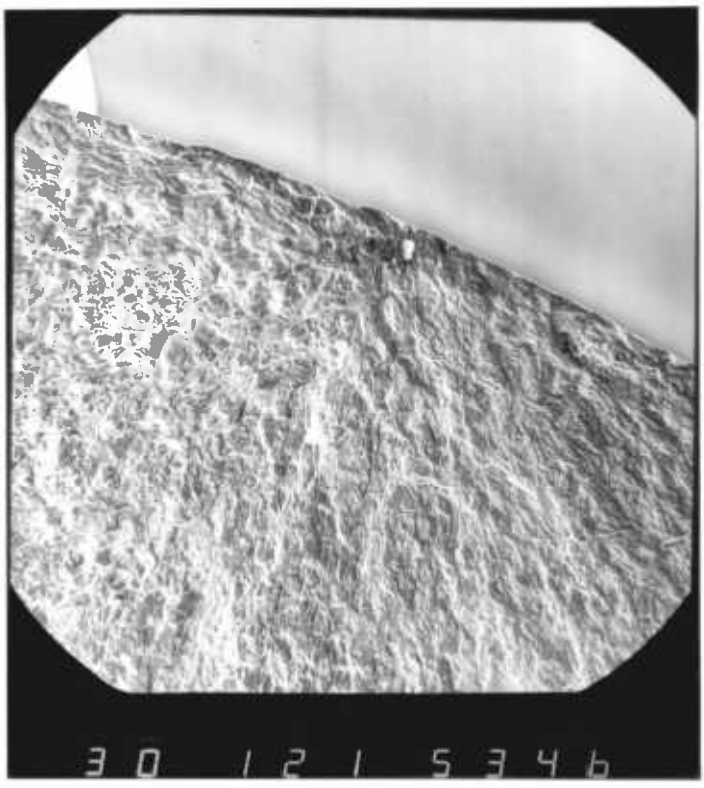

Photograph 5.28

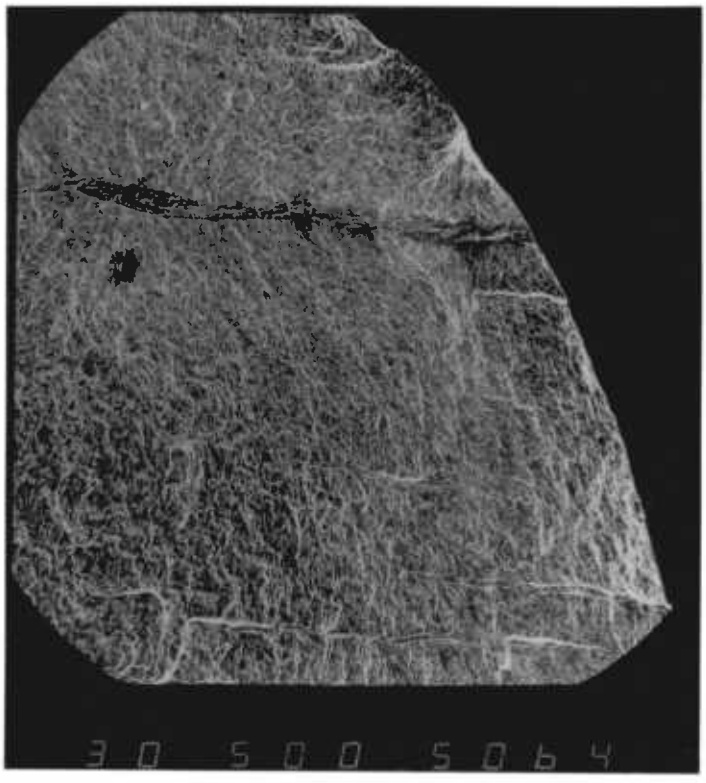

Photograph 5.29

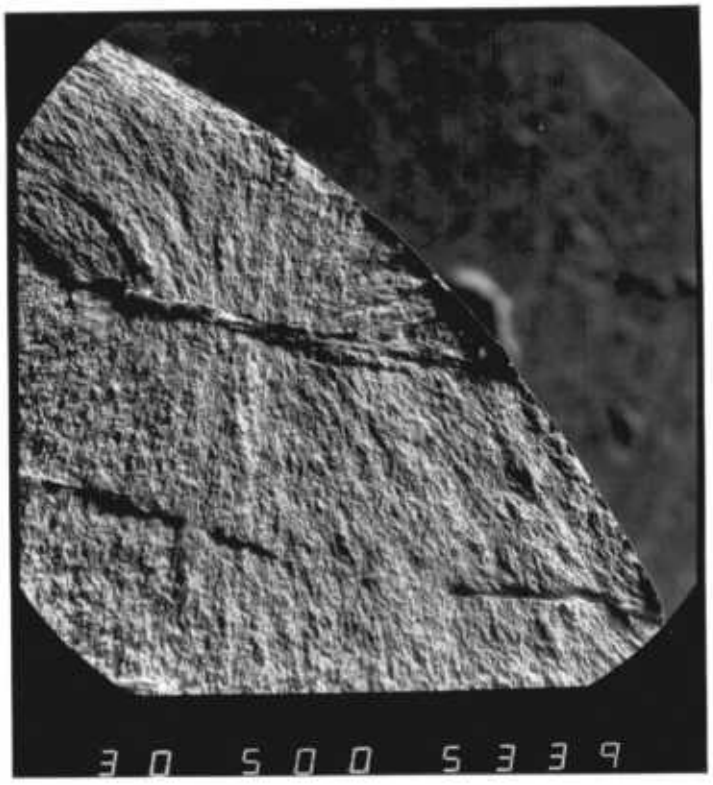

Photograph 5.30

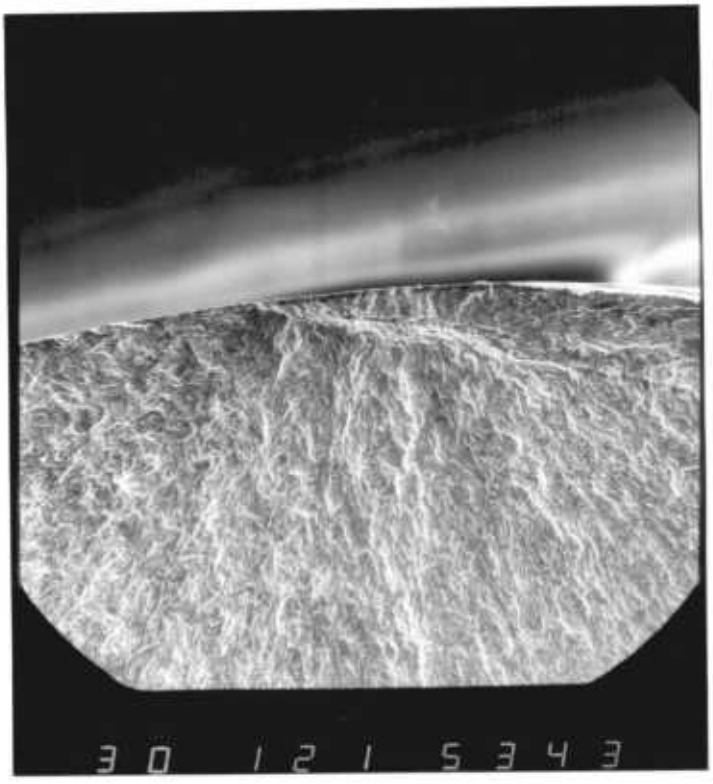

Photograph 5.31

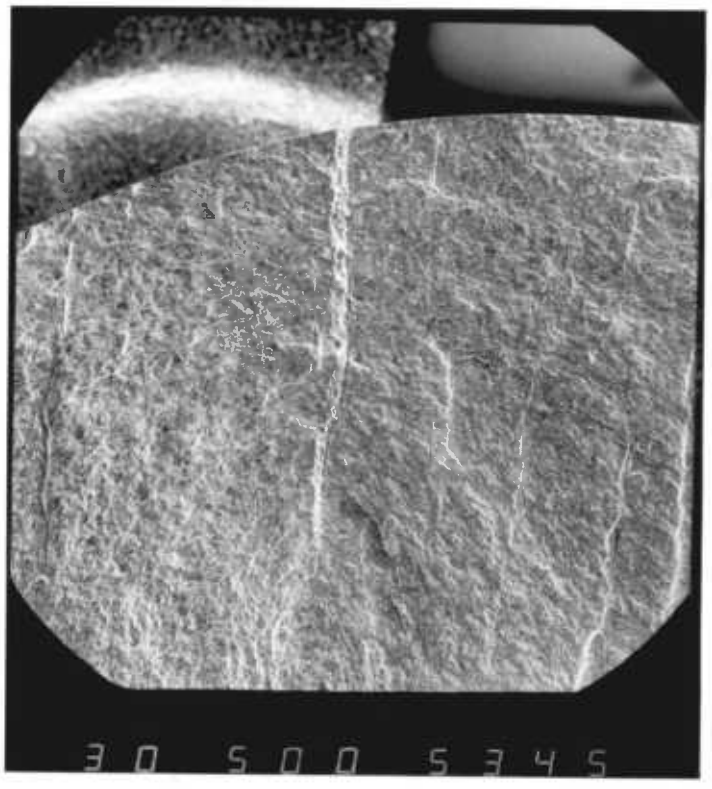

Photograph 5.32

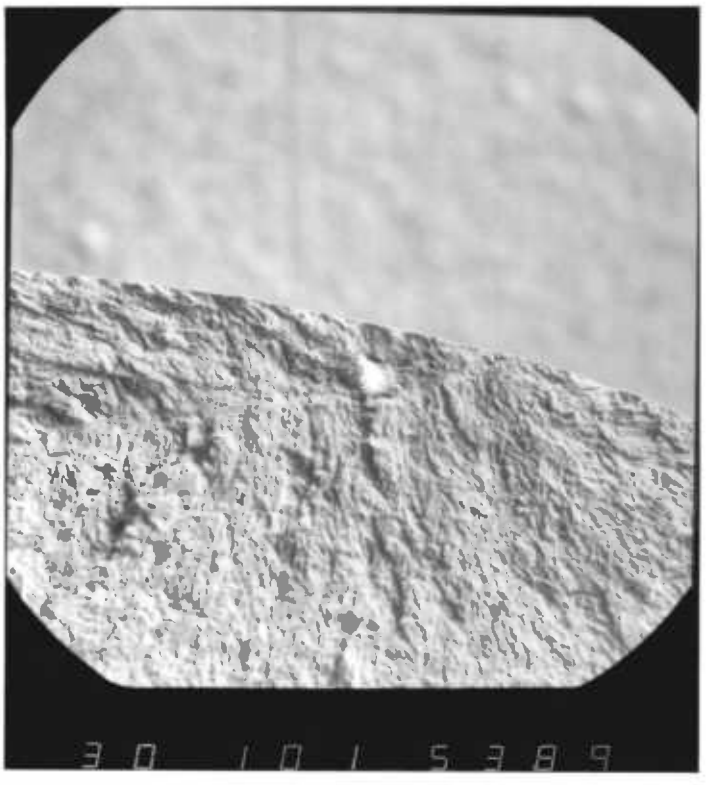

Photograph 5.33

Photograph 5.34

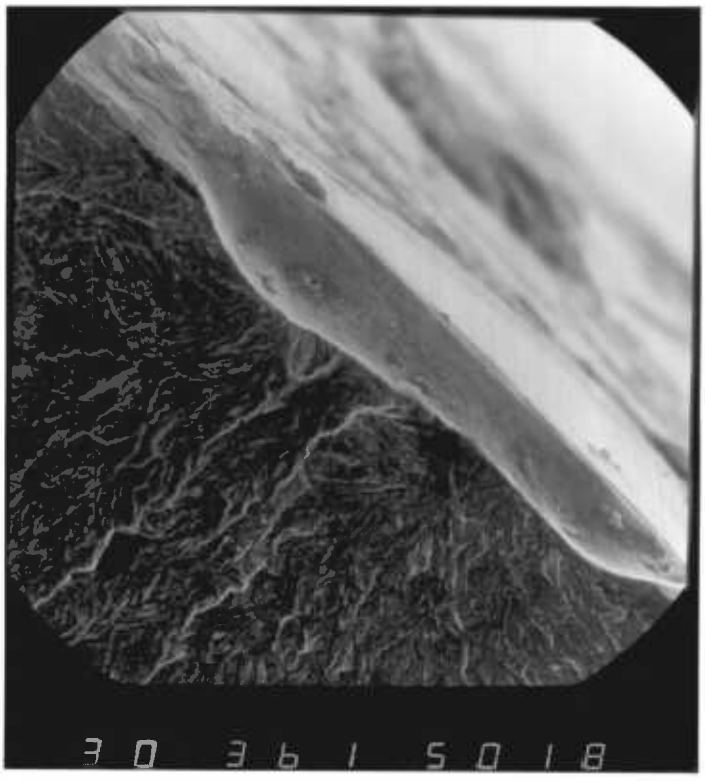

Photograph 5.37

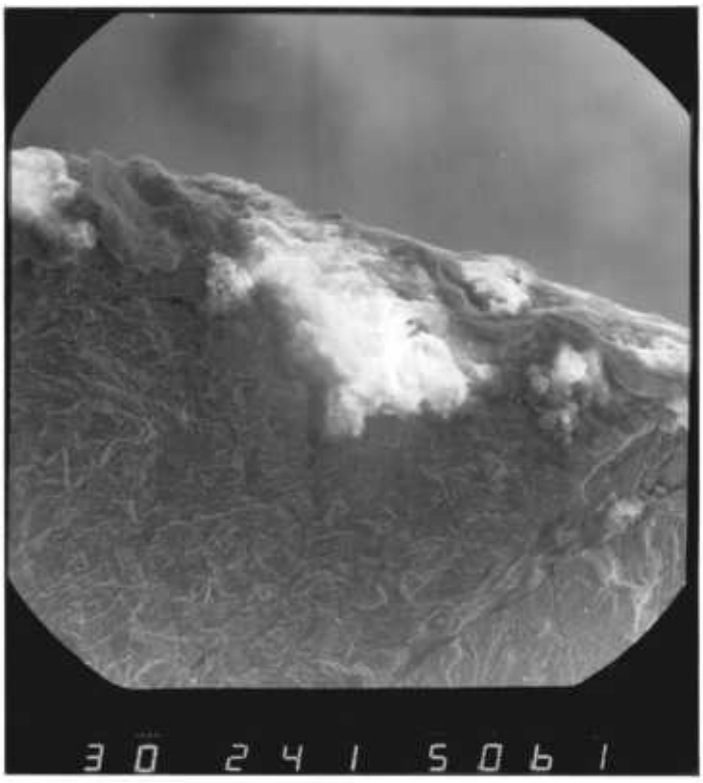

Photograph 5.35

Photograph 5.36

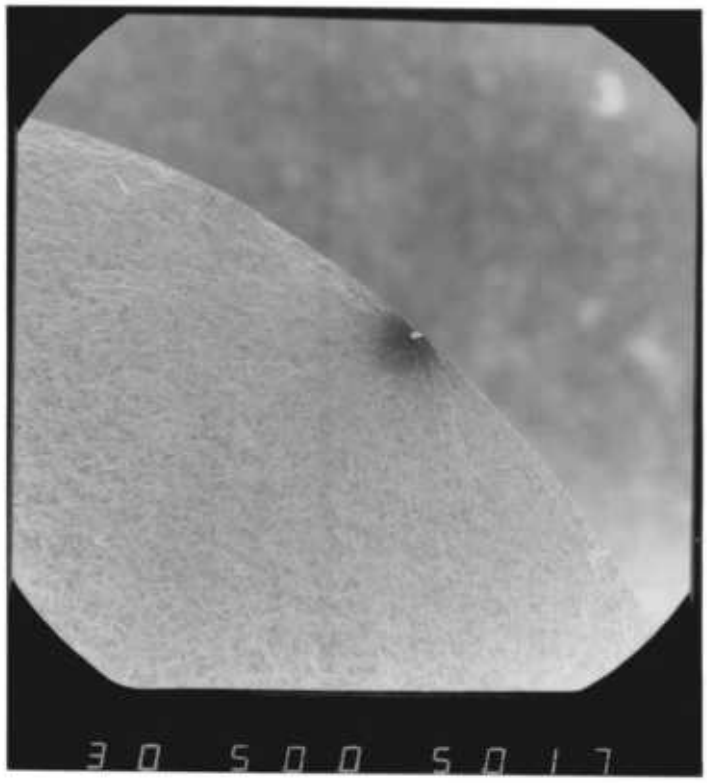

Photograph 5.38

Photograph 5.39

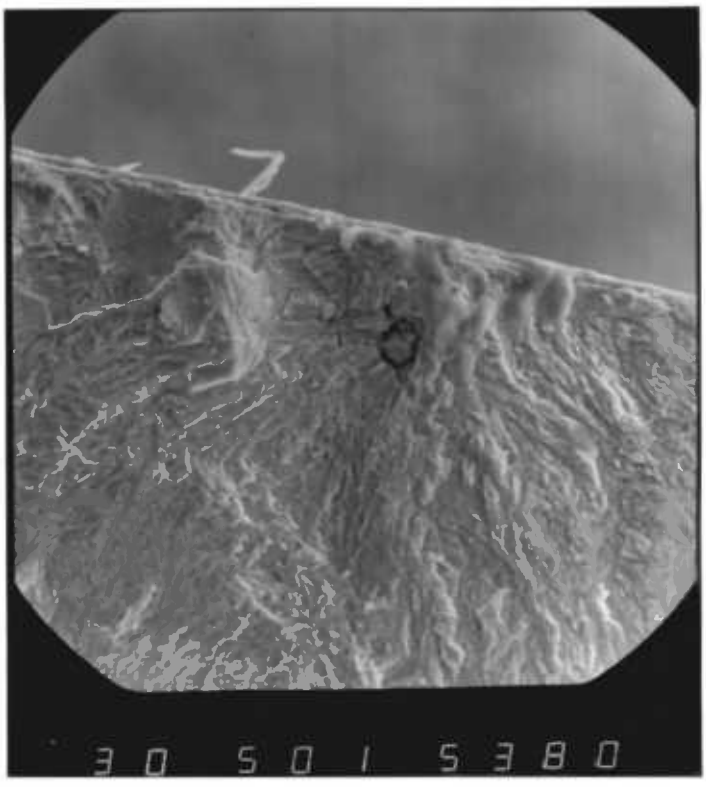

Photograph 5.40

Photograph 5.41

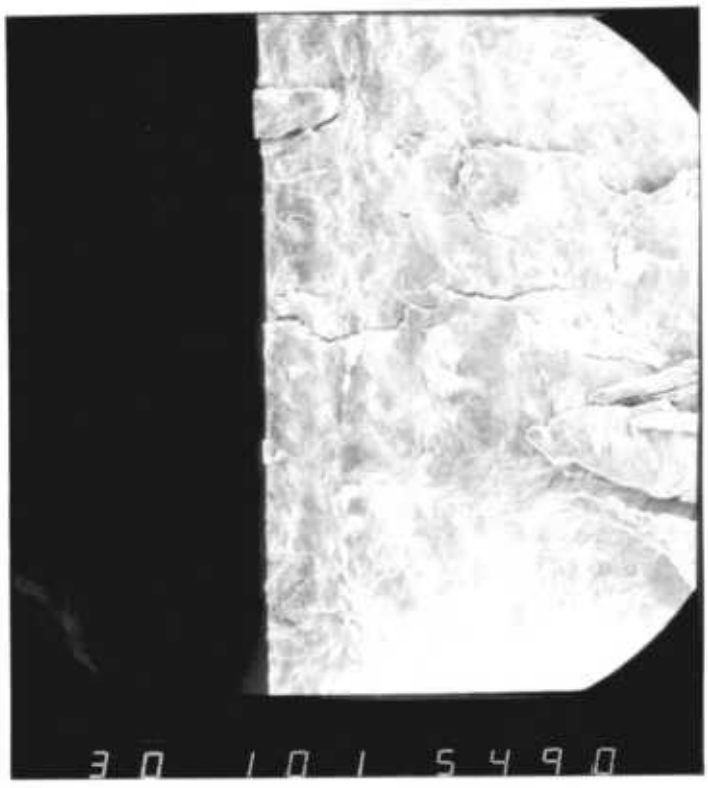

Photograph 5.42

Photograph 5.43

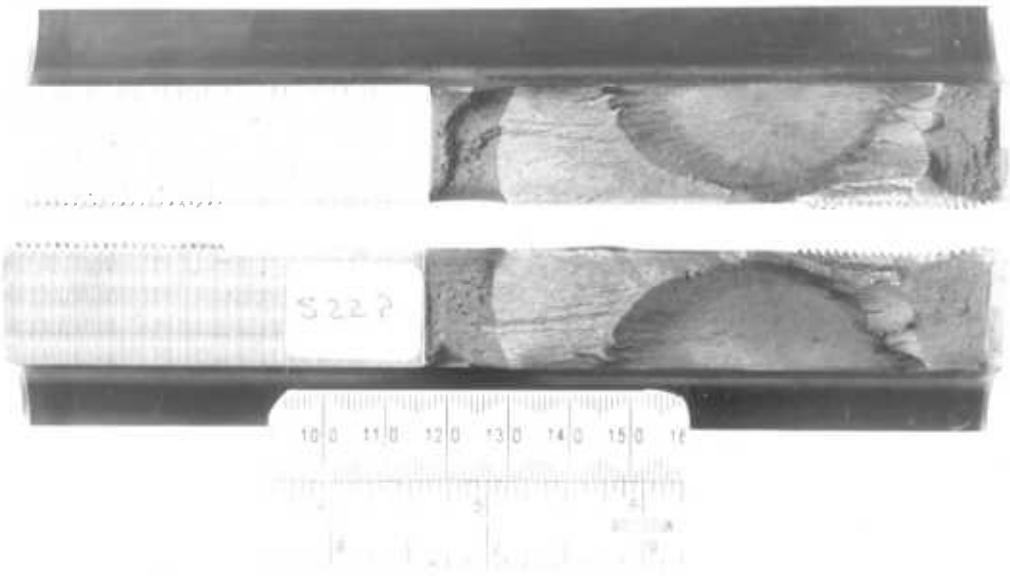

Photograph 5.44

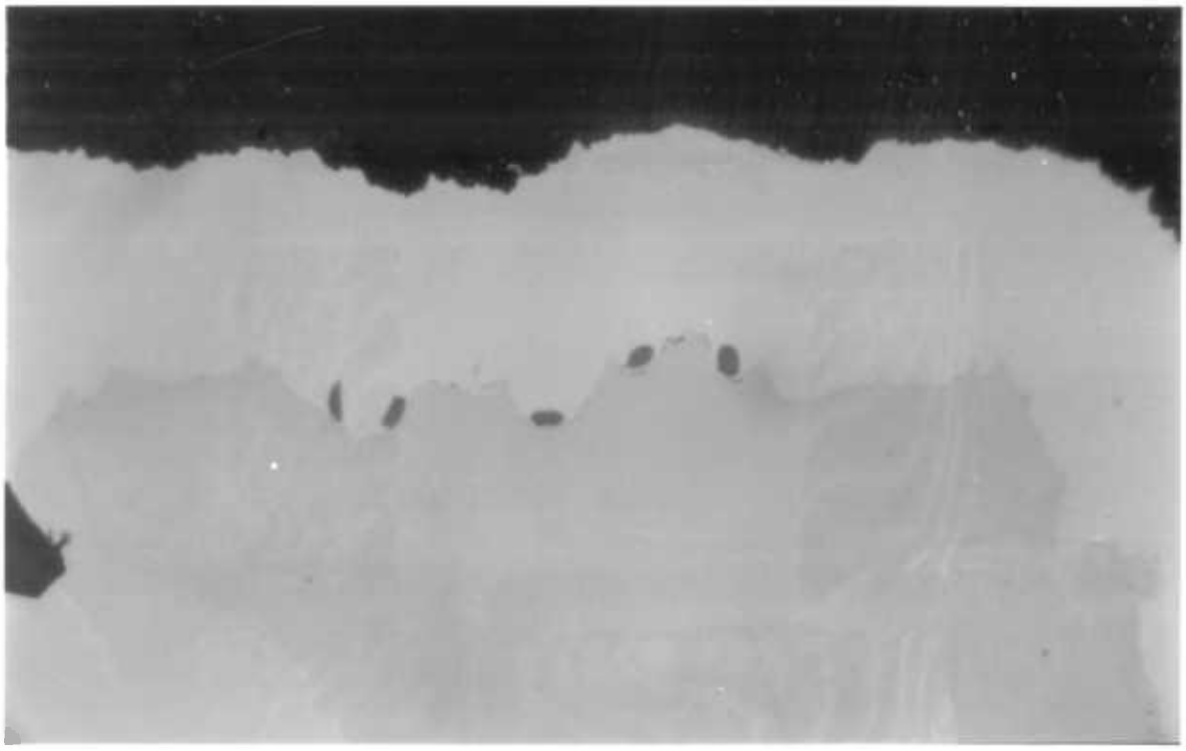

Photograph 5.45 ×100 (×4.4)

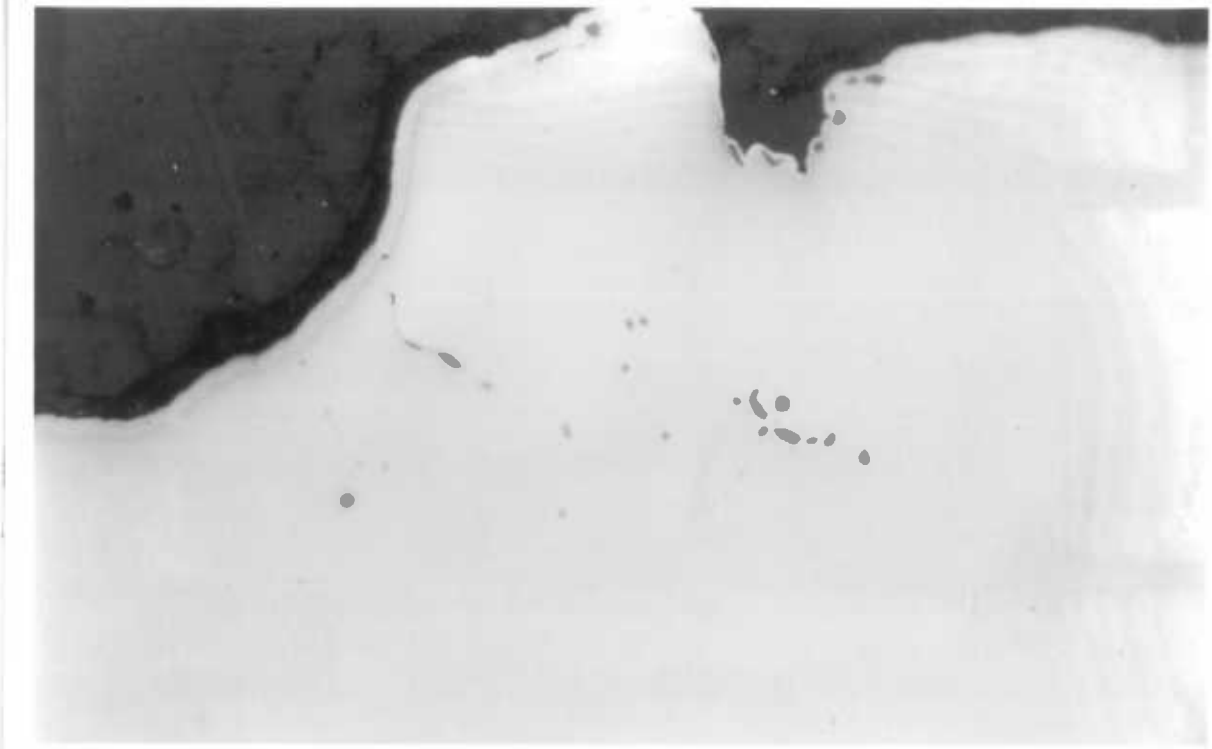

Photograph 5.46 ×100 (×4.4)

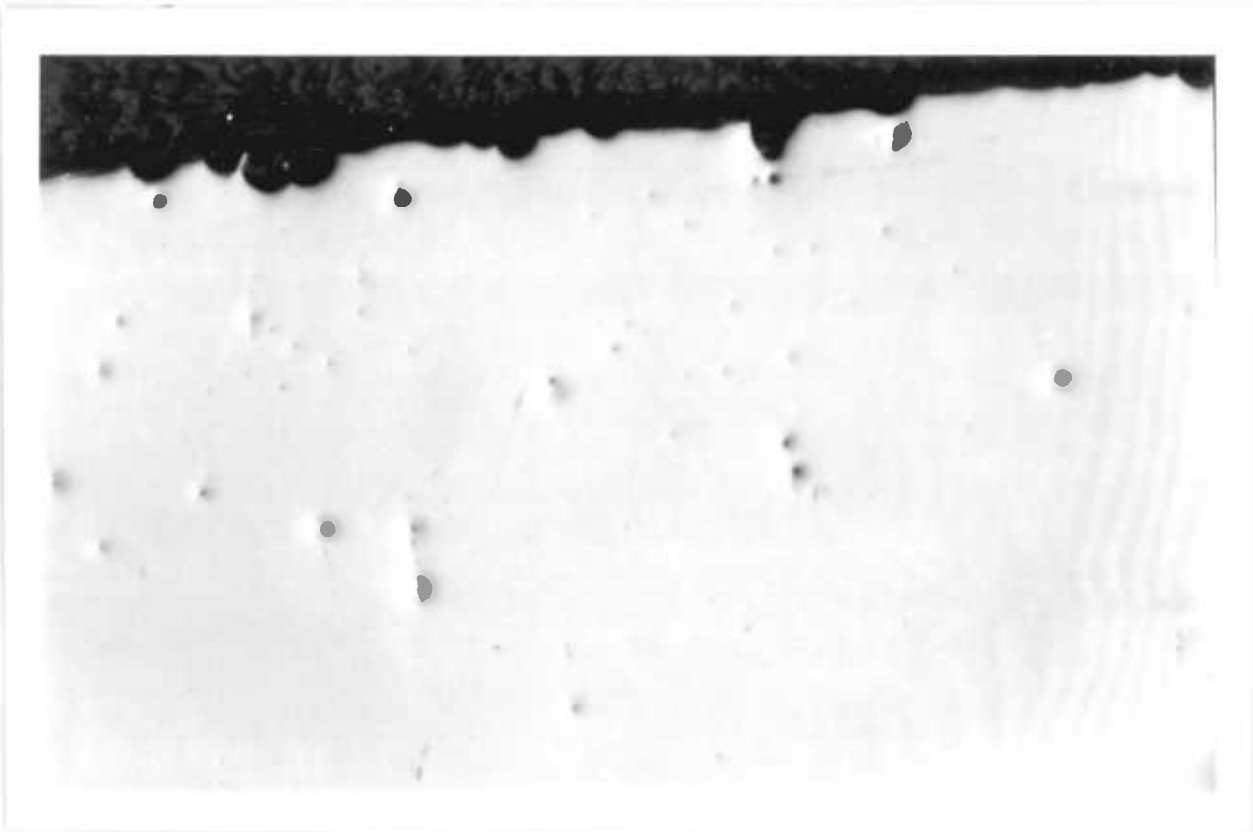

Photograph 5.47 ×12.5 (×4.4)

Photograph 5.48 ×50 (×4.4)

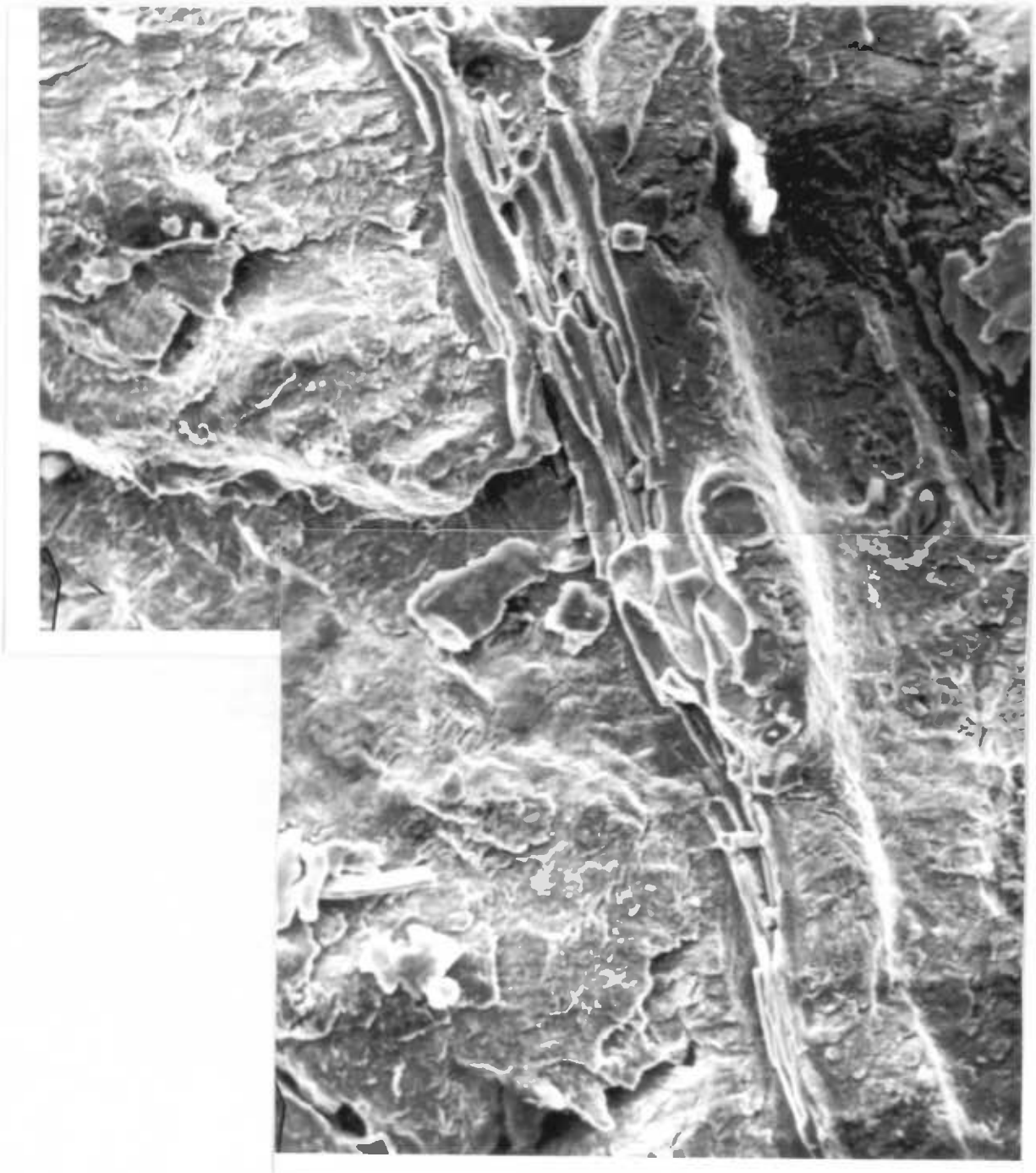

Photograph 5.49

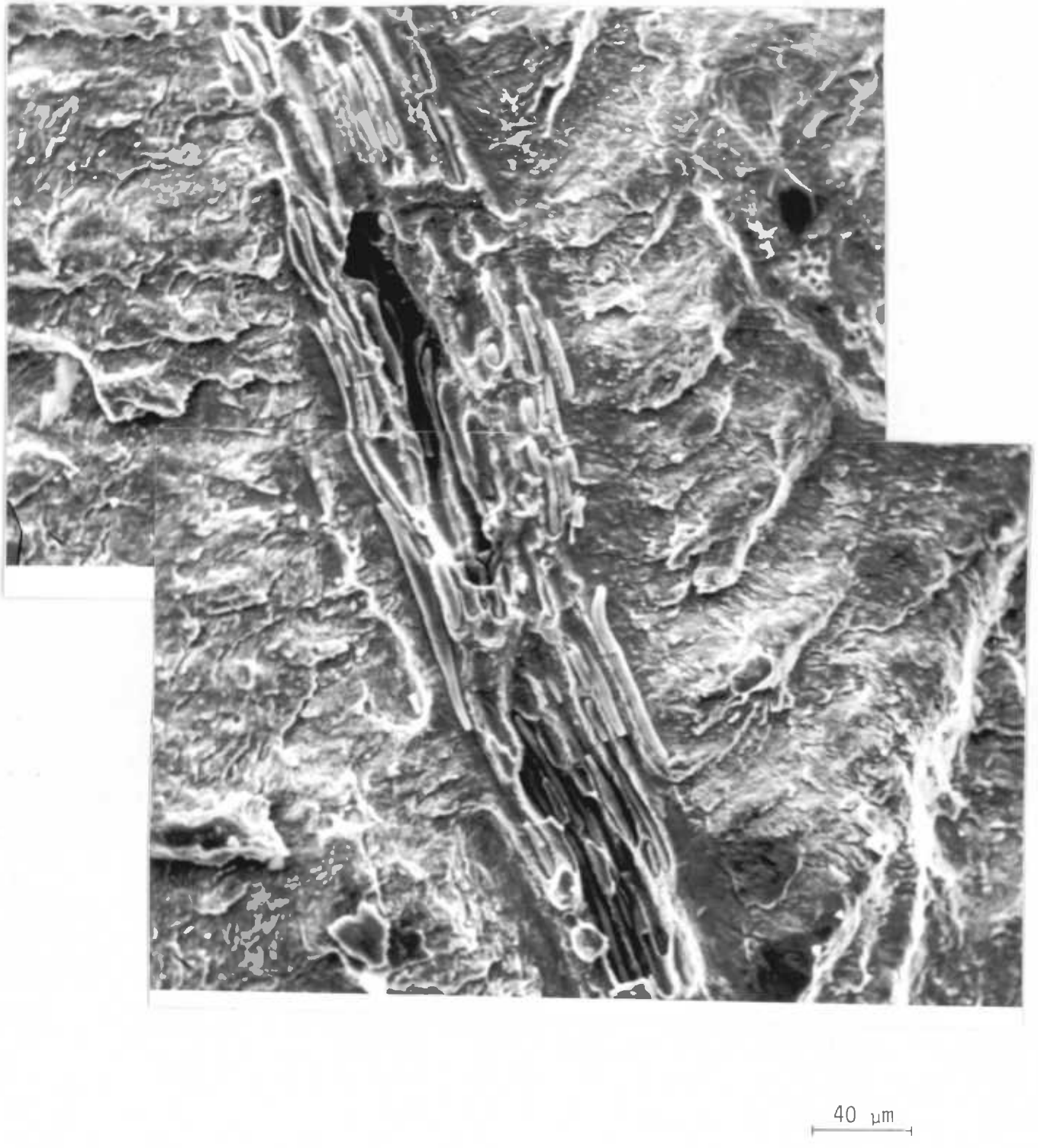

Photograph 5.49

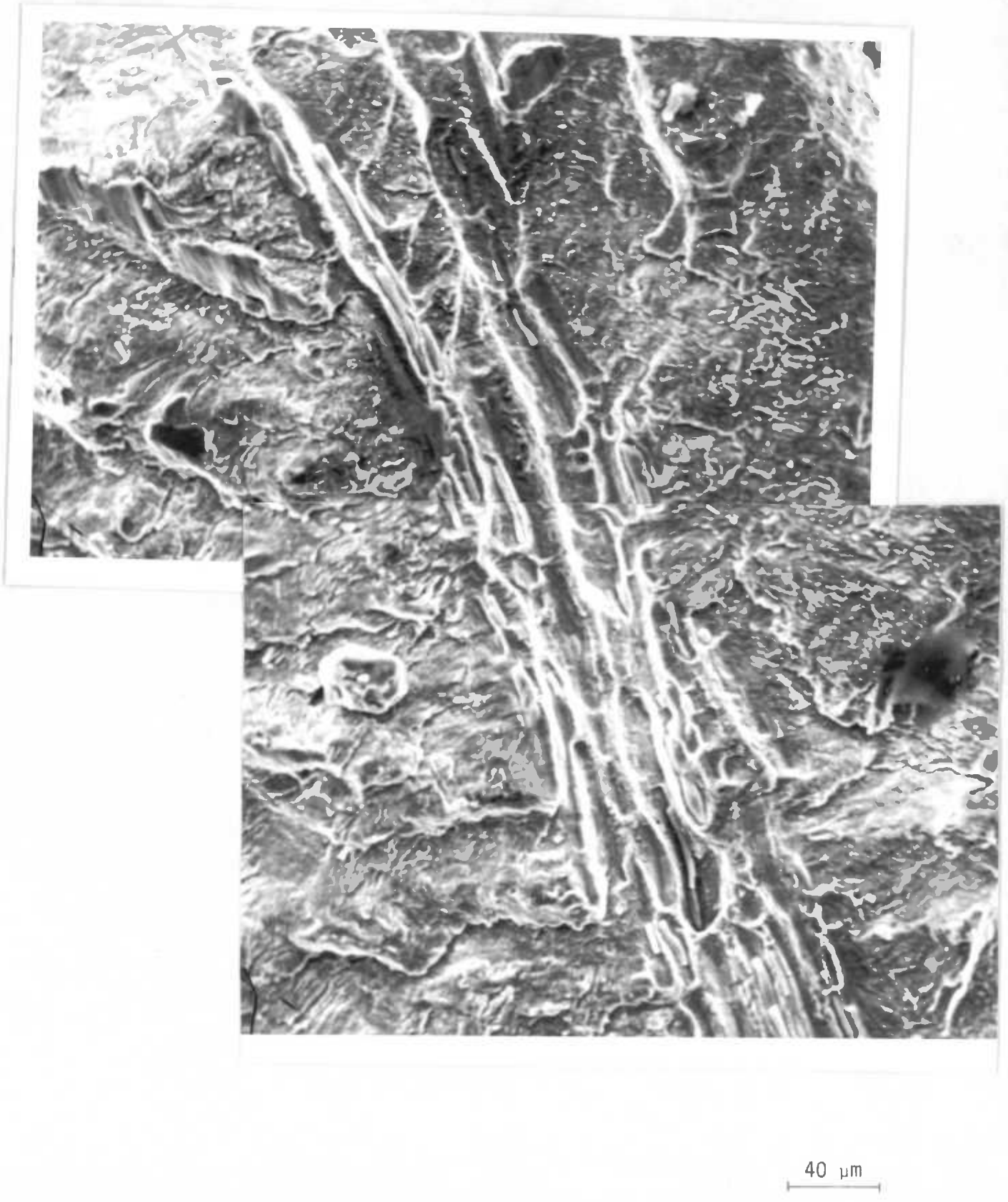

Photograph 5.49